

THE SIGNIFICANCE OF THE "PROTECTION POTENTIAL"
FOR Fe-Cr ALLOYS AT ROOM TEMPERATURE

By

KENNETH KIRCH STARR

A DISSERTATION PRESENTED TO THE GRADUATE
COUNCIL OF THE UNIVERSITY OF FLORIDA IN PARTIAL
FULFILLMENT OF THE REQUIREMENTS FOR THE DEGREE OF
DOCTOR OF PHILOSOPHY

UNIVERSITY OF FLORIDA
1973

© 1974

KENNETH KIRCH STARR

ALL RIGHTS RESERVED

Dedicated to My Wife,

Barbara Jo

ACKNOWLEDGMENTS

I would like to express my thanks to the chairman of my supervisory committee, Dr. Ellis D. Verink, Jr., for his guidance, inspiration and patience. Thanks are also extended to the other members of the committee: Dr. G. M. Schmid, Dr. R. T. DeHoff and Dr. J. J. Hren. Special thanks are extended to Dr. M. Pourbaix for his inspiration and helpful suggestions at several stages of this investigation.

Technical assistance was provided by Mr. P. D. Kalb, Mr. C. J. Minier, Mr. C. M. Simmons, Mr. E. C. Logsdon and Mr. H. W. Willis.

I wish to acknowledge the financial support supplied by the National Science Foundation in the form of an N.S.F. Traineeship. I would also like to acknowledge the financial support supplied by the Advanced Research Project Agency under Contract Number N00014-68-A-0173-0003, administered by the Office of Naval Research, Washington, D.C., and the financial support supplied by the Office of Naval Research under Contract Number N00014-68-A-0173-0015.

The Fe - 12% Cr alloy was donated by the Naval Research Laboratory and the other Fe-Cr alloys were donated by the United States Steel Corporation. These contributions are gratefully acknowledged.

The author is also grateful to his parents, for their help and encouragement, and to his wife, who supported him in many ways.

TABLE OF CONTENTS

	<u>Page</u>
ACKNOWLEDGMENTS.....	iv
LIST OF TABLES.....	xi
LIST OF FIGURES.....	xv
ABSTRACT.....	xxxii
CHAPTERS:	
1. INTRODUCTION.....	1
2. LITERATURE SURVEY.....	5
2.1 Methods of Investigation.....	6
2.1.1 Immersion Tests.....	7
2.1.2 Galvanostatic Tests.....	7
2.1.3 Potentiostatic Tests.....	8
2.1.4 Potentiokinetic Tests.....	8
2.2 Passivity.....	9
2.3 Aggressive Anions.....	12
2.4 Pitting Corrosion.....	13
2.4.1 Pit Initiation.....	14
2.4.1.1 Breakdown of passivity: adsorption theory.....	14
2.4.1.2 Breakdown of passivity: oxide-film theory.....	14
2.4.1.3 Breakdown of passivity: combined theory.....	15
2.4.1.4 Passive film breakdown parameters.....	16
2.4.1.5 Critical pitting potentials...	17
2.4.1.6 Critical chloride ion concentrations.....	19

TABLE OF CONTENTS (Continued)

	<u>Page</u>
2.4.1.7 Effect of pH.....	20
2.4.1.8 Effect of alloy composition...	21
2.4.1.9 Induction periods.....	22
2.4.2 Propagation of Pitting.....	22
2.4.2.1 Geometry of pitting.....	23
2.4.2.2 Current distribution in and around pits.....	25
2.4.2.3 Potential distribution in and around pits.....	27
2.4.2.4 Electrolyte composition inside pits.....	28
2.4.2.5 pH changes in pits.....	29
2.4.2.6 Chemical analysis of artifi- cial pits.....	30
2.4.2.7 Hydrolysis in pits.....	31
2.4.2.8 Electromigration and diffusion.....	32
2.4.2.9 Stability of pitting.....	34
2.5 Crevice Corrosion.....	36
2.5.1 Initiation of Crevice Corrosion.....	37
2.5.1.1 Metal ion cells.....	37
2.5.1.2 Differential aeration cells...	39
2.5.1.3 Passive-active cells.....	39
2.5.1.4 Critical parameter concept....	40
2.5.1.5 Induction periods.....	42
2.5.2 Propagation of Crevice Corrosion.....	42
2.5.2.1 Geometry of crevice corrosion.....	43

TABLE OF CONTENTS (Continued)

	<u>Page</u>
2.5.2.2 Current distribution in and around crevices.....	44
2.5.2.3 Potential distribution in and around crevices.....	45
2.5.2.4 pH changes in crevices.....	48
2.5.2.5 Chemical analysis of crevices.	49
2.5.2.6 Hydrolysis in crevices.....	51
2.6 Limitations of Laboratory Tests.....	52
2.7 The "Protection Potential".....	53
2.7.1 Definition and Verification.....	53
2.7.2 Experimental Methods.....	54
2.7.3 Interpretation of the "Protection Potential" for Cu-Rich Alloys.....	55
2.7.4 Effects of Experimental and Environmental Variables on the "Protection Potential".....	56
2.7.4.1 Effect of alloy composition on E_p	56
2.7.4.2 Effect of pH on E_p	58
2.7.4.3 Effect of $[Cl^-]$ on E_p	58
2.7.4.4 Effect of temperature on E_p ...	60
2.7.4.5 Effect of extent of propagation on E_p	60
2.7.5 Effect of Geometry on E_p	60
2.7.6 Material Vs. Environmental Property....	63
2.7.7 "Repassivation" Vs. "Deactivation".....	64
2.7.8 Experimental Correlation.....	65

TABLE OF CONTENTS (Continued)

	<u>Page</u>
3. EXPERIMENTAL PROCEDURE.....	67
3.1 Potentiostatic Polarization Experiments.....	67
3.2 Potentiokinetic Polarization Experiments.....	67
3.3 Galvanostatic Polarization Experiments.....	68
3.4 Artificial Occluded Cell Experiments.....	71
3.4.1 First Type.....	71
3.4.2 Second Type.....	74
4. RESULTS AND DISCUSSION.....	80
4.1 Potentiokinetic Polarization Results.....	80
4.1.1 Effect of Alloy Composition.....	89
4.1.2 Effect of Bulk Electrolyte pH.....	89
4.1.3 Effect of Bulk Electrolyte Chloride Ion Concentration.....	97
4.1.4 Effect of Extent of Propagation.....	104
4.2 Galvanostatic Polarization Results.....	113
4.3 Artificial Occluded Cell Results.....	119
4.3.1 First Type.....	119
4.3.2 Second Type.....	122
4.4 Thermodynamic Calculations.....	134
4.4.1 Potential Vs. pH (Pourbaix) Diagrams...	134
4.4.2 Hydrolysis Calculations.....	141
4.5 Metal Chloride Solution Scans.....	157
4.6 Potentiostatic Titration Results.....	169
4.6.1 pH Titrations.....	169
4.6.2 Metal Chloride Titrations.....	170

TABLE OF CONTENTS (Continued)

	<u>Page</u>
5. CONCLUSIONS.....	176
6. RECOMMENDATIONS FOR FURTHER RESEARCH.....	181
APPENDICES.....	182
1. ALLOY CHARACTERIZATION.....	183
2. STANDARD ELECTROCHEMICAL POLARIZATION CELL.....	188
3. SAMPLE PREPARATION AND MOUNTING.....	190
4. ELECTROLYTES.....	192
5. DEAERATION OF ELECTROLYTES.....	195
6. LIST OF EQUIPMENT.....	196
7. ZERO-IMPEDANCE AMMETER.....	198
8. EXPERIMENTAL POTENTIAL VS. pH DIAGRAMS AND CHARACTERISTIC VALUES FROM CYCLIC POTENTIOKINETIC POLARIZATION CURVES FOR Fe-Cr ALLOYS IN 0.1 M Cl ⁻ , H ₂ -SATURATED (OR O ₂ -SATURATED) SOLUTIONS.....	200
9. SPECIAL CYCLIC POTENTIOKINETIC POLARIZATION SCANS FOR THE Fe - 12% Cr ALLOY IN 0.1 M Cl ⁻ , H ₂ - SATURATED SOLUTIONS.....	228
10. SPECIAL CYCLIC POTENTIOKINETIC POLARIZATION SCANS FOR THE Fe - 12% Cr ALLOY IN 0.1 M Cl ⁻ , H ₂ - SATURATED SOLUTIONS, USING PAINTED-OFF SAMPLES APPROXIMATELY 1 cm ² IN AREA.....	245
11. EXPERIMENTAL POTENTIAL VS. LOG CHLORIDE ION MOLARITY DIAGRAMS AND CHARACTERISTIC VALUES FROM CYCLIC POTENTIOKINETIC POLARIZATION CURVES FOR Fe-Cr ALLOYS IN H ₂ -SATURATED SOLUTIONS OF NOMINAL pH 5.4, 8.8 AND 10.8.....	262
12. GALVANOSTATIC POLARIZATION EXPERIMENT DATA FOR THE Fe - 12% IN A 0.1 M Cl ⁻ , H ₂ -SATURATED SOLUTIONS OF NOMINAL pH 10.1.....	300
13. GALVANOSTATIC SINGLE-PIT POLARIZATION EXPERIMENT DATA FOR THE Fe - 12% Cr ALLOY IN 0.1 M Cl ⁻ , H ₂ - SATURATED SOLUTIONS OF NOMINAL pH 10.2.....	303

TABLE OF CONTENTS (Continued)

	<u>Page</u>
14. ARTIFICIAL OCCLUDED CELL DATA FOR THE Fe - 12% Cr ALLOY AND ARMCO Fe IN SOLUTIONS INITIALLY 0.1 M Cl ⁻ .	307
15. ANALYSES OF FINAL ARTIFICIAL OCCLUDED CELL SOLUTIONS FOR THE Fe - 12% Cr ALLOY AND ARMCO Fe IN SOLUTIONS INITIALLY 0.1 M Cl ⁻	311
16. CARBIDE CALCULATIONS.....	313
17. CALCULATED EQUILIBRIUM POTENTIAL VS. pH (POURBAIX) DIAGRAMS, THERMODYNAMIC DATA AND PERTINENT EQUATIONS	316
18. HYDROLYSIS CALCULATIONS AND RESULTS.....	331
19. CYCLIC POTENTIOKINETIC POLARIZATION SCAN DATA FOR THE Fe - 12% Cr ALLOY IN H ₂ -SATURATED METAL CHLORIDE SOLUTIONS.....	338
BIBLIOGRAPHY.....	342
BIOGRAPHICAL SKETCH.....	357

LIST OF TABLES

<u>Table</u>		<u>Page</u>
1	Chemical Compositions of Commercial Stainless Steels.....	2
2	Details of Investigations of the "Protection Potential" for Ferrous Alloys.....	57
3	Extent of Propagation Data for the Fe - 12% Cr Alloy in 0.1 M Cl ⁻ , H ₂ -Saturated Solutions of pH Approximately 10.1.....	109
4	Single-Pit Extent-of-Propagation Data for the Fe - 12% Cr Alloy in 0.1 M Cl ⁻ , H ₂ -Saturated Solutions of pH Approximately 10.2.....	112
5	Solubility of Metal Chlorides.....	145
6	Thermodynamic Data for Complex Ion Hydrolysis Reactions.....	146
7	pH's of H ₂ -Deaerated Metal Chloride Solutions.....	152
8	pH Titration Results: Fe-12% Cr Alloy.....	171
9	Metal Chloride Titration Results: Fe-12% Cr Alloy, 0.1 M NaCl, H ₂ -Saturated Initial Solutions.....	173
10	Metal Chloride Titration Results: Fe - 5.0% Cr, Fe - 12% Cr, Fe - 16.9% Cr and Fe - 24.9% Cr Alloys 0.1 M NaCl, H ₂ -Saturated Initial Solutions, Holding Potential -0.250 v _{SCE} (0.000 v _{SHE}).....	175
11	Compositions of Binary Iron-Chromium Alloys Under Investigation.....	184
12	0.1 M Cl ⁻ Electrolytes.....	193
13	Characteristic Values from Cyclic Potentiokinetic Polarization Curves for the Fe-0.5% Cr Alloy in 0.1 M Cl ⁻ , H ₂ -Saturated Solutions.....	213
14	Characteristic Values from Cyclic Potentiokinetic Polarization Curves for the Fe-2.0% Cr Alloy in 0.1 M Cl ⁻ , H ₂ -Saturated Solutions.....	215
15	Characteristic Values from Cyclic Potentiokinetic Polarization Curves for the Fe-5.0% Cr Alloy in 0.1 M Cl ⁻ , H ₂ -Saturated Solutions.....	217

LIST OF TABLES (Continued)

<u>Table</u>		<u>Page</u>
16	Characteristic Values from Cyclic Potentio-kinetic Polarization Curves for the Fe-12% Cr Alloy in 0.1 M Cl ⁻ , H ₂ -Saturated Solutions.....	219
17	Characteristic Values from Cyclic Potentio-kinetic Polarization Curves for the Fe-12% Cr Alloy in 0.1 M Cl ⁻ , O ₂ -Saturated Solutions.....	222
18	Characteristic Values from Cyclic Potentio-kinetic Polarization Curves for the Fe-16.9% Cr Alloy in 0.1 M Cl ⁻ , H ₂ -Saturated Solutions.....	224
19	Characteristic Values from Cyclic Potentio-kinetic Polarization Curves for the Fe-24.9% Cr Alloy in 0.1 M Cl ⁻ , H ₂ -Saturated Solutions.....	226
20	Characteristic Values from Cyclic Potentio-kinetic Polarization Curves for the Fe-0.5% Cr Alloy in H ₂ -Saturated Solutions.....	287
21	Characteristic Values from Cyclic Potentio-kinetic Polarization Curves for the Fe-2.0% Cr Alloy in H ₂ -Saturated Solutions.....	290
22	Characteristic Values from Cyclic Potentio-kinetic Polarization Curves for the Fe-12% Cr Alloy in H ₂ -Saturated Solutions.....	293
23	Characteristic Values from Cyclic Potentio-kinetic Polarization Curves for the Fe-16.9% Cr Alloy in H ₂ -Saturated Solutions.....	297
24	Galvanostatic Polarization Experiment Data for the Fe-12% Cr Alloy in a 0.1 M Cl ⁻ , H ₂ -Saturated Solution of pH 10.1: Run No. KS-145 (Sample Area ≈ 0.95 cm ²).....	301
25	Galvanostatic Polarization Experiment Data for the Fe-12% Cr Alloy in a 0.1 M Cl ⁻ , H ₂ -Saturated Solution of pH 10.0: Run No. KS-146 (Sample Area ≈ 1.13 cm ²).....	301
26	Galvanostatic Polarization Experiment Data for the Fe-12% Cr Alloy in a 0.1 M Cl ⁻ , H ₂ -Saturated Solution of pH 10.1: Run No. KS-148 (Sample Area ≈ 1.33 cm ²).....	302

LIST OF TABLES (Continued)

<u>Table</u>		<u>Page</u>
27	Galvanostatic Polarization Experiment Data for the Fe-12% Cr Alloy in a 0.1 M Cl ⁻ , H ₂ -Saturated Solution of pH 10.1: Run No. KS-149 (Sample Area ≈ 1.33 cm ²).....	302
28	Single-Pit Galvanostatic Polarization Experiment Data for the Fe-12% Cr Alloy in a 0.1 M Cl ⁻ , H ₂ -Saturated Solution of pH 10.2: Run No. KS-185 ² (Sample Area ≈ 0.000883 cm ²).....	304
29	Single-Pit Galvanostatic Polarization Experiment Data for the Fe-12% Cr Alloy in a 0.1 M Cl ⁻ , H ₂ -Saturated Solution of pH 10.1: Run No. KS-186 ² (Sample Area ≈ 0.000883 cm ²).....	305
30	Single-Pit Galvanostatic Polarization Experiment Data for the Fe-12% Cr Alloy in a 0.1 M Cl ⁻ , H ₂ -Saturated Solution of pH 10.2: Run No. KS-187 ² (Sample Area ≈ 0.000883 cm ²).....	306
31	Artificial Occluded Cell Data for the Fe-12% Cr Alloy and Armco Fe in Solutions Initially 0.1 M Cl ⁻	308
32	Analyses of Final Artificial Occluded Cell Solutions for the Fe-12% Cr Alloy and Armco Fe in Solutions Initially 0.1 M Cl ⁻	312
33	Free Energy of Formation Data for Fe-Containing Species Considered.....	323
34	Free Energy of Formation Data for Cr-Containing Species Considered.....	324
35	Pertinent Nernst Equations for the Fe-H ₂ O System Potential Vs. pH (Pourbaix) Diagram (Activities of All Dissolved Species Taken to Be 10 ⁻⁶).....	325
36	Pertinent Nernst Equations for the Fe-Cl ⁻ -H ₂ O System Potential Vs. pH (Pourbaix) Diagram (Activity of Cl ⁻ Taken to Be 0.1 and Activities of All Other Dissolved Species Taken to Be 10 ⁻⁶ ...	326
37	Pertinent Nernst Equations for the Special Fe-Cl ⁻ -H ₂ O System Potential Vs. pH (Pourbaix) Diagram (Activity of Cl ⁻ Taken to Be 0.373 and Activities of All Other Dissolved Species Taken to Be 0.156).....	327

LIST OF TABLES (Continued)

<u>Table</u>		<u>Page</u>
38	Pertinent Nernst Equations for the Fe-H ₂ O System Potential Vs. pH (Pourbaix) Diagram (Activities of all Dissolved Species Taken to Be 10 ⁻⁶).....	328
39	Pertinent Nernst Equations for the Fe-Cl ⁻ -H ₂ O System Potential Vs. pH (Pourbaix) Diagram (Activity of Cl ⁻ Taken to Be 0.1 and Activities of All Other Dissolved Species Taken to Be 10 ⁻⁶)..	329
40	Pertinent Nernst Equations for the Special Cr-Cl ⁻ -H ₂ O System Potential Vs. pH (Pourbaix) Diagram (Activity of Cl ⁻ Taken to Be 0.373 and Activities of all Other Dissolved Species Taken to Be 0.02)..	330
41	Data Used for HYD1E, HYD2E, HYD3A and HYD4A Computer Programs.....	334
42	Hydrolysis Calculation Results.....	335
43	Cyclic Potentiokinetic Polarization Scan Data for the Fe - 12% Cr Alloy in H ₂ -Saturated Metal Chloride Solutions ("Teflon Gasket" Samples).....	339
44	Cyclic Potentiokinetic Polarization Scan Data for the Fe - 12% Cr Alloy in H ₂ -Saturated Metal Chloride Solutions ("Microshield" Samples).....	341

LIST OF FIGURES

<u>Figure</u>		<u>Page</u>
1	Hypothetical cathodic and anodic polarization plots for a passive metallic electrode.....	11
2	Proposed potential vs. concentration ratio plot for an active-passive metal showing regions of active dissolution (and etching), passivity, brightening and transpassivity. Seven possible kinds of reactions are indicated by numbers.....	24
3	Effect of sodium chloride molarity on the "protection potential" for Types 410, 304 and 316 stainless steels in 0.1 M NaHCO ₃ , N ₂ -saturated solutions at 20°C.....	58
4	Effect of chloride ion normality on the "protection potential" for Type 316L stainless steel in stagnant chloride solutions at 70°C.....	59
5	Effect of temperature on the "protection potential" for Types 410, 304 and 316 stainless steels in 0.1 M NaCl + 0.1 M NaHCO ₃ , N ₂ -saturated solutions.....	61
6	Effect of temperature on the "protection potential" for Type 316L stainless steel in stagnant 0.88 N NaCl solutions.....	62
7	Effect of extent of propagation on the "protection potential" for Types 430 and 304 stainless steels in 1 M NaCl, N ₂ -saturated solutions at 25°C. Initial specimen area: 5 cm ²	63
8	Correlation between the "difference potential" (E _R - E _P) and corrosion weight loss of stainless steel alloys exposed in sea water for 4.25 years. The "difference potentials" were determined in 3.5 wt. % NaCl, air-saturated solutions at 25°C...	66
9	Schematic diagram of equipment used to potentiokinetically polarize specimen and record current density as a function of potential.....	69
10	Effect of scan rate on potentiokinetic polarization curves for the Fe-12% Cr alloy in 0.1 M NaCl + 0.1 M NaHCO ₃ , H ₂ -saturated solutions (pH 8.7) at 25°C.....	70

LIST OF FIGURES (Continued)

<u>Figure</u>		<u>Page</u>
11	Schematic diagram of equipment used to galvanostatically polarize sample and record resulting potential as a function of time.....	72
12	Modified sample and sample holder for first type of artificial occluded cell used during this investigation.....	73
13	Schematic diagram of equipment used for first type of artificial occluded cell.....	75
14	Second type of artificial occluded cell used during this investigation.....	76
15	Electrical schematic diagram for the second type of artificial occluded cell.....	78
16	Schematic diagram of equipment used for second type of artificial occluded cell. S_1 and S_2 are the bulk and artificial occluded cell samples, respectively.....	79
17	a. Schematic diagram for the development of an experimental potential vs. pH diagram for iron in chloride-free, N_2 -saturated solutions. The "a" and "b" dashed lines represent the equilibrium hydrogen and oxygen electrodes, respectively.....	81
	b. Schematic diagram for the development of an experimental potential vs. pH diagram for iron in 0.01 M Cl^- , N_2 -saturated solutions. The "a" and "b" lines represent the equilibrium hydrogen and oxygen electrodes, respectively..	81
18	Experimental potential vs. pH diagrams for the series of Fe-Cr alloys under investigation in 0.1 M Cl^- , H_2 -saturated solutions, as reported by Cusumano. The cross-hatched areas represent regions of general corrosion.....	82
19	Some typical potentiokinetic polarization curves for the series of Fe-Cr alloys under investigation in 0.1 M Cl^- , H_2 -saturated solutions, according to Cusumano. E_{pp} : primary passivation potential, E_R : rupture potential, E_p : "protection potential".	83

LIST OF FIGURES (Continued)

<u>Figure</u>		<u>Page</u>
20	Experimental potential vs. pH diagrams for the Fe - 12% Cr alloy in 0.1 M Cl ⁻ , H ₂ -saturated and O ₂ -saturated solutions.....	84
21	Schematic experimental potential vs. pH diagrams for the Fe - 12% Cr alloy in 0.1 M Cl ⁻ , H ₂ -saturated and O ₂ -saturated solutions.....	85
22	Schematic representation of two types of cyclic potentiokinetic polarization curves observed for the Fe - 12% Cr alloy in Cl ⁻ -containing, H ₂ -saturated solutions. E ₀ : zero current potential, E _{pp} : primary passivation potential, E _R : rupture potential, E _p : "protection potential".....	86
23	Experimental potential vs. pH diagrams for the series of Fe-Cr alloys in 0.1 M Cl ⁻ , H ₂ -saturated solutions, including zero current potentials, primary passivation potentials and rupture potentials.....	88
24	"Protection potential" (E _p) data, superimposed on the zero current potential, primary passivation potential and rupture potential lines taken from Figure 23.....	90
25	Results of a series of special cyclic potentiokinetic polarization scans for the Fe - 12% Cr alloy in 0.1 M Cl ⁻ , H ₂ -saturated solutions of pH 3.2, 4.4, 5.5 and 7.1.....	93
26	Results of a series of special cyclic potentiokinetic polarization scans for the Fe - 12% Cr alloy in 0.1 M Cl ⁻ , H ₂ -saturated solutions of pH 8.9, 9.7, 10.9 and 12.0.....	94
27	Results of a series of special cyclic potentiokinetic polarization scans for the Fe - 12% Cr alloy in 0.1 M Cl ⁻ , H ₂ -saturated solutions of pH 3.2, 4.4, 5.5 and 7.2, using painted-off samples (~ 1 cm ² in area).....	95

LIST OF FIGURES (Continued)

<u>Figure</u>		<u>Page</u>
28	Results of a series of special cyclic potentiokinetic polarization scans for the Fe - 12% Cr alloy in 0.1 M Cl ⁻ , H ₂ -saturated solutions of pH 8.9, 9.7, 10.9 and 12.0, using painted-off samples (~ 1 cm ² in area).....	96
29	Experimental potential vs. log chloride ion concentration diagrams for four Fe-Cr alloys in H ₂ -saturated solutions of pH 5.4 to 5.5, including zero current potentials, primary passivation potentials and rupture potentials.....	98
30	Experimental potential vs. log chloride ion concentration diagrams for four Fe-Cr alloys in H ₂ -saturated solutions of pH 8.7 to 8.8, including zero current potentials, primary passivation potentials and rupture potentials.....	99
31	Experimental potential vs. log chloride ion concentration diagrams for four Fe-Cr alloys in H ₂ -saturated solutions of pH 10.8 to 11.0, including zero current potentials, primary passivation potentials and rupture potentials.....	100
32	"Protection potential" (E _p) data, superimposed on the zero current potential, primary passivation potential and rupture potential lines taken from Figure 29.....	101
33	"Protection potential" (E _p) data, superimposed on the zero current potential, primary passivation potential and rupture potential lines taken from Figure 30.....	102
34	"Protection potential" (E _p) data, superimposed on the zero current potential, primary passivation potential and rupture potential lines taken from Figure 31.....	103
35	Plot of "protection potential" (E _p) data vs. total charge passed per unit sample area, Q/A (plotted logarithmically), for the Fe - 12% Cr alloy in 0.1 M Cl ⁻ , H ₂ -saturated solutions of indicated pH's.....	105

LIST OF FIGURES (Continued)

<u>Figure</u>		<u>Page</u>
36	a. Plot of "protection potential" (E_p) data vs. total charge passed per unit (original) sample area, Q/A (plotted logarithmically) for the Fe - 12% Cr alloy in 0.1 M Cl^- , H_2 -saturated solutions of pH approximately 10.1.....	108
	b. Plot of "protection potential" (E_p) data vs. pit density (number of pits divided by original sample area).....	108
	c. Plot of "protection potential" (E_p) data vs. active area fraction, A_A (pitted plus creviced area divided by original sample area). Points connected by a line represent a single sample.....	108
37	Plot of single-pit "protection potential" (E_p) data vs. total charge passed per unit sample area, Q/A (plotted logarithmically), for the Fe - 12% Cr alloy in 0.1 M Cl^- , H_2 -saturated solutions of pH approximately 10.2. Points connected by a line represent a single sample.....	111
38	Instantaneous mixed potential vs. total charge passed, Q (plotted logarithmically) for the Fe - 12% Cr alloy in 0.1 M Cl^- , H_2 -saturated solutions of pH approximately 10.1. Sample areas $\approx 1 \text{ cm}^2$. Each diagram presents results for a single sample.....	115
39	Superposition of data from Figures 36a and 38d. A superposition of potentiokinetic and galvanostatic results.....	116
40	Single-pit instantaneous mixed potential vs. total charge passed per unit sample area, Q/A (plotted logarithmically), for the Fe - 12% Cr alloy in 0.1 M Cl^- , H_2 -saturated solutions of pH approximately 10.2. Each diagram presents results for a single sample.....	118

LIST OF FIGURES (Continued)

<u>Figure</u>		<u>Page</u>
41	Potentiokinetic plot of applied potential vs. Ag-AgCl electrode potential for the first type of Fe - 12% Cr artificial occluded cell in a 0.1 M Cl ⁻ , H ₂ -saturated solution of pH 5.4. The zero current potential, rupture potential and "protection potential," observed with an ammeter incorporated into the potentiostat, are indicated with arrows.....	120
42	Potentiokinetic plots of applied current vs. Ag-AgCl electrode potential for the first type of Fe - 12% Cr artificial occluded cell in 0.1 M Cl ⁻ , H ₂ -saturated solutions of pH 8.8.....	121
43	a. Progress of artificial occluded cell experiments for the Fe - 12% Cr alloy in solutions initially 0.1 M NaCl + 0.01 M NaHCO ₃ , with H ₂ -saturated bulk solutions.....	124
	b. Progress of artificial occluded cell experiments for the Fe - 12% Cr alloy in solutions initially 0.1 M NaCl + 0.01 M NaHCO ₃ , with O ₂ -saturated bulk solutions. The results are superimposed on the experimental potential vs. pH diagram (0.1 M Cl ⁻ , H ₂ -saturated solutions) for the same alloy.....	124
44	Progress of artificial occluded cell experiments for the Fe - 12% Cr alloy in solutions initially 0.1 M NaCl, adjusted to approximately pH 10 with 0.1 M NaOH. The bulk solutions were O ₂ -saturated. The results are superimposed on the experimental potential vs. pH diagram (0.1 M Cl ⁻ , H ₂ -saturated solutions) for the same alloy.....	125
45	Progress of two artificial occluded cell experiments conducted with Armco Fe in solutions initially 0.1 M NaCl, adjusted to approximately pH 10 with 0.1 M NaOH. The bulk solutions were O ₂ -saturated. The results are superimposed on the experimental potential vs. pH diagram for the Fe - 12% Cr alloy (0.1 M Cl ⁻ , H ₂ -saturated solutions) for purposes of comparison.....	128

LIST OF FIGURES (Continued)

<u>Figure</u>		<u>Page</u>
46	Minimum pH and corresponding potential attained in the Fe - 12% Cr artificial occluded cell experiments presented in Figures 43a, 43b and 44, superimposed on the experimental potential vs. pH diagram for the same alloy in 0.1 M Cl ⁻ , H ₂ -saturated solutions.....	130
47	Return zero current potentials and their corresponding pH's measured for some of the artificial occluded cell samples, superimposed on the results of Figure 46. Run numbers are included for reference.....	131
48	Results of atomic absorption spectrophotometric analyses of the final artificial occluded cell solutions for the Fe - 12% Cr alloy. The solid and dashed lines were calculated assuming no macroscopic dealloying occurred.....	133
49	Plot of chloride concentrations (determined by AgNO ₃ titrations) vs. linear combinations of the data shown in Figure 48. The solid line was calculated assuming the predominant corrosion products to be FeCl ₂ ·xH ₂ O and CrCl ₃ ·yH ₂ O.....	135
50	Comparison of calculated equilibrium potential vs. pH (Pourbaix) diagrams for the Fe-H ₂ O system and experimentally determined potential vs. pH diagrams for the Fe - 12% Cr alloy in 0.1 M Cl ⁻ solutions.....	136
51	Calculated equilibrium potential vs. pH (Pourbaix) diagram for the Fe-FeCl ₂ ·4H ₂ O-H ₂ O system, assuming a solution saturated in FeCl ₂ ·4H ₂ O.....	137
52	Calculated equilibrium potential vs. pH diagrams for the Cr-H ₂ O system. Cr(OH) ₃ ·nH ₂ O is assumed to form in the presence of chloride solutions.....	139
53	a. Calculated equilibrium potential vs. pH (Pourbaix) diagrams for the Fe-H ₂ O and Fe-Cl ⁻ -H ₂ O systems: The activity of Cl ⁻ was taken to be 0.1 and the activities of all other dissolved species were taken to be 10 ⁻⁶	140

LIST OF FIGURES (Continued)

<u>Figure</u>		<u>Page</u>
53	b. Calculated equilibrium potential vs. pH (Pourbaix) diagrams for the Cr-H ₂ O and Cr-Cl ⁻ -H ₂ O systems.....	140
54	Specially calculated equilibrium potential vs. pH (Pourbaix) diagrams for the Fe-Cl ⁻ -H ₂ O and Cr-Cl ⁻ -H ₂ O systems.....	142
55	Results of hydrolysis calculations for Fe ⁺⁺ , Fe ⁺⁺⁺ , Cr ⁺⁺⁺ and Ni ⁺⁺	147
56	a. Potential vs. pH curves calculated by combining hydrolysis equations and Nernst Equations for pure Fe.....	150
	b. Potential vs. pH curves calculated by combining hydrolysis equations and Nernst Equations for pure Cr and for pure Ni.....	150
	c. Potential vs. pH curves calculated by combining hydrolysis equations and Nernst Equations for the Fe - 12% Cr alloy.....	150
57	Superposition of Fe - 12% Cr artificial occluded cell results and hydrolysis calculations for aquo-complex ions involving Cr.....	154
58	a. Potential vs. log chromic ion molarity diagrams for the Fe - 12% Cr alloy in 0.1 M NaCl, H ₂ -saturated solutions with CrCl ₃ ·6H ₂ O and FeCl ₂ ·4H ₂ O added.....	159
	b. "Protection potentials" (E _p), return peak potentials, return zero current potentials and second feature potentials (all determined from return scans), superimposed on the zero current potential, primary passivation potential and rupture potential lines taken from Figure 58a.....	159
59	Some of the metal chloride solution scan data for the "Teflon Gasket" samples, superimposed on the experimental potential vs. pH diagram for the Fe - 12% Cr alloy in 0.1 M Cl ⁻ , H ₂ -saturated solutions.	162

LIST OF FIGURES (Continued)

<u>Figure</u>		<u>Page</u>
60	Log passivation current density (a/cm^2) vs. log chromic ion molarity diagrams constructed from the metal chloride solution scan data for "Teflon Gasket" samples and for "Microshield" samples of the Fe - 12% Cr alloy.....	163
61	Log current density (a/cm^2) vs. log chromic ion molarity diagrams constructed from the metal chloride solution scan data for "Teflon Gasket" samples and for "Microshield" samples of the Fe - 12% Cr alloy.....	164
62	Log passivation current density (a/cm^2) vs. log chloride ion molarity diagrams constructed from potentiokinetic polarization data for the Fe - 12% Cr alloy in H_2 -saturated solutions of pH 5.4, 8.8 and 10.8.....	166
63	Log passivation current density (a/cm^2) vs. pH diagram constructed from potentiokinetic polarization data for the Fe - 12% Cr alloy in 0.1 M (molar) Cl^- , H_2 -saturated solutions.....	167
64	Metal chloride solution ($[Fe]/[Cr] = 7.82$) scan data superimposed on the log passivation current density (a/cm^2) line for the Fe - 12% Cr alloy in 0.1 M (Molar) Cl^- , H_2 -saturated solutions (from Figure 63).....	168
65	Phase diagram for the Fe-Cr system, according to Hansen.....	185
66	Photomicrograph of the as-forged Fe - 12% Cr alloy showing delta ferrite in a martensite matrix (magnification 500 X).....	186
67	Photomicrograph of the annealed Fe - 12% Cr alloy showing a matrix of equiaxed ferrite grains, with randomly dispersed particles of chromium carbide (magnification 500 X).....	186
68	Standard electrochemical polarization cell used during this investigation.....	189
69	Assembled and exploded views of sample holder.....	191
70	Electrical schematic diagram of zero-impedance ammeter used to eliminate internal resistance errors during current measurements.....	199

LIST OF FIGURES (Continued)

<u>Figure</u>		<u>Page</u>
71	Experimental potential vs. pH diagram for the Fe - 0.5% Cr alloy in 0.1 M Cl ⁻ , H ₂ -saturated solutions.....	201
72	"Protection potential" (E _p) data for the Fe - 0.5% Cr alloy, superimposed on the zero current potential, primary passivation potential and rupture potential lines taken from Figure 71.....	202
73	Experimental potential vs. pH diagram for the Fe - 2.0% Cr alloy in 0.1 M Cl ⁻ , H ₂ -saturated solutions.....	203
74	"Protection potential" (E _p) data for the Fe - 2.0% Cr alloy, superimposed on the zero current potential, primary passivation potential and rupture potential lines taken from Figure 73.....	204
75	Experimental potential vs. pH diagram for the Fe - 5.0% Cr alloy in 0.1 M Cl ⁻ , H ₂ -saturated solutions.....	205
76	"Protection potential" (E _p) data for the Fe - 5.0% Cr alloy, superimposed on the zero current potential, primary passivation potential and rupture potential lines taken from Figure 75.....	206
77	Experimental potential vs. pH diagram for the Fe - 12% Cr alloy in 0.1 M, H ₂ -saturated solutions.....	207
78	"Protection potential" (E _p) data for the Fe - 12% Cr alloy, superimposed on the zero current potential, primary passivation potential and rupture potential lines taken from Figure 77.....	208
79	Experimental potential vs. pH diagram for the Fe - 16.9% Cr alloy in 0.1 M Cl ⁻ , H ₂ -saturated solutions.....	209
80	"Protection potential" (E _p) data for the Fe - 16.9% Cr alloy, superimposed on the zero current potential, primary passivation potential and rupture potential lines taken from Figure 79.....	210
81	Experimental potential vs. pH diagram for the Fe - 24.9% Cr alloy in 0.1 M Cl ⁻ , H ₂ -saturated solutions.....	211

LIST OF FIGURES (Continued)

<u>Figure</u>		<u>Page</u>
82	"Protection potential" (E_p) data for the Fe - 24.9% Cr alloy, superimposed on the zero current potential, primary passivation potential and rupture potential lines taken from Figure 81.....	212
83	Out-scan portion of special cyclic potentiokinetic polarization scan for the Fe - 12% Cr alloy in 0.1 M Cl^- , H_2 -saturated solution of pH 3.2.....	229
84	Return-scan portion of special cyclic potentiokinetic polarization scan for the Fe - 12% Cr alloy in 0.1 M Cl^- , H_2 -saturated solution of pH 3.2.....	230
85	Out-scan portion of special cyclic potentiokinetic polarization scan for the Fe - 12% Cr alloy in 0.1 M Cl^- , H_2 -saturated solution of pH 4.4.....	231
86	Return-scan portion of special cyclic potentiokinetic polarization scan for the Fe - 12% Cr alloy in 0.1 M Cl^- , H_2 -saturated solution of pH 4.4.....	232
87	Out-scan portion of special cyclic potentiokinetic polarization scan for the Fe - 12% Cr alloy in 0.1 M Cl^- , H_2 -saturated solution of pH 5.5.....	233
88	Return-scan portion of special cyclic potentiokinetic polarization scan for the Fe - 12% Cr alloy in 0.1 M Cl^- , H_2 -saturated solution of pH 5.5.....	234
89	Out-scan portion of special cyclic potentiokinetic polarization scan for the Fe - 12% Cr alloy in 0.1 M Cl^- , H_2 -saturated solution of pH 7.1.....	235
90	Return-scan portion of special cyclic potentiokinetic polarization scan for the Fe - 12% Cr alloy in 0.1 M Cl^- , H_2 -saturated solution of pH 7.1.....	236
91	Out-scan portion of special cyclic potentiokinetic polarization scan for the Fe - 12% Cr alloy in 0.1 M Cl^- , H_2 -saturated solution of pH 8.9.....	237

LIST OF FIGURES (Continued)

<u>Figure</u>	<u>Page</u>	
92	Return-scan portion of special cyclic potentiokinetic polarization scan for the Fe - 12% Cr alloy in 0.1 M Cl ⁻ , H ₂ -saturated solution of pH 8.9.....	238
93	Out-scan portion of special cyclic potentiokinetic polarization scan for the Fe - 12% Cr alloy in 0.1 M Cl ⁻ , H ₂ -saturated solution of pH 9.7.....	239
94	Return-scan portion of special cyclic potentiokinetic polarization scan for the Fe - 12% Cr alloy in 0.1 M Cl ⁻ , H ₂ -saturated solution of pH 9.7.....	240
95	Out-scan portion of special cyclic potentiokinetic polarization scan for the Fe - 12% Cr alloy in 0.1 M Cl ⁻ , H ₂ -saturated solution of pH 10.9.....	241
96	Return-scan portion of special cyclic potentiokinetic polarization scan for the Fe - 12% Cr alloy in 0.1 M Cl ⁻ , H ₂ -saturated solution of pH 10.9.....	242
97	Out-scan portion of special cyclic potentiokinetic polarization scan for the Fe - 12% Cr alloy in 0.1 M Cl ⁻ , H ₂ -saturated solution of pH 12.0.....	243
98	Return-scan portion of special cyclic potentiokinetic polarization scan for the Fe - 12% Cr alloy in 0.1 M Cl ⁻ , H ₂ -saturated solution of pH 12.0.....	244
99	Out-scan portion of special cyclic potentiokinetic polarization scan for the Fe - 12% Cr alloy in 0.1 M Cl ⁻ , H ₂ -saturated solution of pH 3.2, using painted-off sample approximately 1 cm ² in area.....	246
100	Return-scan portion of special cyclic potentiokinetic polarization scan for the Fe - 12% Cr alloy in 0.1 M Cl ⁻ , H ₂ -saturated solution of pH 3.2, using painted-off sample approximately 1 cm ² in area.....	247

LIST OF FIGURES (Continued)

<u>Figure</u>		<u>Page</u>
101	Out-scan portion of special cyclic potentiokinetic polarization scan for the Fe - 12% Cr alloy in 0.1 M Cl ⁻ , H ₂ -saturated solution of pH 4.4, using painted-off sample approximately 1 cm ² in area.....	248
102	Return-scan portion of special cyclic potentiokinetic polarization scan for the Fe - 12% Cr alloy in 0.1 M Cl ⁻ , H ₂ -saturated solution of pH 4.4, using painted-off sample approximately 1 cm ² in area.....	249
103	Out-scan portion of special cyclic potentiokinetic polarization scan for the Fe - 12% Cr alloy in 0.1 M Cl ⁻ , H ₂ -saturated solution of pH 5.5, using painted-off sample approximately 1 cm ² in area.....	250
104	Return-scan portion of special cyclic potentiokinetic polarization scan for the Fe - 12% Cr alloy in 0.1 M Cl ⁻ , H ₂ -saturated solution of pH 5.5, using painted-off sample approximately 1 cm ² in area.....	251
105	Out-scan portion of special cyclic potentiokinetic polarization scan for the Fe - 12% Cr alloy in 0.1 M Cl ⁻ , H ₂ -saturated solution of pH 7.2, using painted-off sample approximately 1 cm ² in area.....	252
106	Return-scan portion of special cyclic potentiokinetic polarization scan for the Fe - 12% Cr alloy in 0.1 M Cl ⁻ , H ₂ -saturated solution of pH 7.2, using painted-off sample approximately 1 cm ² in area.....	253
107	Out-scan portion of special cyclic potentiokinetic polarization scan for the Fe - 12% Cr alloy in 0.1 M Cl ⁻ , H ₂ -saturated solution of pH 8.9, using painted-off sample approximately 1 cm ² in area.....	254

LIST OF FIGURES (Continued)

<u>Figure</u>		<u>Page</u>
108	Return-scan portion of special cyclic potentiokinetic polarization scan for the Fe - 12% Cr alloy in 0.1 M Cl ⁻ , H ₂ -saturated solution of pH 8.9, using painted-off sample approximately 1 cm ² in area.....	255
109	Out-scan portion of special cyclic potentiokinetic polarization scan for the Fe - 12% Cr alloy in 0.1 M Cl ⁻ , H ₂ -saturated solution of pH 9.7, using painted-off sample approximately 1 cm ² in area.....	256
110	Return-scan portion of special cyclic potentiokinetic polarization scan for the Fe - 12% Cr alloy in 0.1 M Cl ⁻ , H ₂ -saturated solution of pH 9.7, using painted-off sample approximately 1 cm ² in area.....	257
111	Out-scan portion of special cyclic potentiokinetic polarization scan for the Fe - 12% Cr alloy in 0.1 M Cl ⁻ , H ₂ -saturated solution of pH 10.9, using painted-off sample approximately 1 cm ² in area.....	258
112	Return-scan portion of special cyclic potentiokinetic polarization scan for the Fe - 12% Cr alloy in 0.1 M Cl ⁻ , H ₂ -saturated solution of pH 10.9, using painted-off sample approximately 1 cm ² in area.....	259
113	Out-scan portion of special cyclic potentiokinetic polarization scan for the Fe - 12% Cr alloy in 0.1 M Cl ⁻ , H ₂ -saturated solution of pH 12.0, using painted-off sample approximately 1 cm ² in area.....	260
114	Return-scan portion of special cyclic potentiokinetic polarization scan for the Fe - 12% Cr alloy in 0.1 M Cl ⁻ , H ₂ -saturated solution of pH 12.0, using painted-off sample approximately 1 cm ² in area.....	261
115	Potential vs. log chloride ion molarity diagram for the Fe - 0.5% Cr alloy in H ₂ -saturated solutions of pH 5.5.....	263

LIST OF FIGURES (Continued)

<u>Figure</u>		<u>Page</u>
116	"Protection potential" (E_p) data, superimposed on the zero current potential, primary passivation potential and rupture potential lines taken from Figure 115.....	264
117	Potential vs. log chloride ion molarity diagram for the Fe - 0.5% Cr alloy in H_2 -saturated solutions of pH 8.7.....	265
118	"Protection potential" (E_p) data, superimposed on the zero current potential, primary passivation potential and rupture potential lines taken from Figure 117.....	266
119	Potential vs. log chloride ion molarity diagram for the Fe - 0.5% Cr alloy in H_2 -saturated solutions of pH 10.8.....	267
120	"Protection potential" (E_p) data, superimposed on the zero current potential, primary passivation potential and rupture potential lines taken from Figure 119.....	268
121	Potential vs. log chloride ion molarity diagram for the Fe - 2.0% Cr alloy in H_2 -saturated solutions of pH 5.5.....	269
122	"Protection potential" (E_p) data, superimposed on the zero current potential, primary passivation potential and rupture potential lines taken from Figure 121.....	270
123	Potential vs. log chloride ion molarity diagram for the Fe - 2.0% Cr alloy in H_2 -saturated solutions of pH 8.7.....	271
124	"Protection potential" (E_p) data, superimposed on the zero current potential, primary passivation potential and rupture potential lines taken from Figure 123.....	272
125	Potential vs. log chloride ion molarity diagram for the Fe - 2.0% Cr alloy in H_2 -saturated solutions of pH 11.0.....	273

LIST OF FIGURES (Continued)

<u>Figure</u>		<u>Page</u>
126	"Protection potential" (E_p) data, superimposed on the zero current potential, primary passivation potential and rupture potential lines taken from Figure 125.....	274
127	Potential vs. log chloride ion molarity diagram for the Fe - 12% Cr alloy in H_2 -saturated solutions of pH 5.4.....	275
128	"Protection potential" (E_p) data, superimposed on the zero current potential, primary passivation potential and rupture potential lines taken from Figure 127.....	276
129	Potential vs. log chloride ion molarity diagram for the Fe - 12% Cr alloy in H_2 -saturated solutions of pH 8.8.....	277
130	"Protection potential" (E_p) data, superimposed on the zero current potential, primary passivation potential and rupture potential lines taken from Figure 129.....	278
131	Potential vs. log chloride ion molarity diagram for the Fe - 12% Cr alloy in H_2 -saturated solutions of pH 10.8.....	279
132	"Protection potential" (E_p) data, superimposed on the zero current potential, primary passivation potential and rupture potential lines taken from Figure 131.....	280
133	Potential vs. log chloride ion molarity diagram for the Fe - 16.9% Cr alloy in H_2 -saturated solutions of pH 5.4.....	281
134	"Protection potential" (E_p) data, superimposed on the zero current potential, primary passivation potential and rupture potential lines taken from Figure 133.....	282
135	Potential vs. log chloride ion molarity diagram for the Fe - 16.9% Cr alloy in H_2 -saturated solutions of pH 8.8.....	283

LIST OF FIGURES (Continued)

<u>Figure</u>	<u>Page</u>
136 "Protection potential" (E_p) data, superimposed on the zero current potential, primary passivation potential and rupture potential lines taken from Figure 135.....	284
137 Potential vs. log chloride ion molarity diagram for the Fe - 16.9% Cr alloy in H_2 -saturated solutions of pH 10.8.....	285
138 "Protection potential" (E_p) data, superimposed on the zero current potential, primary passivation potential and rupture potential lines taken from Figure 137.....	286
139 Calculated equilibrium potential vs. pH (Pourbaix) diagram for the Fe- H_2O system. The activities of all dissolved species were taken to be 10^{-6}	317
140 Calculated equilibrium potential vs. pH (Pourbaix) diagram for the Fe- Cl^- - H_2O system. The activity of Cl^- was taken to be 0.1 and the activities of all other dissolved species were taken to be 10^{-6} ...	318
141 Specially calculated equilibrium potential vs. pH (Pourbaix) diagram for the Fe- Cl^- - H_2O system. The activity of Cl^- was taken to be 0.373 and the activities of all other dissolved species were taken to be 0.156.....	319
142 Calculated equilibrium potential vs. pH (Pourbaix) diagram for the Cr- H_2O system. The activities of all dissolved species were taken to be 10^{-6}	320
143 Calculated equilibrium potential vs. pH (Pourbaix) diagram for the Cr- Cl^- - H_2O system. The activity of Cl^- was taken to be 0.1 and the activities of all other dissolved species were taken to be 10^{-6} ..	321
144 Specially calculated equilibrium potential vs. pH (Pourbaix) diagram for the Cr- Cl^- - H_2O system. The activity of Cl^- was taken to be 0.373 and the activities of all other dissolved species were taken to be 0.02.....	322

Abstract of Dissertation Presented to the
Graduate Council of the University of Florida in Partial Fulfillment
of the Requirements for the Degree of Doctor of Philosophy

THE SIGNIFICANCE OF THE "PROTECTION POTENTIAL"
FOR Fe-Cr ALLOYS AT ROOM TEMPERATURE

By

Kenneth Kirch Starr

March, 1973

Chairman: Dr. Ellis D. Verink, Jr.
Major Department: Materials Science and Engineering

The significance of the "protection potential," a potential below which active pits cease to propagate (a critical potential for pit propagation), was investigated using electrochemical hysteresis (cyclic potentiokinetic polarization), artificial occluded cell, atomic absorption analysis and wet chemical analysis techniques.

The effects of certain material, environmental and experimental variables on the "protection potential" were studied: alloy composition, pH, chloride ion concentration and extent of propagation. Results from artificial occluded cells were compared with thermodynamic calculations. Preliminary studies of the passive-active behavior of certain Fe-Cr alloys in the presence of metal chloride solutions were undertaken.

The "protection potential" appeared to be influenced by both alloy composition and environment. Both "repassivation" and "deactivation" mechanisms appeared to be operative for the Fe-Cr

alloys, depending upon the particular alloy/environment system. Evidence was obtained which suggested that an active occluded cell of at least one alloy (Fe - 12% Cr) could propagate to an extent precluding any possibility of a "repassivation" mechanism unless there was dilution of the contents of the occluded cell. Hydrolysis calculations indicated that the CrOH^{++} complex ion may be one of the hydrolysis products primarily responsible for localized acidification of active occluded cells of Fe-Cr alloys.

CHAPTER 1

INTRODUCTION

The great utility of stainless steel alloys is common knowledge. There are many commercially available stainless steel alloys, each designed to have the mechanical properties and corrosion resistance necessary for particular applications. Table 1 lists the nominal compositions of a number of these alloys.

The martensitic chromium steels, Group I, can be hardened by heat treatment. The ferritic steels, Group II, cannot be hardened by heat treatment but possess better corrosion resistance. Groups I and II are basically Fe-Cr alloys.

The austenitic stainless steels, Group III, are basically Fe-Cr-Ni alloys, with a few notable exceptions. These alloys also cannot be hardened by heat treatment but possess better corrosion resistance than either Group I or II.

The age-hardenable steels, Group IV, possess both reasonably good corrosion resistance and the ability to be hardened by heat treatment.

The alloys studied in this investigation are Fe-Cr alloys of 0.5% Cr, 2.0% Cr, 5.0% Cr, 12% Cr, 16.9% Cr and 24.9% Cr. The 0.5% Cr, 2.0% Cr and 5.0% Cr alloys are called chromium steels. The 12% Cr alloy is a martensitic stainless steel, and the 16.9% Cr and 24.9% Cr alloys are ferritic stainless steels. The detailed compositions and characterization of these alloys are given in Appendix 1.

Fe-Cr and stainless steel alloys may suffer pitting and/or

TABLE 1

CHEMICAL COMPOSITIONS OF COMMERCIAL STAINLESS STEELS [1, p. 164]

AISI type	% C	% Cr	% Ni	% Other Elements
Group I: Martensitic Cr Steels				
410	0.15 max	11.5-13.5	-	-
416	0.15 max	12-14	-	Se, Mo, or Zr
420	0.35-0.45	12-14	-	-
431	0.2 max	15-17	1.25-2.5	-
440A	0.60-0.75	16-18	-	-
Group II: Ferritic Nonhardenable Steels				
405	0.08 max	11.5-14.5	0.5 max	0.1-0.3 Al
430	0.12 max	14-18	0.5 max	-
442	0.25 max	18-23	0.5 max	-
446	0.20 max	23-27	0.5 max	0.25 N max
Group III: Austenitic Cr-Ni Steels				
201	0.15 max	16-18	3.5-5.5	5.0-7.5 Mn 0.25 N max
302	0.15 max	17-19	4-6	7.5-10 Mn 0.25 N max
301	0.15 max	16-18	6-8	2 Mn max
302	0.15 max	17-19	8-10	2 Mn max
302B	0.15 max	17-19	8-10	2-3 Si
304	0.08 max	18-20	8-12	1 Si max
304L	0.03 max	18-20	8-12	1 Si max
308	0.08 max	19-21	10-12	1 Si max
309	0.2 max	22-24	12-15	1 Si max
309S	0.08 max	22-24	12-15	1 Si max
310	0.25 max	24-26	19-22	1.5 Si max
310S	0.08 max	24-26	19-22	1.5 Si max

TABLE 1 (Continued)

AISI type	% C	% Cr	% Ni	% Other Elements
314	0.25 max	23-26	19-22	1.5-3.0 Si
316	0.10 max	16-18	10-14	2-3 Mo
316L	0.03 max	16-18	10-14	2-3 Mo
317	0.08 max	18-20	11-14	3-4 Mo
321	0.08 max	17-19	8-11	Ti 4 x C (min)
347	0.08 max	17-19	9-13	Cb + Ta 10 x C (min)
Alloy 20	0.07 max	29	20	3.25 Cu, 2.25 Mo
Group IV: Age-Hardenable Steels				
322	0.07	17	7	0.07 Ti, 0.2 Al
17-7PH	0.07	17	7	1.0 Al
17-4PH	0.05	16.5	4.25	4.0 Cu
A-8MoPH	0.05 max	14	8.5	2.5 Mo, 1 Al
AM350	0.10	16.5	4.3	2.75 Mo
CD4MCu	0.03	25	5	3.0 Cu, 2.0 Mo

crevice corrosion in particular environments such as sea water. Interest has arisen in the possibility of protecting these alloys against localized attack by altering or controlling their electrode potentials. The Fe-Cr alloys are of special interest for three reasons:

1. they contain only one basic alloying element and thus have only one basic composition variable,
2. the martensitic grades can be hardened by heat treatment and
3. they are the least expensive of the stainless steels.

The "protection potential," a potential below (more active than) which active pits cease to propagate (i.e., a critical potential for pit propagation), has been the subject of considerable debate among corrosion experts in recent years.

The purpose of this research was to characterize the material, environmental and experimental aspects of the "protection potential," and to distinguish between the possibilities of "repassivation" and "deactivation" mechanisms.

The approach has been to study the effects of alloy composition, bulk electrolyte pH, bulk electrolyte chloride ion concentration and extent of propagation on the "protection potential." Results from artificial occluded cells were compared with thermodynamic calculations. These results primarily concern the "repassivation" vs. "deactivation" question. In addition, preliminary work was carried out involving the passive-active behavior of alloys exposed to artificial pit or crevice solutions.

CHAPTER 2
LITERATURE SURVEY

Two phrases need to be clarified: "protection potential" and "occluded cell." The phrase "occluded corrosion cell" was used by B. F. Brown [2] to tie together in a general way a number of forms of localized corrosion. These included crevice corrosion, pitting, stress corrosion cracking, turberculation, intergranular corrosion, filiform corrosion and exfoliation. Brown concluded that the unifying feature of these different forms of corrosion was localized acidification by hydrolysis and that this localized acidification was largely responsible for their self-perpetuating character.

In this study, an occluded cell will be considered to be an electrochemical system involving a solid metallic electrode in contact with an electrolyte of restricted volume. The restriction may result from any combination of the following conditions:

1. limited total quantity of electrolyte,
2. confining geometry of cell [2],
3. presence of corrosion product [2],
4. stagnation.

The phrase "protection potential" was used by M. Pourbaix and coworkers [3] in reference to the experimental observation that, for stainless steels in chloride solutions, the propagation of active pits could be stopped by making the sample potential more negative (active) than a critical value. This critical potential was considered to be the "protection potential" against pitting.

This survey will be focused on the discussion of crevice corrosion and pitting of stainless steel alloys, although mention will be made of stress corrosion cracking and other types of occluded cell corrosion. Emphasis will be placed on the significance of the "protection potential" concept with respect to crevice corrosion and pitting.

Some of the terms used are defined as follows:

1. Corrosion - The deterioration of a substance, usually a metal, because of a reaction with its environment.
2. Passivation - The process or processes by means of which a metal becomes inert to a given environment or environments.
3. Crevice Corrosion - Localized corrosion as a result of the formation of a crevice between a metal and a nonmetal, or between two metal surfaces.
4. Pitting - Localized corrosion taking the form of cavities at the surface.
5. Stress Corrosion Cracking - Spontaneous cracking produced by the combined action of corrosion and static stress (residual or applied). [4, pp. 267t-268t)

2.1 Methods of Investigation

Experimental techniques which have been employed in the study of crevice corrosion and pitting phenomena include immersion tests, galvanostatic polarization techniques, potentiostatic polarization techniques, potentiokinetic polarization techniques, the use of artificial occluded cells, indicator techniques, autoradiography, chemical analysis, X-ray analysis, electron probe microanalysis, optical microscopy, electron microscopy and scanning electron microscopy.

Greene and Fontana [5] discussed advantages and disadvantages

of a number of these techniques. The first four techniques listed will be briefly described here. Other methods of investigation will be described later.

2.1.1 Immersion Tests

Immersion tests involve the placing of a sample or samples within a suitable environment. The environment may consist of any combination of gaseous, liquid or solid phases. Atmospheric exposure is an important type of immersion test involving gaseous, liquid and solid phases. Frequently, immersion tests involve samples totally immersed in liquid electrolytes at ambient temperatures. Dissolved gases and solid objects may also be present.

Information obtained may result from visual observations, metallographic examinations, weight-loss measurements and potential measurements. Such potentials are "free-corrosion" or "mixed" potentials [6, 7]. They are determined only by the metal-environment system.

In the case of stainless steel alloys, there exists an ASTM Standard Method for total immersion corrosion tests, ASTM Designation: A279-63 [8]. This standard discusses general considerations, leaving specifics to the individual investigator.

2.1.2 Galvanostatic Tests

"Galvanostatic" implies a technique of applying a constant current to a sample immersed in an electrolyte [9]. Current is the independent variable and usually potential is the dependent variable. Visual observations may also be made.

In normal practice the current is varied, either stepwise or continuously (galvanokinetically), and the potential is monitored. Brenner [10] employed such a technique to measure his "break-through" potentials, denoting the initiation of pitting of stainless steel samples.

2.1.3 Potentiostatic Tests

"Potentiostatic" implies the potential of an electrode being held constant during some experimental procedure, such as measuring the current over a time interval [9]. Potential is the independent variable and usually current is the dependent variable. Visual observations may be made and weight-loss data may be obtained.

In normal practice the potential is varied in a stepwise manner and the current is monitored. A brief review concerning "the classical potentiostat" and some simplified circuitry was given by Greene [11]. He also showed that such an instrument was particularly useful in the study of passivity.

2.1.4 Potentiokinetic Tests

"Potentiokinetic" (also "potentiodynamic") implies a technique of varying the potential of an electrode in a continuous manner at a preset rate, frequently used to prepare polarization plots [9]. Potential is the independent variable and usually current is the dependent variable.

The rate of potential scan (scan rate) may be a significant variable [12, 13]. ASTM Standard Number G5-69 [14] presents a

reference method for conducting both potentiostatic and potentiokinetic anodic polarization measurements. Greene [15] has given a detailed treatment of experimental aspects of electrode kinetics.

2.2 Passivity

Fontana and Greene stated that

...the nature of the passive film, and consequently the basic nature of passivity, still remains an unsolved problem. [1, p. 321]

However, the fact that many passivable metals are particularly susceptible to pitting [16, 17, 18] and/or crevice corrosion [19] under particular conditions makes it imperative that some thought be given to the passivation process itself.

Today there are two basic theories of passivity. The first theory, sometimes referred to as the "oxide-film theory," holds that passivity is due to a diffusion barrier of reaction products. These reaction products are usually considered to be oxides of some sort, although they may not necessarily correspond to bulk oxides [20, 21, 22, 23, 24].

The second theory attributes passivity to the chemical adsorption of atoms, ions, or molecules on the surface of a metal. The adsorbed layer may be only a monolayer thick and probably contains chemically adsorbed oxygen ions and/or hydroxide ions in many cases [20, 22, 23].

Tomashov and Chernova [22] attributed the first description of passivity in metals to Lomonosov in 1738. Tomashov and Chernova [22] and Uhlig and Wulff [25] attributed the original "oxide-film

theory" to Faraday in 1836.

Uhlig [26], in a paper tying together the concepts of chemisorption and the "adsorption theory" of passivity, attributed the original suggestion to Langmuir in 1916. Uhlig and Wulff [25] developed a theoretical basis for the "adsorption theory" of passivity in alloys according to an electron-sharing scheme.

It appears that the "adsorption theory" of passivity, in its strictest sense, is presently being abandoned or modified [18].

However, Tomashov and Chernova have stated that:

It must be pointed out that the oxide-film and adsorption theories do not contradict, but rather supplement one another. As the adsorbed film in the process of thickening gradually passes into an oxide film, the retardation of the anodic process promoted by change in the double-layer structure will also be supplemented by the greater difficulty encountered by ions passing directly through the protective film. Thus, one may speak of a combined oxide-film-adsorption theory of passivity. [22, p. 13]

Figure 1 shows schematic apparent anodic and cathodic polarization curves for a passive metal in an aqueous electrolyte containing aggressive anions, representing steady-state conditions. More will be said later about "aggressive anions." The plot in Figure 1 is according to the conventions outlined in ASTM Standard Designation G3-68 [9], with slight modifications [27]. The critical points on that curve may be defined as follows:

1. E_{corr} - corrosion potential - The potential of a corroding electrode in a stated environment. Often used to mean the open circuit (also called "steady state," freely corroding or "rest") potential in an electrochemical cell; that is, the potential without any external current flowing. [9, pp. 546-548]

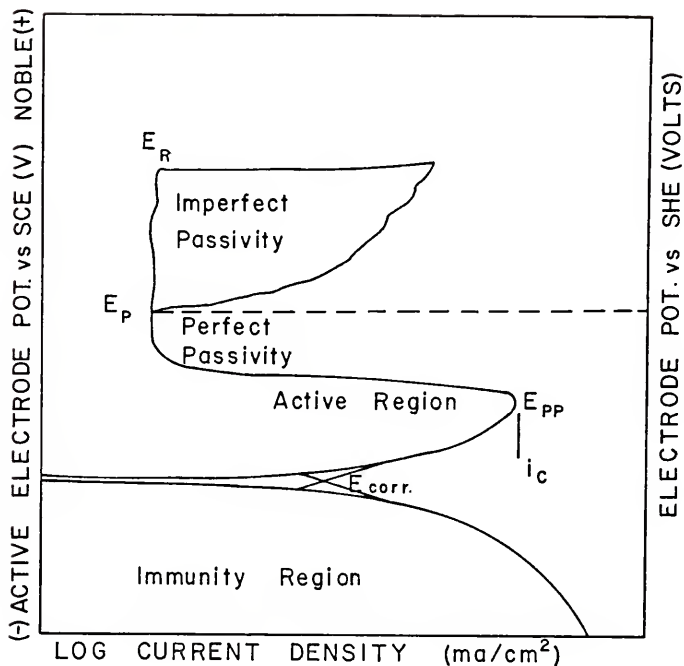


Figure 1. Hypothetical cathodic and anodic polarization plots for a passive metallic electrode [9, 27].

2. E_{pp} - primary passive potential - The potential corresponding to the maximum active current density in an electrode which exhibits active-passive corrosion behavior. [Also called primary passivation potential.] [9, pp. 546-548]
3. i_c - critical anodic current density - The maximum anodic current density observed in the active region with a metal or alloy electrode which exhibits active-passive behavior in the environment studied. [9, pp. 546-548]
4. E_R - rupture potential - The potential above which the passivating film becomes locally non-protective leading to pitting. [Also called "breakthrough potential," pitting potential, critical pitting potential or critical potential for pit initiation.] [27, p. 431]

5. E_p - protection potential - The potential below which formed pits will not grow and thus become harmless. [Also called critical potential for pit propagation (or growth).] [27, p. 431]

2.3 Aggressive Anions

The terms "aggressive anions" and "unaggressive anions" are misleading if taken too literally, but are useful for general classification. Kolotyrkin [17] used the former term with reference to specifically acting anions, particular Cl^- , Br^- or I^- . He used the latter term with reference to SO_4^{--} , ClO_3^- , CO_3^{--} , NO_3^- and CrO_4^{--} , with ClO_4^- falling into both categories.

Borgmann [28] found that the initial corrosion rates of iron in salt solutions were similar for chloride, iodide and sulfate solutions. Foley [29] reviewed the literature on the role of the chloride ion in the corrosion of iron. Although there was no general agreement in the literature, it appeared that many ions could be either aggressive or inhibitive, depending upon their concentrations [30]. The situation was even more complicated for solutions containing two or more anions (other than OH^-).

Leckie and Uhlig [31] studied the effects of additions of SO_4^{--} , ClO_4^- , OH^- and NO_3^- to chloride solutions on pitting of an 18% Cr - 8% Ni stainless steel. They found, for each anion, a critical activity ratio of anion to chloride ion necessary to inhibit pitting corrosion.

It becomes clear that the aggressiveness of any particular anion depends upon several factors, including the nature of the

metal, whether or not it is passivated, the concentration of the anion, and the presence and concentration of other anions.

Greene and Fontana [5] noted, however, that the halides and halogen-containing anions were almost always associated with the pitting of metals. In particular, chlorides, bromides and hypochlorites were usually the most aggressive of the halogen-containing anions. It is in this context that the term "aggressive anion" will be used in this discussion.

2.4 Pitting Corrosion

Reviews of the literature of pitting corrosion have been published by Greene and Fontana [5], Kolotyrkin [17], and Szklarska-Smialowska [32]. It has been found meaningful and convenient to divide pitting into two steps [33, 34, 5, 32]: pit initiation or surface breakdown and pit growth in depth and volume [34], or more simply, initiation and propagation [33]. Any complete theory of pitting must take both steps into account in a consistent manner.

Szklarska-Smialowska [32] expressed the opinion that none of the existing theories was completely successful. A brief look will be taken at some of the theories concerning pit initiation and a more thorough look taken at the theories and experiments concerning pit growth.

Any theory of pit initiation must apply to at least one theory of passivity. In fact, the two basic theories of passivation have attendant theories of pit initiation. Aggressive anions, usually halide ions, will be assumed present in the electrolytes.

2.4.1 Pit Initiation

2.4.1.1 Breakdown of passivity: adsorption theory

According to the adsorption theory, chloride ions [35, 5, 20, 32] or other aggressive anions [17] competitively or preferentially adsorb on a passive metal surface, displacing oxygen [35, 5, 17, 20, 32] or hydroxide ions [20]. Substitution of adsorbed oxygen by chloride ions has also been suggested [36]. Pitting is then assumed to initiate at sites or areas where the passivating species has been successfully displaced or replaced by aggressive anions.

2.4.1.2 Breakdown of passivity: oxide-film theory

Numerous theories of the breakdown of passive oxide films have been proposed. Since these theories are well described in the previously mentioned review articles on pitting corrosion [5, 17, 18], only a few of the more important historical and current theories will be mentioned here.

The penetration theory was suggested by Evans [37] in 1927. According to this theory, the small diameter of the chloride ion allowed it to penetrate the protective oxide layer on passive iron.

The acid theory was proposed by Hoar [38] in 1947. According to Hoar, who then assumed the passive oxide film on iron to be $\text{Fe}(\text{OH})_2$, transference of chloride ions to the anode surface allowed the electrolyte next to the anode to become acidified. Eventually this localized acidification led to destruction and undermining of the passive film. In a later work Hoar [39] assumed the existence of incipient cracks or pores in the passive oxide film.

Thermodynamic theories of pit initiation have been given in the literature [40, 41, 42]. These theories suggest that at some critical anodic potential, conversion of a protective oxide film into a nonprotective phase (such as a metal chloride) becomes energetically possible. Unfortunately, the thermodynamic theories offer only a qualitative description of the pit initiation process.

2.4.1.3 Breakdown of passivity: combined theory

Assuming a modern combined theory of passivation to be operative, Hoar and Jacob [43] proposed a plausible mechanism for the breakdown of passivity of stainless steels by halide ions. Their theory proceeded as follows:

Three or four halide ions jointly "adsorb" on the oxide film surface around a lattice cation--one next to a surface anion for preference. The transitional complex thus formed will be of high energy and the probability of its formation at any instant will be very small. But, once formed, the complex can readily and immediately separate from the oxide ions in the lattice, the cation dissolving in the solution, very much more readily than the non- or aquo-complexed cations present in the film surface in the absence of halide ion. Under the anodic field, a further cation comes up through the film to replace the dissolved cation--the field at constant anode potential increases at the "thinned" point of the film; but arriving at the film/solution interface, it finds, not stabilizing oxide ion formed from water (nor, in de-aerated solution, oxygen molecules), but several halide ions, so that the catalytic process, once begun, has a strong probability of repeating itself, and of accelerating because of the increasing electrostatic field. Thus, once localized breakdown starts with the initial transitional complex, it accelerates "explosively." [43, p. 1300]

However, for the case of iron, Hoar suggested that

...a process of migration through the passivating film of one chloride ion at a time may determine the breakdown rate. [18, p. 20C]

One apparent weakness of the existing theories of the breakdown of passive films by aggressive anions is that they are unable to predict or even explain observed experimental values of critical pitting potentials.

Some of the experimental methods available for studying the breakdown of passive films by aggressive anions will now be discussed.

2.4.1.4 Passive film breakdown parameters

Reinoehl and Beck [44] noted that for an active metal to become passive there existed a number of critical parameters, including a critical concentration of oxidizing agent, a critical potential, a critical anodic current density, a critical temperature, a critical pressure and a critical pH. It seems reasonable that many of these parameters should also be important in the breakdown of passivity. In pitting, an additional parameter is a critical concentration of aggressive anion [45, 40].

The critical parameters most often used in experimental studies of pit initiation are potential, pH, and aggressive anion concentration (usually chloride ion concentration). Oxidizing agents (particularly oxidizing metal chlorides) have been used to promote pitting of passive metals [46, 47, 34], but as a first approximation the action of oxidizing agents should be describable in terms of potential, pH, and aggressive anion concentration.

Uhlig [46] proposed that only solutions capable of forming sufficiently noble oxidation-reduction potentials would cause pitting of stainless steels. Kolotyrkin later suggested a general rule:

At present, the following general rule can possibly be formulated: a metal is subject to pitting corrosion only if the redox potential of the solution containing aggressive anions lies at values more positive than V_c [critical pitting potential]. In other words, the redox system can stimulate the development of pits only on those metals for which the V_c lies at more negative values than the redox potential of the system. [17, p. 263t]

Streicher [34] found that the pitting intensity of Type 304 stainless steel at 25°C in nine different chloride salts was largely a function of the pH of the solutions (due to hydrolysis). Oxidizing agents may also affect pitting by contributing an aggressive anion to the electrolyte. The concentration of that particular anion would depend upon the concentration of the oxidizing salt.

Szklarska-Smialowska [32] noted that no systematic work had been done on temperature effects in pitting. The work that had been done indicated a greater tendency for pitting at higher temperatures [3, 32]. Little or no work has been done on pressure effects.

2.4.1.5 Critical pitting potentials

Electrical stimulation of pit initiation may be accomplished galvanostatically, galvanokinetically (continuously increasing applied current), potentiostatically, potentiokinetically or with simple applied voltages.

Uhlig and Wulff [25] used a battery and slide wire resistances to apply a voltage across a cell consisting of a stainless steel anode and a silver-silver chloride cathode. As long as the anode remained passive and little current flowed, the silver-silver chloride electrode should not have been appreciably polarized. Under those

conditions the anode potential would have been nearly equal to the applied potential and the apparatus should have operated as a potentiostat. However, the relatively large currents associated with pitting would have polarized the silver-silver chloride cathode and potential control would then have become uncertain.

Uhlig and Wulff [25] noted that Donker and Dengg had used a similar apparatus to make film breakdown measurements on iron in 1927. The procedure was to increase the applied voltage (equal to the potential) until a large increase in current was measured by an ammeter, corresponding to the initiation of pitting. The applied potentials at the moment of film rupture were called "threshold potentials."

In 1937, just prior to the work of Uhlig and Wulff, Brennert [10] had developed a slightly different method of evaluating the pitting resistance of stainless steels. Brennert used an auxiliary cathode and a reference electrode instead of a combined cathode-reference electrode. He applied an increasing voltage between the anode and auxiliary cathode until the passive film ruptured, at that point measuring his "breakthrough potentials."

Mahla and Nielsen [48] used a similar apparatus to study the effects of prepassivation and inhibitors. Streicher [34] also used a similar apparatus in his studies of pit initiation. Streicher, however, maintained a breakthrough voltage for a fixed time and used the resulting density of pits as a measure of pit initiation resistance.

Pourbaix et al. [49, 3] employed a potentiokinetic method to determine "breakdown" and "protective tensions" for AISI Types 410, 304, and 316 stainless steels in bicarbonate solutions at temperatures of 20°, 40° and 80°C. Such terms as "breakthrough potential," "threshold

potential," and "breakdown potential" are somewhat confusing. In addition, the terms "critical pitting potential" and "critical potential for pit initiation" have been used in the literature. All of these potentials are related to the rupture potential. Szklarska-Smialowska and Janik-Czachor [50] presented a critical analysis of the experimental methods available for the determination of characteristic potentials of pitting corrosion. Bond [51] has also reviewed testing methods for pitting corrosion and their interpretation.

2.4.1.6 Critical chloride ion concentrations

Some early work to determine the critical minimum chloride ion concentration necessary for the initiation of pitting was published by Fenwick [45] in 1935, describing an "electrometric titration" method. This method involved the titration of a standard chloride solution into an electrolyte containing a carbon steel or stainless steel sample and a bridge tube leading to a silver-silver chloride reference electrode.

Usually, a sudden change in the electrode potential of up to one volt occurred at some critical chloride ion concentration. Fenwick took this critical concentration to be a measure of the relative resistance to corrosion (pitting) of a ferrous alloy in the passive state.

Pourbaix et al. [52, 3] used a modification of this technique for a similar purpose. Their method consisted of a continuous chloride titration, under potentiostatic conditions, while monitoring the applied current. A sharp increase of applied current was noted at

a critical value of chloride ion concentration. The anode material in this case was an AISI Type 304 stainless steel rod.

Nobe and Tobias [53] used a similar technique as part of their study of the effects of chloride ions on the potentiostatic anodic polarization of iron.

Pourbaix et al. [52, 3] used rupture potentials, determined potentiokinetically for stainless steels in solutions of known chloride ion concentrations, to study the effect of chloride ion concentration on the initiation of pitting.

Leckie and Uhlig [31] used a potentiostatic method for studies of an 18% Cr - 8% Ni stainless steel. Verink [54] employed a potentiokinetic method to study the effect of chloride ion concentration on rupture potentials for a series of binary Fe-Cr alloys.

The results of the studies mentioned indicate that the breakdown of passivity is strongly influenced by the chloride ion concentration in solution. Higher chloride ion concentrations result in lower rupture potentials and an increased tendency for the initiation of pitting corrosion.

2.4.1.7 Effect of pH

Szklarska-Smialowska [32] indicated that most of the recent literature suggested the rupture potential to be rather insensitive to pH. Streicher [34] found pitting intensity of Type 304 stainless steel to decrease with increasing pH. Pourbaix et al. [3] found the addition of NaHCO_3 to chloride solutions (thus buffering the pH at around 8.3) to raise the rupture potential as much as several hundred millivolts.

Leckie and Uhlig [31] noted a small increase in the critical pitting potential with pH (18% Cr - 8% Ni stainless steel in 0.1 N NaCl) up to a pH of about 8, where a large increase occurred. Pourbaix [27] presented experimental potential vs. pH diagrams for iron and stainless steels showing a considerable increase (as much as several hundred millivolts) in the rupture potential with pH, depending upon the chloride ion concentration.

Verink [54] and Cusumano [55] found both dependent and relatively independent behavior for a series of binary Fe-Cr alloys, depending upon the particular alloy.

Both Pourbaix's [27] and Cusumano's [55] work indicated that at some critical pH value the primary passivation and rupture potentials should become equal, and that below this pH value passivation should not occur at all.

Leckie [13] determined critical pitting potentials for Type 304 stainless steel as a function of pH in 0.01 M, 0.1 M, and 1.0 M NaCl. His values were nearly constant up to a pH of 10 to 12, depending on chloride concentration, where a marked shift to more noble potentials occurred.

2.4.1.8 Effect of alloy composition

A wide variation in rupture potentials has been found between different metals and/or alloys. Hoar [18] cited a few typical examples for a given electrolyte ranging from a few tenths of a volt to approximately thirty volts.

Kolotyrkin [17] studied the effect of Cr in Fe-Cr alloys and

Ni in Fe-Ni alloys on the critical pitting potential (0.1 N chloride solutions of pH \sim 2). An abrupt increase (more noble) was observed at 28-30% Cr for the Fe-Cr alloys. Steigerwald [56] also found 28-30% Cr to be critical for stabilizing the passive state in both ferric chloride and 0.1 N NaCl solutions.

2.4.1.9 Induction periods

Induction periods for the initiation of pitting corrosion have been noted in the literature [57, 40, 58, 59, 43, 60, 32]. Engell and Stolica [40] found the induction time and the chloride ion concentration to be inversely proportional for carbon steels. This relationship was confirmed for stainless steel samples by Schwenk [58].

Hoar and Jacob [43], however, found $1/T$ for an 18% Cr - 8% Ni stainless steel in chloride solutions (T = induction time) to be proportional to the n th power of the chloride ion concentration, where $2.5 < n < 4.5$. For bromide solutions the exponent was between 4 and 4.5. The authors calculated an apparent energy of activation of 60 kcal/mole. They used this information as a basis for their theory of the breakdown of passivity, cited in Section 2.4.1.3.

It has also been established that the induction time depends upon potential [59, 43] and temperature [43]. In general, it appears that the induction time decreases with increasing potential, temperature or chloride ion concentration.

2.4.2 Propagation of Pitting

The second stage of pitting, propagation, contains several important aspects: the geometry of pitting (the size, shape, structure,

and distribution of pits); the current distribution in and around pits; the potential distribution and resistance effects in and around pits; the electrolyte composition within pits; mass transport and diffusion in pits; and stability and reversibility considerations in pitting corrosion.

2.4.2.1 Geometry of pitting

Champion [61] characterized the possibilities of variations in intensity and distribution of metallic corrosion. He suggested a scheme of classification ranging from general corrosion to cracking and graduations in pit number and size. The tools of investigation were visual observation, optical microscopy and radiography. More recently, transmission electron microscopy [62] and scanning electron microscopy [63, 64] have been used to study pit morphology.

Szklarska-Smialowska [32] reviewed the recent literature on the subject of pit morphology. Her conclusion was that the shape of a pit depended on both the environmental conditions within the pit and the composition, properties and structure of the particular metal.

Schwenk [58] found that at low potentials and current densities regularly etched pits (mostly hexagons and squares) were sometimes formed. High potentials and current densities lead to isotropic (hemispherical) pits. Schwenk noted that these conditions were similar to those present in electrolytic polishing, although the pit areas might look either dull or polished.

Hoar [65] proposed a schematic diagram of potential vs. anion/water concentration ratio, shown in Figure 2, on which he

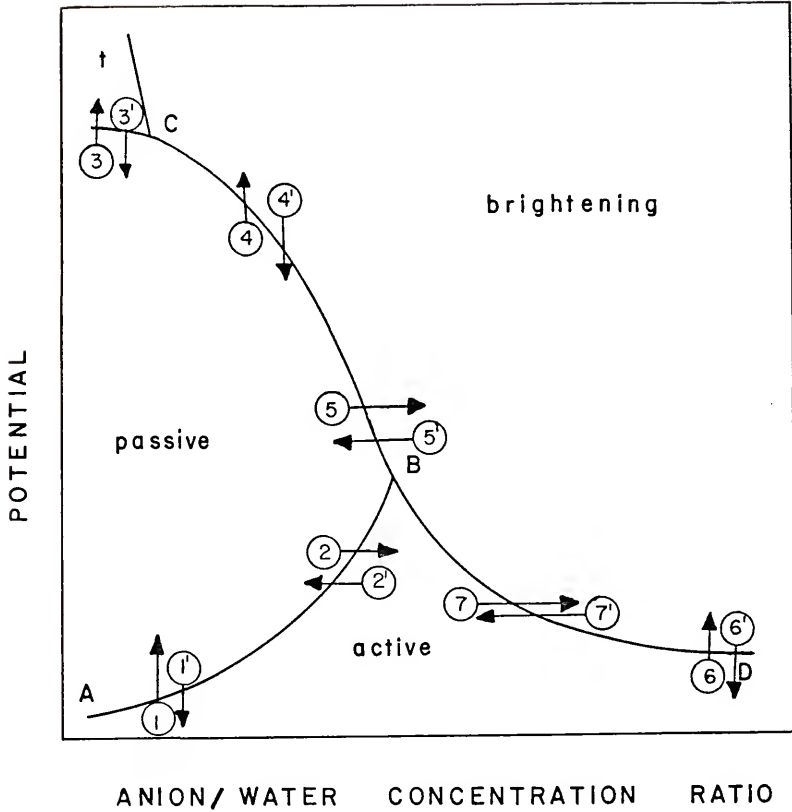


Figure 2. Proposed potential vs. concentration ratio plot for an active-passive metal showing regions of active dissolution (and etching), passivity, brightening and transpassivity. Seven possible kinds of reactions are indicated by numbers [65, p. 354].

delineated areas of active dissolution (and etching), passivity, brightening and transpassivity.

In addition to pit shape, pit size and distribution can be important. Agar and Hoar [66] noted that the e.m.f. of an active cell had to overcome electrolyte resistance, electrode polarization and external circuit resistance. Thus, very large cells (referring to current path distance) are frequently limited by electrolyte resistance and very small cells are often limited by electrode polarization.

Waber [67] treated the problem similarly, but in more depth. He referred to the above-mentioned limiting cases as "macroscopic" and "microscopic" cells. For coplanar electrodes, Waber found the potential of the "composite electrode" (the potential measured at large enough distances to be a negligible function of position) to be proportional to the anode area fraction.

Artificial pits have been employed from time to time in the study of pitting corrosion, particularly the second stage. Greene and Fontana [5] cited as one criticism of this technique the fact that most artificial pit designs were not geometrically similar to actual corrosion pits.

2.4.2.2 Current distribution in and around pits

Three types of current measurements have been made with respect to pitting corrosion: total applied current measurements (normally under potentiostatic control), localized current measurements in the vicinity of pits and current measurements associated with artificial pits.

Szklarska-Smialowska [32] also reviewed the recent literature pertaining to pit growth kinetics. A semiempirical current equation for potentiostatic control of the form $i = kt^b$, where i = applied current, k = constant depending upon chloride ion concentration, b = constant (sometimes 2 or 3) and t = time, has been found to hold in some cases.

Rosenfeld and Danilov [36] employed a twin probe method to measure the field strength in the solution adjacent to an active stainless steel pit. They were then able to calculate the current distribution adjacent to the pit. The effect of time on this distribution was also studied.

Rosenfeld and Danilov discovered, as they traversed an active pit, that the anodic current density was a maximum at the center of the pit and the cathodic current density was a maximum near the edge of the pit. The apparent current density of a pit decreased with time according to the equation $i_a = kt^{-1/2}$, where k = constant and t = time.

Artificial pits have been employed for current measurements, the determination of electrochemical control and the effects of additions of cathodic depolarizers.

Brown and Mears [68-70] developed their well-known "scratch technique" and applied it to electrochemical studies of Al [68], stainless steel (18% Cr - 8% Ni) [69], and steel and Mg [70]. This method involved the short-circuited coupling, through a zero-resistance ammeter, of a waxed anode with one or more scratches present and a waxed cathode of definite exposed area. The potential was also monitored. The technique gave an indication of anodic, cathodic or mixed electrochemical control.

Another type of artificial pit was developed by Greene and Fontana [71] and used for a similar purpose [72]. Their artificial pit consisted of a sheet cathode with a hole in it, through which passed a small diameter anode wire, electrically insulated. It was hoped that such an arrangement would approximate the geometry of an actual pitted metal surface, neglecting pit interaction. Murray [73] demonstrated the use of a somewhat similar artificial pit, using a drilled plate cathode backed by an anode plate, electrically insulated.

The general result of Brown and Mears' work [69] and Greene and Fontana's work [72], for stainless steels, seems to have been that electrochemical control could change, depending upon such factors as time, presence of depolarizers and extent of propagation. As pointed out by Greene and Fontana [5], the presence of local-action currents on any artificial pit could lead to questionable results.

2.4.2.3 Potential distribution in and around pits

Herbsleb and Engell [74] used a fine Haber-Luggin capillary (0.08 mm) to measure the potential inside pits under potentiostatic control. They found that for an iron electrode in a 1 N H_2SO_4 + 0.003 M Cl^- solution, potentiostated to +1.230 v_{SHE} , the potential inside an active pit was as low as +0.100 v_{SHE} . Rosenfeld and Danilov [36] measured a substantial variation in electric field strength as a function of position in the electrolyte just outside of an active pit. Pickering and Frankenthal [75], also using a fine Haber-Luggin capillary probe, measured a potential drop corresponding to their calculated electrolyte IR drop (~ 100 mv) as they lowered the probe into an

active iron pit. However, within 50 μm of the bottom of the pit, they observed larger potential drops and sharp transients that were 1.2 v more negative (active) than the applied potential. They also observed H_2 gas bubbles emanating from iron and stainless steel pits under similar conditions of applied potential.

Akimov [76] discussed the potential drop due to current flow through a solution for a pair of electrochemically coupled electrodes. This is similar to the potential drop between the auxiliary and working (specimen) electrodes in a potentiostatic circuit. Piontelli [77] showed that "additional resistance" and "screen" effects, due to positioning of the Haber-Luggin capillary and current flow, could introduce significant experimental errors into measured potentials.

2.4.2.4 Electrolyte composition inside pits

Pryor [78] used X-ray diffraction to identify the corrosion products of steel after immersion in several electrolytes exposed to air. He found α and $\gamma\text{-FeO}\cdot\text{OH}$ to be a common constituent.

Fontana and Greene [1] noted that "corrosion tubes" could form on ferrous alloys due to the action of dissolved oxygen in the electrolyte. Here X-ray diffraction showed the presence of several layers or "rings" of iron in various oxidation states.

Heyn and Bauer [79], and later Foroulis and Uhlig [80], identified iron carbide (Fe_3C) as a corrosion residue. Herbsleb and Engell [81] identified Fe_3C in pits of mild steel, but no solid corrosion products in pits of spectroscopically pure iron. Staehle et al. [82] observed the stability of iron carbide structures to be a function of potential, pH and anion.

Strehblow and Vetter [83] developed a technique for transferring a sample with active pits into an electron probe microanalyzer. The pits were grown potentiostatically on iron samples in chloride and chloride/sulfate solutions. In order to prevent chloride precipitation inside the pits, it was found necessary to limit the diameters of the pits to between 5 and 10 μm .

Enrichment in chloride was measured inside previously active (5-10 μm) pits, but no solid corrosion products were observed for chloride solutions. A thick, porous sulfate layer was observed over the chloride layer for chloride/sulfate solutions.

2.4.2.5 pH changes in pits

Ideally, it would be best to analyze for the chemical composition of actual "in-service" pits. In 1926, Baylis [84] carried out such an analysis of the tubercles on the inside of cast-iron pipe exposed to a public water system. He noted pH's of about 6 and the presence of Fe, chlorides, sulfates and other constituents.

The difficulty of making in situ analyses on actual corrosion pits has led many investigators to the use of artificial pit devices. These devices, although varying in size and design, usually possessed a common feature: an anode compartment of restricted volume separated from the bulk or cathode compartment by some sort of diffusion barrier (porous ceramic material, parchment or paper, asbestos fibers or fritted glass). Porous debris [85], corrosion products [86, 85] and migrational screening effects [5] have been viewed as possible diffusion barriers in real pits.

2.4.2.6 Chemical analysis of artificial pits

Evans [85] used his "parchment cell apparatus" to study differential aeration conditions. He noted a much larger accumulation of iron in the anode (unaerated) compartment. He did not determine the final pH's of the compartment electrolytes.

Uhlig [46] employed a porous cup, a piece of 18% Cr - 8% Ni stainless steel pipe and a graphite cathode to simulate a natural pit. He passed a constant direct current through a 5% NaCl aqueous solution, with the stainless steel anode inside the porous cup. After the experiment, the anode was found to have pitted over its entire surface.

Analysis of the anolyte solution revealed no preferential dissolution of the alloy constituents (Fe, Cr, Ni). Chloride ion increased in concentration within the porous cup and decreased outside. The catholyte reached a pH of about 11 and the anolyte attained of pH of less than 2.

Parsons et al. [87] constructed artificial pits using Fe anodes and Cu cathodes. Their starting solutions contained 9 parts of 0.1 N NaCl and 1 part of 0.1 N NaOH, giving an initial pH of about 12. A yellowish membrane formed between the electrodes. In those cases where the membrane remained intact, it acted as a diffusion barrier.

Analyses of cells forming a single membrane yielded Fe^{++} concentrations of 0.085 M to 0.276 M, Cl^- concentrations of 0.154 M to 0.324 M and pH's of 5.8 to 6.3. Analyses of a few multiple-membrane pits gave slightly lower pH's and nearly double the Fe^{++} and Cl^- concentrations of single-film pits.

Pryor [78] employed an artificial pit device, making use of a porous alundum pot, to study the behavior of steel anodes. He applied a constant anodic current for a period of 24 hours and then analyzed the anolyte. The resulting pH's were found to vary from 3.4 to 6.7. In those solutions containing chlorides, 230 to 290 percent increases in chloride concentration were observed.

More recently, Wilde and Williams [88] devised an artificial pit anode consisting of an AISI Type 304 stainless steel wire embedded in epoxy. The sample was potentiostated at various potentials in 1 M NaCl at 25°C. Each sample, after having been maintained at a given potential for an appropriate time, was quickly frozen in liquid nitrogen. The frozen plug of corrosion products was then melted and analyzed for pH and $\text{Fe}^{++}/\text{Fe}^{+++}$ concentration ratio.

For applied potentials ranging from +0.500 to -0.200 v_{SCE} , they observed pH's ranging from 3.6 to 0.0 and $\text{Fe}^{++}/\text{Fe}^{+++}$ concentration ratios ranging from 1.59 to 9.8. An unexpected result was that more noble applied potentials resulted in higher pit pH's (lower H^+ concentrations).

2.4.2.7 Hydrolysis in pits

In a general sense, hydrolysis has been defined as the reaction of any substance with water [89]. In a more restricted sense, it has been defined as the reaction of an ion with water to form an associated species plus H^+ or OH^- [89]. Cation hydrolysis can result in an increase in H^+ concentration and thus a reduction in pH.

Whitman et al. [90] attributed the nearly constant corrosion rate of steel in natural waters of pH 4 to 10 as being due to the formation of a constant pH of 9.5 at the surface of the steel (relating to the solubility product of $\text{Fe}(\text{OH})_2$).

A number of authors [28, 46, 47, 27, 88] have noted that iron and chromium chloride solutions tended to be acidic. There appears to be no general agreement as to what hydrolysis products form from iron and stainless steel reaction products in chloride solutions.

Uhlig [46] found the corrosion products of an 18% Cr - 8% Ni stainless steel (driven anodes in NaCl solutions) to be Fe^{++} , Cr^{+++} and Ni^{++} chlorides. Stolica [60] suggested that, according to his data, Cr^{++} was formed as a primary reaction product and was oxidized to Cr^{+++} by the electrolyte.

Pourbaix [27] attributed hydrolysis of iron to the formation of Fe_3O_4 and $\text{Fe}(\text{OH})_3$. Wilde and Williams [88] tabulated a number of possible hydrolysis reactions involving Fe^{++} , Fe^{+++} , Cr^{++} , Cr^{+++} and Ni^{++} , but were unable to decide which reaction or reactions predominated.

2.4.2.8 Electromigration and diffusion

The observed tendency for chloride ions to concentrate in active pits may be accounted for in two ways:

1. Chloride ions react directly or indirectly with metal inside pits to form a corrosion product or associated species, resulting in a drop in chloride ion activity in the pits. Inward diffusion of chloride ions follows.
2. The rapid production of positively charged metal ions

inside pits tends to cause a local charge imbalance. This must be offset by the outward movement of cations or the inward movement of anions.

The first possibility would seem difficult to prove, due to the known high solubilities of many metal chlorides in water [91, 92, 93]. In addition, if operative, such a process should not result in any increase in chloride ion activities in pits.

The second possibility can be dealt with using the concept of transference or transport numbers. Assuming a current passing through an electrolyte, transference numbers can be defined as follows [94]:

t_+ = fraction of current carried by cation,

t_- = fraction of current carried by anion,

where $t_+ + t_- = 1$.

This definition could be extended to include transference numbers for each individual cation and anion present in the electrolyte.

The anions in solution tend to migrate toward the anode under the influence of an applied electric field and the cations tend to migrate toward the cathode. If particular ions are discharged at the appropriate electrode, a buildup in concentration may not occur. If discharge does not occur, there may be a buildup in concentration near the appropriate electrode.

A situation can be envisioned where the transference number of a particular anion, such as the chloride ion, might be high. At potentials below that required for chlorine evolution, chloride ions should concentrate themselves in the vicinity of the anode. Local electrical neutrality (down to molecular dimensions) must be

maintained in an electrolyte [94]. Thus, a large concentration of metal ions in a pit must be accompanied by enough anions to assure an equal number of positive and negative charges.

The ionic mobility is defined as the average velocity with which an ion moves toward an electrode under the influence of a potential of 1 v applied across a 1 cm cell [94]. H^+ and OH^- ions have the highest ionic mobilities at infinite dilution in aqueous solutions, with other ions possessing lower but about equal mobilities [94]. It would appear that the transference number for a given ion would depend on both availability (concentration) and mobility. This would imply that an increase of chloride ion concentration in a pit would be due to the requirement for electrical neutrality and to ready availability, rather than to an inherently high ionic mobility.

A number of authors have suggested that migration [46, 47, 78, 95] and diffusion [47, 78, 17] effects were instrumental in the changes of electrolyte composition occurring in active pits. Other authors [96, 97, 98, 5] discussed an ion-screening mechanism with reference to the diffusion of oxygen into a pit. Their view was that corrosion products reacted with oxygen and hindered or prevented it from entering the interior of a pit. This concept might be applied to other species in solution, such as the OH^- ion for pits on ferrous alloys (due to the formation of $Fe(OH)_2$).

2.4.2.9 Stability of pitting

Franck [99] showed that there should be two stable stationary states (active and passive) for an open system involving an active-

passive metal or alloy. Franck also showed (mathematically) that only one stationary state should be stable at a time. This implied that pitting corrosion should be an unstable process, since both active and passive areas existed simultaneously.

Realizing that pitting corrosion did exist, Franck made further assumptions. Using an analog computer simulation of pitting, involving two variables, he was able to show mathematically that there were cases where pitting corrosion was stable, unstable, or oscillatory. The presence of a very high-resistance polishing film was postulated, whose rate of dissolution determined the corrosion current. The true potential of a pit was viewed as lying in the active corrosion region.

Brauns and Schwenk [100] suggested that perhaps both the resistance effect and the electrolyte composition change (concentration) effect were required for stable pitting. Schwenk [101] later showed that the concentration effect could lead to stable pitting under galvanostatic conditions (only at the pitting potential) and that the resistance effect could lead to stable pitting under potentiostatic conditions at any potential within the pitting range. In this [101] and another work [58] Schwenk again noted that both the resistance and concentration effects might be necessary for stable pitting corrosion.

Rosenfeld and Danilov [36] helped to confirm this idea by showing that pits could be deactivated by destroying the protecting layer over the pits, thus allowing access to the bulk electrolyte.

Pickering and Frankenthal [75] presented evidence that the potential in a localized corrosion cell (pit or crevice) was in the

active part of the anodic polarization curve of the metal, even when the specimen surface was potentiostated to more noble potentials. They attributed this effect to the presence of high-resistance paths in the form of H_2 gas bubbles within pits or crevices.

Hoar et al. [102] held the opinion that the anode potential within pits could not be more than a few mv different from that measured and controlled (potentiostatically) outside. They based their conclusion partly on the fact that crystallographic etching (often found with active dissolution) was suppressed, with anodic brightening type of attack occurring instead (characteristic of higher anode potentials). The authors suggested the presence of a "contaminated oxide" compact solid film of high cation conductivity on the pit anode.

At about the same time Vetter [42] expressed similar doubts about the validity of the resistance effect. He also developed a thermodynamic theory for the stability of pitting, postulating the coexistence of passivating oxide layers and nonpassivating salt layers (Cl^- , Br^- , I^-).

2.5 Crevice Corrosion

As in the case of pitting corrosion, two stages or steps in crevice corrosion are generally recognized: initiation and propagation [103]. Bombara [104] noted that initiation and propagation were two well-distinguished stages in stress corrosion cracking and in many forms of localized attack.

A number of authors [105, 34, 1, 106, 107, 75] have noted similarities between the propagation stages of pitting and crevice

corrosion. Schafer et al. [103] stated that they were identical processes. Bombara [104] went so far as to suggest that a strict analogy might exist between the electrochemical mechanisms of localized attack and stress corrosion cracking in both the initiation and propagation stages. For this reason, some results from the literature pertaining to stress corrosion cracking will be included here.

2.5.1 Initiation of Crevice Corrosion

France [106] recently reviewed the literature of crevice corrosion (Rosenfeld and Marshakov [108] had done so earlier). He categorized the currently popular mechanisms under a general heading of "concentration cells." The categories included metal-ion cells, differential aeration cells, active-passive cells and other concentration cells. The final category included hydrogen-ion, neutral salt and inhibitor cells. Primary emphasis will be placed on crevice corrosion of previously passive metals.

2.5.1.1 Metal ion cells

The metal ion cell is a special case of the electrolyte concentration cell. A concentration cell is an electrolytic cell, the e.m.f. of which is due to differences in composition of the electrolyte at anode and cathode areas [4]. McKay [109] studied such a cell in 1922 by measuring the potential between a pair of Monel^{*} metal electrodes (70% Ni - 30% Cu) in sulfuric acid solutions of different concentrations of cupric sulfate, separated by a porous cup.

By the use of current and weight-loss measurements, McKay

*Trade name of International Nickel Co.

verified that the Monel electrode immersed in the solution of lower copper ion concentration was the anode. He correlated these results with those predicted by the Nernst equation for pure Cu. In addition, McKay demonstrated that corrosion could be produced by cells due to differences in the concentration of acids, concentration of dissolved oxygen or hydrogen, or concentration of dissolved oxidizing and reducing salts.

Evans [85] made some calculations on the possible effects of stirring, using the Nernst equation. Assuming fixed electrode potentials of +0.1, +0.2, and +0.3 v_{SHE} , he calculated the equilibrium concentration of metal ions (assuming the Nernst equation to be valid) for several metals. The results showed that equilibrium concentrations could be attained for Ag and Cu, but that equilibrium concentrations for Pb, Cd, Fe and Zn (according to the Nernst equation) were clearly unattainable.

In a later paper, McKay extended an existing definition of concentration cell to

...cells whose e.m.f. is set up by two electrodes of the same material in different electrolytes. [110, p. 23]

LaQue et al. [19] used the metal ion cell concept to explain a type of crevice corrosion observed on Cu alloys, where the attack was limited to the area just outside a crevice. Schafer and Foster [111] argued that the metal ion cell, in order to operate, would have to violate the laws of chemical diffusion. They suggested that the type of attack referred to by LaQue et al. was in fact a special case of differential aeration.

2.5.1.2 Differential aeration cells

Differential aeration cell has been defined as an electrolytic cell, the e.m.f. of which is due to a difference in oxygen concentration at two otherwise similar electrodes [4]. McKay [109, 110] recognized the existence of such a cell in the early 1920's.

Evans [85, 112, 96, 113] treated the subject in a number of his papers. It was established that, in general, the electrode immersed in the solution of lower dissolved oxygen concentration became the anode and that the electrode immersed in the solution of higher dissolved oxygen concentration became the cathode [85, 110, 96, 113]. More recently, Korovin and Ulanovskii [114] have studied the effects of dissolved oxygen concentration on the electrode potentials of stainless steels. Schafer et al. [103] noted that the differential aeration cell mechanism should be operative primarily only in the initiation stage of crevice corrosion.

2.5.1.3 Passive-active cells

Passive-active cell (or active-passive cell) has been defined as a cell, the e.m.f. of which is due to the potential difference between a metal in an active state and the same metal in a passive state [4]. Uhlig [20] attributed the formation of passive-active cells in chloride solutions to the localized breakdown of passivity by chloride ions. France [106] discussed the mechanism in terms of a localized deficiency in oxidizers (e.g., dissolved oxygen, Cu^{+2} or Fe^{+3}).

Although the concept of localized cells being responsible for the initiation of crevice corrosion is well established, another

possible way of viewing the subject for the case of previously passive metals in chloride solutions (or solutions containing other aggressive anions) presents itself. This is by way of the concept of critical parameters for the breakdown of passivity.

2.5.1.4 Critical parameter concept

The concept of critical parameters for the breakdown of passivity was discussed in Section 2.4.1.4. It was noted then that in solutions containing chloride or other aggressive anions, breakdown of passivity could be attained by reaching a critical potential (rupture potential), a critical chloride concentration (or aggressive anion concentration) or a critical pH.

Thus, the initiation of crevice corrosion on a previously passive metal might be affected by raising the potential of the metal above (more noble than) the critical pitting or rupture potential in an existing crevice. The potential might be maintained electronically, through the use of a potentiostat, or chemically, by the use of oxidizing agents. The role of dissolved oxygen might then be viewed as twofold: to maintain the potential (in the absence of any applied current) and to alter the rupture potential.

The data of Wilde and Williams [115] indicated a higher (more noble) rupture potential for aerated solutions than for deaerated solutions, although a more exhaustive study might be required to verify the point. Accepting their data, one could envision the rupture potential in an existing inactive crevice to be lower (due to a lower concentration of dissolved oxygen) than that outside the crevice

in solutions containing dissolved oxygen. If the potential were maintained between the two rupture potentials (more noble than the crevice rupture potential), breakdown of passivity could be expected to occur inside the crevice.

If the chloride ion concentration inside an existing inactive crevice were increased while the potential was maintained at a constant value, a critical concentration necessary for the breakdown of passivity might be reached. Such a concentration increase could conceivably result from the electromigration of chloride ions accompanying the small corrosion current present in the passive state. This type of mechanism would depend upon the relative transference of the various ions present in solution.

If the pH inside an existing inactive crevice were lowered while the potential was maintained at a constant value, a critical pH necessary for the breakdown of passivity might be attained. Such a pH decrease might result from the hydrolysis of metal ions, slowly formed by the dissolution process in the passive state. This type of mechanism would depend upon the relative diffusion rates of the various ions present in solution. In reality all three processes, or any combination thereof, might operate simultaneously.

Some aspects of this approach follow closely the reasoning put forth by Fontana and Greene [1, 106] in a unified mechanism of crevice corrosion (e.g., chloride ion migration and metal-ion hydrolysis), but the additional possibility of critical parameters may be useful for better understanding of the initiation of crevice corrosion on previously passive metals in solutions containing aggressive anions.

2.5.1.5 Induction periods

Another aspect of the initiation stage of crevice corrosion should be mentioned: the existence of an induction period for the initiation of crevice corrosion. France [106] attributed the existence of an incubation period to the time required for consuming the oxygen in a shielded crevice area. Indirect experimental verification of this process was obtained by Karlberg and Wranglen [116] through the use of an artificial crevice.

The critical parameter concept would also be amenable to the existence of an induction period for crevice corrosion initiation. Wilde [117] claimed the induction period for crevice corrosion to be shorter than that of pitting. Fontana and Greene stated that pitting

...is a self-initiating form of crevice corrosion.
...it does not require a crevice--it creates its own.
[1, p. 54]

The existing geometry at a crevice helps to rationalize a longer induction period for the initiation of pitting than for the initiation of crevice corrosion.

2.5.2 Propagation of Crevice Corrosion

As was mentioned at the beginning of Section 2.5, the propagation stages of pitting and crevice corrosion (and perhaps other forms of localized corrosion) appear to proceed by similar mechanisms. For this reason a subject order similar to that used in the section on the propagation stage of pitting will be followed.

Rosenfeld [118] reviewed the literature of crevice corrosion,

with particular emphasis on the propagation stage. One observation that he made was that it was not clear just which hydrolysis process was responsible for acidification of the electrolyte in a crevice.

2.5.2.1 Geometry of crevice corrosion

The name given to the type of attack presently under consideration implies the presence of a small interstice or crevice. In practice, it can be very difficult to eliminate unwanted crevices. It has been shown that some of the materials commonly used for mounting or partial incasement of electrochemical samples can form crevices at material/sample interfaces [119, 120].

Crevice corrosion has been known to occur under a number of materials, including fabrics, plastics, wood, porcelain, glass, rubber, wax, mica, asbestos, packing (especially when graphite was present) and marine growths [19]. Rosenfeld and Marshakov [121] studied the nature of attack produced under a series of dielectrics on the surface of iron and between two homogeneous iron samples, and observed no differences. Some crevice-forming substances may contain reactive constituents such as sulfur in sulfur-bearing rubbers [19].

The geometry, or shape and size, of a crevice can be important in characterizing crevice corrosion. This is due partly to the effect of geometry on diffusion and electromigration processes and partly to the effect of geometry (relative surface distribution of anodic and cathodic areas) on electrochemical polarization.

Ellis and LaQue [122] studied area effects on crevice corrosion of an Fe - 17% Cr stainless steel exposed to fresh sea

water. Using machined samples of known crevice dimensions, they found both the average weight loss and the average maximum pit depth to be directly proportional to the exposed area of sample outside the crevice.

Other authors have shown that intensity of attack within a crevice may vary with width or depth. Rosenfeld and Marshakov [108] noted that a maximum of corrosion intensity occurred at an intermediate crevice width. Bombara et al. [123] showed that a maximum rate of crevice attack occurred at a depth which depended upon the externally applied potential and the crevice width. Vermilyea and Tedmon [124] made calculations based on experimental work which predicted how the metal-ion concentration and potential should vary with depth for a simple type of crevice. Some of the mathematical treatments of crevice corrosion are quite involved and fraught with simplifying assumptions. Nevertheless, they can be instructive and useful by pointing out the danger of intuitive reasoning.

2.5.2.2 Current distribution in and around crevices

The several types of current measurements that conceivably might be made include the total net sample current (including crevices and other areas), the total net crevice current, and net local currents inside and outside crevices.

Measurements of the total net sample (working electrode) current can be made using standard potentiostatic or potentiokinetic apparatus. These were the kinds of measurements made by Greene et al. [119], and Lizlovs and Bond [120]. The presence of crevices resulted in higher measured applied currents in passive potential ranges.

Lizlovs [125] designed a more reproducible crevice assembly, in which the crevice could be introduced or removed at will. Large current increases were frequently observed when the artificial crevice was introduced.

The "scratch technique" of Brown and Mears [68-70] was briefly discussed in Section 2.4.2.2. Their scratches (in the wax) might be considered to be shallow artificial crevices. Thus, their conclusions regarding the observation that all types of electrochemical control could be observed in pitting corrosion probably also apply to crevice corrosion. If this is true they were, in fact, measuring the total crevice currents of artificial crevices.

Rosenfeld and Marshakov [108] presented a plot of current vs. depth in crevice (for an Fe - 13% Cr alloy in 0.5 N NaCl) [There is some question as to the alloy composition.] which showed the crevice edges to be functioning as cathodes and the interior of the crevice to be functioning as anode. The authors also employed a sectional artificial crevice to measure current and potential as a function of depth inside the crevice.

2.5.2.3 Potential distribution in and around crevices

The potential, as measured experimentally, of an electrode possessing an active crevice, may depend upon the position of the measuring apparatus (i.e., the position of the Haber-Luggin capillary) [77, 76, 67]. The measured potential may be that of a "composite electrode" [67] (a sort of average potential) or that of a local electrode process (a local potential). The measured potential conceivably may also fall between these two extremes.

Bombara et al. [126, 104] determined potentiokinetic polarization curves for several austenitic stainless steels at 40°C in solutions of 0.75 M H_2SO_4 , with and without 0.01 M NaCl. They then maintained samples potentiostatically for appropriate times and later examined them metallographically. Combining the data, they delineated potential ranges according to attack morphology.

Larin and Iofa [127] expressed an opinion that, for the case of the crevice corrosion of iron at three-phase boundaries, the potential of the anodic area could not be very different from that of the cathodic area, due to their close proximity. This statement of opinion was similar to that expressed by Hoar et al. [102] for the case of pitting corrosion.

Localized anodic and cathodic polarization curves (potential vs. current density) were determined for iron in 0.5 N NaCl by Rosenfeld and Marshakov [108]. A sectional artificial crevice was employed and curves were presented for several depths inside the crevice. They found the anodic process to be greatly accelerated and the cathodic process to be retarded inside a narrow crevice.

Somewhat related experiments were conducted by France and Greene [128] in 1 N H_2SO_4 for Type 304 and 18% Cr - 12% Ni stainless steels. They used an electrode assembly fabricated from a plastic block, with internal probe openings spaced at 0.5-in. intervals. They maintained the potential of the external crevice face potentiostatically. Potential differences of up to approximately 1 v were measured in some cases.

Another type of artificial crevice was developed by Vermilyea

and Tedmon [124]. Their (calculated) potential differences for iron were smaller than those observed by France and Greene [128], of the order of 100 mv. Similar results were obtained directly by Karlberg and Wranglen [116] for stainless steels, using yet another type of artificial crevice. Pourbaix [129, 27] presented data relating potential and pH inside an artificial crevice to the potential and pH outside the crevice for an ordinary carbon steel. Efird [130] used an improved artificial crevice design to obtain data for a Cu-Ni alloy.

A. Pourbaix [131, 132] used a modified version of the artificial crevice employed by M. Pourbaix [129, 27] to determine simultaneous polarization curves for duplex (active and passive segments) steel electrodes in 10^{-3} M NaOH and either 10^{-3} or $10^{-0.3}$ M NaCl solutions. The device consisted of a large "bulk" (cathode) compartment and a small "crevice" (anode) compartment, separated by a diffusion barrier in the form of a hole filled with asbestos fibers.

Pickering and Frankenthal [75] observed H_2 gas bubbles emanating from pits and crevices on iron and stainless steel samples, even with the external applied potential as noble as $+1.4 v_{SHE}$. Similar observations were made by Rhodes [133] for the case of stress corrosion cracking. B. F. Brown et al. observed potential differences between stress corrosion cracks and unaffected material for freely corroding [134, 135] and potentiostatically controlled [135] samples. They studied 4340 [135] and other alloy steels [134], and found the potential of the stress corrosion crack in every case to be below that of the equilibrium hydrogen electrode.

2.5.2.4 pH changes in crevices

A number of authors have reported pH changes (from the bulk solution pH) in crevices [136, 137, 27, 116] and stress corrosion cracks [138, 134, 135]. Most of the work concerning crevice corrosion was done with the aid of artificial crevices, but the work concerning stress corrosion cracks was performed in situ on real cracks.

Ulanovskii and Korovin [136] reported attempts to make direct pH measurements on crevices, using both a potentiometric method and an indicator method. Details were not given, but a minimum pH of about 3 was noted for an Fe - 13% Cr stainless steel. They then polarized specimens in a cell of limited volume (about 5 ml of electrolyte) and monitored pH. The pH was found to decrease towards a steady-state value, both with increasing applied current (for a constant time) and with increasing time (for a constant current). A pH of about 2 was attained after a period of 24 hours with an applied current density of $+0.20 \text{ ma/cm}^2$.

Peterson et al. [137] used a thymol blue indicator to make direct pH measurements of active crevices on a Type 304 stainless steel exposed to sea water. They estimated the pH to range from 1.2 to 2.0. The authors also found that cathodic protection yielded alkaline pH's, above 10 for specimens coupled to zinc anodes (probably due to H_2 gas evolution).

Pourbaix [27] showed, on potential vs. pH diagrams, a dependence of the pH of an artificial crevice on the externally applied potential. He reported a steady-state crevice pH of about 4.7 for ordinary carbon steel with an applied potential (due to oxygen reduction) of about

$-0.1 v_{SHE}$. Pourbaix observed that the crevice pH could become either more acidic than or more basic than the bulk solution, depending on the externally applied potential. Acidification was attributed to metal-ion hydrolysis and alkalization was attributed to H_2 gas evolution.

Karlberg and Wranglen [116] measured the pH of a freely corroding artificial crevice (after up to 14 days) on an Fe - 13% Cr stainless steel. The external potential was about $-0.15 v_{SHE}$ and the crevice potential was about $-0.3 v_{SHE}$. The measured pH was 4.0, although the authors noted that the pH may have been lower locally.

Brown et al. employed chemical indicator [138, 135], indicator electrode [135] and colorimetric methods [134] in their studies of chemistry changes within actual stress corrosion cracks. Early work [138] reported pH values at crack fronts of 3.5, 3.8 and 1.7 for an Al alloy, a carbon steel and a Ti alloy, respectively, in solutions of 3-1/2% NaCl by weight.

Later work [135] on an AISI 4340 steel showed the pH at crack tips to be virtually independent of the bulk pH and that electrochemical conditions at the crack tips were favorable for H_2 gas evolution regardless of the externally applied potential. Work [134] performed on a series of alloy steels (including an Fe - 12% Cr alloy) in solutions of 3-1/2% NaCl by weight, under freely corroding conditions, yielded pH values at the crack tips of about 3.7 for all steels.

2.5.2.5 Chemical analysis of crevices

Some of the authors cited in the previous section also attempted chemical analyses of solutions within crevices [137, 130, 131, 132] and

stress corrosion cracks [138, 134]. Brown et al. employed chemical indicator [138, 134] and colorimetric [134] methods to study the solution chemistry of actual stress corrosion cracks. Their chemical indicator work identified Fe^{++} , but not Fe^{+++} , in the crack solution of a 0.45% C steel exposed to a 3-1/2% NaCl solution by weight [138]. Similar results were obtained in later work [134] done on several alloy steels. In addition, the alloying elements in the steels were found in the solution near the crack tip (analyzed colorimetrically) in approximately the same proportions as in the original steel compositions.

Peterson et al. [137] used a similar chemical indicator technique to analyze qualitatively for the presence of Fe^{++} and Fe^{+++} in crevice solutions of a Type 304 stainless steel exposed to sea water. They noted a strong indication for Fe^{++} and only a trace for Fe^{+++} .

Any buildup of ions in crevices (or other occluded cells) may result in indirect effects. One of these is a decrease in oxygen solubility with increasing concentrations of salt solutions [139, 140]. This may tend to decrease the rate of transfer of oxygen into an active occluded cell.

The topics of hydrolysis, electromigration and diffusion, and stability (of pitting) were discussed in the section on the propagation of pitting (2.4.2). The pertinent remarks made there should also apply, at least qualitatively, to the propagation stage of crevice corrosion. Consideration should be made of the different geometries involved.

2.5.2.6 Hydrolysis in crevices

It was implied in Section 2.5.1.3 that the concentration of oxidizing agents (e.g., dissolved oxygen, Cu^{++} or Fe^{+++}) in an active crevice or occluded cell should be lower than that in the bulk solution. Whether or not oxidizing conditions are maintained would depend on the relative rates of oxidizer reduction inside the crevice and mass transport into the crevice.

The reason for concern as to whether or not oxidizing conditions exist in a given occluded cell is that hydrolysis reactions depend on the oxidation state of any ionic species involved. The only general statement that can be made is that many authors [108, 106, 118, 75] consider the dissolved oxygen concentration inside an active crevice or occluded cell to be low.

As was done in the case of pitting corrosion, the acidity frequently found in crevice solutions has been attributed to metal or metal-ion hydrolysis [108, 137, 27, 116]. Similar conclusions were reached for the case of stress corrosion cracking [138, 133, 134, 135]. There has, however, been no general agreement as to the responsible hydrolysis products.

Several authors [108, 133, 27, 116] considered only solid reaction products. Other authors [138, 134, 135] considered only soluble hydrolysis products. Finally, Peterson et al. [137] did consider a number of possible solid and soluble hydrolysis products. In addition, these authors suggested that the most likely reaction under their particular conditions (Type 304 stainless steel in sea water) was the hydrolysis of Cr^{+++} .

Brown et al. [134] measured the acidity of freshly prepared aqueous solutions of 1 M $\text{FeCl}_2 \cdot 4\text{H}_2\text{O}$ (Parsons et al. [87] may have done a similar experiment earlier). These solutions were prepared both with boiled (to lower dissolved oxygen content) and unboiled distilled water. The initial pH's of both solutions were 4.0. The pH of the solution prepared with boiled distilled water slowly drifted to a value of about 3.2. The "unboiled" solution attained about the same pH, but much more rapidly. The authors then interpreted their pH results on stress corrosion cracks of alloy steels as being due to the hydrolysis of partially oxidized (by dissolved oxygen) ferrous ions.

2.6 Limitations of Laboratory Tests

One criticism of relatively rapid laboratory corrosion tests (both freely corroding and with externally applied current) has been that results might not correlate with in-service tests. Induction periods have been observed for the initiation of occluded cell corrosion, leading some authors [141, 18] to question the validity of short-term laboratory corrosion tests. Other authors [13, 107] have attempted to show that short-term data could be applicable to longer exposures.

France and Greene [95] questioned the correspondence between chemically and electrolytically induced pitting corrosion. Brigham [142], and Wilde and Williams [143] appear to have countered their arguments.

The extrapolation of data obtained for salt solutions or synthetic sea water solutions to an actual sea water environment is

generally not encouraged. This attitude arises from the known fact that salt solutions and synthetic sea water solutions may be different in their "corrosiveness" from fresh, live sea water [144, 145].

2.7 The "Protection Potential"

"Tension de protection," translated as "protective tension" [3] or "protection potential," [27] was a term coined by M. Pourbaix et al. [52] in 1962. The original work was done for Types 410, 304 and 316 stainless steels [52, 146, 49, 147, 3]. Work also was done involving the "protection potential" for copper [148, 149, 150, 27].

2.7.1 Definition and Verification

The "protective tension" (later the "protection potential") was defined in the following manner:

If after polarizing the steel at an increasing tension beyond this breakdown tension it is then polarized at a decreasing tension, a tension [potential]/current curve is obtained which does not coincide with the curve for increasing tension, but lies considerably below it. The curve meets the ordinate axis (with a practically zero current density) at an electrode tension representing a second well-defined critical value, which we have called the "protective tension" E_p , below which the steel stops corroding. [3, p. 245]

Three electrode potential regions have been recognized [151, 143]:

- (1) Above (more noble than) the rupture potential, new pits can initiate and propagate and existing pits can continue to propagate.
- (2) Between the rupture potential and the "protection

potential," existing pits can continue to propagate but no new pits can initiate.

- (3) Below (more active than) the "protection potential," pits can neither initiate nor propagate.

Pourbaix et al. [52, 3] conducted a series of chronoamperometric experiments (monitored current as a function of time at a fixed potential) for a Type 410 stainless steel. They observed that the applied current for actively pitting specimens (whose potentials had previously been raised above (more noble than) the rupture potential) approached low values when the potential was lowered below (more active than) the "protection potential." Physical examination of the specimens after conclusion of the experiments confirmed the current measurements.

Verink et al. [152] employed a diamond scribe to further verify the "protection potential" concept for an Fe - 16.9% Cr alloy. It was observed that scratches made on the surface of the sample, in solution, would not propagate as active pits at potentials below (more active than) the rupture potential for the alloy. It was also observed that scratches, activated at potentials above (more noble than) the rupture potential, would cease to propagate when the potential was lowered below (more active than) the "protection potential."

It should be noted that completely meaningful "protection potential" data can be obtained only in solutions containing negligible quantities of dissolved oxidizing species [3, 153, 154].

2.7.2 Experimental Methods

An electrochemical hysteresis technique [153, 154] (a cyclic

potentiokinetic method), developed by Pourbaix et al. [52, 49, 3] has been the usual method used for determining "protection potentials." Details of this method will be given in Chapter 3.

Szklarska-Smialowska and Janik-Czachor [50] discussed various potentiostatic, potentiokinetic, galvanostatic and galvanokinetic methods for the determination of characteristic pitting potentials. The characteristic pitting potentials were a critical potential for pit initiation (rupture potential) and a critical potential for pit propagation ("protection potential").

Up to the present time the experimental work has primarily been done on iron-rich alloys (Fe [129, 27], Fe-Cr [54, 55, 153, 154] and stainless steel [52, 49, 3, 88, 155]), copper-rich alloys (Cu [149, 150, 156], Cu-Ni [157, 156] and Cu-Zn [158, 159, 160]) and nickel-rich alloys (Ni-Cu [156]).

2.7.3 Interpretation of the "Protection Potential" for Cu-Rich Alloys

One result of the research mentioned above was that the "protection potential" for copper and copper-rich alloys was observed to be relatively pH-independent [157, 158, 159, 160, 156] and approximately equal to $+0.200 \text{ v}_{\text{SHE}}$ [149, 150, 157, 158, 159, 160, 156]. This potential appeared to correspond to the potential for the reaction $\text{Cu} + \text{Cl}^- = \text{CuCl} + \text{e}^-$ [158, 159, 160] (assuming an activity for Cl^- of 0.1), as given by Pourbaix et al. [161,149].

The "protection potential" of copper and copper-rich alloys may also correspond to the potential for the reaction



Lee [156] investigated this possibility for a Cu - 10% Ni alloy in 0.1 M chloride solutions and obtained good agreement.

2.7.4 Effects of Experimental and Environmental Variables on the "Protection Potential"

The effects of a number of experimental and environmental variables on the "protection potential" have been investigated for iron-rich alloys [52, 49, 54, 27, 88, 155]. These are described chronologically in Table 2.

Pourbaix et al. [52] observed "protection potential" results for Type 410 stainless steel to be nearly the same for mechanically and electrolytically polished specimens. The authors also observed lower (more active) "protection potentials" for samples which had received a sensitizing heat treatment (10 minutes at 1000-1050°C).

2.7.4.1 Effect of alloy composition on E_p

The results of Pourbaix et al. [52], as given in Figure 3, showed the "protection potential" to increase (become more noble) with increasing chromium or nickel content (in the order Types 410, 304 and 316). Cusumano concluded that the "protection potential"

...rises to more noble values with increasing chromium content. [55, p. 106]

The data of Wilde and Williams [88] also showed a similar trend, becoming more noble in the order Type 410, USS 100, Types 430, 446, 304, 316, and Hastelloy C.

TABLE 2
 DETAILS OF INVESTIGATIONS OF THE "PROTECTION POTENTIAL" FOR FERROUS ALLOYS

<u>Year</u>	<u>Authors</u>	<u>Alloy</u>	<u>Electrolyte</u>	<u>Gas</u>	<u>pH</u>	<u>[Cl]</u>	<u>Prop.</u>	<u>Temp.</u>	<u>S.P.</u>	<u>H.T.</u>
1962	Pourbaix <u>et al.</u> , [52]	410 304 316	0.1 M NaHCO ₃	N ₂		X X X			X	X X X
1962	Pourbaix <u>et al.</u> , [49]	410 304 316	0.1 M NaHCO ₃	N ₂				X X X		
1970	Verink [54]	Fe-0.5% Cr Fe-2.0% Cr Fe-5.0% Cr Fe-12% Cr Fe-16.9% Cr Fe-24.9% Cr	buffers	H ₂	X X X X X X	X X				
1970	Pourbaix [27]	iron	buffers	N ₂	X	X				
1971	Wilde and Williams [88]	USS 100 410 430 446 304 316 Hastelloy C 430 304	3.5 wt. % NaCl	air						
1972	Suzuki and Kitamura [155]	316L	chlorides	stag- nant air	X	X				
									X X	

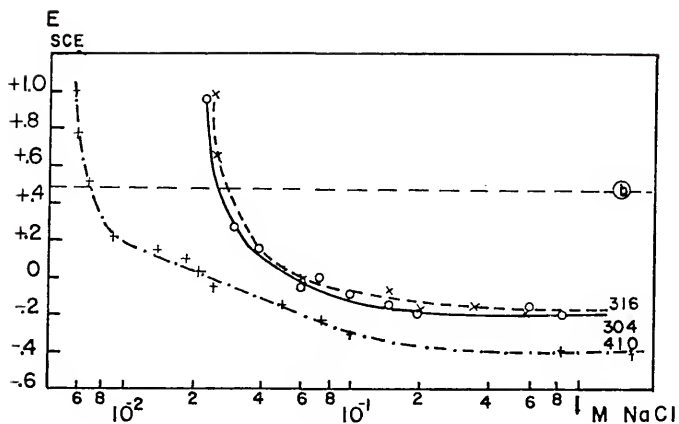


Figure 3. Effect of sodium chloride molarity on the "protection potential" for Types 410, 304 and 316 stainless steels in 0.1 M NaHCO_3 , N_2 -saturated solutions at 20°C [52].

2.7.4.2 Effect of pH on E_p

Previous authors have reported the "protection potential" to be either independent of [155] or only slightly dependent on [27, 54, 55, 153, 154] the bulk solution pH.

2.7.4.3 Effect of $[\text{Cl}^-]$ on E_p

Pourbaix *et al.* [52] observed the "protection potential" for some stainless steel alloys to become more active with increasing bulk solution chloride concentration, as shown in Figure 3. Suzuki and Kitamura [155] obtained qualitatively similar results, shown in Figure 4. Other workers [27, 54, 153, 154] have reported the "protection potential" to be relatively independent of chloride concentration.

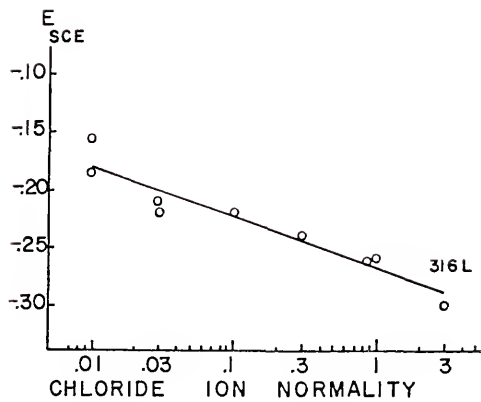


Figure 4. Effect of chloride ion normality on the "protection potential" for Type 316L stainless steel in stagnant chloride solutions at 70°C [155, p. 5].

2.7.4.4 Effect of Temperature on E_p

Pourbaix et al. [49] presented a plot of "protection potential" vs. temperature, reproduced in Figure 5, showing a decrease with increasing temperature for Types 316 and 304 stainless steels, and a decrease followed by an increase with increasing temperature for Type 410 stainless steel. Suzuki and Kitamura [155] observed a decrease of the "protection potential" with increasing temperature for Type 316L stainless steel, as shown in Figure 6.

2.7.4.5 Effect of extent of propagation on E_p

Wilde and Williams [88] studied the effect of extent of propagation on the "protection potential" for Types 430 and 304 stainless steels. They observed that the "protection potential" decreased (became more active) linearly with the increasing logarithm of the charge passed (obtained by integration of cyclic potentiokinetic polarization scans). Their results are shown in Figure 7.

2.7.5 Effect of Geometry on E_p

Suzuki and Kitamura [155] employed artificial occluded cells to study the "protection potential" for pits, crevices and stress corrosion cracks. They observed the "protection potential" for pitting to be more noble than the "protection potential" for crevice corrosion, and that the latter was approximately equal to that for stress corrosion cracking.

Wilde concluded [117] that the breakdown of passivity on stainless alloys occurred by either pit initiation or crevice initiation, possessing differing kinetics. He also concluded that the initiation

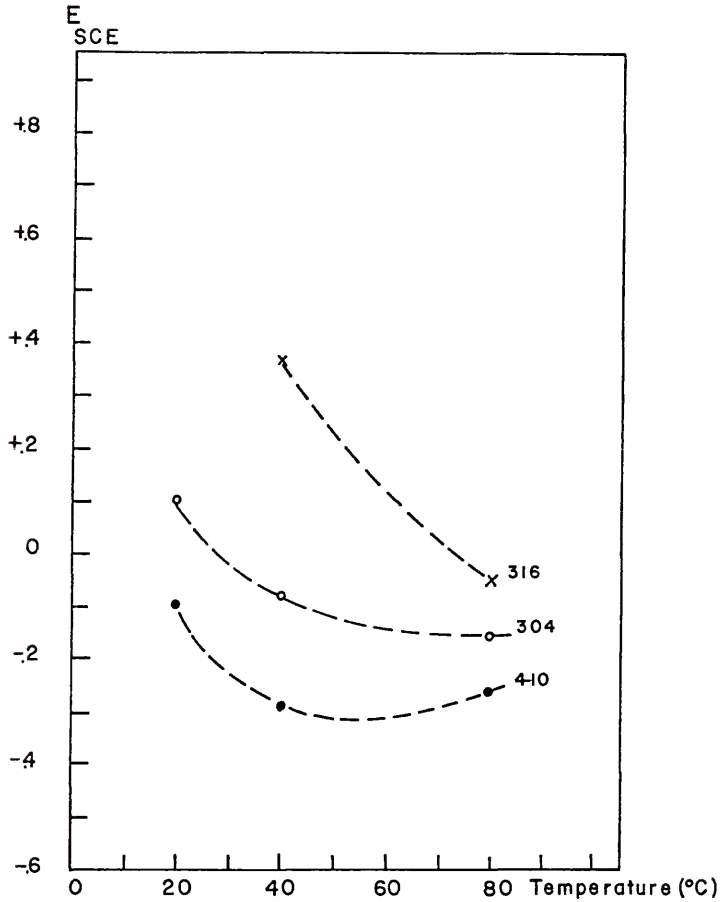


Figure 5. Effect of temperature on the "protection potential" for Types 410, 304 and 316 stainless steels in 0.1 M NaCl + 0.1 M $NaHCO_3$, N_2 -saturated solutions [49].

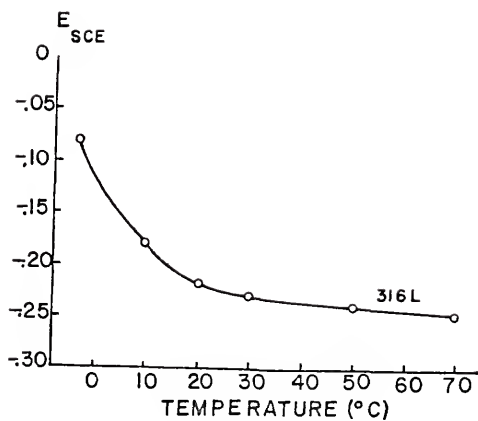


Figure 6. Effect of temperature on the "protection potential" for Type 316L stainless steel in stagnant 0.88 N NaCl solutions [155, p. 5].

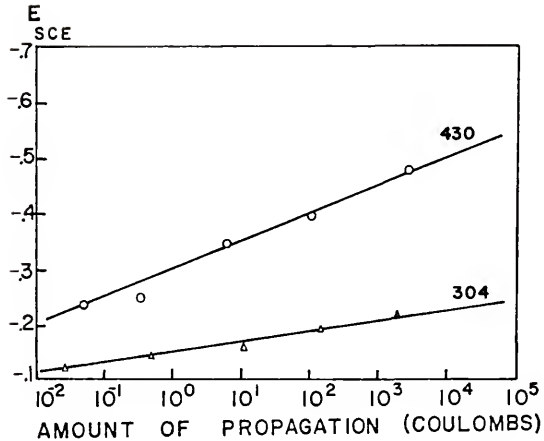


Figure 7. Effect of extent of propagation on the "protection potential" for Types 430 and 304 stainless steels in 1 M NaCl, N₂-saturated solutions at 25°C. Initial specimen area: 5 cm² [88, p. 1980].

kinetics of crevice corrosion appeared to be more rapid than those of pit initiation.

2.7.6 Material Vs. Environmental Property

The "protection potential" has apparently not been established as either a material property or as an environmental property. Some authors [3, 27, 54, 153, 154, 155], although admitting the "protection potential" might be somewhat dependent on both material and environment, considered it to be potentially more useful than the rupture potential

(which was strongly dependent on environmental variables) in predicting "safe" electrochemical potential ranges for ferrous alloys and stainless steels in chloride solutions.

Other authors [31, 162, 117] considered the "protection potential" to be unreliable. Leckie and Uhlig expressed the opinion that the "repassivation" of active pits would depend

...on accidental favorable geometry of the pit cavities and a stirring rate high enough to mix electrolyte inside the pits with electrolyte outside. [31, p. 1267]

Pessall and Lui [163] tried to show that a true critical pitting potential fell between the rupture potential and the "protection potential."

Pickering [162] considered the "protection potential" to be unpredictable due to the constant egress of H_2 gas bubbles from active pits and crevices. Wilde went a step further and concluded that the "protection potential" was not a material property and that it varied

...in magnitude with the experimental conditions used to evaluate it. [117, p. 290]

2.7.7 "Repassivation" Vs. "Deactivation"

A number of authors [31, 36, 125, 163, 164, 117] considered the "protection potential" to involve some sort of "repassivation" process. Other authors [27, 153, 154, 131, 132, 162] considered a "deactivation" process to be operative. By "deactivation" it is meant that the sample potential is lowered (made more active) enough to cause it to become thermodynamically immune to corrosion (i.e., a form of cathodic protection).

Pourbaix has interpreted the "protection potential" as being

...approximately equal to (or better slightly higher than) the potential...inside these pits. [27, p. 432]

This appears to be equivalent to saying that the "protection potential" is approximately equal to an instantaneous mixed potential involving active metal dissolution and H_2 gas evolution inside active pits (implying a "deactivation" mechanism).

2.7.8 Experimental Correlation

Wilde and Williams [88] were able to obtain a linear correlation between a "difference potential" (rupture potential minus "protection potential") as measured in the laboratory and weight loss of stainless steel alloys exposed to sea water. Their results are given in Figure 8, although no definite theoretical basis is available at the present time.

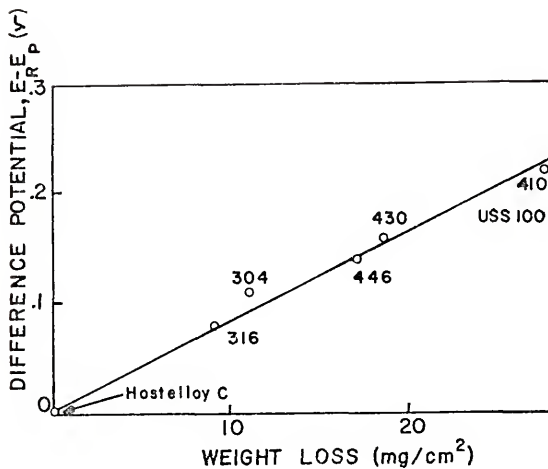


Figure 8. Correlation between the "difference potential" ($E_R - E_P$) and corrosion weight loss of stainless steel alloys exposed in sea water for 4.25 years. The "difference potentials" were determined in 3.5 wt. % NaCl, air-saturated solutions at 25°C [88, p. 1978].

CHAPTER 3
EXPERIMENTAL PROCEDURE

The standard electrochemical polarization cell, described in Appendix 2, was modified (by drilling an additional hole in the Teflon^{*} lid) to permit the insertion of a combination glass/Ag-AgCl pH electrode into the cell when desirable. Sample preparation and mounting techniques are discussed in Appendix 3. Electrolyte compositions are given in Appendix 4. The vacuum deaeration of electrolytes is discussed in Appendix 5. A list of equipment is given in Appendix 6.

3.1 Potentiostatic Polarization Experiments

Potentiostatic polarization experiments were conducted in the standard corrosion cell described in Appendix 2. Applied potentials were measured with an electrometer or with an electrometer/digital voltmeter combination. Applied currents were measured with an ammeter incorporated into the potentiostat or with an electrometer (ammeter mode).

When desired a burette was put in place of the thermometer in the cell lid so that solutions could be introduced into the cell during the course of an experiment. The duration of the experiments ranged from a few minutes to a few days.

3.2 Potentiokinetic Polarization Experiments

Potentiokinetic polarization experiments were conducted in

* Trade name of E. I. DuPont de Nemours Co., Inc.

the standard corrosion cell described in Appendix 2. The technique, the basic theories involved and the equipment have been discussed previously [27, 157, 55, 153, 154]. The equipment is shown schematically in Figure 9, and listed in Appendix 6.

The scanning potentiostat applies a continuously varying potential to the sample over a preset range. The differential amplifier isolates the potentiostat from the recording equipment and eliminates ground loops. The logarithmic converter allows the applied current to be plotted as a logarithm on the x-axis of the x-y recorder, while the applied sample potential is plotted linearly on the y-axis. An automatic step-switching apparatus [165] extends the range of the logarithmic converter and allows the continuous recording of applied currents from 5×10^{-8} to 10 a. The low-pass RC filter, consisting of a 100 μf capacitor in parallel with a 25 $\text{k}\Omega$ potentiometer adjusted to 10 $\text{k}\Omega$, reduces the electrical noise in the system to negligible values.

The effects of polarization scan rate have been discussed elsewhere [3, 12, 55]. It was concluded that although current densities varied with scan rate, characteristic potentials remained nearly the same. Figure 10 shows potentiokinetic polarization curves determined at three different scan rates for the Fe-12% Cr alloy used in this investigation [55]. The scan rates employed in this investigation ranged from 2,000 to 4,000 mv/hr.

3.3 Galvanostatic Polarization Experiments

Galvanostatic polarization experiments were conducted in the

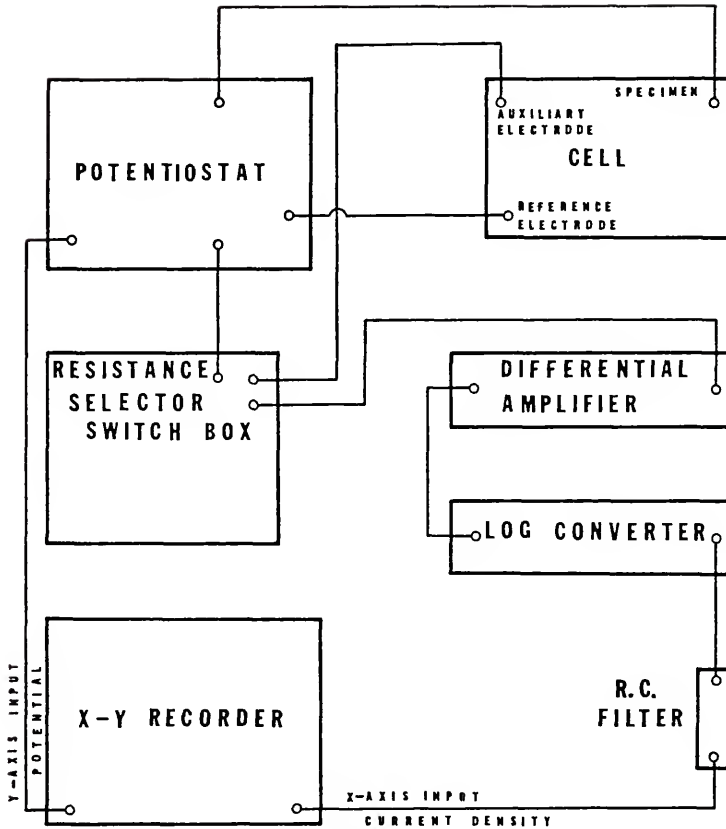


Figure 9. Schematic diagram of equipment used to potentiokinetically polarize specimen and record current density as a function of potential.

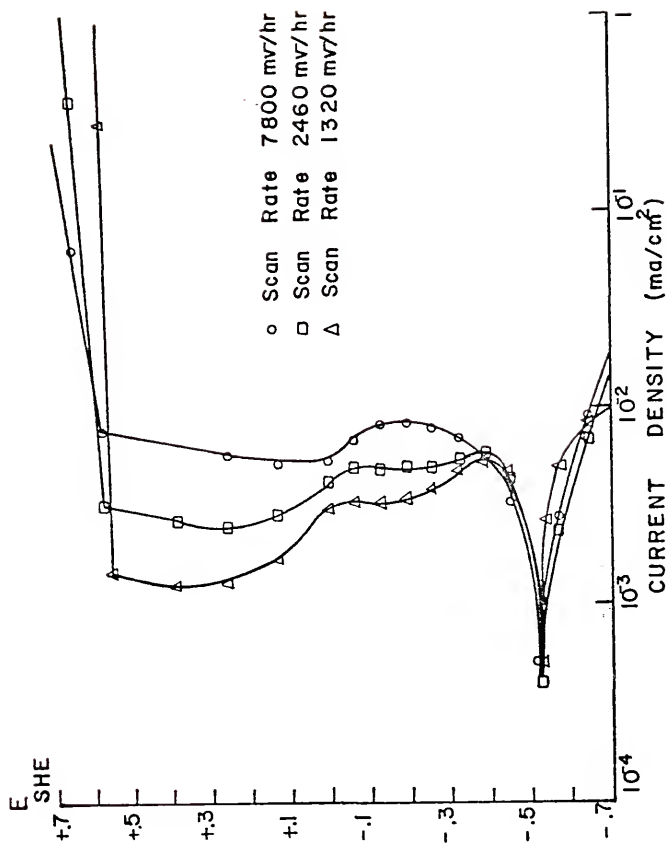


Figure 10. Effect of scan rate on potentiokinetic polarization curves for the Fe-12% Cr alloy in 0.1 M NaCl + 0.1 M NaHCO₃, H₂-saturated solutions (pH 8.7) at 25°C [55, p. 39].

standard corrosion cell described in Appendix 2. The potentiostat was converted into a galvanostat by the use of appropriate precision resistors. Resulting sample potentials were monitored with an electrometer in conjunction with an x-time recorder, or with an oscilloscope.

A schematic diagram of the equipment is shown in Figure 11. The procedure was to apply a constant current to the sample for a predetermined time. The product of the current and the time gives the net electrical charge passed during the experiment. After the time had elapsed, the applied current was stopped by removing the electrical contact to the auxiliary (Pt) electrode. The increase or decay of the sample potential was monitored as a function of time.

3.4 Artificial Occluded Cell Experiments

3.4.1 First Type

The first type of artificial occluded cell consisted of a specially recessed sample combined with a modified sample holder, shown in Figure 12.

A 1/4-in. diameter end mill was used to recess the sample, allowing a glass-enclosed Ag-AgCl electrode* to be placed inside. The opposite (exposed) side of the sample was surface ground to a thickness of 0.030 in. A number 80 wire drill (0.0132 in. in diameter) was used to drill a hole in the center of the exposed side of the sample, thus

*The Ag-AgCl electrodes were prepared by chloridizing exposed cross sections of 0.051 in. diameter Ag wire in 0.1 N HCl, according to [166, p. 205].

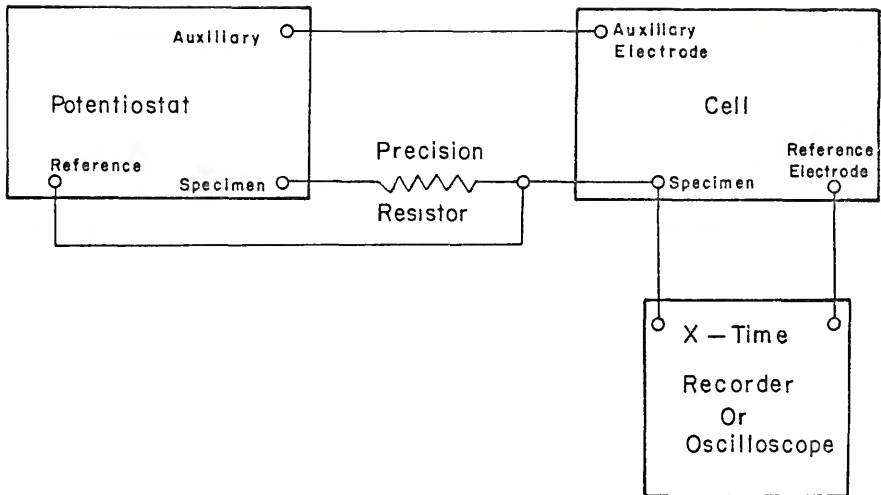


Figure 11. Schematic diagram of equipment used to galvanostatically polarize sample and record resulting potential as a function of time.

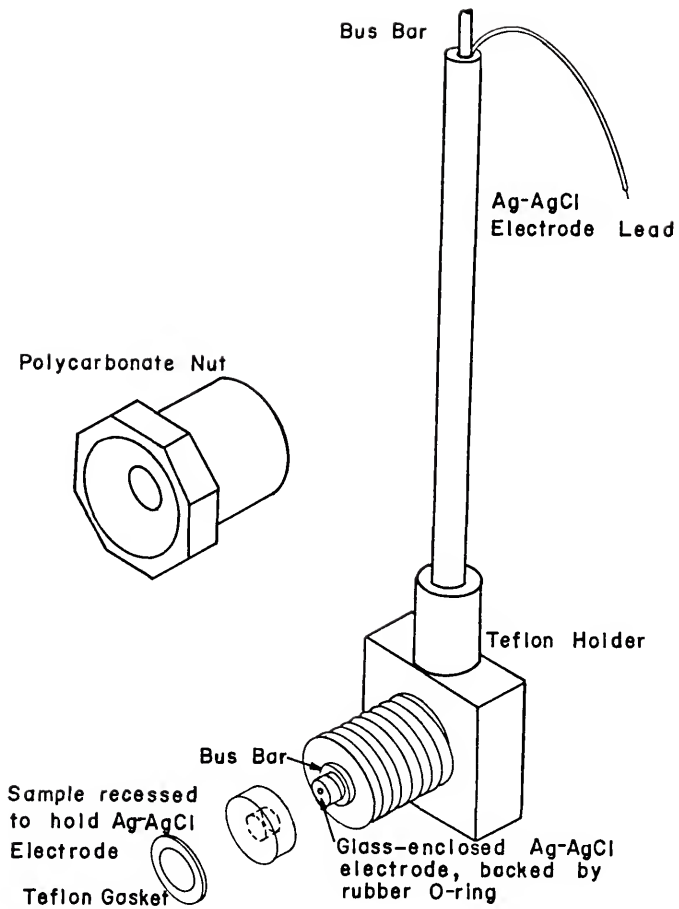


Figure 12. Modified sample and sample holder for first type of artificial occluded cell used during this investigation.

forming a cylindrical artificial pit 0.0132 in. in diameter and 0.030 in. in length.

The modified sample and sample holder were used in conjunction with the standard corrosion cell described in Appendix 2. A schematic diagram of the equipment is shown in Figure 13.

The modified samples were potentiostated in the normal way while the potential of the Ag-AgCl electrode (which was in contact with the solution at the base of the artificial pit) was monitored with respect to the saturated calomel reference electrode. In addition, either applied potential (with respect to SCE) vs. Ag-AgCl electrode potential (also with respect to SCE) or applied current vs. Ag-AgCl electrode potential (with respect to SCE) could be plotted on an x-y recorder.

3.4.2 Second Type

The second type of artificial occluded cell, similar to one used by Pourbaix [129, 27], developed by Efird [130], is presented schematically in Figure 14.

The special cell is constructed of Pyrex* glass and consists of large and small compartments, each containing the same solution initially, separated by a fritted glass disc. The large or bulk compartment contains similar parts to those contained in the standard cell described in Appendix 2. The small or artificial occluded cell

*Trade name of Corning Glass Works.

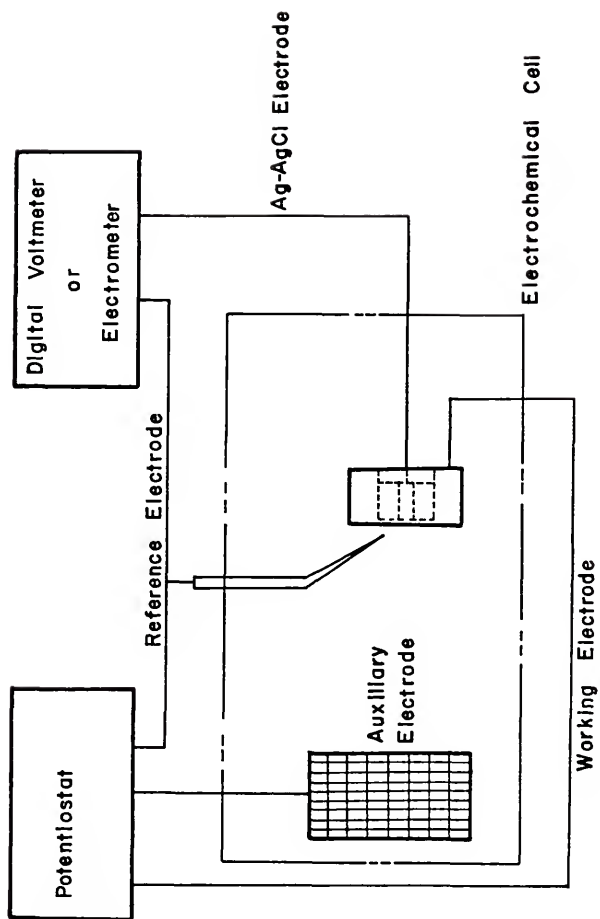


Figure 13. Schematic diagram of equipment used for first type of artificial occluded cell.

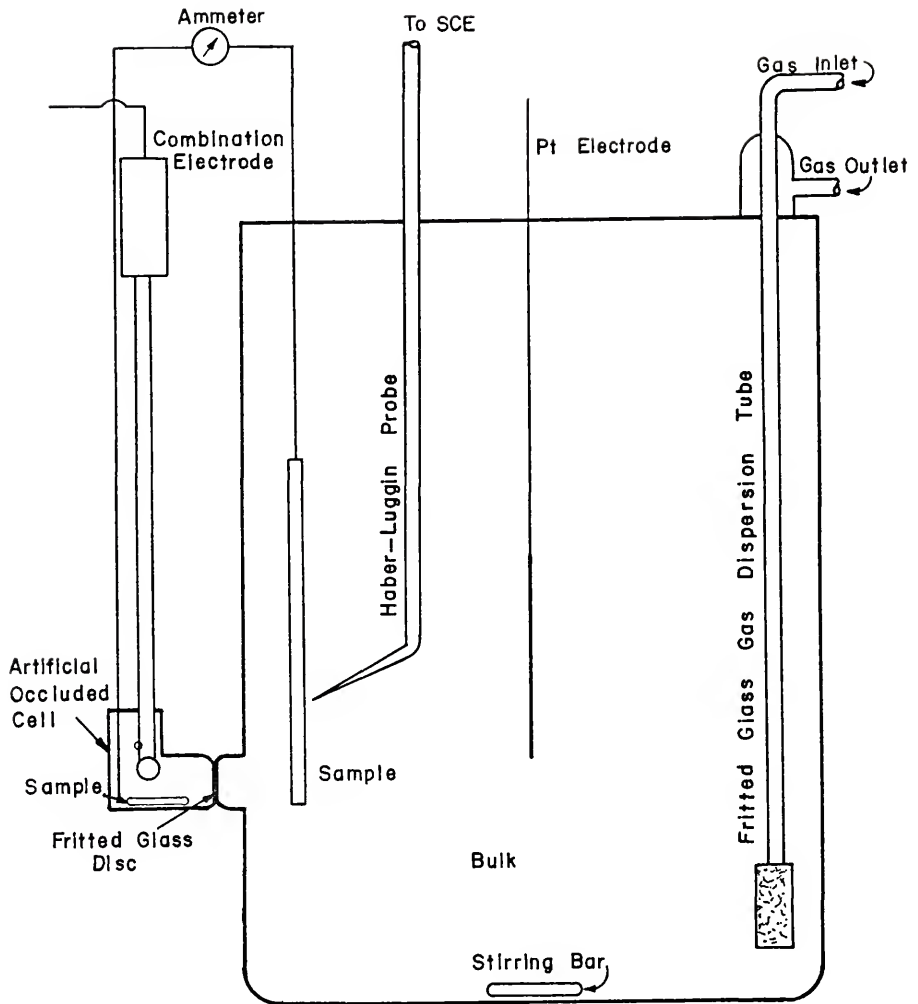


Figure 14. Second type of artificial occluded cell used during this investigation [130, p. 31].

compartment, sealed with a rubber stopper, contains a combination glass/Ag-AgCl pH electrode. An electrical schematic is shown in Figure 15 [130].

A sample is placed in each compartment and the two samples are connected electrically. The large (bulk) samples are approximately 3 cm^2 in area and the small (occluded cell) samples are approximately 0.5 cm^2 in area. The potential is controlled potentiostatically in the large compartment. When corrosion of the sample in the small compartment occurs, the composition of the solution inside changes as it might in an actual occluded cell. The time required to reach steady-state for the Fe - 12% Cr alloy varies from a few days to nearly a week.

A schematic diagram of the equipment is shown in Figure 16. During the course of an experiment the potential, pH and current of the artificial occluded cell are monitored. The total applied current and the bulk electrode current are also monitored. Currents are measured with an electrometer (ammeter mode) or with a zero-impedance ammeter, a brief description of which is given in Appendix 7.

After the experiment has been concluded, the final artificial occluded cell solution is analyzed for iron and chromium concentration by atomic absorption spectrophotometric analysis and for chloride concentration by potentiometric AgNO_3 titration [167, pp. 372-374].

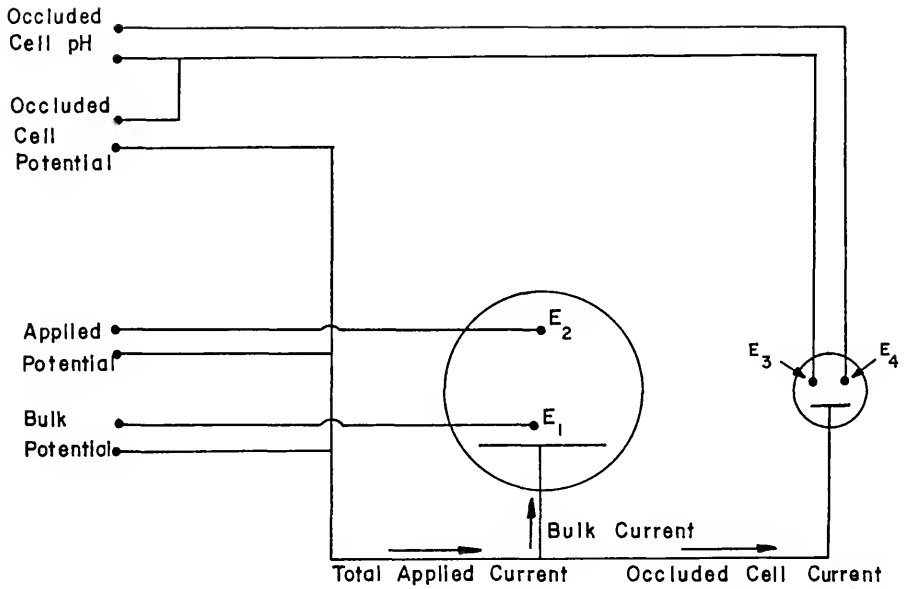


Figure 15. Electrical schematic diagram for the second type of artificial occluded cell [130, p. 32].

E_1 = saturated calomel electrode (SCE)

E_2 = Pt auxiliary electrode

E_3 = Ag-AgCl electrode (SSC)

E_4 = glass electrode

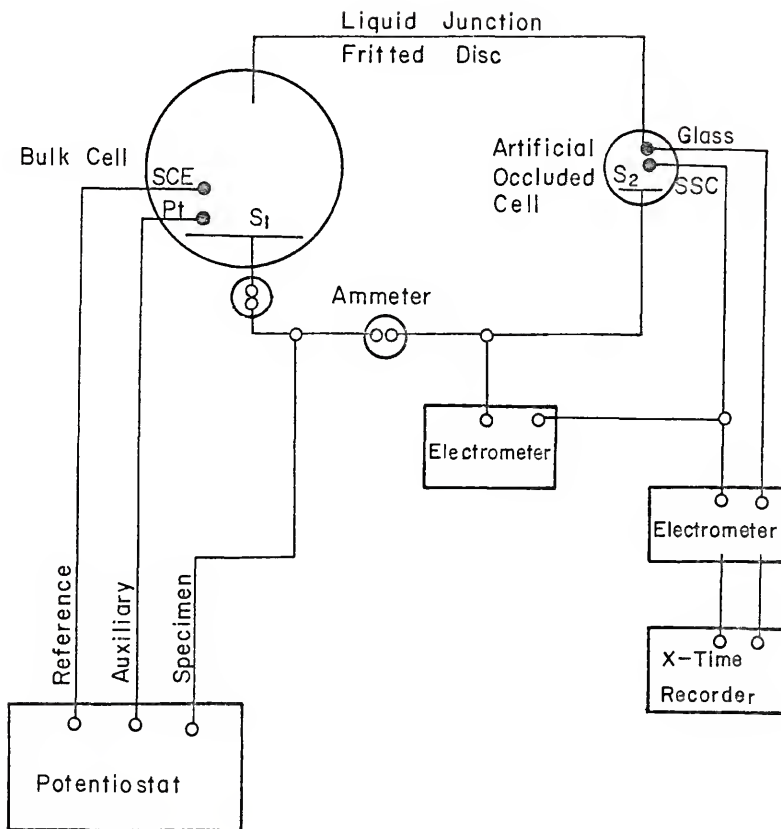


Figure 16. Schematic diagram of equipment used for second type of artificial occluded cell. S_1 and S_2 are the bulk and artificial occluded cell samples, respectively.

CHAPTER 4

RESULTS AND DISCUSSION

4.1 Potentiokinetic Polarization Results

Figures 17a and 17b show schematically the development of experimental potential vs. pH diagrams for Armco* Fe from cyclic [107] potentiokinetic polarization curves, according to Pourbaix [27]. Figure 18 shows experimental potential vs. pH diagrams for the series of Fe-Cr alloys under investigation in 0.1 M Cl^- , H_2 -saturated solutions, as reported by Cusumano [55]. Figure 19 shows schematically some typical cyclic potentiokinetic polarization curves used to obtain the diagrams shown in Figure 18.

Figure 20 presents experimental potential vs. pH diagrams for the Fe - 12% Cr alloy in 0.1 M Cl^- , H_2 -saturated and O_2 -saturated solutions. Figure 21, a schematic version of Figure 20, shows potential/pH regions of immunity, corrosion, passivation and pitting. The data are given in Appendix 8.

There may be some expansion of the passive region at low pH's in O_2 -saturated solutions. As mentioned in Section 2.5.1.4, there is evidence that rupture potentials may be higher (more noble) in O_2 -saturated solutions than in H_2 -saturated solutions.

Figures 22a and 22b are schematic representations of two types of cyclic potentiokinetic polarization curves observed for the Fe - 12%

* Armco Steel Corp., Middletown, Ohio.

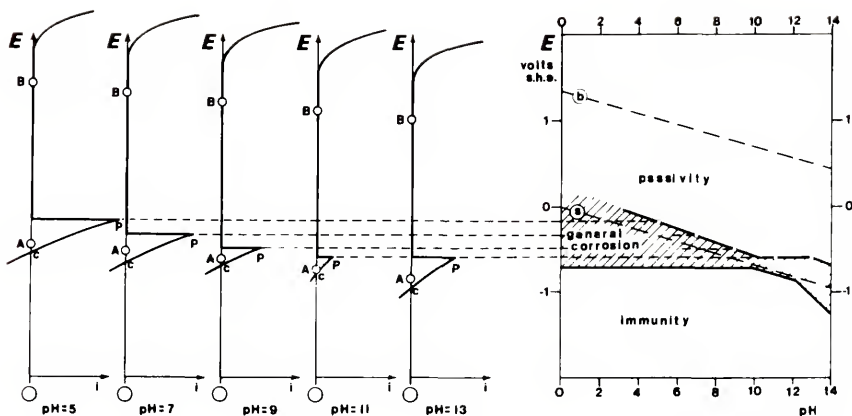


Figure 17a. Schematic diagram for the development of an experimental potential vs. pH diagram for iron in chloride-free, N_2 -saturated solutions [27, p. 431]. The "a" and "b" dashed lines represent the equilibrium hydrogen and oxygen electrodes, respectively.

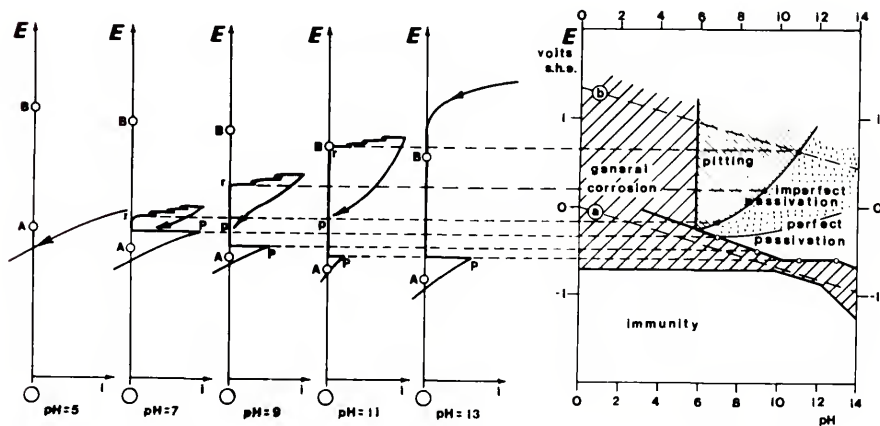


Figure 17b. Schematic diagram for the development of an experimental potential vs. pH diagram for iron in $0.01 M Cl^-$, N_2 -saturated solutions [27, p. 431]. The "a" and "b" lines represent the equilibrium hydrogen and oxygen electrodes, respectively.

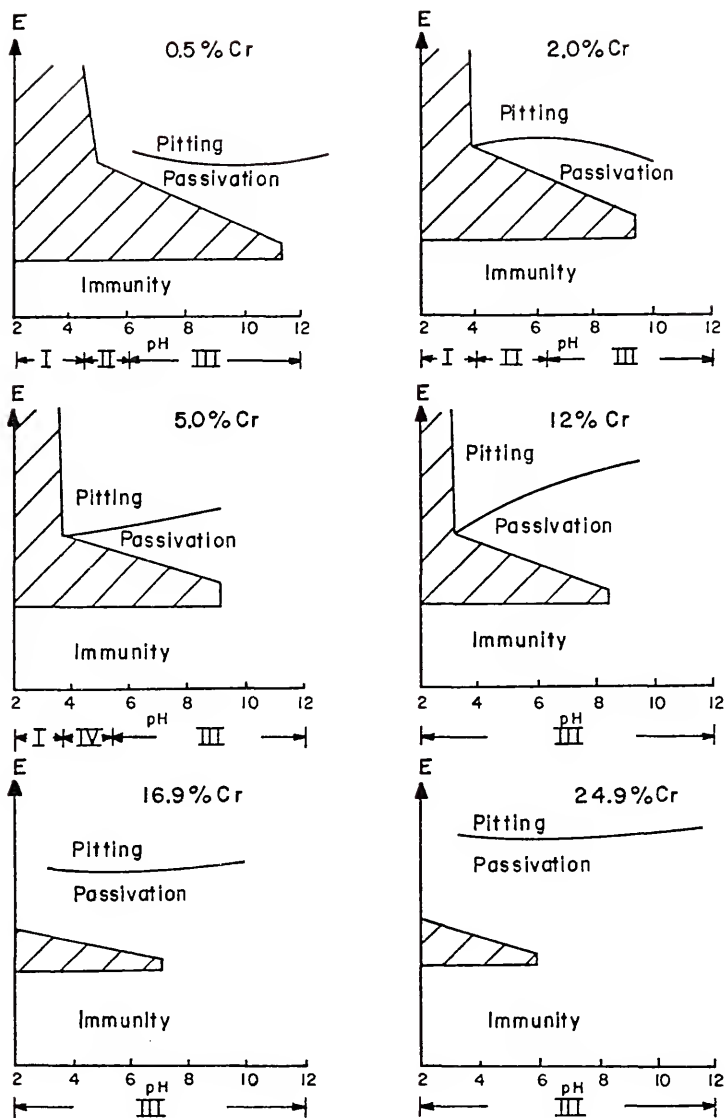


Figure 18. Experimental potential vs. pH diagrams for the series of Fe-Cr alloys under investigation in 0.1 M Cl^- , H_2 -saturated solutions, as reported by Cusumano [55, p. 61]. The cross-hatched areas represent regions of general corrosion.

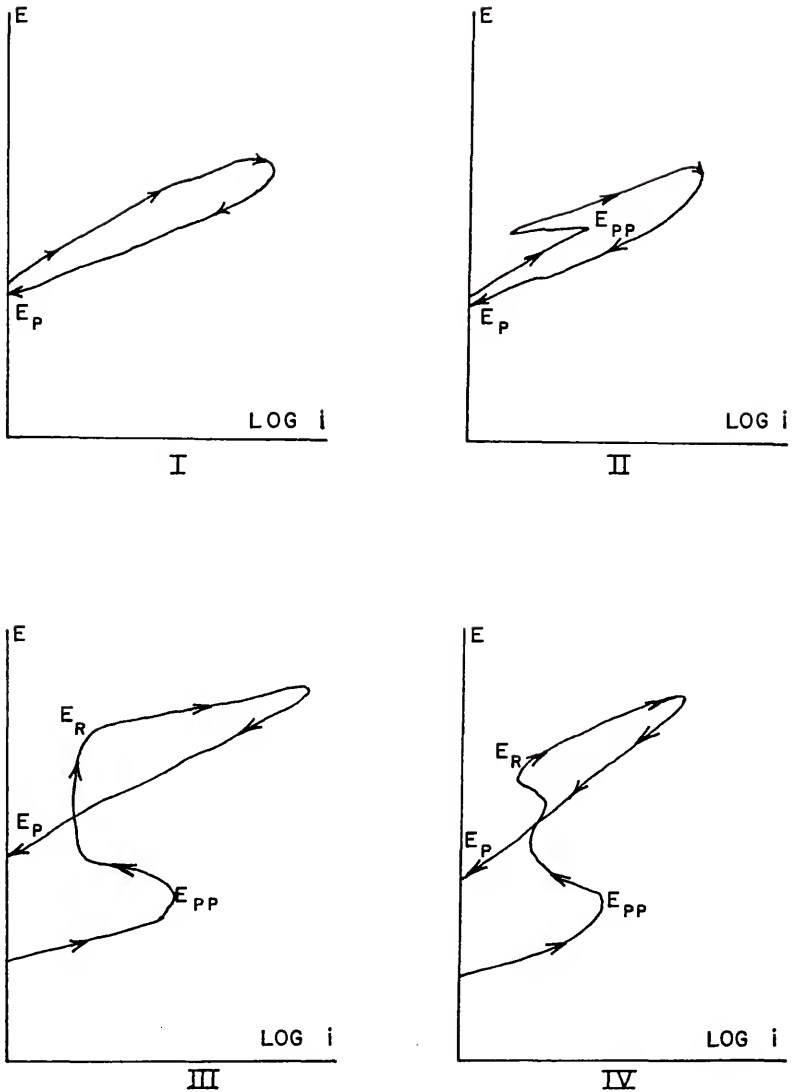


Figure 19. Some typical potentiokinetic polarization curves for the series of Fe-Cr alloys under investigation in 0.1 M Cl^- , H_2 -saturated solutions, according to Cusumano [55, p. 60]. E_{PP} : primary passivation potential, E_R : rupture potential, E_P : "protection potential."

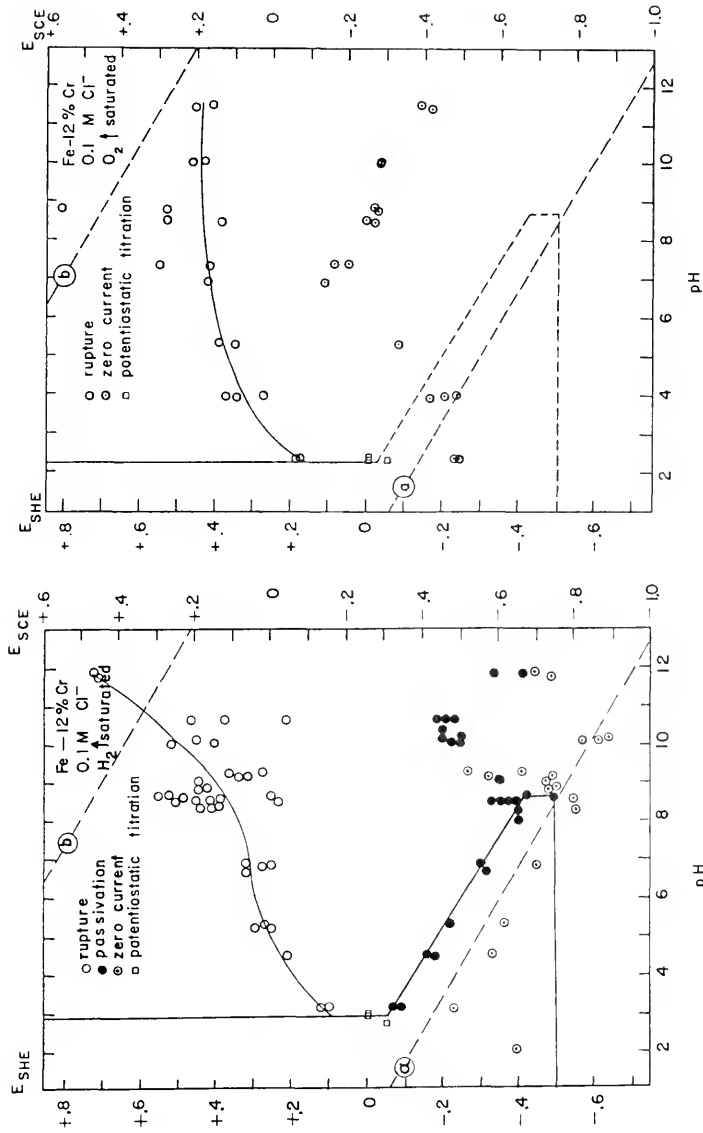


Figure 20. Experimental potential vs. pH diagrams for the Fe - 12% Cr alloy in 0.1 M Cl⁻, H₂-saturated and O₂-saturated solutions.

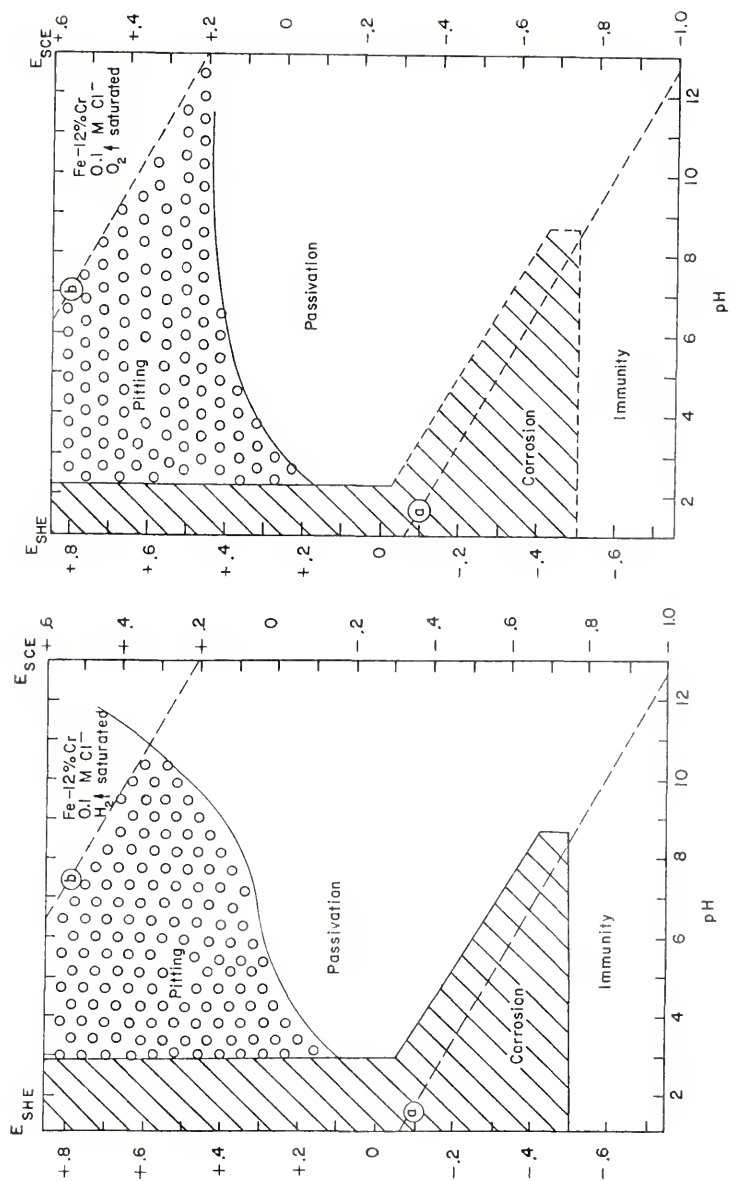


Figure 21. Schematic experimental potential vs. pH diagrams for the Fe - 12% Cr alloy in 0.1 M Cl⁻, H₂-saturated and O₂-saturated solutions.

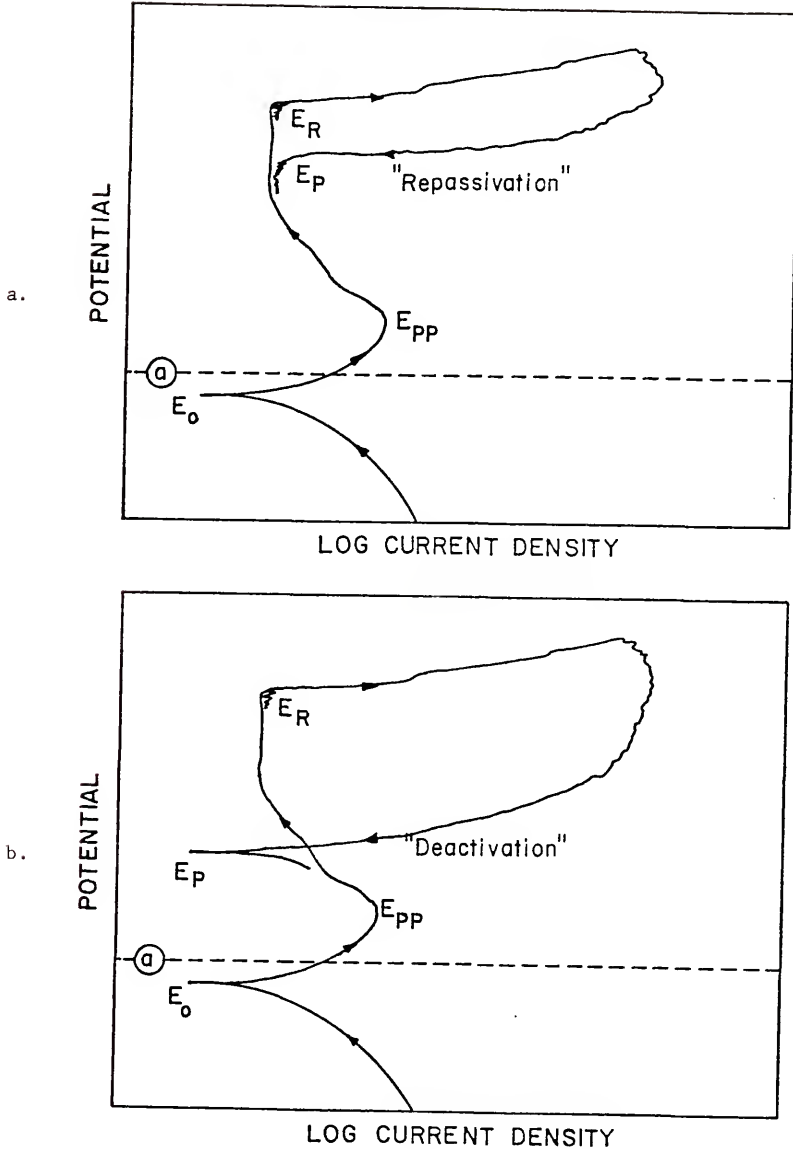


Figure 22. Schematic representation of two types of cyclic potentiokinetic polarization curves observed for the Fe - 12% Cr alloy in Cl^- -containing, H_2 -saturated solutions. E_0 : zero current potential, E_{PP} : primary passivation potential, E_R : rupture potential, E_P : "protection potential."

Cr alloy in Cl^- -containing, H_2 -saturated solutions. These curves exhibit what has been termed "electrochemical hysteresis [154]," since the out scans and the return scans do not coincide.

The features of interest on these curves are the zero current potentials (E_o), the primary passivation potentials (E_{pp}), the rupture or critical pitting potentials (E_R) and the "protection potentials" (E_p). Note that the two types of E_p 's shown are extreme cases of those normally found experimentally.

A sharp "protection potential," like the one exhibited in Figure 22b, is similar to the zero current potential observed for the active metal. However, an active zero current potential falls below the equilibrium hydrogen electrode line (marked "a" in Figures 22a and 22b), indicating an instantaneous mixed potential involving metal dissolution and H_2 gas evolution.

A blunt or smooth "protection potential," like the one shown in Figure 22a, may be indicative of a "repassivation" mechanism. High (noble) values of the "protection potential," above 0 v_{SHE} (more noble than the equilibrium standard hydrogen electrode (SHE)), are almost certainly associated with a "repassivation" mechanism.

Although the occurrence of two types of observed "protection potentials" suggests the possibility of both "repassivation" and "deactivation" mechanisms being operative for this alloy, additional work is needed to verify this point. The terms "deactivation" and "repassivation" were discussed in Section 2.7.7.

Figure 23 contains experimental potential vs. pH diagrams for the series of Fe-Cr alloys in 0.1 M Cl^- , H_2 -saturated solutions,

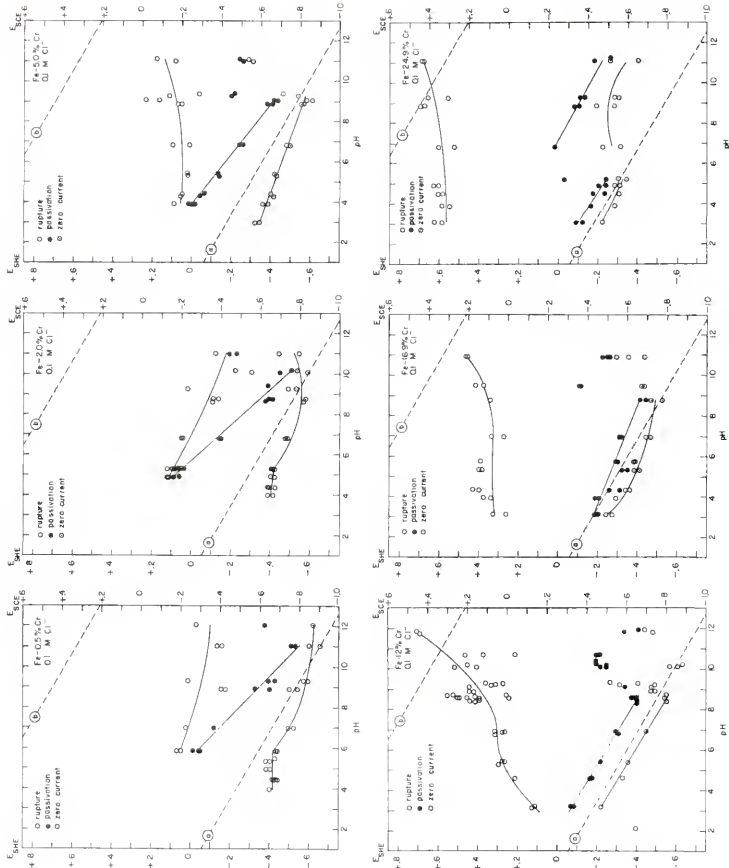


Figure 23. Experimental potential vs. pH diagrams for the series of Fe-Cr alloys in 0.1 M Cl⁻, H₂-saturated solutions, including zero current potentials, primary passivation potentials and rupture potentials.

including zero current potentials, primary passivation potentials and rupture potentials. The individual diagrams and data are included in Appendix 8.

Figure 24 contains "protection potential" (E_p) data, superimposed on the zero current potential, primary passivation potential and rupture potential lines taken from Figure 23. The individual diagrams and data are included in Appendix 8.

4.1.1 Effect of Alloy Composition

The "protection potential" (E_p) data presented in Figure 24 show that the "protection potential" commonly tends to increase (become more noble) with increasing chromium content, in agreement with previous work described in Section 2.7.4.1. The relatively low (active) values of the "protection potential" for the Fe - 0.5% Cr, Fe - 2.0% Cr and Fe - 5.0% Cr alloys suggest that a "deactivation" mechanism may be operative. The relatively high (noble) values of the "protection potential" for the Fe - 16.9% Cr and Fe - 24.9% Cr alloys suggest that a "repassivation" mechanism may be operative. The data for the Fe - 12% Cr alloy suggest transitional behavior.

4.1.2 Effect of Bulk Electrolyte pH

The "protection potential" (E_p) data presented in Figure 24 for the Fe - 0.5% Cr, Fe - 2.0% Cr and Fe - 5.0% Cr alloys show that the "protection potential" decreases (becomes more active) with increasing pH, with a break in the data occurring at about pH 8. The data for pH's up to and including 7 fall in the vicinity of the zero current potential lines, indicative of "deactivation." The data for pH's above 8

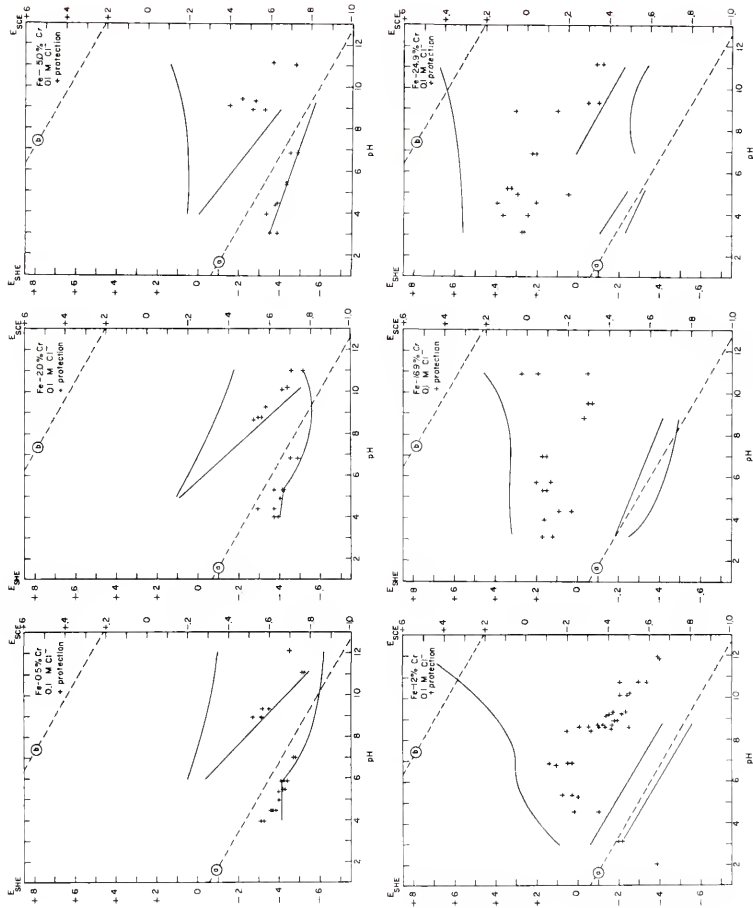


Figure 24. "Protection potential" (E_p) data, superimposed on the zero current potential, primary passivation potential and rupture potential lines taken from Figure 23.

roughly parallel the "a" line. Assuming that hydrolysis occurs within occluded cells (pits or crevices), as discussed in Sections 2.4.2.7 and 2.5.2.6, localized pH changes may account for the break in the data.

The occlusion may be due, in part, to the formation of either Fe_3O_4 [27] or $\text{Fe}(\text{OH})_2$. A white, gelatinous precipitate, thought to be $\text{Fe}(\text{OH})_2$, was sometimes observed to form over active pits on the Fe - 12% Cr alloy in alkaline solutions.

The "protection potential" (E_p) data for the Fe - 16.9% Cr and Fe - 24.9% Cr alloys for pH's up to and including 7 are relatively independent of pH. The data for pH's above 8 are erratic, but may show some tendency to decrease (becoming more active) with increasing pH.

The "protection potential" (E_p) data for the Fe - 12% Cr alloy for pH's up to and including 7 increase (become more noble) with increasing pH. The data for pH's above 8 decrease (become more active) with increasing pH, roughly paralleling the "a" line. The data suggest a "deactivation" mechanism for pH's up to 4.5, a repassivation mechanism for pH's from 4.5 to 9, and again a "deactivation" mechanism for pH's 9 and above.

In order to verify the transitional behavior of the Fe - 12% Cr alloy, special cyclic potentiokinetic polarization scans were conducted. These differed from ordinary potentiokinetic polarization scans in that, immediately after recording the "protection potential" on the return scan, the scan direction was again reversed and a second out scan was made.

According to M. Pourbaix [168], either of two types of behavior might be expected:

- (1) a rapid increase of current density, indicative of active corrosion and a "deactivation" mechanism, or
- (2) little or no increase of current density, indicative of passivity and a "repassivation" mechanism.

Figures 25 and 26 present the results of a series of special cyclic potentiokinetic polarization scans for the Fe - 12% Cr alloy in 0.1 M Cl^- , H_2 -saturated solutions. These results agree partially with earlier conjectures. There appears to be a transition from "deactivation" to "repassivation" between pH 3.2 and 4.4, and a transition from "repassivation" to "deactivation" between pH 9.7 and 10.9. The individual diagrams are included in Appendix 9.

Additional scans made at pH 10.1 (adjusted with 0.1 M NaOH) indicated a deactivation mechanism. Apparently, the pH 8.9 and 9.7 solutions were buffered well enough to help neutralize local acidity and thus aid in "repassivation." It should be noted, however, that it may be possible for a sample to first "deactivate," then quickly "repassivate," giving the appearance of a "repassivation" mechanism.

Figures 27 and 28 present the results of a similar series of special potentiokinetic polarization scans for the Fe - 12% Cr alloy in 0.1 M Cl^- , H_2 -saturated solutions, using samples painted off with Microshield* lacquer. The exposed areas of the samples were approximately 1 cm^2 . Qualitatively, these results appear to be similar to those for sample-holder mounted samples, suggesting that the sample holder, despite its Teflon gasket, does a reasonably good job of minimizing

* Trade name of Michigan Chrome and Chemical Co.

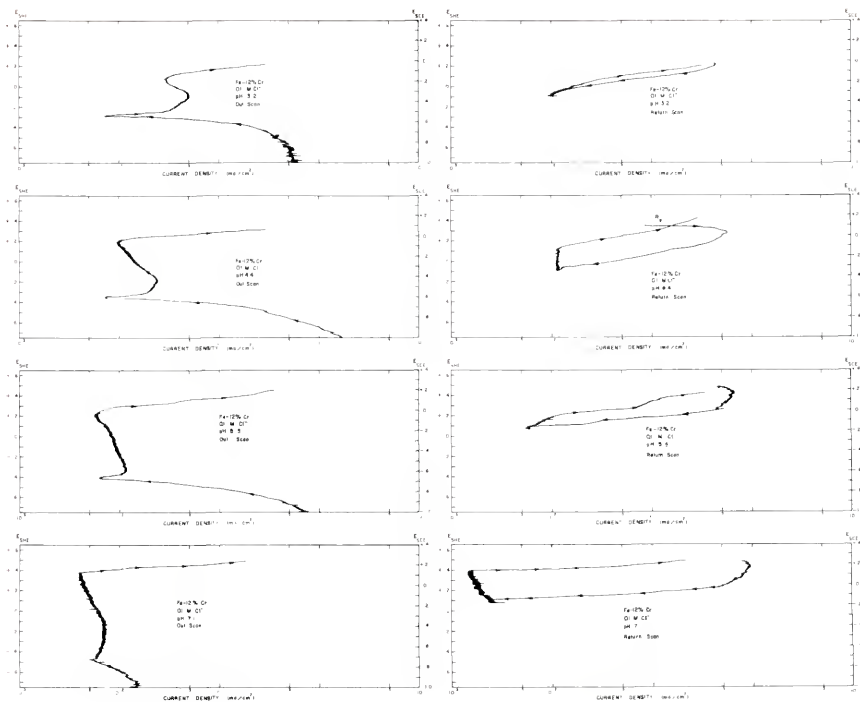


Figure 25. Results of a series of special cyclic potentiokinetic polarization scans for the Fe - 12% Cr alloy in 0.1 M Cl⁻, H₂-saturated solutions of pH 3.2, 4.4, 5.5 and 7.1.

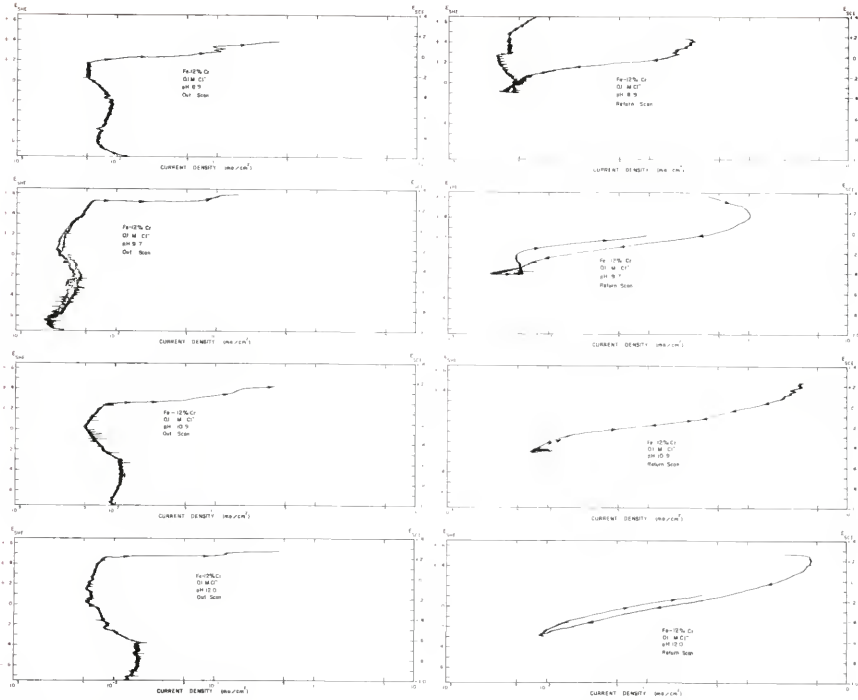


Figure 26. Results of a series of special cyclic potentiokinetic polarization scans for the Fe - 12% Cr alloy in 0.1 M Cl⁻, H₂-saturated solutions of pH 8.9, 9.7, 10.9 and 12.0.

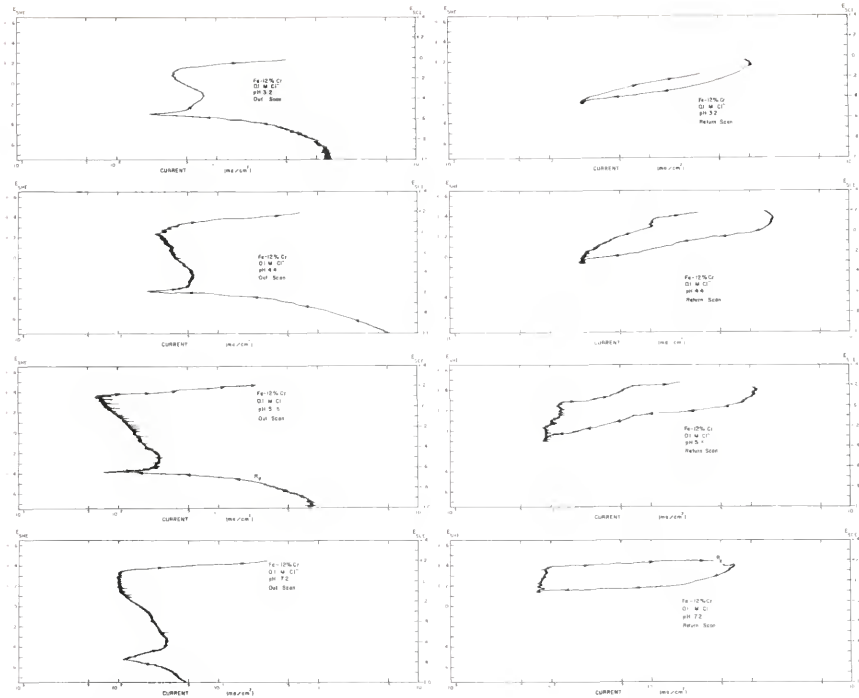


Figure 27. Results of a series of special cyclic potentiokinetic polarization scans for the Fe - 12% Cr alloy in 0.1 M Cl^- , H_2 -saturated solutions of pH 3.2, 4.4, 5.5 and 7.2, using painted-off samples ($\sim 1 \text{ cm}^2$ in area).

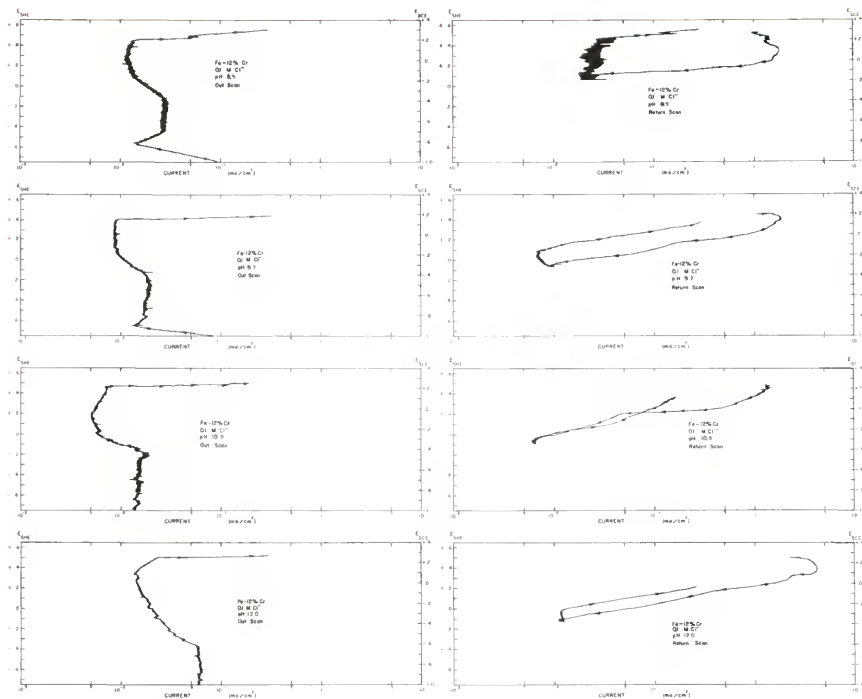


Figure 28. Results of a series of special cyclic potentiokinetic polarization scans for the Fe - 12% Cr alloy in 0.1 M Cl⁻, H₂-saturated solutions of pH 8.9, 9.7, 10.9 and 12.0, using painted-off samples ($\sim 1 \text{ cm}^2$ in area).

crevice effects. The individual diagrams are included in Appendix 10.

4.1.3 Effect of Bulk Electrolyte Chloride Ion Concentration

Figures 29, 30 and 31 contain experimental potential vs. log chloride ion concentration (molarity) diagrams, including zero current potentials, primary passivation potentials and rupture potentials. Figure 29 contains data for the Fe - 0.5% Cr, Fe - 2.0% Cr, Fe - 12% Cr and Fe - 16.9% Cr alloys in H₂-saturated solutions of pH 5.4 to 5.5. Figures 30 and 31 contain data for the same alloys in H₂-saturated solutions of pH 8.7 to 8.8 and 10.8 to 11.0, respectively. The individual diagrams and data are included in Appendix 11.

Figures 32, 33 and 34 contain "protection potential" (E_p) data superimposed on the zero current potential, primary passivation potential and rupture potential lines taken from Figures 29, 30 and 31, respectively. The individual diagrams and data are included in Appendix 11.

It was found that the pH's of the prepared electrolytes were slightly more acidic for concentrated chloride solutions than for dilute chloride solutions. Thus, the calculated equilibrium hydrogen and oxygen electrode lines (marked "a" and "b", respectively) in Figures 29 through 34 curve upward slightly at high chloride ion concentrations.

The "protection potential" (E_p) data presented in Figures 31 through 34 show that the "protection potential" commonly tends to decrease (become more active) with increasing chloride ion concentration, in agreement with some of the previous work cited in Section 2.7.4.3.

For some alloy/electrolyte combinations (high chromium content and/or low chloride ion concentration) no pitting (or crevice corrosion)

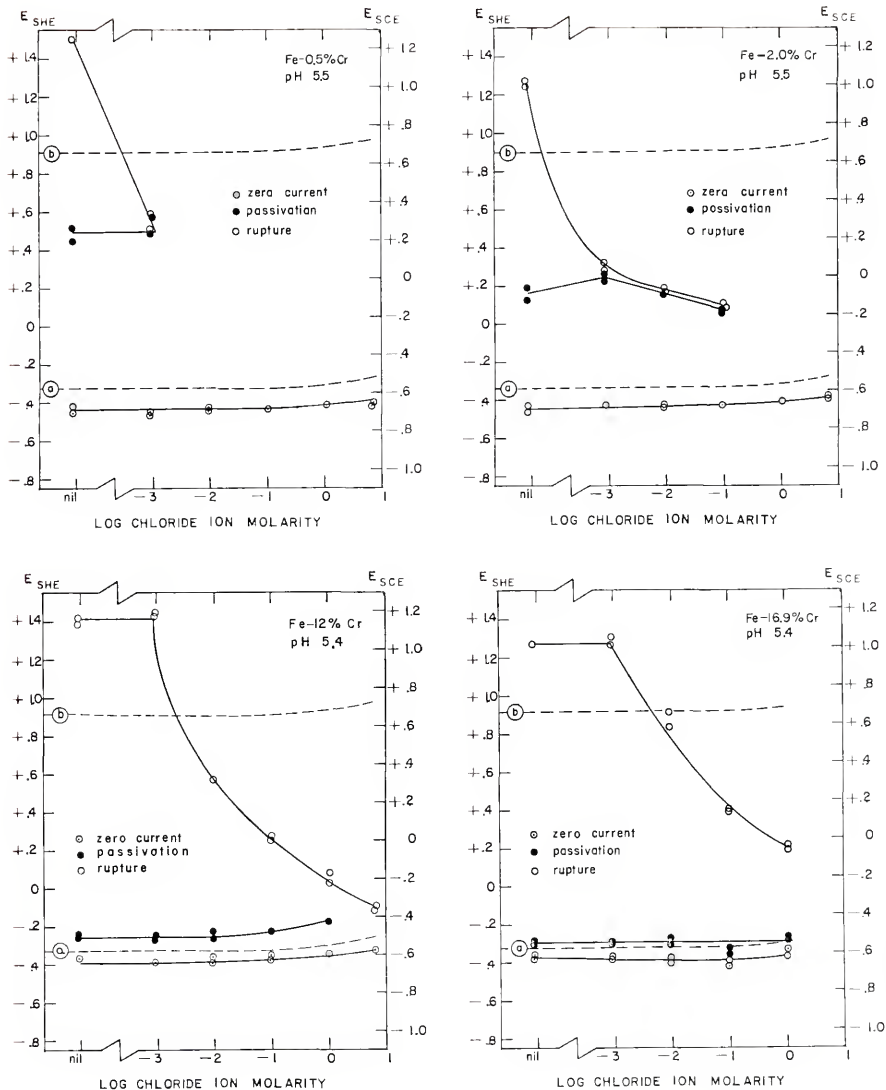


Figure 29. Experimental potential vs. log chloride ion concentration diagrams for four Fe-Cr alloys in H_2 -saturated solutions of pH 5.4 to 5.5, including zero current potentials, primary passivation potentials and rupture potentials.

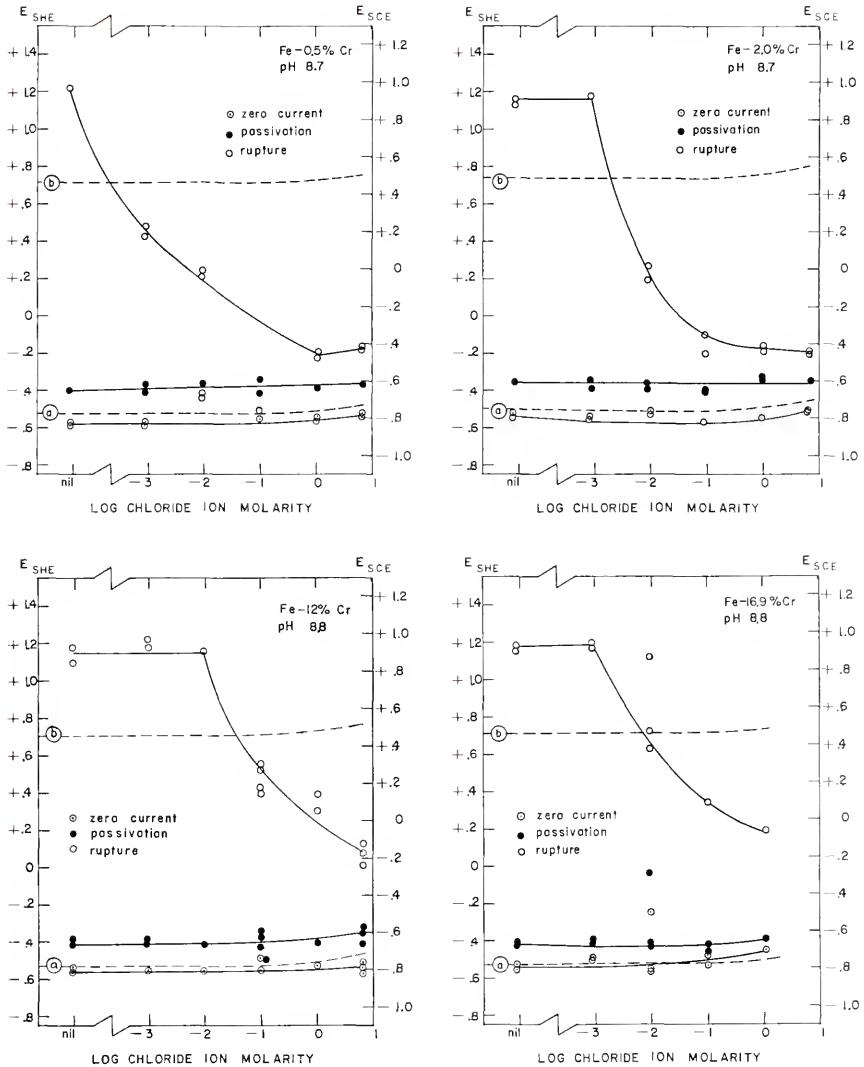


Figure 30. Experimental potential vs. log chloride ion concentration diagrams for four Fe-Cr alloys in H_2 -saturated solutions of pH 8.7 to 8.8, including zero current potentials, primary passivation potentials and rupture potentials.

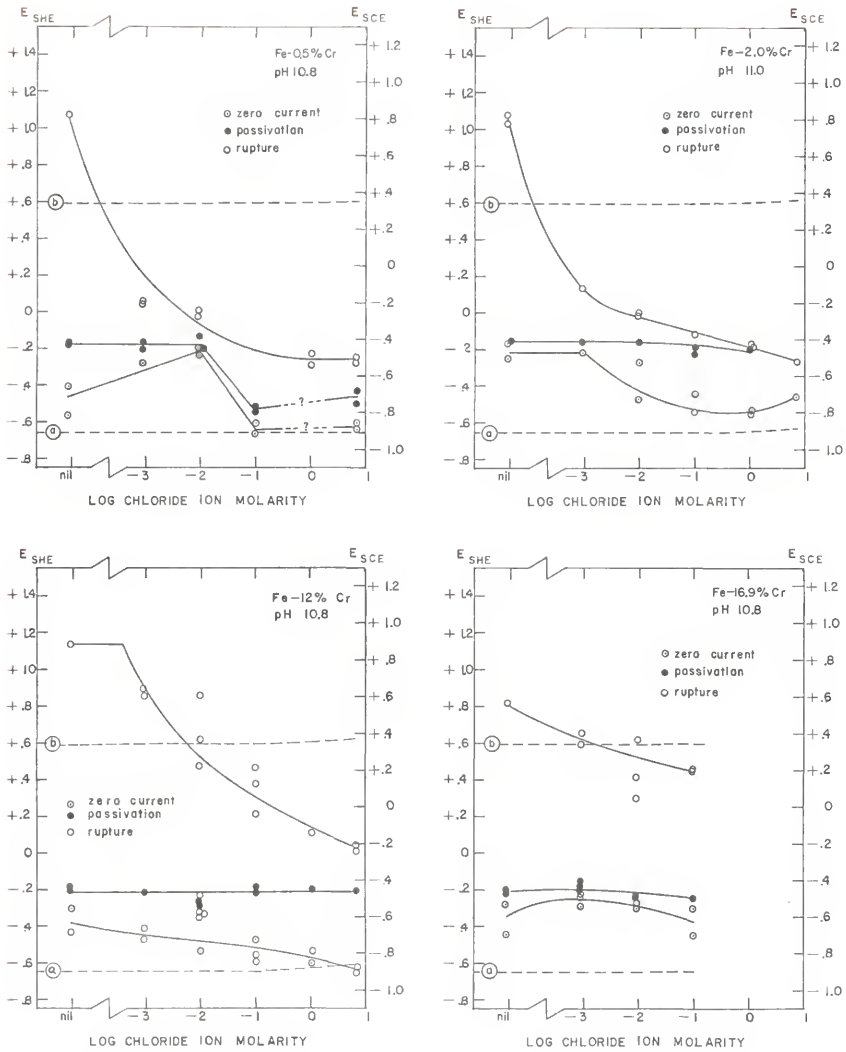


Figure 31. Experimental potential vs. log chloride ion concentration diagrams for four Fe-Cr alloys in H_2 -saturated solutions of pH 10.8 to 11.0, including zero current potentials, primary passivation potentials and rupture potentials.

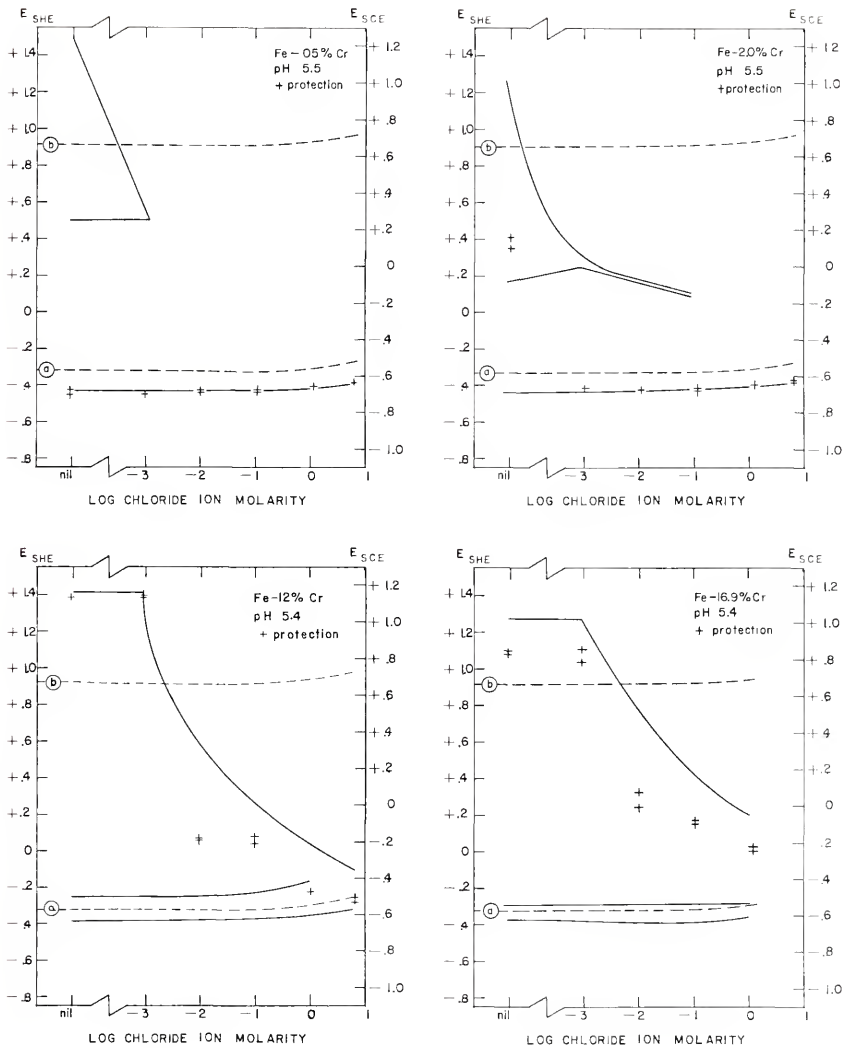


Figure 32. "Protection potential" (E_p) data, superimposed on the zero current potential, primary passivation potential and rupture potential lines taken from Figure 29.

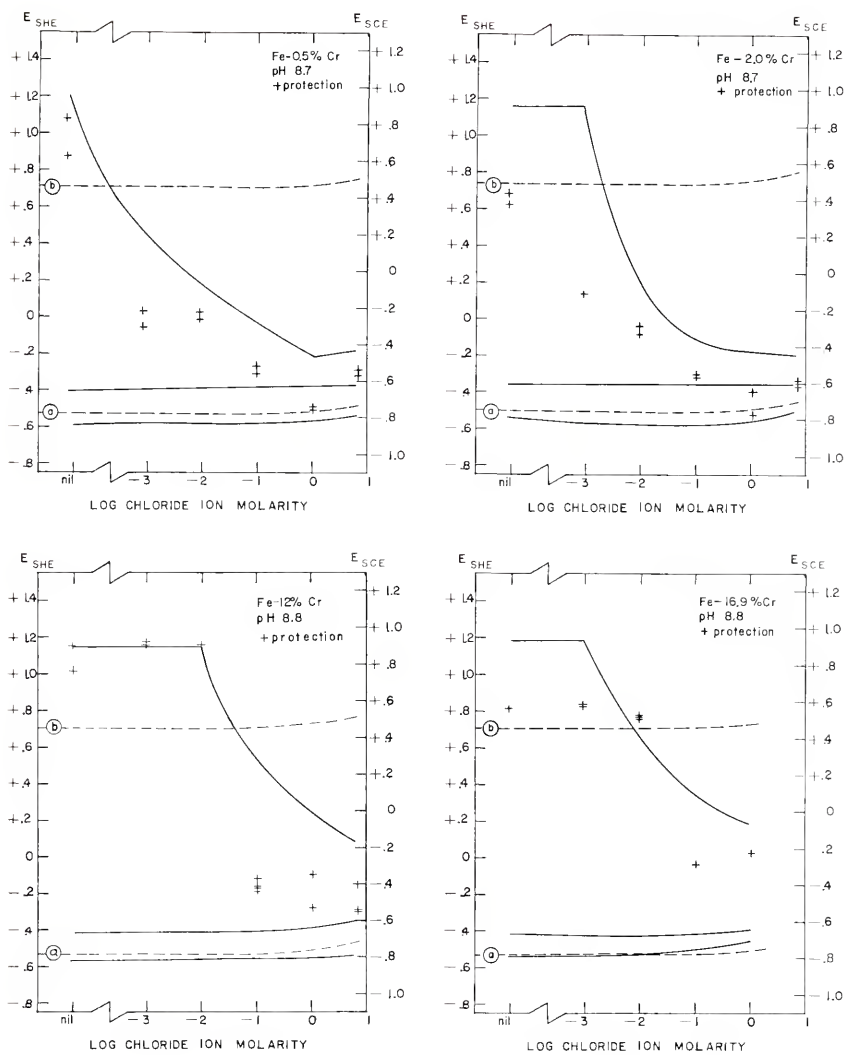


Figure 33. "Protection potential" (E_p) data, superimposed on the zero current potential, primary passivation potential and rupture potential lines taken from Figure 30.

was observed. Strictly speaking, there can be no "protection potential" (against pitting) when no pitting occurs. Under these circumstances the zero current potentials on the return scans were above (more noble) than the "b" line and coincided with the potentials at which currents became significant on the corresponding out scans. These potentials are believed to be related with the O_2 gas evolution reaction [3].

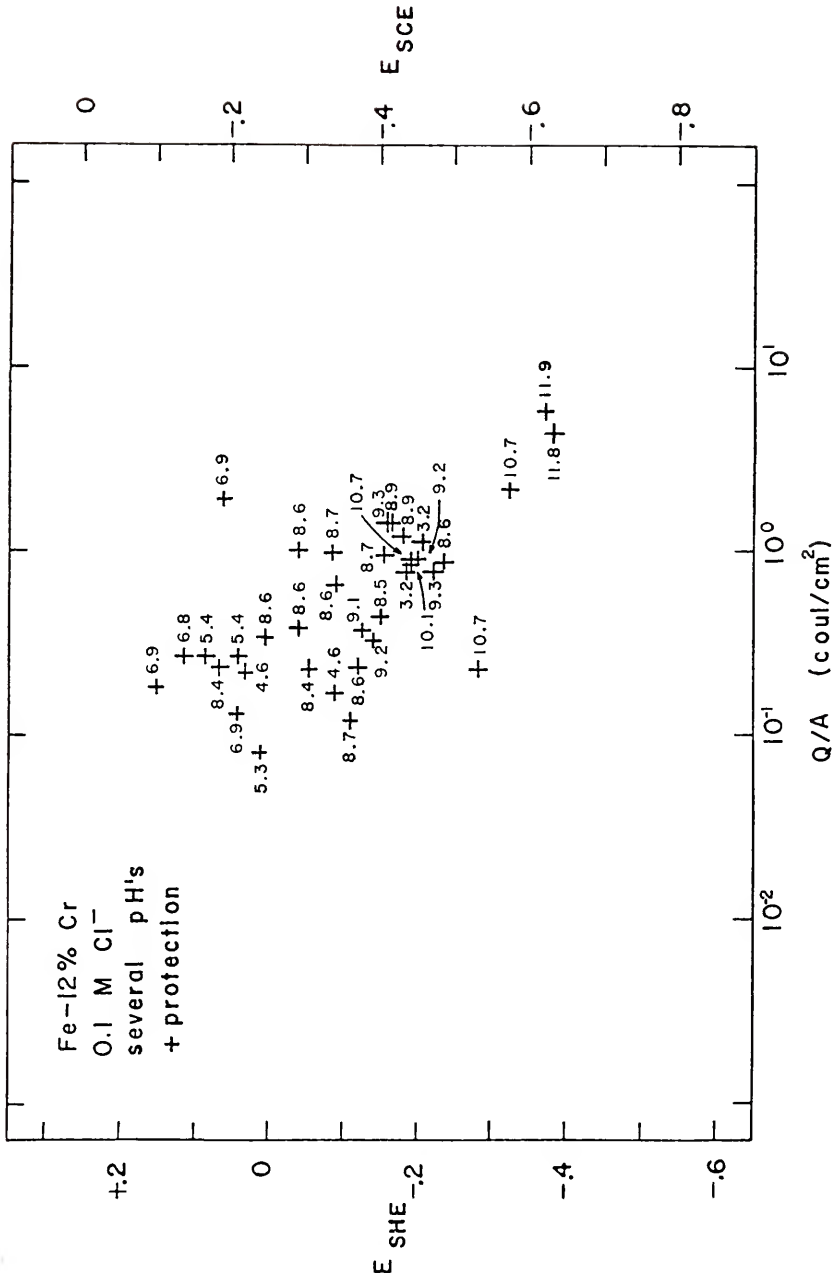
For other alloy/electrolyte combinations (low chromium content and/or high chloride ion concentration) the "protection potentials" are approximately equal to zero current potentials, indicating a "deactivation" mechanism to be operative.

For still other alloy/electrolyte combinations the "protection potentials," while falling below (more active than) the "b" lines, are relatively noble, suggesting that a "repassivation" mechanism may be operative.

4.1.4 Effect of Extent of Propagation

Figure 35 is a plot of the "protection potential" (E_p) vs. total charge passed per unit (original) sample area, Q/A (plotted logarithmically), for the Fe - 12% Cr alloy in 0.1 M Cl^- , H_2 -saturated solutions of indicated pH's. The Q/A values were calculated by integration of cyclic polarization curves between the rupture potential and the "protection potential" for each curve. The data are given in Appendix 8.

This plot serves to show that, although there may be a downward (more active) trend in the "protection potential" with increasing extent of propagation, the extent of propagation variable does not appear to overshadow the pH variable.



Figures 36a, b and c deal with the effect of the extent of propagation on the "protection potential" for the Fe - 12% Cr alloy in 0.1 M Cl^- , H_2 -saturated solutions of pH approximately 10.1. The three figures were drawn using data obtained from one set of nine samples. The data are given in Table 3.

Figure 36a is a plot of the "protection potential" (E_p) vs. total charge passed per unit (original) sample area, Q/A (plotted logarithmically) as determined by integration of cyclic potentiokinetic polarization curves. Experimentally, the extent of propagation was increased by allowing the scans to proceed to higher (more noble) potentials after the onset of pitting before reversing the scan direction for the return scan.

The data indicate that the "protection potential" (E_p) decreases (becomes more active) with increasing extent of propagation, in agreement with previous work for other alloys discussed in Section 2.7.4.5, except that a break in the data occurs for the Fe - 12% Cr alloy.

The dual points in Figures 36a, b and c, recording the occurrence of both types of "protection potentials" (blunt and sharp) on a single return scan, are believed indicative of transitional behavior. The data suggest the possibility that a "repassivation" mechanism is operative for small Q/A values, a "deactivation" for large Q/A values and a combination of both mechanisms for intermediate Q/A values.

Figure 36b is a plot of the "protection potential" (E_p) vs. pit density (number of pits divided by original sample area). The number of pits for each (except the KS-169) sample was determined by counting, using a hand-held magnifying glass. The number of pits on the KS-169

- Figure 36. a. Plot of "protection potential" (E_p) data vs. total charge passed per unit (original) sample area, Q/A (plotted logarithmically) for the Fe - 12% Cr alloy in 0.1 M Cl^- , H_2 -saturated solutions of pH approximately 10.1.
- b. Plot of "protection potential" (E_p) data vs. pit density (number of pits divided by original sample area).
- c. Plot of "protection potential" (E_p) data vs. active area fraction, A_A (pitted plus creviced area divided by original sample area). Points connected by a line represent a single sample.

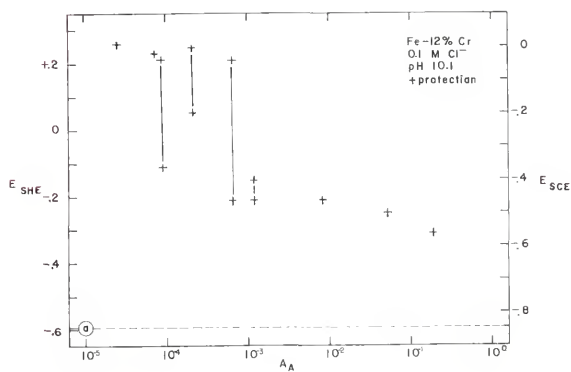
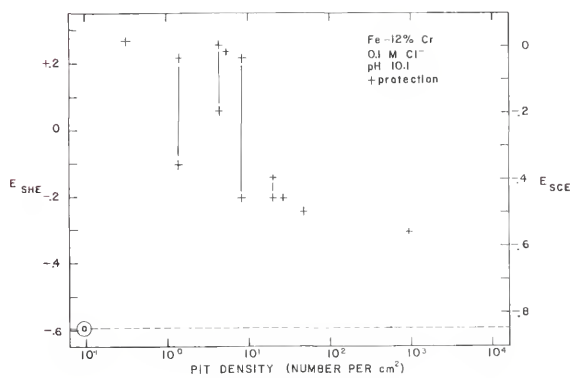
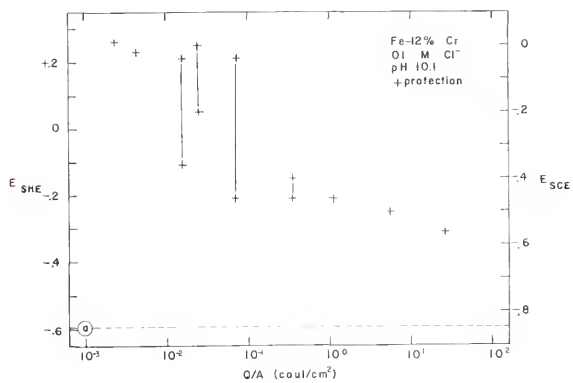


TABLE 3

EXTENT OF PROPAGATION DATA FOR THE Fe - 12% Cr ALLOY
IN 0.1 M Cl^- , H_2 -SATURATED SOLUTIONS OF pH APPROXIMATELY 10.1

(Original Sample Areas = 2.5 - 2.9 cm^2)

<u>Run No.</u>	<u>"Protection Potential" (v_{SCE})</u>	<u>Q/A (coul/cm²)</u>	<u>Pit Density (No. per cm²)</u>	<u>A_A (cm²/cm²)</u>
KS-164	+0.010	0.00265	0.346	0.0000281
KS-166	-0.020	0.00457	5.19	0.0000775
KS-172	-0.040 -0.360	0.0176	1.38	0.0000917
KS-167	0.000 -0.200	0.0271	4.30	0.000223
KS-173	-0.040 -0.460	0.0755	8.65	0.000678
KS-170	-0.400 -0.460	0.371	20.6	0.00117
KS-168	-0.460	1.16	27.6	0.00746
KS-171	-0.500	6.37	48.6	0.0514
KS-169	-0.560	25.4	934	0.188

sample was estimated by making twenty-six separate counts of the number of pits lying inside a 0.742 cm x 0.742 cm grid (using a metallurgical microscope) and normalizing the total to the original sample area.

Figure 36c is a plot of the "protection potential" (E_p) vs. active area fraction, A_A (sum of pitted and creviced areas, divided by original sample area). The active area fraction, A_A , was determined for each sample by multiplying an average pit area (as viewed vertical to the pitted surface) by the total number of pits present on the sample, adding this to the measured area of crevice attack (if any), and dividing by the original sample area. Only the KS-171 and 169 samples exhibited severe crevice corrosion. It is felt that the logarithmic plotting of the active area fraction should not be sensitive to small errors inherent in this method of estimation.

Many of the pits were approximately the same size. This may partially explain why Figures 36b and c are similar in appearance to 36a. It is not clear, however, which of the variables are dependent and which is independent.

Figure 37 is a plot of single-pit "protection potential" (E_p) data vs. total charge passed per unit sample area, Q/A (plotted logarithmically), for the Fe - 12% Cr alloy in 0.1 M Cl^- , H_2 -saturated solutions of pH approximately 10.2. The data are given in Table 4.

The single-pit samples were prepared by first painting off an entire sample with Microshield lacquer and then drilling just through the Microshield with a number 80 wire drill (0.0132 in. in diameter), giving an initial exposed surface area of approximately 0.000137 in.^2 (0.000883 cm^2).

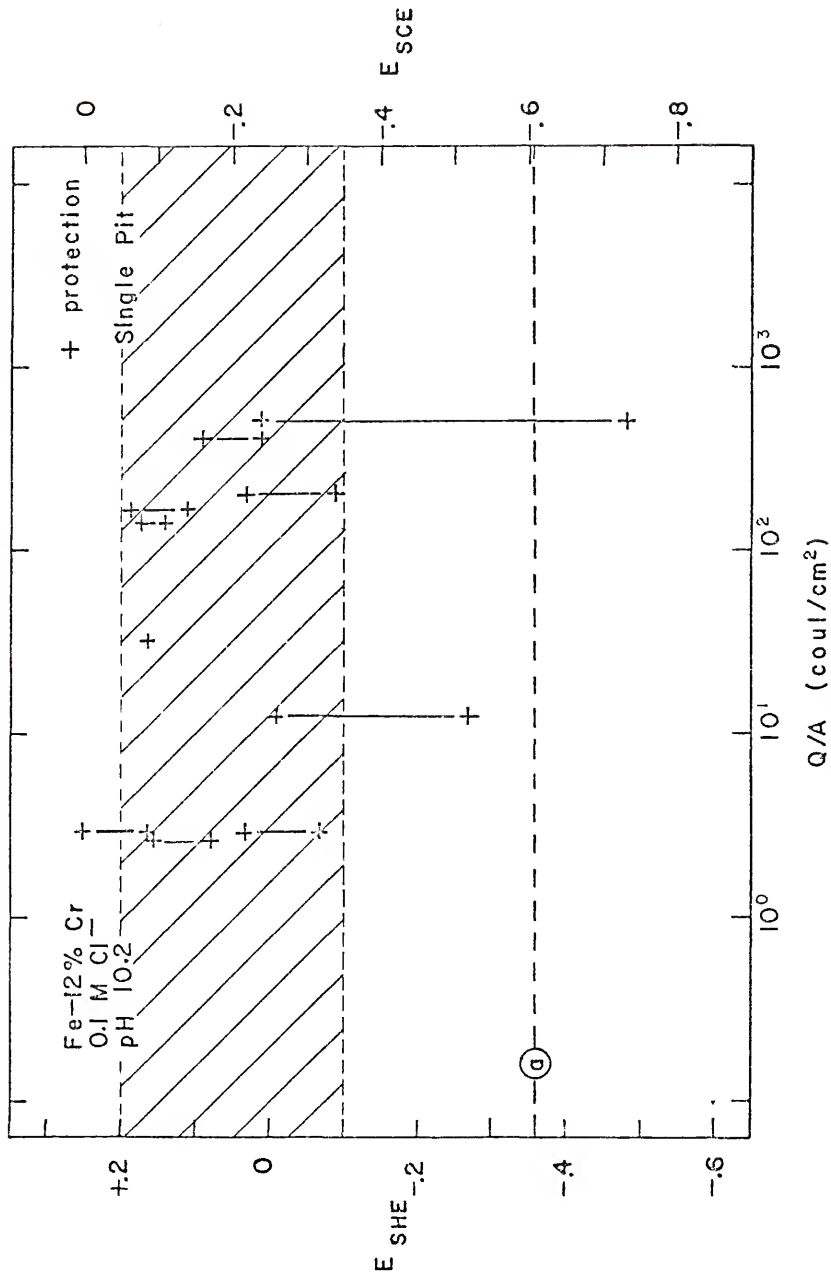


Figure 37. Plot of single-pit "protection potential" (E_p) data vs. total charge passed per unit sample area, Q/A (plotted logarithmically), for the Fe - 12% Cr alloy in 0.1 M Cl^- , H_2 -saturated solutions of pH approximately 10.2. Points connected by a line represent a single sample.

TABLE 4

SINGLE-PIT EXTENT-OF-PROPAGATION DATA FOR THE Fe - 12% Cr
 ALLOY IN 0.1 M Cl^- , H_2 -SATURATED SOLUTIONS OF
 pH APPROXIMATELY 10.2

(Original Sample Areas $\approx 0.000883 \text{ cm}^2$)

<u>Run No.</u>	<u>"Protection Potential"</u> <u>(v_{SCE})</u>	<u>Q/A</u> <u>(coul/cm²)</u>
KS-179	+0.005 -0.075	2.72
KS-181	0.000 -0.090	2.99
KS-175	-0.220 -0.320	3.01
KS-174	-0.260 -0.520	13.6
KS-176	-0.090	32.5
KS-177	-0.080 -0.110	148
KS-178	-0.065 -0.140	173
KS-180	-0.220 -0.340	202
KS-183	-0.160 -0.240	404
KS-182	-0.240 -0.730	507

During the course of the experiments bubbles (assumed to be H_2 gas) were occasionally observed to emerge from the single pits, in agreement with previous work described in Section 2.4.2.3. The dual points in Figure 37 are used to indicate some uncertainty. The upper (more noble) points represent a potential at which the applied current had dropped to low values. The lower (more active) points represent a potential at which the applied current had leveled off at a value approximately equal to the passive current.

Although the data presented in Figure 37 are erratic, they appear to be rather independent of the extent of propagation. The lowest (most active) point occurred when a bubble (again, assumed to be H_2 gas) remained trapped at the entrance of the single pit. This suggests the possibility that the effect of increased extent of propagation for ordinary multiple-pit specimens may be primarily to increase the number of active pits, and thus to statistically increase the chances for one or more pits remaining in the active state (rather than repassivating).

4.2 Galvanostatic Polarization Results

The galvanostatic polarization technique was used to study the concept of the "protection potential" being approximately equal to the potential inside active pits. Instantaneous mixed potential vs. time curves were obtained, both on an x-time recorder and on an oscilloscope.

The oscilloscope and the x-time recorder results showed the instantaneous mixed potentials to change smoothly and continuously, from an applied current potential to a final steady-state value, after

the applied current was stopped. The writing rate of the oscilloscope was 100 cm/msec or faster.

Figure 38 shows x-time recorder results for runs KS-145, 146, 148 and 149, plotted for particular times after the applied currents were stopped. The data are given in Appendix 12. The "0 min" values were the earliest readings possible using the recorder (minimum response of 10 in./sec). The plots are of instantaneous mixed potential vs. total charge passed, Q (product of applied current and time duration of application, plotted logarithmically), for the Fe - 12% Cr alloy in 0.1 M Cl^- , H_2 -saturated solutions of pH approximately 10.1. The exposed areas of the samples were roughly 1 cm^2 . A single sample was used for each run.

The data appear to indicate a tendency for a decrease (become more active) in the instantaneous mixed potential with increasing extent of propagation. The data also appear to indicate that the instantaneous mixed potentials rapidly approach an active value (within 15 sec).

Figure 39 is a superposition of data from Figures 36a and 38d (a superposition of potentiokinetic and galvanostatic results). Although any apparent agreement between the two types of experiments is probably fortuitous, the data do again suggest the possibility of both "repassivation" and "deactivation" mechanisms being operative.

Figure 40 shows single-pit x-time recorder results for runs KS-185, 186 and 187. The data are given in Appendix 13. The single pits were prepared in the same way as for the single-pit potentiokinetic experiments. The plots are of single-pit instantaneous mixed potential

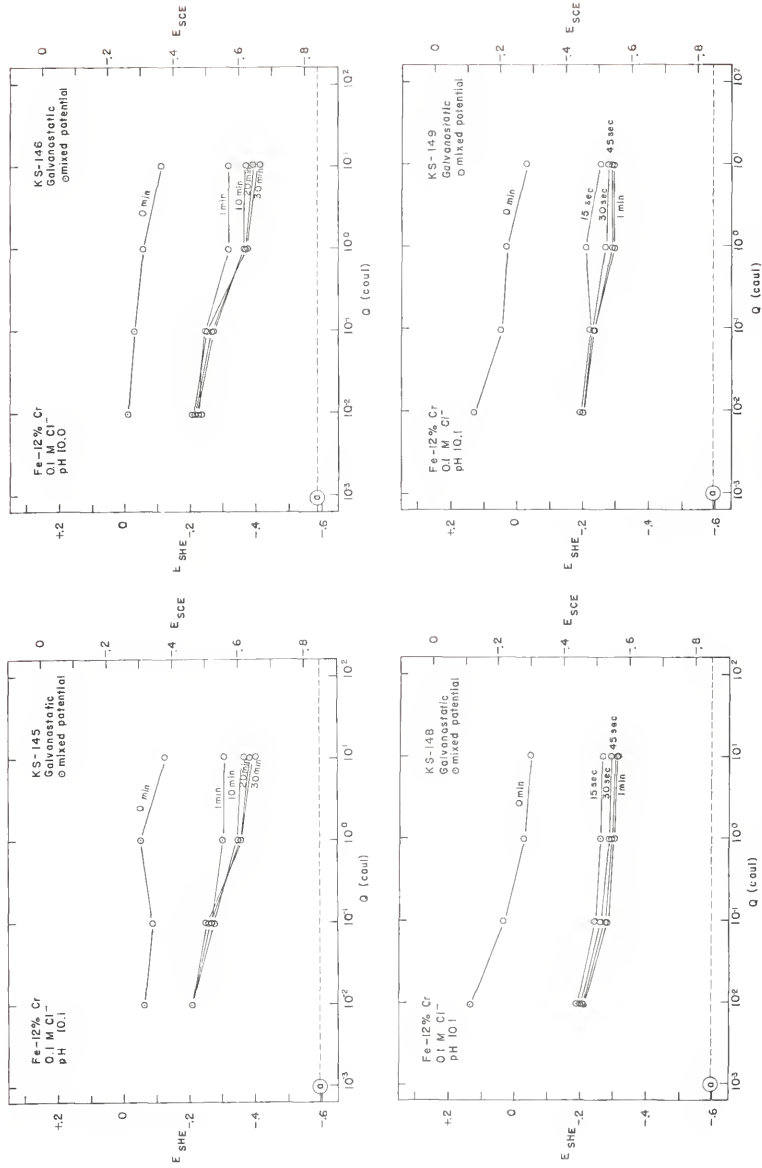
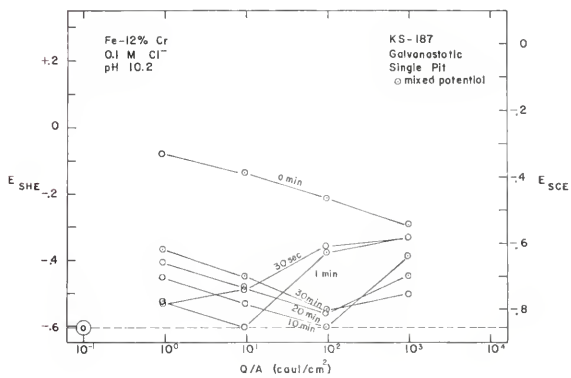
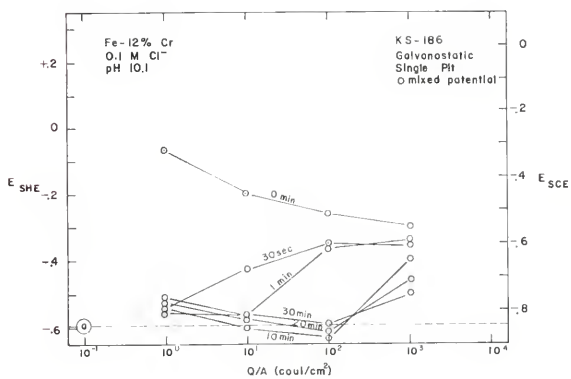
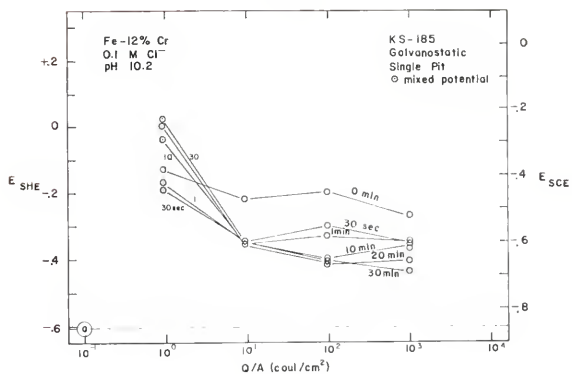


Figure 38. Instantaneous mixed potential vs. total charge passed, Q (plotted logarithmically) for the Fe - 12% Cr alloy in 0.1 M Cl⁻, H₂-saturated solutions of pH approximately 10.1. Sample areas ≈ 1 cm². Each diagram presents results for a single sample.

Figure 40. Single-pit instantaneous mixed potential vs. total charge passed per unit sample area, Q/A (plotted logarithmically), for the Fe - 12% Cr alloy in 0.1 M Cl^- , H_2 -saturated solutions of pH approximately 10.2. Each diagram presents results for a single sample.



vs. total charge passed per unit area, Q/A (plotted logarithmically), for the Fe - 12% Cr alloy in 0.1 M Cl^- , H_2 -saturated solutions of pH approximately 10.2.

The data presented in Figure 40, while erratic, are reminiscent of the single-pit potentiokinetic data (not clearly a function of extent of propagation). Thus, it does seem, as discussed earlier, that the effect of extent of propagation on a given single pit is uncertain.

4.3 Artificial Occluded Cell Results

4.3.1 First Type

Figure 41 is a potentiokinetic plot of applied potential vs. Ag-AgCl electrode potential (both measured with respect to SCE) for the first type of Fe - 12% Cr artificial occluded cell (modified sample and sample holder) in a 0.1 M Cl^- , H_2 -saturated solution of pH 5.4. The zero current potential, rupture potential and "protection potential," observed with an ammeter incorporated into the potentiostat, are indicated with arrows.

Figure 41 is essentially a plot of applied potential vs. the difference between the applied potential and the resulting potential at the deepest point inside the artificial occluded cell (assuming a relatively constant Cl^- activity). The similarity in shape to ordinary potentiokinetic scans suggests the possibility that the apparent Ag-AgCl electrode potential as observed in this experiment may be a function of the applied current.

Figure 42 presents two potentiokinetic plots of applied current

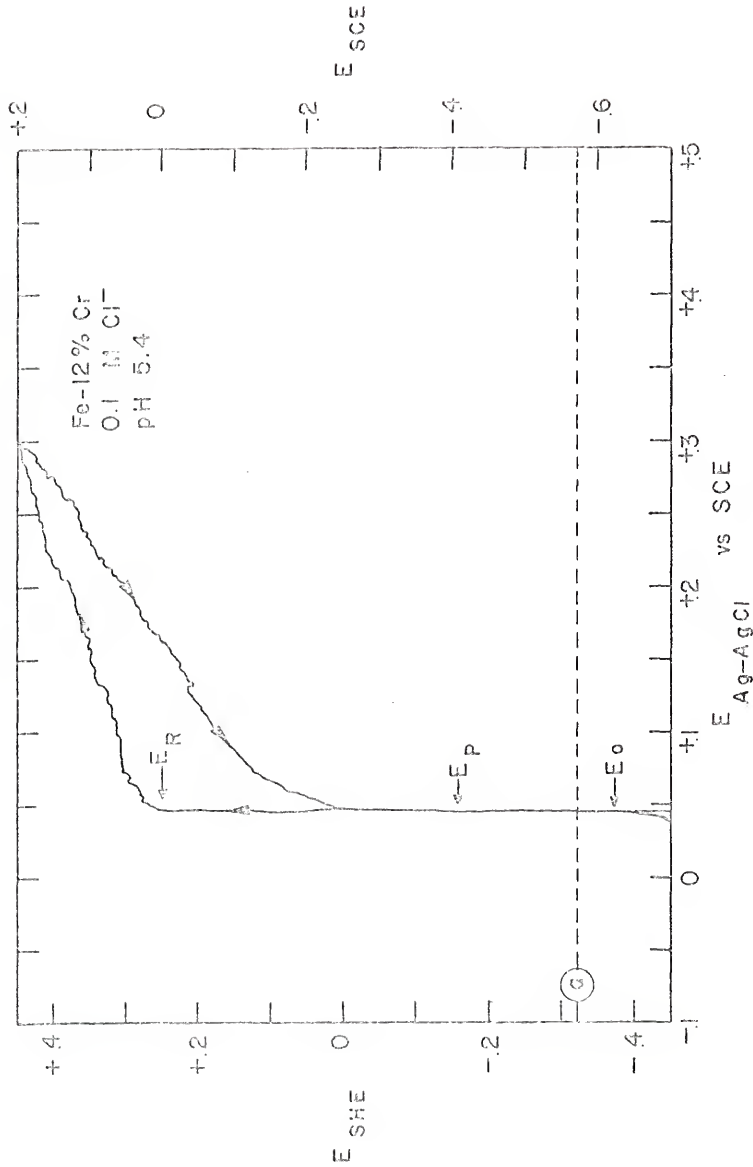


Figure 41. Potentiokinetic plot of applied potential vs. Ag-AgCl electrode potential for the first type of Fe - 12% Cr artificial occluded cell in a 0.1 M Cl⁻, H₂-saturated solution of pH 5.4. The zero current potential, rupture potential and "protection potential," observed with an ammeter incorporated into the potentiostat, are indicated with arrows.

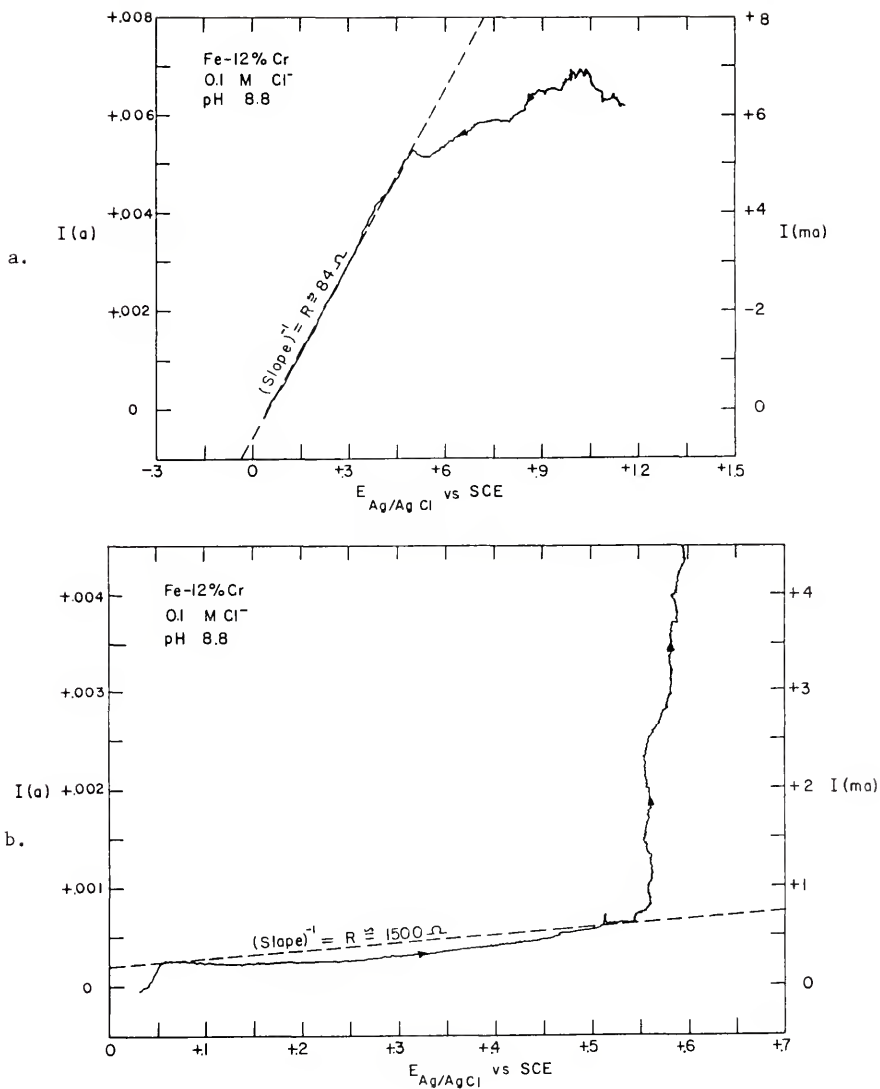


Figure 42. Potentiokinetic plots of applied current vs. Ag-AgCl electrode potential for the first type of Fe - 12% Cr artificial occluded cell in 0.1 M Cl⁻, H₂-saturated solutions of pH 8.8.

vs. Ag-AgCl electrode potential for the first type of Fe - 12% Cr artificial occluded cell in 0.1 M Cl^- , H_2 -saturated solutions of pH 8.8. The inverse of the slope of the roughly linear portion of each plot yields an apparent resistance.

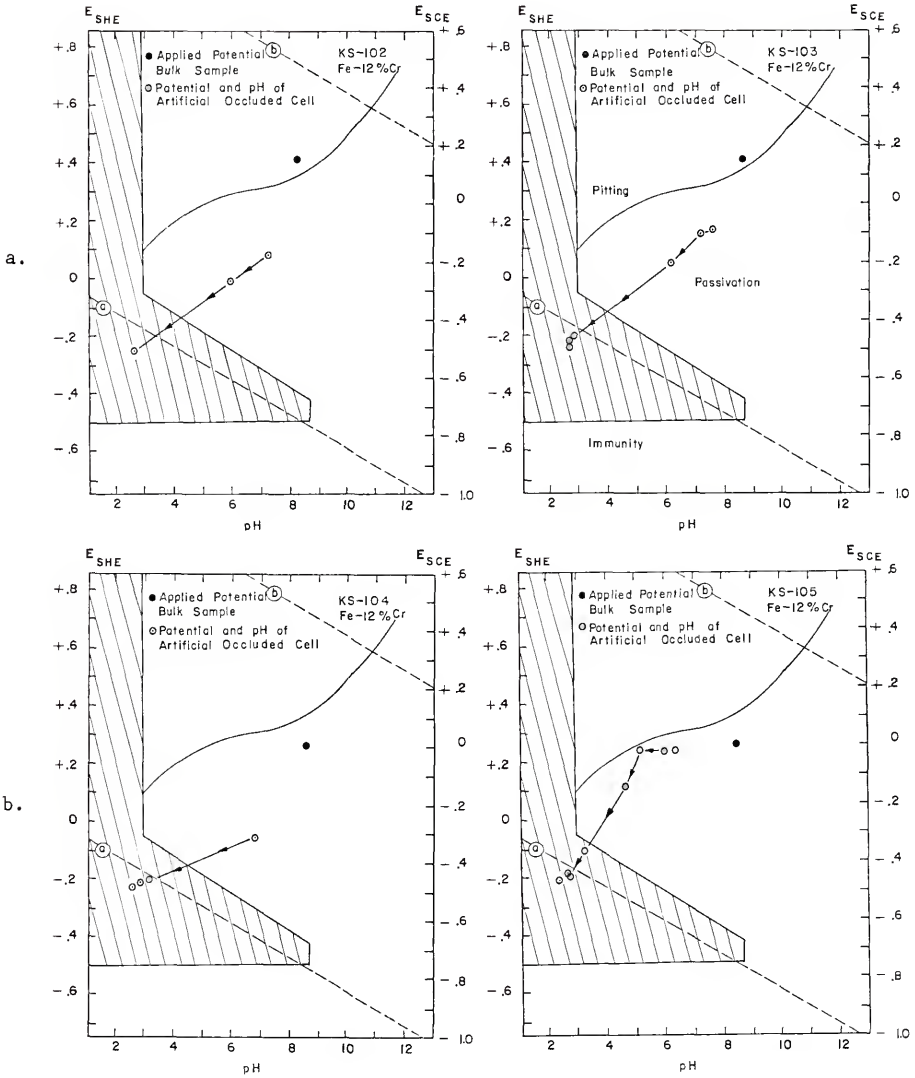
The calculated apparent resistance of 84 Ω for Figure 42a may be fairly reasonable for a concentrated Cl^- electrolyte [169]. The calculated apparent resistance of 1500 Ω (the apparent resistance could be much higher) for Figure 42b is nearly 18 times as large. Large potential drops, far exceeding those calculated for electrolyte resistance, have been attributed by Pickering and Frankenthal [75] to the observed presence of H_2 gas bubbles in active pits and crevices on Fe. Possibly, entrapment of H_2 gas bubbles accounts for the high calculated values of apparent resistance for Figure 42b.

The first type of artificial occluded cell was constructed primarily for the purpose of measuring the Cl^- activity and pH inside active pits. It was envisioned that a Ag-AgCl electrode (reversible to Cl^-) or a Pd electrode (reversible to H^+) would be used. However, the occurrence of large potential drops (much larger than those potentials which were to be measured) with applied current prevented its use for the intended purpose. For this reason the second type of artificial occluded cell was employed for the remainder of this investigation.

4.3.2 Second Type

Figures 43a, 43b and 44 show the progress of several of the second type of artificial occluded cell experiments conducted with the Fe - 12% Cr alloy, superimposed on the potential vs. pH diagram (0.1 M

- Figure 43. a. Progress of artificial occluded cell experiments for the Fe - 12% Cr alloy in solutions initially 0.1 M NaCl + 0.01 M NaHCO₃, with H₂-saturated bulk solutions.
- b. Progress of artificial occluded cell experiments for the Fe - 12% Cr alloy in solutions initially 0.1 M NaCl + 0.01 M NaHCO₃, with O₂-saturated bulk solutions. The results are superimposed on the experimental potential vs. pH diagram (0.1 M Cl⁻, H₂-saturated solutions) for the same alloy.



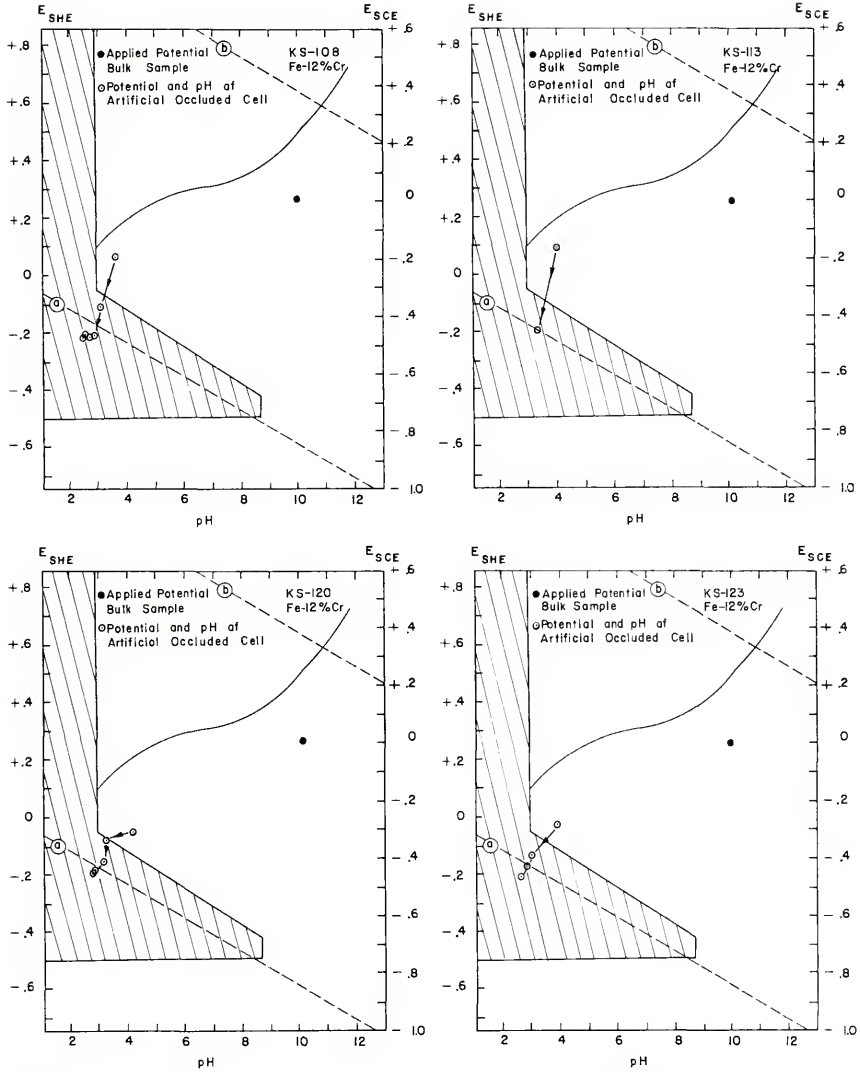


Figure 44. Progress of artificial occluded cell experiments for the Fe - 12% Cr alloy in solutions initially 0.1 M NaCl, adjusted to approximately pH 10 with 0.1 M NaOH. The bulk solutions were O₂-saturated. The results are superimposed on the experimental potential vs. pH diagram (0.1 M Cl⁻, H₂-saturated solutions) for the same alloy.

Cl^- , H_2 -saturated solutions) for the same alloy. The black circles represent the applied potentials of the bulk samples and the initial pH's of the solutions. The data are given in Appendix 14.

The results of Figures 43a and b correspond to solutions initially 0.1 M NaCl + 0.01 M NaHCO_3 . Figure 43a presents results for H_2 -saturated bulk solutions and Figure 43b presents results for O_2 -saturated bulk solutions. The bulk samples were observed to become active eventually (due to crevice corrosion) during the experiments referred to in Figure 43b. No bulk samples were used in the experiments referred to in Figure 43a.

The results of Figure 44 correspond to solutions initially 0.1 M NaCl, adjusted to approximately pH 10 with 0.1 M NaOH. The bulk solutions were O_2 -saturated. The bulk samples remained passive in runs KS-108 and 120, while the bulk samples eventually became active in runs KS-113 and 123.

Normally, in the second type of artificial occluded cell experiments, the occluded cell (small compartment) samples were initially activated by briefly raising the applied potential (with the bulk sample disconnected) above (more noble than) the rupture potential.

An apparent resistance may be calculated for the second type of artificial occluded cell by dividing the potential difference (corrected to 0 for 0 current) between the Ag-AgCl reference electrode located in the artificial occluded cell compartment and the saturated calomel reference electrode located outside the cell by the measured current of the small sample located in the artificial occluded cell, $\Delta E/I_{\text{occ}}$.

A number of such calculations were carried out for runs KS-108 and 120, for different times during the experiments. The calculated apparent resistances ranged from 534 Ω to 1217 Ω for run KS-108 and from 610 Ω to 2157 Ω for run KS-120.

The initial artificial occluded cell resistance was determined for 0.1 M NaCl by placing a Pt wire and a Ag wire in solution on each side of the fritted glass disc. A known current was passed between the two Pt wires and the potential difference between the two Ag wires was measured. An apparent resistance was calculated by dividing the potential difference by the applied current, $\Delta E/I_{\text{appl}}$.

For applied currents ranging from 0.1 ma to 10.0 ma, the calculated apparent resistance ranged from 362 Ω to 390 Ω . A similar determination made in the bulk solution (with the spacing of the wires about the same) for applied currents ranging from 1.0 ma to 50 ma yielded calculated apparent resistances ranging from 18.3 Ω to 23.3 Ω .

It appears that the apparent resistance of the second type of artificial occluded cell, although initially due primarily to the presence of the fritted glass disc, may later be due in part to the presence of a corrosion product adhering to the bulk solution side of the fritted glass disc. This corrosion product appeared to be a hydrated ferric oxide (reddish-orange rust) in O_2 -saturated bulk solutions. Thus, the fritted glass disc and its adhering corrosion product may function reasonably well as a substitute for the trapped H_2 gas bubbles and porous corrosion products which may occur in actual occluded corrosion cells.

Figure 45 shows the progress of two artificial occluded cell

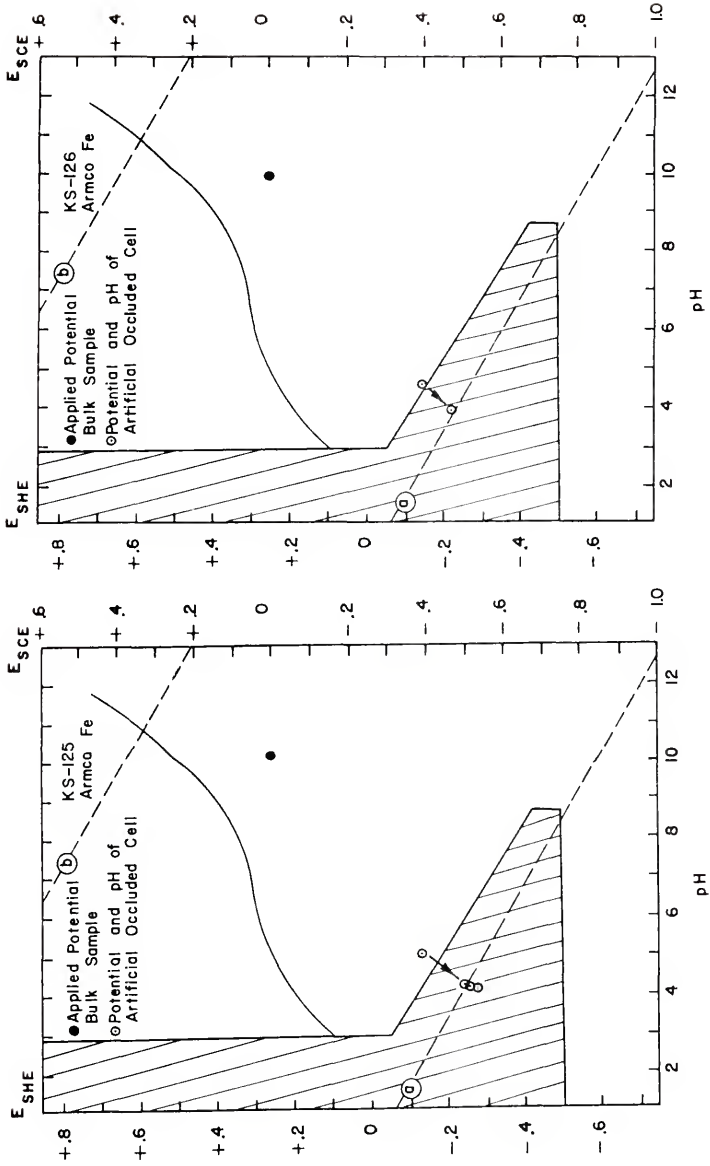


Figure 45. Progress of two artificial occluded cell experiments conducted with Armco Fe in solutions initially 0.1 M NaCl, adjusted to approximately pH 10 with 0.1 M NaOH. The bulk solutions were O_2 -saturated. The results are superimposed on the experimental potential vs. pH diagram for the Fe - 12% Cr alloy (0.1 M Cl^- , H_2 -saturated solutions) for purposes of comparison.

experiments conducted with Armco^{*} Fe, superimposed on the experimental potential vs. pH diagram for the Fe - 12% Cr alloy (0.1 M Cl⁻, H₂-saturated solutions) for purposes of comparison. The initial solutions were 0.1 M NaCl, adjusted to approximately pH 10 with 0.1 M NaOH. The bulk solutions were O₂-saturated. The bulk samples eventually became active. The data are given in Appendix 14.

The minimum pH's attained with Armco Fe artificial occluded cells are less acidic than those attained with the Fe - 12% Cr alloy. This is in qualitative agreement with much of the existing literature discussed in Sections 2.4.2.6 and 2.5.2.4.

Figure 46 is a plot of the minimum pH and corresponding potential attained in the Fe - 12% Cr artificial occluded cell experiments presented in Figures 43a, 43b and 44, superimposed on the experimental potential vs. pH diagram for the same alloy in 0.1 M Cl⁻, H₂-saturated solutions. The minimum pH's and corresponding potentials attained are nearly the same, and all fall in a region of active metal dissolution. The results indicate that an active pit or crevice on this alloy may propagate to an extent precluding the possibility of a "repassivation" mechanism unless there is dilution of the contents of the pit or crevice.

Figure 47 is a plot of the return zero current potentials (marked "+" at their corresponding pH's) measured for some of the artificial occluded cell samples, superimposed on the results of Figure 46. Run

* Armco Ingot Iron HP, Armco Steel Corp., Middletown, Ohio (typically 0.003% C and less than 0.2% total impurities).

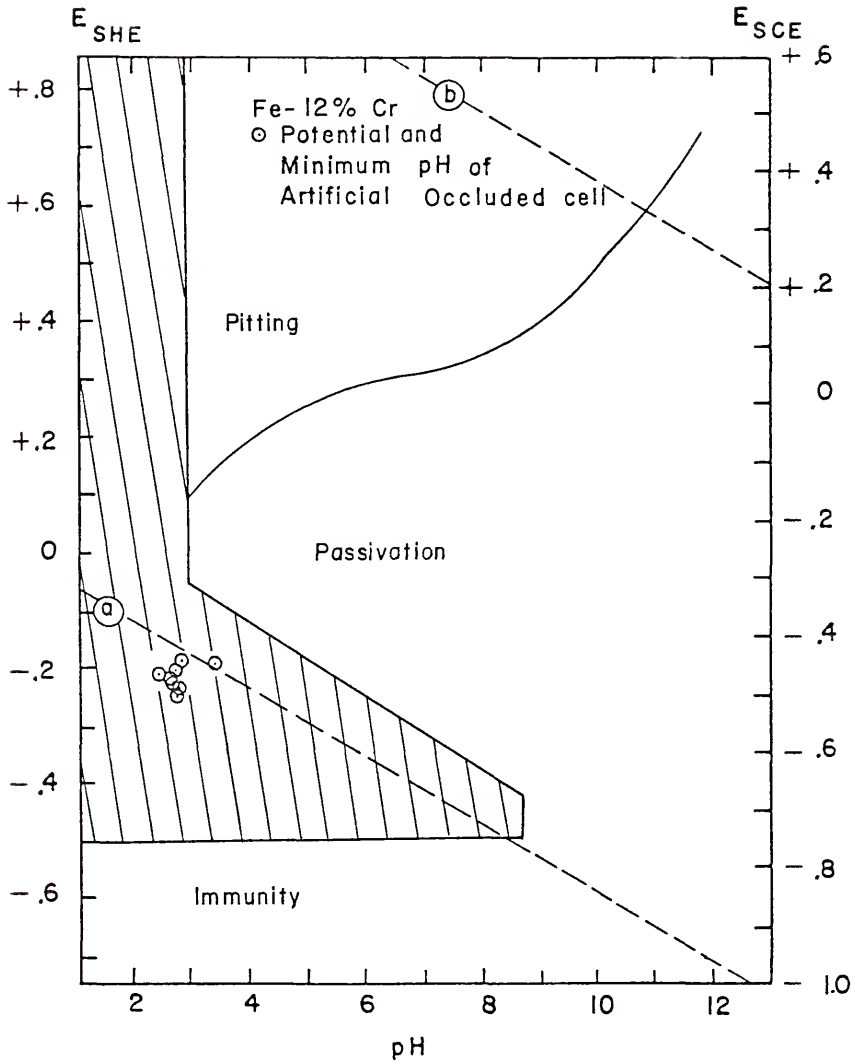


Figure 46. Minimum pH and corresponding potential attained in the Fe - 12% Cr artificial occluded cell experiments presented in Figures 43a, 43b and 44, superimposed on the experimental potential vs. pH diagram for the same alloy in 0.1 M Cl⁻, H₂-saturated solutions.

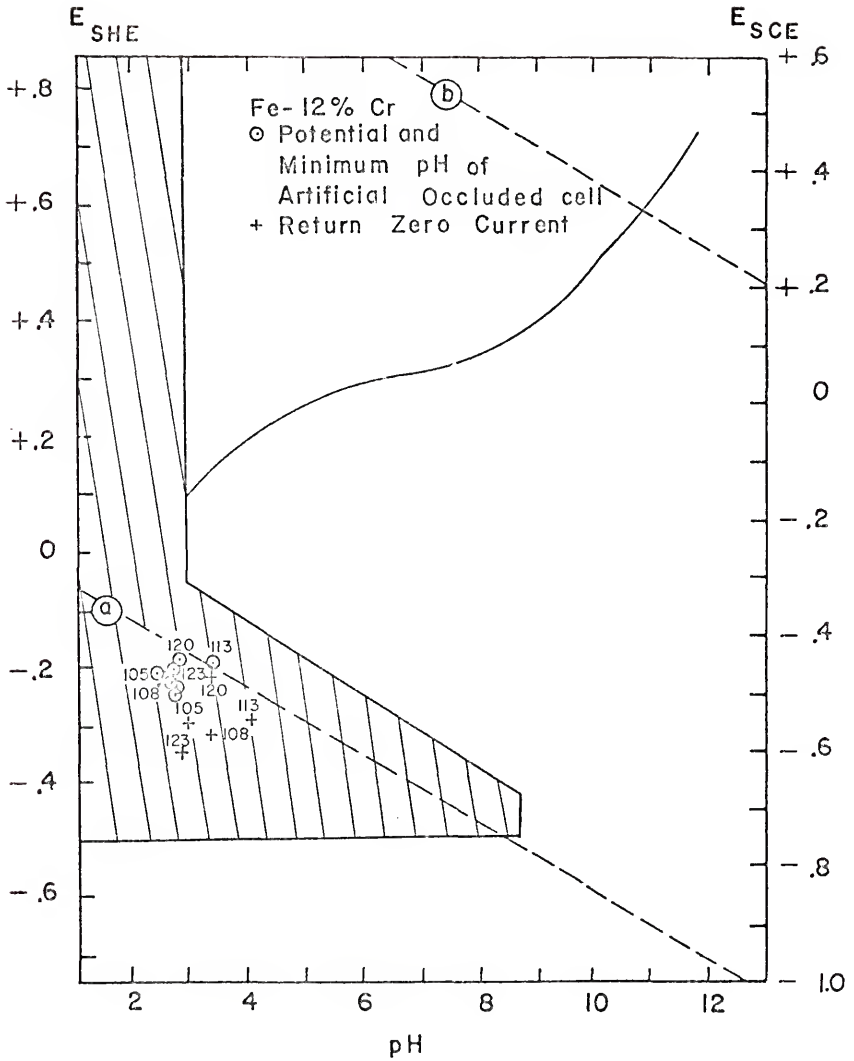


Figure 47. Return zero current potentials and their corresponding pH's measured for some of the artificial occluded cell samples, superimposed on the results of Figure 46. Run numbers are included for reference.

numbers are included for reference. These potentials are more negative (active) than the steady-state values and the corresponding pH's are slightly higher than the steady-state values. The higher pH's are experienced on the basis of H_2 gas evolution inside the artificial occluded cell, as discussed in Sections 2.4.2.3 and 2.5.2.4. The lower (more active) potentials are in qualitative agreement with the results of A. Pourbaix [131, 132].

Figure 48 shows the results of atomic absorption spectrophotometric analyses of the final artificial occluded cell solutions for the Fe - 12% Cr alloy. The experimental technique and individual peculiarities of the Heath spectrophotometer have been discussed elsewhere [158, 159]. The sensitivity of the instrument for Fe and Cr was approximately 2 ppm. The confidence limits [158] shown in Figure 48 were calculated assuming a possible ± 2 ppm deviation from the original instrument reading for the sample in question. The data are given in Appendix 15.

The total volume (3-5 ml) of artificial occluded cell solution was first spun down with a centrifuge. Then, 1 ml aliquots were taken and diluted with 0.5 M HCl + 0.01 M $NaHCO_3$ (1000:1 for Fe analyses and 100:1 for Cr analyses).

The solid line in Figure 48 was calculated ignoring the presence of carbides and assuming the Fe/Cr concentration ratio to be equal to that in the alloy. The dashed line was calculated taking into account the presence of $Cr_{23}C_6$. The details of the calculation are given in Appendix 16. It indicates that no macroscopy dealloying occurred in this case since the corrected ratio of alloy constituents in the

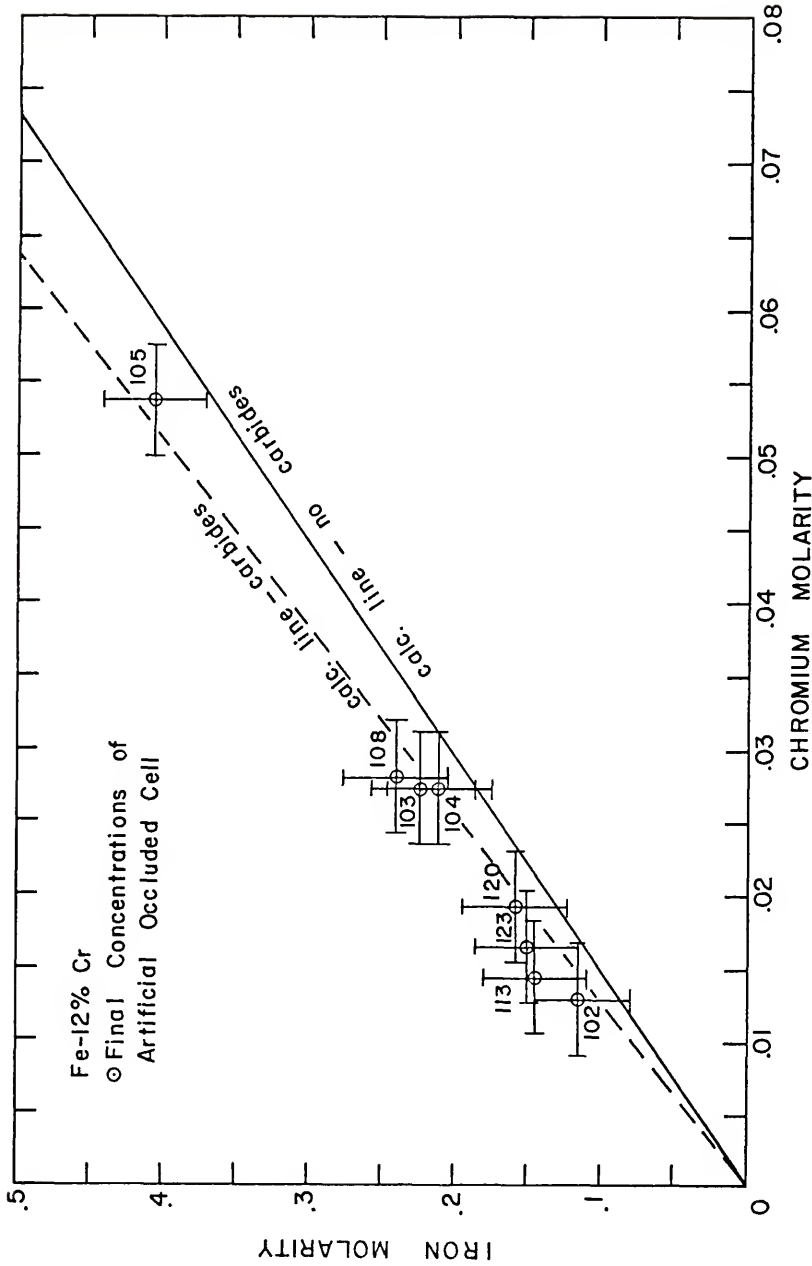


Figure 48. Results of atomic absorption spectrophotometric analyses of the final artificial occluded cell solutions for the Fe - 12% Cr alloy. The solid and dashed lines were calculated assuming no macroscopic dealloying occurred.

alloy and in the solutions were about the same, in agreement with the results of Uhlig [46] for an 18% Cr - 8% Ni alloy (see Section 2.4.2.6) and Stolica [60] for Fe-Cr alloys.

Figure 49 shows the previous results and the chloride analyses (1 ml aliquot samples) compared in such a way as to test the assumption of Fe^{++} and Cr^{+++} , in the form of $\text{FeCl}_2 \cdot x\text{H}_2\text{O}$ and $\text{CrCl}_3 \cdot y\text{H}_2\text{O}$, being the predominant corrosion products in Fe - 12% Cr artificial occluded cells. The data are given in Appendix 15. The results appear to indicate this assumption to be reasonable and are in qualitative agreement with the results of Uhlig [46] for an 18% Cr - 8% Ni alloy (see Section 2.4.2.7).

4.4 Thermodynamic Calculations

The graphic presentation of equilibrium data has been reviewed by Sillen [170]. Pourbaix [171] compiled an atlas of potential vs. pH diagrams for pure elements in aqueous solutions. The Atlas also contains information concerning the effect of pH on the solubility of oxides and hydroxides. Metal ions and complex ion hydrolysis products are considered in terms of relative predominance.

4.4.1 Potential Vs. pH (Pourbaix) Diagrams

Figure 50 compares calculated equilibrium potential vs. pH (Pourbaix) diagrams for the Fe- H_2O system [171] with experimentally determined potential vs. pH diagrams for the Fe - 12% Cr alloy in 0.1 M Cl^- solutions. Figure 51 presents a calculated equilibrium potential vs. pH (Pourbaix) diagram for the Fe - $\text{FeCl}_2 \cdot 4\text{H}_2\text{O} - \text{H}_2\text{O}$ system [172, 173, p. 37], assuming a solution saturated in $\text{FeCl}_2 \cdot 4\text{H}_2\text{O}$.

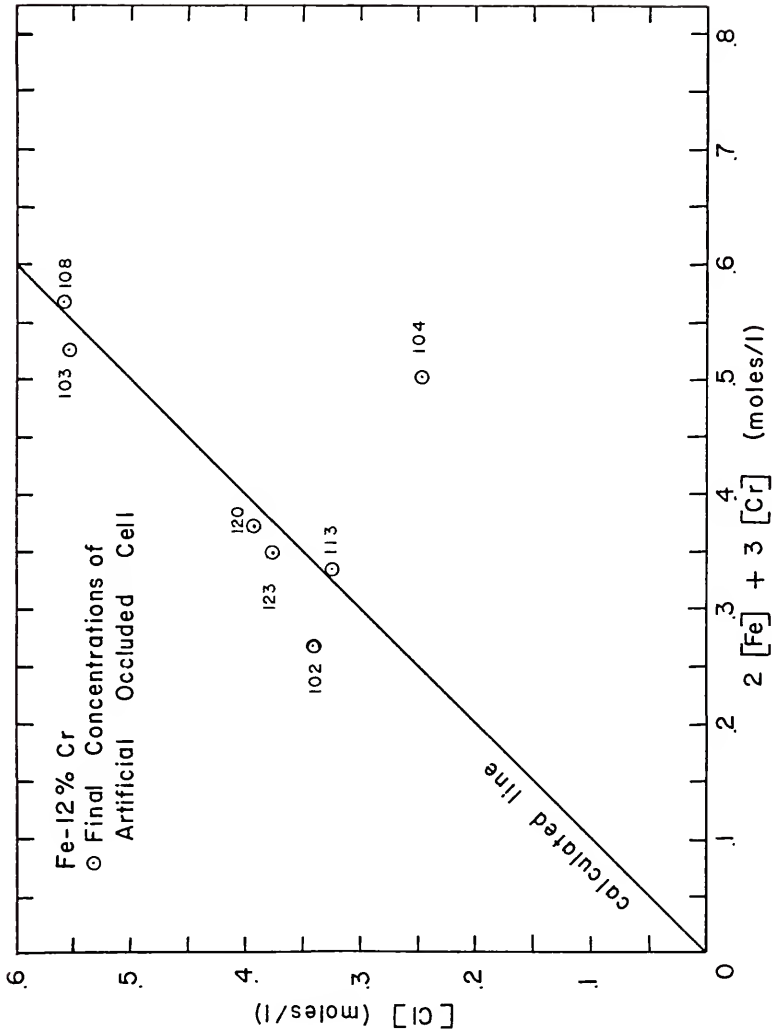


Figure 49. Plot of chloride concentrations (determined by AgNO_3 titrations [167]) vs. linear combinations of the data shown in Figure 48. The solid line was calculated assuming the predominant corrosion products to be $\text{FeCl}_2 \cdot x \text{H}_2\text{O}$ and $\text{CrCl}_3 \cdot y \text{H}_2\text{O}$.

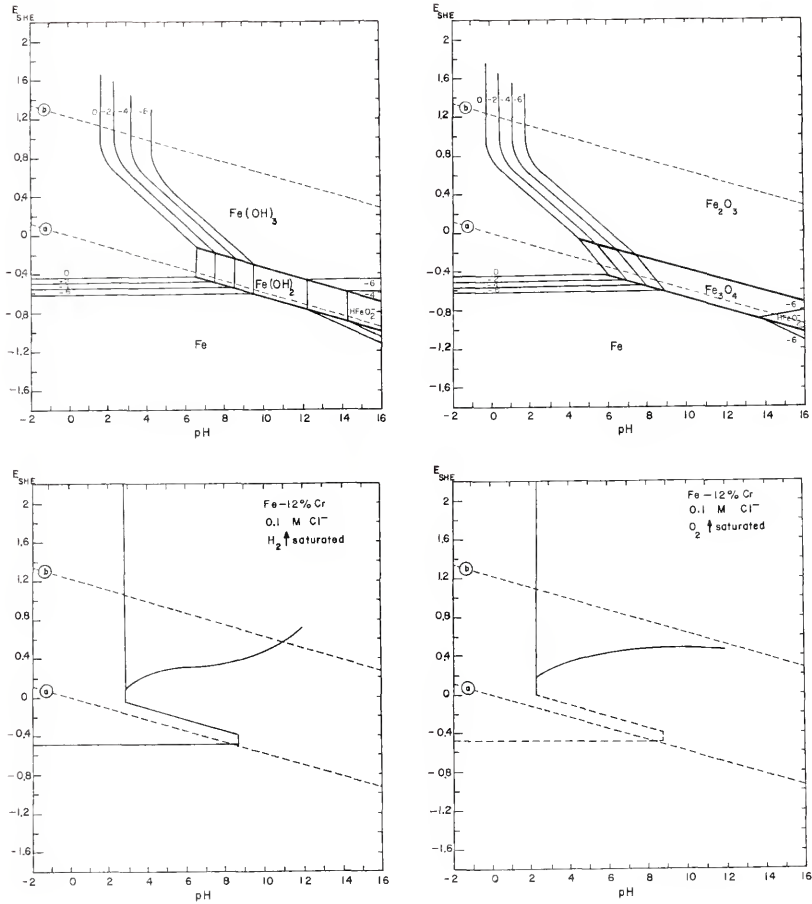


Figure 50. Comparison of calculated equilibrium potential vs. pH (Pourbaix) diagrams for the Fe-H₂O system [171, pp. 312-313] and experimentally determined potential vs. pH diagrams for the Fe - 12% Cr alloy in 0.1 M Cl⁻ solutions.

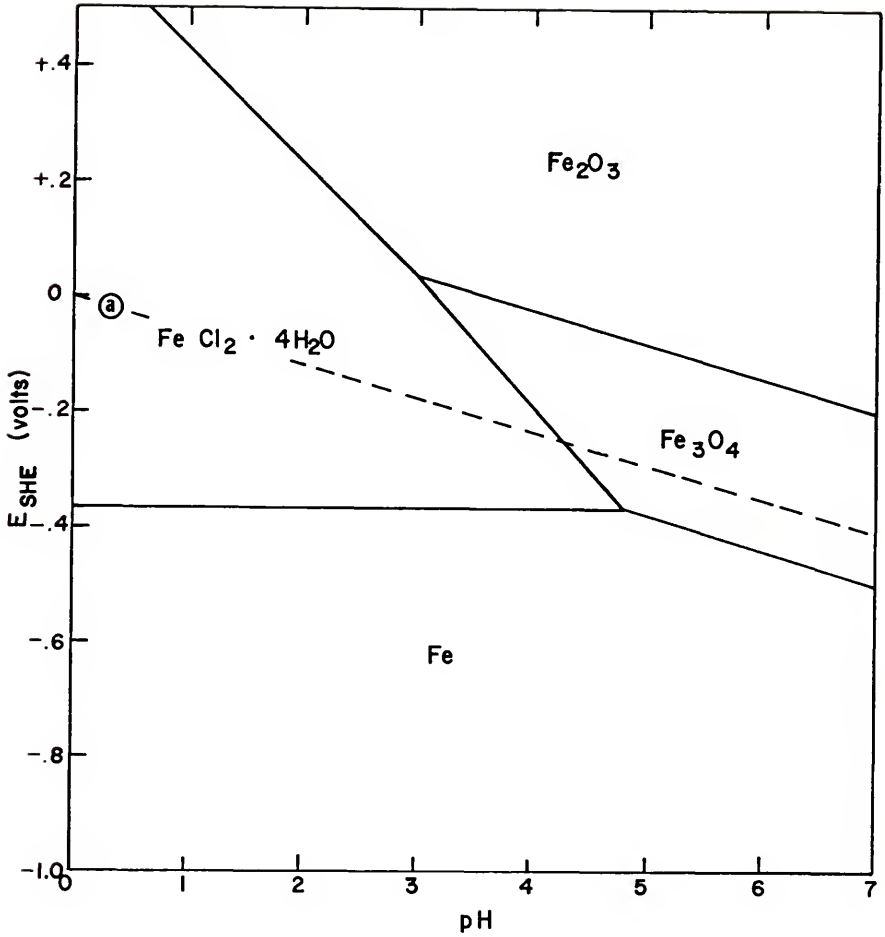


Figure 51. Calculated equilibrium potential vs. pH (Pourbaix) diagram for the Fe-FeCl₂·4H₂O-H₂O system [172, 173, p. 37], assuming a solution saturated in FeCl₂·4H₂O.

Figure 52 contains calculated equilibrium potential vs. pH diagrams for the Cr-H₂O system [171]. Cr(OH)₃·nH₂O is assumed to form in the presence of chloride solutions.

It appears that the experimental results for the Fe - 12% Cr alloy agree more closely with the calculated diagrams for the Fe-H₂O system than with the calculated diagrams for the Cr-H₂O system. In addition, the calculated diagram for the Fe-FeCl₂·4H₂O-H₂O system appears to be similar in many respects to the calculated diagrams for the Fe-H₂O system.

Figure 53a presents calculated equilibrium potential vs. pH (Pourbaix) diagrams for the Fe-H₂O and Fe-Cl⁻-H₂O systems. The activity of Cl⁻ was taken to be 0.1 and the activities of all other dissolved species were taken to be 10⁻⁶. Figure 53b presents calculated equilibrium potential vs. pH (Pourbaix) diagrams for the Cr-H₂O and Cr-Cl⁻-H₂O systems. The activity of Cl⁻ was taken to be 0.1 and the activities of all other dissolved species were taken to be 10⁻⁶.

The diagrams were calculated and rough-plotted completely by an IBM-370 computer, using a Fortran IV computer program written by Bowers, Lee and Maitra [174]. The thermodynamic data, pertinent equations and individual diagrams are included in Appendix 17. The calculation and interpretation of equilibrium potential vs. pH diagrams has been discussed in depth by Pourbaix [171]. A simplified procedure for constructing these diagrams was given by Verink [175].

The diagrams for Cl⁻-containing solutions (Cl⁻ activity of 0.1) are very similar in appearance to the diagrams for Cl⁻-free solutions. Apparently, the complex ions FeCl⁺⁺ and CrCl⁺⁺ predominate over Fe⁺⁺⁺ and Cr⁺⁺⁺ in this case.

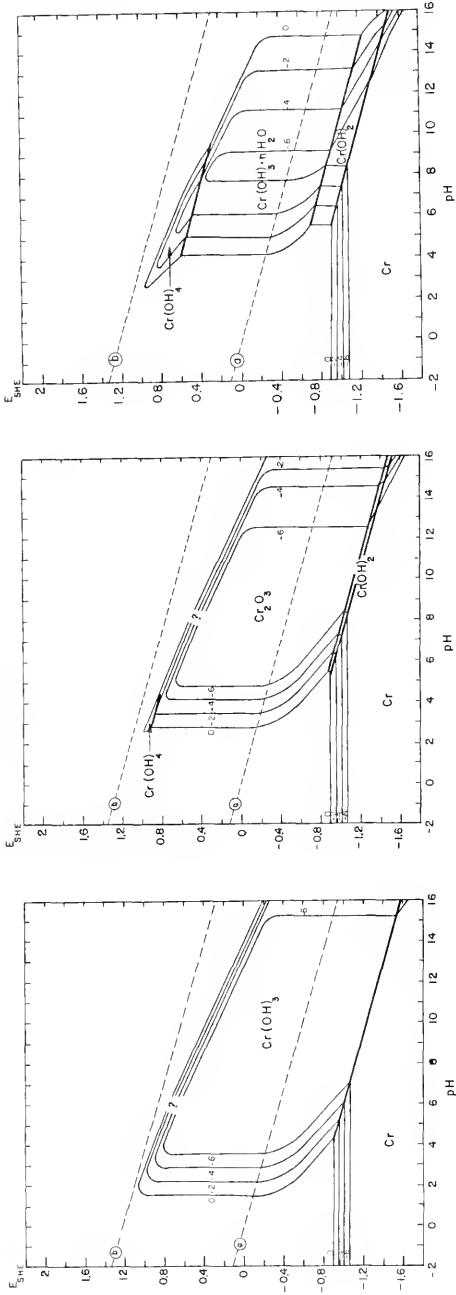


Figure 52. Calculated equilibrium potential vs. pH diagrams for the Cr-H₂O system [171, pp. 262-264]. Cr(OH)₃·nH₂O is assumed to form in the presence of chloride solutions.

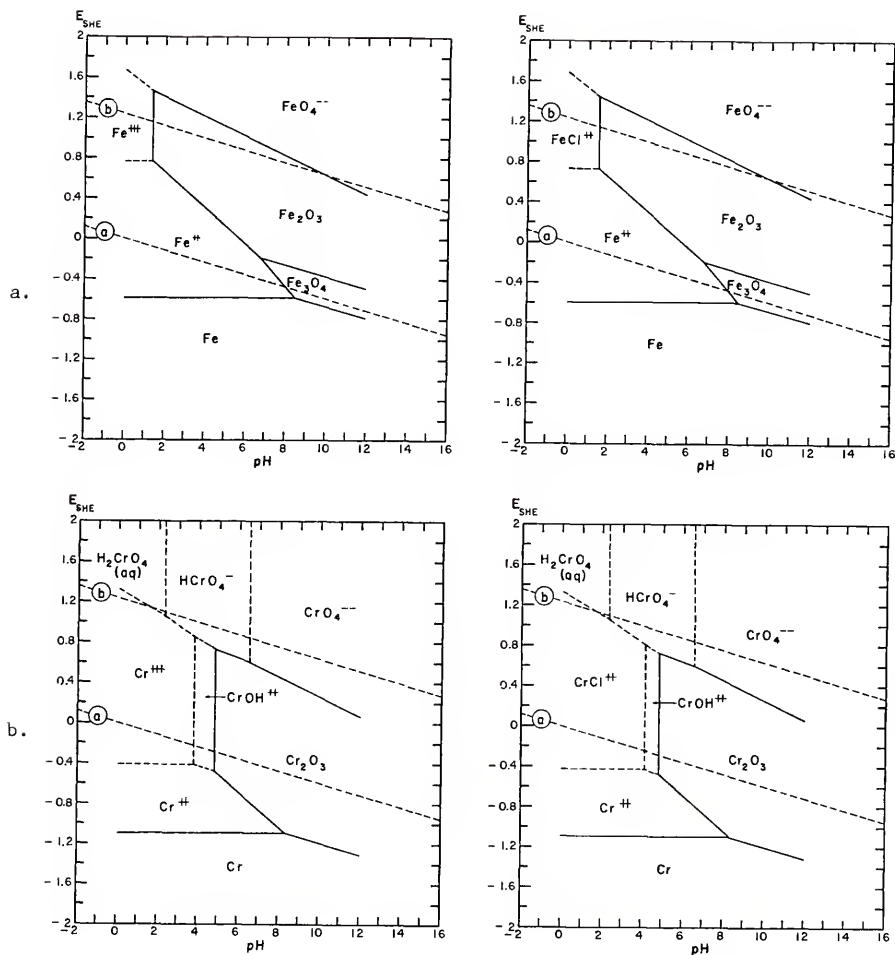


Figure 53. a. Calculated equilibrium potential vs. pH (Pourbaix) diagrams for the Fe-H₂O and Fe-Cl⁻-H₂O systems: The activity of Cl⁻ was taken to be 0.1 and the activities of all other dissolved species were taken to be 10⁻⁶.

b. Calculated equilibrium potential vs. pH (Pourbaix) diagrams for the Cr-H₂O and Cr-Cl⁻-H₂O systems. The activity of Cl⁻ was taken to be 0.1 and the activities of all other dissolved species were taken to be 10⁻⁶.

Figure 54 presents specially calculated (by computer) equilibrium potential vs. pH (Pourbaix) diagrams for the Fe-Cl⁻-H₂O and Cr-Cl⁻-H₂O systems. For the Fe-Cl⁻-H₂O diagram, the activity of Cl⁻ was taken to be 0.373 and the activities of all other dissolved species were taken to be 0.156. For the Cr-Cl⁻-H₂O diagram, the activity of Cl⁻ was taken to be 0.373 and the activities of other dissolved species were taken to be 0.02. The thermodynamic data, pertinent equations and individual diagrams are included in Appendix 17.

These particular activities were chosen in order to approximate the measured final concentrations of the Fe - 12% Cr artificial occluded cells (discussed in the previous section). Taking the activities of soluble Cr species to be 0.02, the activities of soluble Fe species were calculated to be $(7.82)(0.02) = 0.156$. The activity of Cl⁻ was calculated to be $(3)(0.02) + (2)(0.156) = 0.373$.

The black circles in Figure 54 represent approximately the minimum pH's and corresponding potentials attained in the Fe - 12% Cr artificial occluded cell experiments. According to the diagrams, Fe⁺⁺ and CrCl⁺⁺ appear to be the predominant species under these circumstances.

4.4.2 Hydrolysis Calculations

The fact that the particular hydrolysis products in stainless steel pits and crevices which are pH-limiting has not been firmly established was discussed in Sections 2.4.2.7 and 2.5.2.6. The possible role of complex ion hydrolysis products has been largely neglected by other authors, possibly because of the scarcity of thermodynamic data and because the solid hydrolysis products are less difficult to deal with thermodynamically.

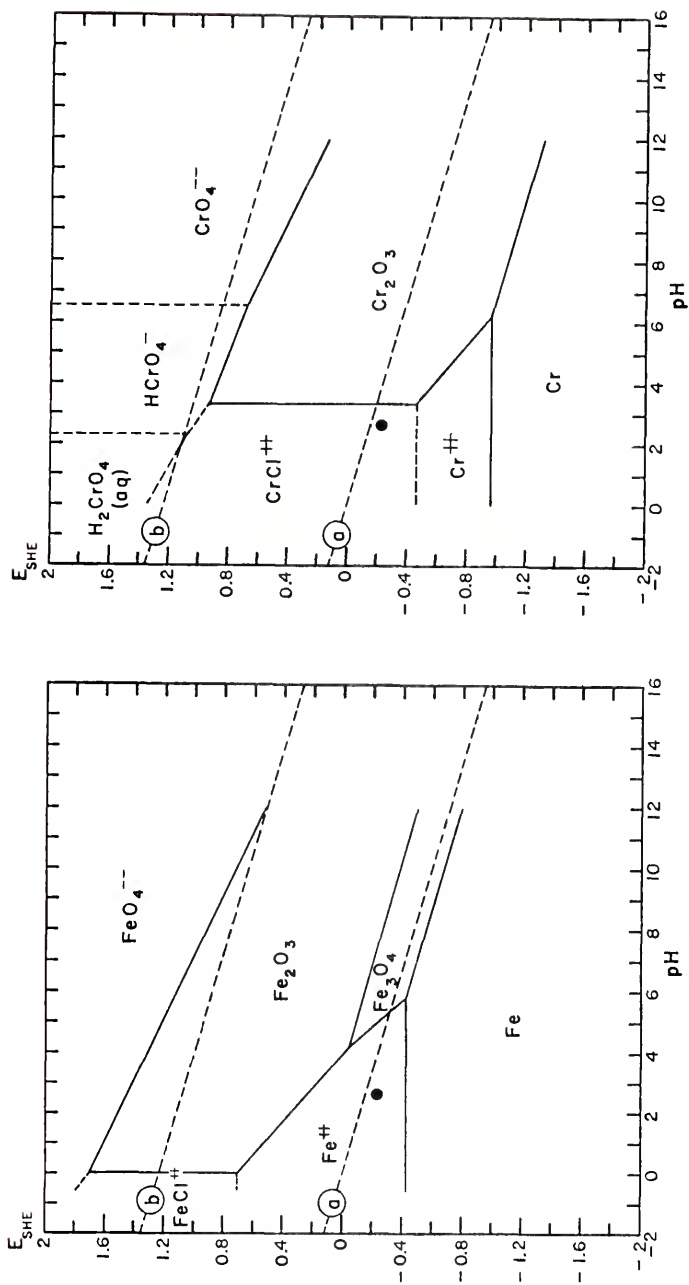
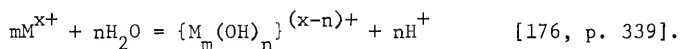


Figure 54. Specially calculated equilibrium potential vs. pH (Pourbaix) diagrams for the Fe-Cl⁻-H₂O and Cr-Cl⁻-H₂O systems. For the Fe-Cl⁻-H₂O diagram, the activity of Cl⁻ was taken to be 0.373 and the activities of all other dissolved species were taken to be 0.156. For the Cr-Cl⁻-H₂O diagram, the activity of Cl⁻ was taken to be 0.373 and the activities of all other dissolved species were taken to be 0.02.

Since there has been some evidence and opinion [96, 46, 87, 97, 29] that the corrosion products inside active pits and other occluded cells may be predominantly soluble chlorides, it seems reasonable to attempt to calculate values of pH due to the presence of complex ion hydrolysis products of Fe, Cr and Ni which might reasonably be expected to be present in occluded cells.

An equation representing the hydrolysis of metal ions to form aquo-complexes may be written as



An equilibrium constant in terms of concentration may be written as

$$K = \frac{[\{M_m(OH)_n\}^{(x-n)+}][H^+]^n}{[M^{x+}]^m[H_2O]^n}.$$

Taking $[H_2O]$ as being nearly unity,

$$K \approx \frac{[\{M_m(OH)_n\}^{(x-n)+}][H^+]^n}{[M^{x+}]^m}.$$

As is normally done [177], it is taken that

$$[\{M(OH)_n\}^{(x-n)+}] = \frac{1}{n} ([H^+] - [OH^-]).$$

Thus,

$$K = \left(\frac{1}{n}\right) \frac{[H^+]^{(n+1)} - [H^+]^n [OH^-]}{[M^{x+}]^m} = \left(\frac{1}{n}\right) \frac{[H^+]^{(n+1)} - K_w [H^+]^{(n-1)}}{[M^{x+}]^m}.$$

Knowing K , an algebraic equation relating $[H^+]$ and $[M^{x+}]$ can be calculated. Since $pH \approx -\log[H^+]$, this can be converted to an

equation relating pH and $\log [M^{x+}]$. A value for K may sometimes be obtained directly from the literature. If the free energy change for a hydrolysis reaction is given, however, K can be calculated according to

$$K = e^{-\frac{\Delta G}{RT}}, \quad \text{where}$$

R = gas constant

T = absolute temperature.

The maximum allowable value of $[M^{x+}]$ was assumed to be that corresponding to a saturated solution of $FeCl_2$, $CrCl_3$ or $NiCl_2$. Table 5 lists the data used and the calculated concentrations for saturated solutions (sat. sol). The formula used was

$$M = \frac{10 \rho Q}{W}, \quad \text{where}$$

M = molarity of sat. sol. (moles/l)

ρ = density of sat. sol. (gm/ml)

Q = quantity of chloride per 100 gm sat. sol. (gm/100 gm)

W = molecular weight of metal chloride (gm/mole).

Table 6 contains thermodynamic data for the complex ion hydrolysis reactions considered. The actual calculations were carried out with the aid of Fortran IV computer programs, implemented through the Interpreter mode on an IBM-360 computer. The programs and results are included in Appendix 18.

Figure 55 shows the results of hydrolysis calculations for Fe^{++} , Fe^{+++} , Cr^{+++} and Ni^{++} , plotted in terms of log metal ion concentration vs pH.

At this point, the additional assumption was made that the

TABLE 5

SOLUBILITY OF METAL CHLORIDES

	Density of Sat. Sol., ρ (gm/ml)	Quantity of Chloride per 100 gm Sat. Sol., Q (gm/100 gm)	Molecular Weight of Metal Chloride, W (gm/mole)	Molarity of Sat. Sol., M (moles/l)
FeCl ₂	1.443 [92]	39.2 [91]	126.75 [93]	4.463
FeCl ₃	1.793 [178]	49.76 [91]	162.21 [93]	5.497
CrCl ₃	2.092*	68.50 [91]	158.35 [93]	9.050
NiCl ₂	1.443**	39.6 [91]	129.62 [93]	4.409

*Estimated from FeCl₃ data.

**Assumed same as for FeCl₂.

TABLE 6
THERMODYNAMIC DATA FOR COMPLEX ION HYDROLYSIS REACTIONS

Hydrolysis Product	Valence	AG (kcal/mole)	Log K	Source	Computer Program
FeOH^+	+2		-9.58	[179]	HYD1E
FeOH^{++}	+3	+ 2.96	-2.17	[176]	HYD1E
$\text{Fe}(\text{OH})_2^+$	+3	+ 8	-5.87	[176]	HYD3A
$\text{Fe}_2(\text{OH})_2^{4+}$	+3	+ 2.92	-2.14	[176]	HYD2A
$\text{Fe}_4(\text{OH})_3^{9+}$	+3	+ 8	-5.87	[176]	HYD4A
CrOH^{++}	+3	+ 5.1	-3.74	[176]	HYD1E
$\text{Cr}(\text{OH})_2^+$	+3		-9.96	*	HYD3A
NiOH^+	+2	+13.3	-9.75	[176]	HYD1E

* Calculated from data given in [180].

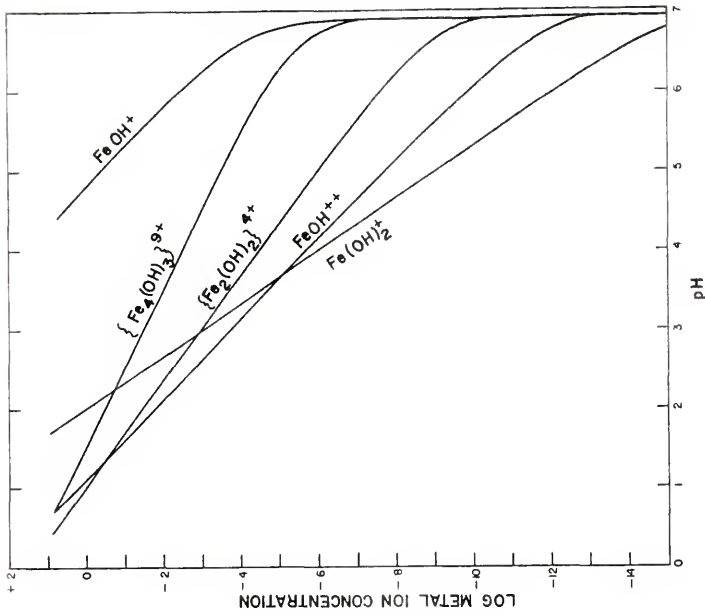
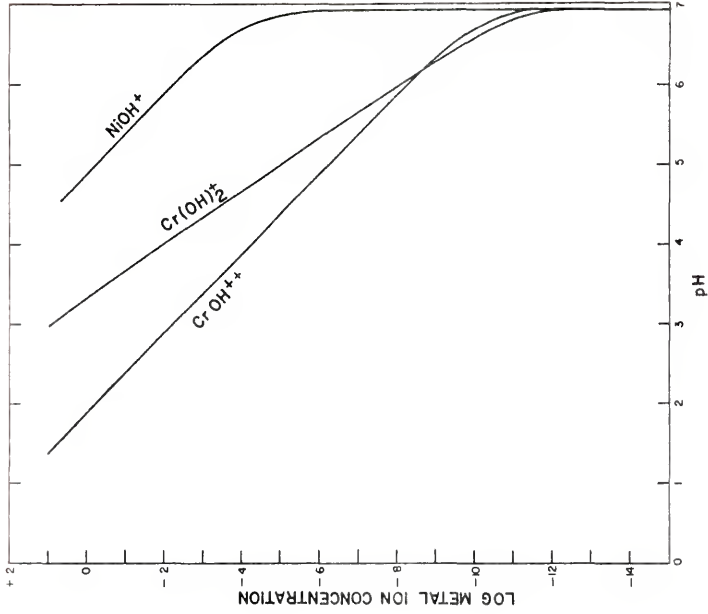
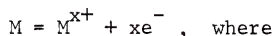


Figure 55. Results of hydrolysis calculations for Fe^{2+} , Fe^{3+} , Cr^{3+} and Ni^{2+} . Log metal ion concentration refers to the concentration (M) of the nonhydrolyzed metal ions.

metal ion concentration inside an occluded cell could be predicted according to the Nernst Equation [131, 132]:

$$E = E^{\circ} + \frac{RT}{xF} \ln[M^{x+}] \quad (\text{assuming concentration} = \text{activity})$$

for the reaction



R = gas constant

T = absolute temperature

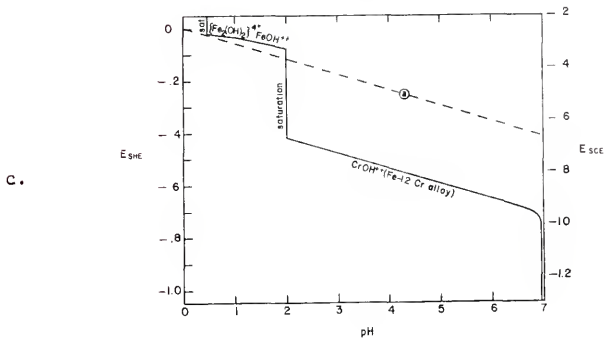
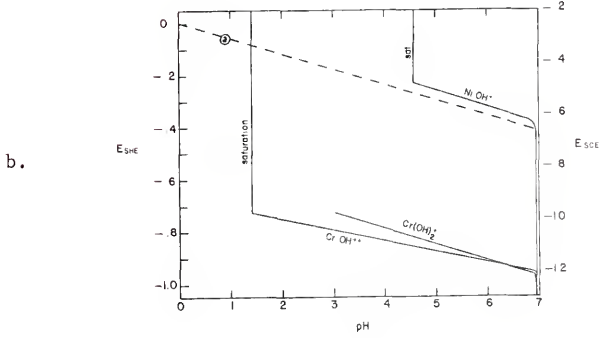
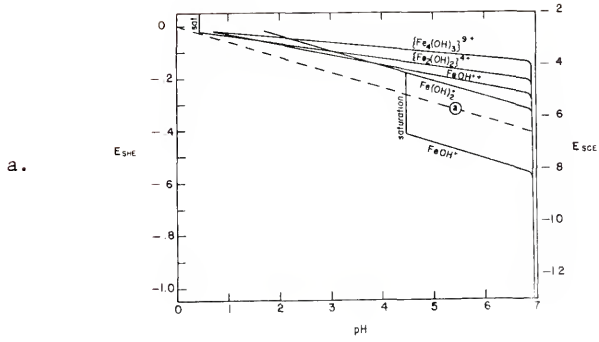
F = Faraday Constant.

Applying the Nernst Equation resulted in an algebraic equation relating electrode potential and metal ion concentration. By combining the hydrolysis equation and the Nernst Equation, a relationship between electrode potential and pH could be established. This method of calculation was used to obtain the curves presented in Figures 56a and 56b. The computer programs and results are included in Appendix 18.

Figure 56c shows potential vs. pH curves calculated by combining hydrolysis equations and Nernst Equations for the Fe - 12% Cr alloy. The CrOH^{++} line reflects an additional assumption of perfect mechanical blocking by the more noble alloying element, Fe (implying $[\text{Fe}^{++}]/[\text{Cr}^{+++}] = 7.82$). It appears from Figure 56c that at potentials lower (more active) than the "a" line the dominant (pH-limiting) complex ion for the Fe - 12% Cr alloy should be the CrOH^{++} ion.

At the potentials attained in the Fe - 12% Cr artificial occluded cell experiments (approximately $-0.2 v_{\text{SHE}}$), the results presented in Figure 56c indicate that the artificial occluded cell

- Figure 56.
- a. Potential vs. pH curves calculated by combining hydrolysis equations and Nernst Equations for pure Fe.
 - b. Potential vs. pH curves calculated by combining hydrolysis equations and Nernst Equations for pure Cr and for pure Ni.
 - c. Potential vs. pH curves calculated by combining hydrolysis equations and Nernst Equations for the Fe - 12% Cr alloy. The CrOH^{++} line reflects an additional assumption of perfect mechanical blocking by the more noble alloying element, Fe.



solutions should have eventually become saturated in ferrous chloride. Since this did not occur, either the experiments were not continued for a long enough period of time or diffusion of metal ions through the fritted glass disc prevented saturated solutions from being attained.

It should be noted that no corrections were made in the calculations for concentrated electrolytes, so the results are not necessarily applicable to such solutions. H_2 -deaerated solutions were made up with $FeCl_2 \cdot 4H_2O$ and/or $CrCl_3 \cdot 6H_2O$, and the resulting pH's were measured. These results are given in Table 7.

Solutions 1 through 3 (Table 7) were chosen to approximate the final iron and chromium chloride concentrations found in artificial occluded cell experiment KS-108 (Fe - 12% Cr alloy). The dominant influence of chromium with respect to the resulting pH can be seen.

Solutions 4 through 6 (Table 7) were chosen for the purpose of observing the effect of concentrated electrolytes on the resulting pH's. The dominant influence of chromium with respect to the resulting pH is still evident. Solution 6 should be indicative of the most aggressive occluded cell solution possible for the Fe - 12% Cr alloy, assuming no gross dealloying. The ratio of the concentrations of $FeCl_2 \cdot 4H_2O$ and $CrCl_3 \cdot 6H_2O$ of $(4.46)/(0.570) = 7.82$ is the same as the $[Fe]/[Cr]$ ratio in the alloy.

The resulting pH of ~ 0 for solution 6 lends credence to the idea of a "repassivation" mechanism being operative (for the Fe - 12% Cr alloy) for measured "protection potentials" above (more noble than) $\sim 0 v_{SHE}$. As was discussed in Section 2.7.7, a "deactivation" type of "protection potential" implies an instantaneous mixed potential

TABLE 7

pH'S OF H₂-DEAERATED METAL CHLORIDE SOLUTIONS

<u>Solution</u>	<u>Resulting pH</u>
1. 0.240 M FeCl ₂ ·4H ₂ O	3.22
2. 0.0281 M CrCl ₃ ·6H ₂ O	2.75
3. 0.240 M FeCl ₂ ·4H ₂ O + 0.0281 M CrCl ₃ ·6H ₂ O	2.72
4. 0.5 M CrCl ₃ ·6H ₂ O	0.60
5. sat. sol. (4.5 M) FeCl ₂ ·4H ₂ O	1.50
6. sat. sol. (4.5 M) FeCl ₂ ·4H ₂ O + 0.570 M CrCl ₃ ·6H ₂ O	-0.11

involving active metal dissolution and H_2 gas evolution. If the minimum pH inside active occluded cells for the Fe - 12% Cr alloy is ~ 0 , the pH at which the potential for the equilibrium hydrogen electrode is $\sim 0 \text{ v}_{\text{SHE}}$, this implies that a measured "protection potential" above (more noble than) $\sim 0 \text{ v}_{\text{SHE}}$ cannot involve H_2 gas evolution (at atmospheric pressure) and therefore may be indicative of a "repassivation" mechanism being operative.

Figure 57 shows a superposition of the Fe - 12% Cr artificial occluded cell results (Figure 46) and the hydrolysis calculations for aquo-complex ions involving Cr (Figure 55). The results appear to indicate that the presence of the CrOH^{++} complex ion could account for localized acidification in this alloy.

Colorimetric spot tests were used on the final artificial occluded cell solutions to check for the presence of Fe^{++} and Fe^{+++} . 0.1 M potassium ferricyanide [138], $\text{K}_3\text{Fe}(\text{CN})_6$, was used to test for Fe^{++} and 0.1 M potassium thiocyanate [181], KSCN , was used to test for Fe^{+++} . As expected, the tests for Fe^{++} were all positive (Fe^{++} present). It was found that those tests for Fe^{+++} conducted immediately after the conclusion of artificial occluded cell experiments were negative. One test made two weeks after the conclusion of an experiment was weakly positive and one test made one month after the conclusion of an experiment was positive. The two positive tests are believed due to the oxidizing action of the air during the time the samples were stored.

The limit of detection of the thiocyanate test for Fe^{+++} is about 10^{-5} M [89]. Thus, since $[\text{Fe}^{+++}] \leq 10^{-5} \text{ M}$, the presence of Fe^{+++} and the ferric complex ion hydrolysis products in the final artificial

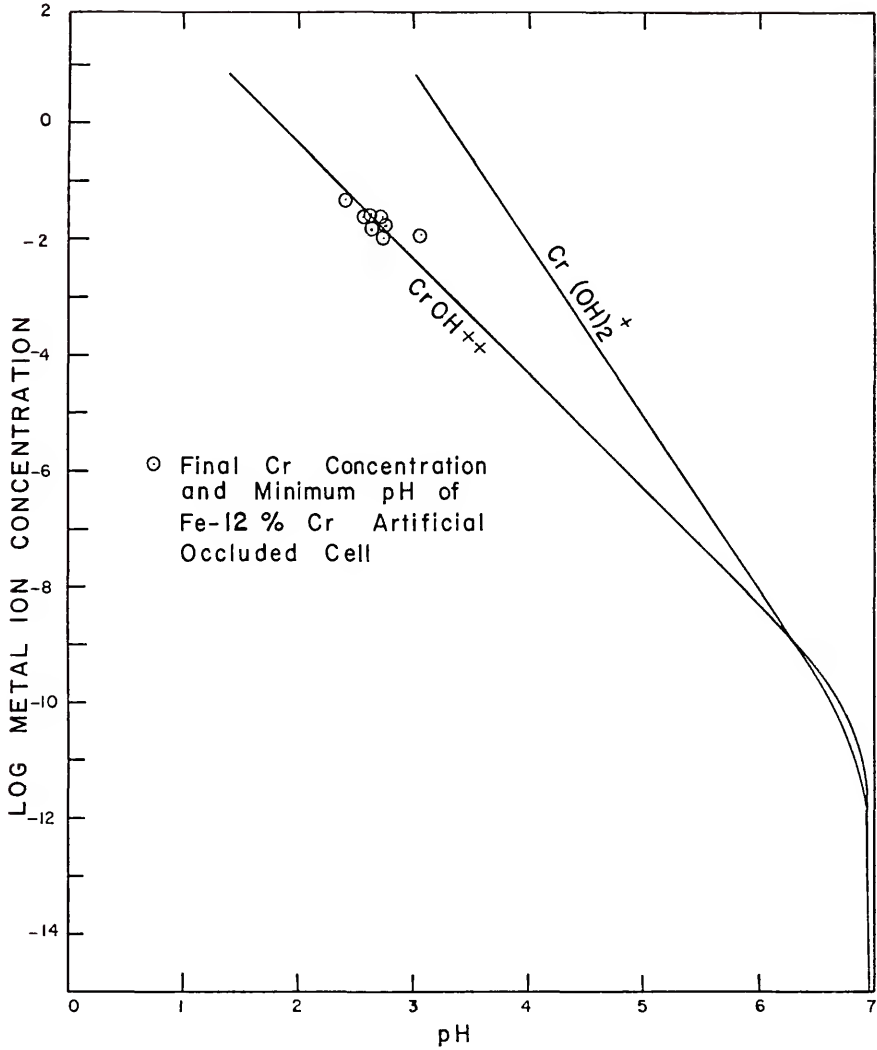
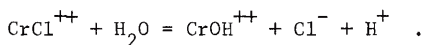


Figure 57. Superposition of Fe - 12% Cr artificial occluded cell results and hydrolysis calculations for aquo-complex ions involving Cr. Log metal ion concentration refers to the concentration (M) of the nonhydrolyzed metal ions.

occluded cell solutions may be neglected for purposes of establishing pH-limiting species.

In the superposition of Fe - 12% Cr artificial occluded cell results and hydrolysis calculations for aquo-complex ions involving Cr, Figure 57, it was assumed that the total [Cr] found for the artificial occluded cells was in the form of Cr^{+++} . The specially calculated equilibrium potential vs. pH (Pourbaix) diagram for the $\text{Cr}-\text{Cl}^--\text{H}_2\text{O}$ system (Figure 54) indicates that CrCl^{++} may be the predominant Cr species.

A reaction for the hydrolysis of CrCl^{++} may be written as



An equilibrium constant for this reaction (in terms of concentrations) may be written as

$$K = \frac{[\text{CrOH}^{++}][\text{Cl}^-][\text{H}^+]}{[\text{CrCl}^{++}][\text{H}_2\text{O}]} .$$

Taking $[\text{CrOH}^{++}] \approx [\text{H}^+]^*$ and $[\text{H}_2\text{O}] \approx 1$,

$$K = \frac{[\text{H}^+]^2 [\text{Cl}^-]}{[\text{CrCl}^{++}]} .$$

From the results of an Fe - 12% Cr artificial occluded cell experiment (KS-103), $[\text{Cr}] = 0.0273$ and $\text{pH} = 2.75$. Taking

*Strictly speaking, $[\text{CrOH}^{++}] = [\text{H}^+] - [\text{OH}^-]$ (as was indicated earlier), but $[\text{OH}^-]$ can be neglected when dealing with acidic solutions.

$$[\text{Fe}] = (7.82)[\text{Cr}] = (7.82)(0.0273) = 0.2135 \quad \text{and}$$

$$[\text{Cl}] = 3[\text{Cr}] + 2[\text{Fe}] = (3)(0.0273) + (2)(0.2135) = 0.5089,$$

$$[\text{CrCl}^{++}] + [\text{CrOH}^{++}] = 0.0273 \quad \text{and}$$

$$[\text{CrCl}^{++}] + [\text{Cl}^-] = 0.5089 - [\text{FeCl}^+] - 2[\text{FeCl}_2] \quad .$$

Although Fe^{++} appeared to predominate over FeCl^+ and FeCl_2 (on a thermodynamic basis), for concentrated electrolytes it may be reasonable to assume the existence of FeCl^+ due to ion association. If this assumption is made,

$$[\text{CrCl}^{++}] + [\text{Cl}^-] = 0.5089 - [\text{FeCl}^+] = (0.5089) - (0.2135)$$

$$[\text{CrCl}^{++}] + [\text{Cl}^-] = 0.2954.$$

Substituting this into the equation for K,

$$K = \frac{[\text{H}^+]^2 (0.2681 + [\text{H}^+])}{(0.0273 - [\text{H}^+])} \quad .$$

Simplifying and rearranging terms,

$$[\text{H}^+]^3 + 0.2681 [\text{H}^+]^2 + K[\text{H}^+] - 0.0273 K = 0 \quad .$$

K for the hydrolysis reaction of CrCl^{++} (using free-energy data from Appendix 17) being 7.405×10^{-6} ,

$$[\text{H}^+]^3 + 0.2681 [\text{H}^+]^2 + 7.405 \times 10^{-6} [\text{H}^+] - 2.0216 \times 10^{-7} = 0 \quad .$$

A trial-and-error solution of this equation gives

$$[\text{H}^+] = 8.51 \times 10^{-4}, \text{ or } \text{pH} = 3.07.$$

This value of pH (3.07) is approximately 0.3 pH units higher than the experimentally measured value (2.75) for the artificial occluded cell in question. This would appear to be reasonably good agreement, in view of the fact that such equilibrium calculations are generally known not to be highly accurate when applied to concentrated electrolytes.

Suzuki et al. [182], unable to account for the low ($\sim 0-1$) pH values attained by their artificial pits (Types 304L and 316L stainless steels, and 18% Cr - 16% Ni - 5% Mo, 0.5 N NaCl initial solutions, 70°C) with solid hydroxide hydrolysis products, hypothesized the existence of "hydroxy-chloro-complexes" (CrOHCl^+ might be an example) in concentrated metal chloride solutions. Unfortunately, thermodynamic data for such complexes are apparently not yet available.

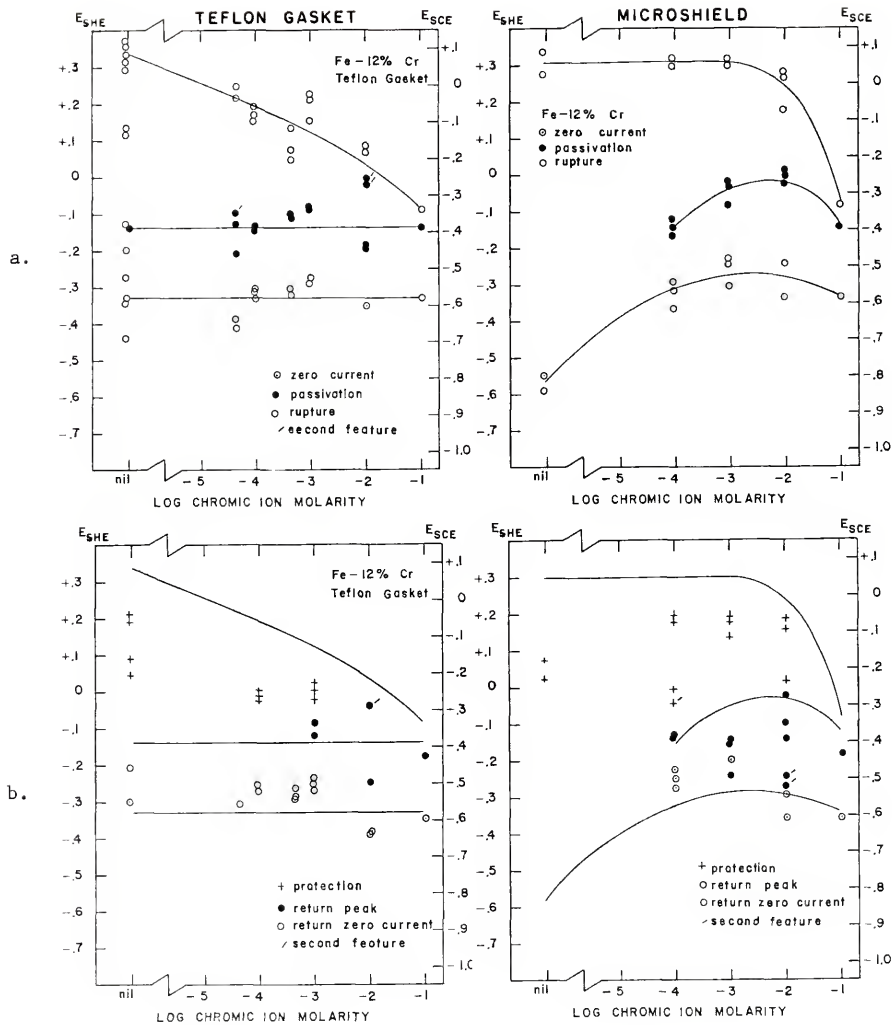
4.5 Metal Chloride Solution Scans

In order to understand better the behavior of the Fe - 12% Cr alloy in metal chloride solutions, potentiokinetic polarization scans were conducted in 0.1 M NaCl, H_2 -saturated solutions with $\text{CrCl}_3 \cdot 6\text{H}_2\text{O}$ and $\text{FeCl}_2 \cdot 4\text{H}_2\text{O}$ added in proper proportions so as to maintain the correct $[\text{Fe}]/[\text{Cr}]$ ratio of 7.82 for the alloy (taking into account the presence of carbides).

The results, plotted in terms of potential vs. log chromic ion molarity, are presented in Figure 58. Figure 58a contains zero current potentials, primary passivation potentials, rupture potentials and second feature* potentials (all determined from out scans) for

* Second peak, zero, etc. during a single out scan or return scan.

- Figure 58. a. Potential vs. log chromic ion molarity diagrams for the Fe - 12% Cr alloy in 0.1 M NaCl, H₂-saturated solutions with CrCl₃·6H₂O and FeCl₂·4H₂O added ([Fe]/[Cr] ratio of 7.82). The diagrams contain zero current potentials, primary passivation potentials, rupture potentials and second feature potentials (all determined from out scans), for samples mounted in the standard sample holder ("Teflon Gasket") and for samples painted off with Microshield.
- b. "Protection potentials" (E_p), return peak potentials, return zero current potentials and second feature potentials (all determined from return scans), superimposed on the zero current potential, primary passivation potential and rupture potential lines taken from Figure 58a.



samples mounted in the standard sample holder ("Teflon^{*} Gasket") and for samples painted off with Microshield⁺ lacquer. Figure 58b contains "protection potentials," return peak potentials, return zero current potentials and second feature[‡] potentials (all determined from return scans), superimposed on the zero current potential, primary passivation potential and rupture potential lines taken from Figure 58a. The data are given in Appendix 19.

The most significant point to be made concerning the diagrams presented in Figure 58a is that while the rupture potential decreases (becomes more active) with increasing chromic ion molarity for the "Teflon Gasket" samples, the rupture potential is independent of chromic ion molarity up to and including 10^{-3} M for the "Microshield" samples. This may be indicative of an increased tendency for crevice attack of the "Teflon Gasket" samples in these solutions.

In Figure 58b, the return scan-data appear to be somewhat similar to the out-scan data presented in Figure 58a. The measured "protection potentials," which were in some cases better described as arrests (probably not true "protection potentials"), were sometimes only about 0.1 v below (more active) than the corresponding rupture potentials. The similarity between out scans and return scans in these particular metal chloride solutions, at least in the more concentrated solutions, may be due to the possibility that the solutions existing inside active

*Trade name of E. I. DuPont de Nemours and Co., Inc.

+Trade name of Michigan Chrome and Chemical Co.

‡Second peak, zero, etc. during a single out scan or return scan.

occluded cells are not unlike the respective bulk solutions.

Figure 59 shows some of the metal chloride solution scan data for the "Teflon Gasket" samples, superimposed on the experimental potential vs. pH diagram for the Fe - 12% Cr alloy in 0.1 M Cl^- , H_2 -saturated solutions. Those data plotted correspond to metal chloride solutions of not more than 0.14 M total chloride. The rough agreement suggests that the predominant role of the metal chlorides in dilute solutions may be to control the solution pH. The scatter of the zero current potential data for $\text{pH} \sim 6$ may reflect the fact that these solutions (0.1 M NaCl with no metal chlorides added) contained no buffers.

Figure 60 presents log passivation current density vs. log chromic ion molarity diagrams constructed from the metal chloride solution scan data (Appendix 19) for the "Teflon Gasket" samples and for the "Microshield" samples. The passivation current density refers to the current density corresponding to the primary passivation potential. The results indicate a tendency for an increasing passivation current density with increasing chromic ion molarity. Note that all current densities are expressed in terms of a/cm^2 , unless otherwise noted.

Figure 61 presents log current density vs. log chromic ion molarity diagrams constructed from the metal chloride solution scan data (Appendix 19) for the "Teflon Gasket" samples and for the "Microshield" samples. Plotted are the minimum current densities and second feature current densities (second minimums) attained during the out scans, superimposed on the primary passivation current density lines from Figure 60.

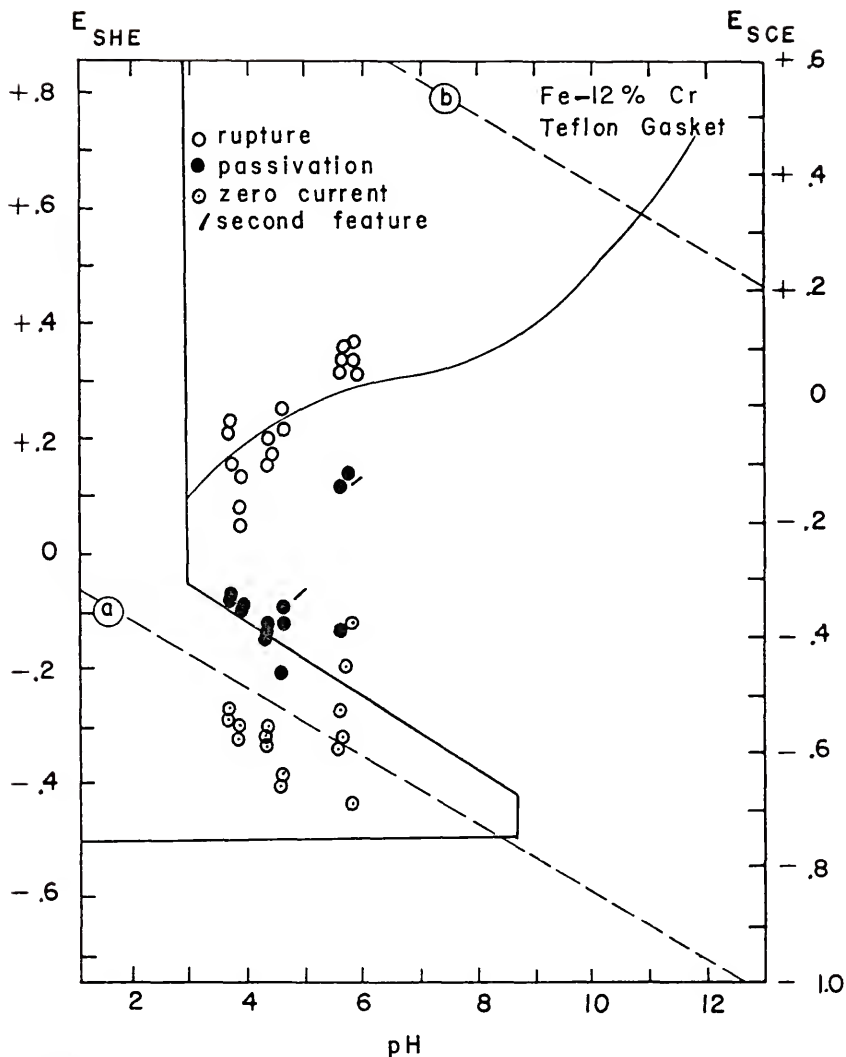


Figure 59. Some of the metal chloride solution scan data for the "Teflon Gasket" samples, superimposed on the experimental potential vs. pH diagram for the Fe - 12% Cr alloy in 0.1 M Cl⁻, H₂-saturated solutions. Those data plotted correspond to metal chloride solutions of not more than 0.14 M total chloride. Included are zero current potentials, primary passivation potentials, rupture potentials and second feature potentials.

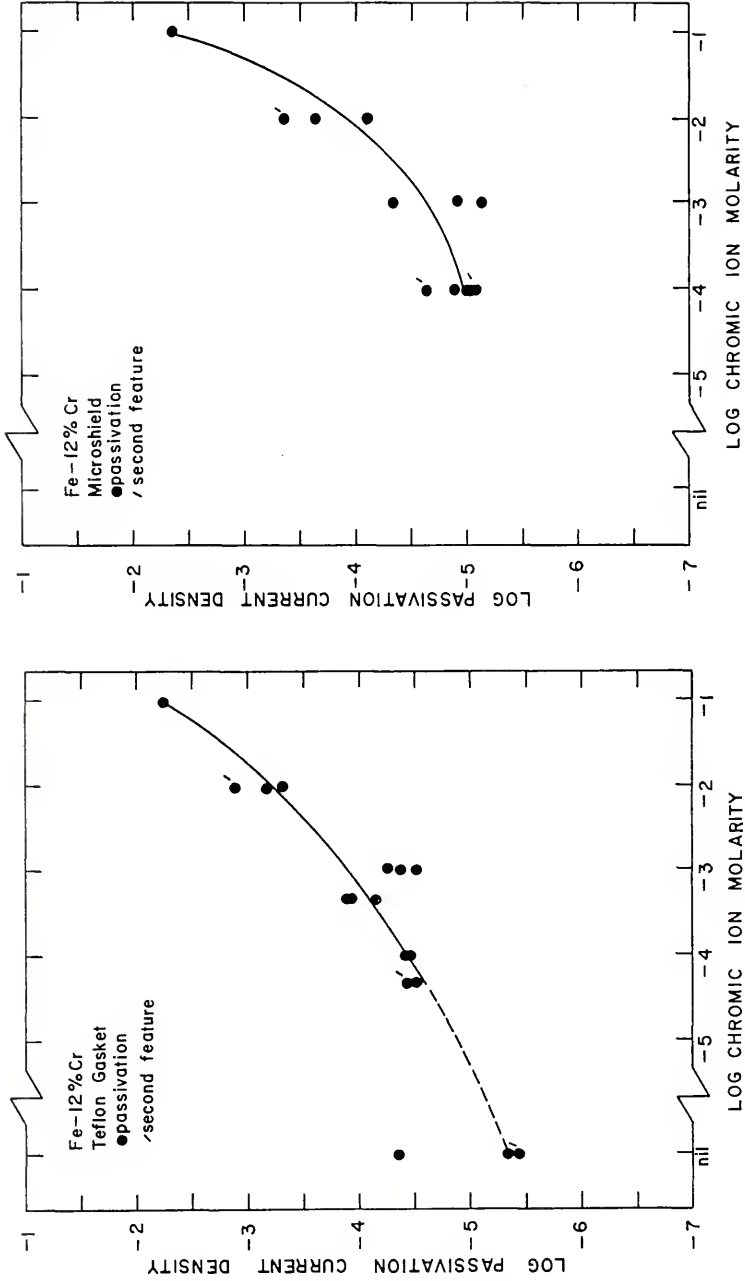


Figure 60. Log passivation current density (a/cm^2) vs. log chromic ion molarity diagrams constructed from the metal chloride solution scan data for "Teflon Gasket" samples and for "Microshield" samples of the Fe - 12% Cr alloy.

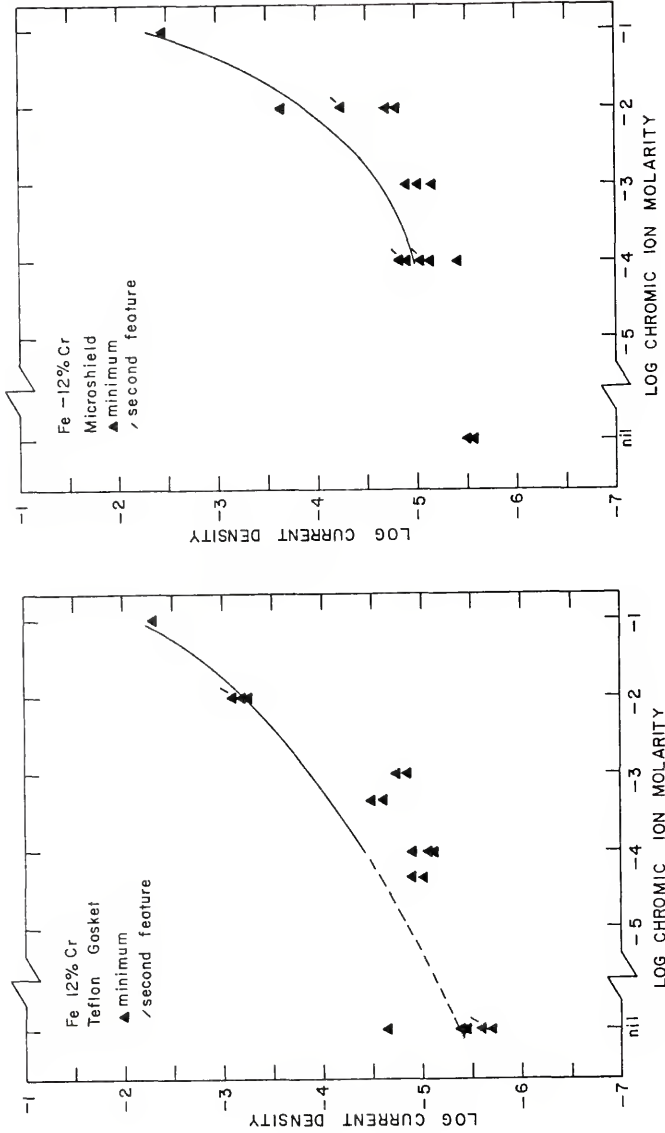


Figure 61. Log current density (a/cm^2) vs. log chromic ion molarity diagrams constructed from the metal chloride solution scan data for "Teflon Gasket" samples and for "Microshield" samples of the Fe - 12% Cr alloy. Plotted are the minimum current densities attained during the out scans and second features (second minimum current densities attained during out scans), superimposed on the primary passivation current density lines from Figure 60.

The data plotted in Figure 61 emphasize that the minimum current densities attained during the out scans in metal chloride solutions were nearly as high as the passivation current densities. The relatively high minimum current densities corresponding to the more concentrated metal chloride solutions (10^{-2} and 10^{-1} M chromic ion) suggest a tendency for the metal chloride solutions to interfere with or detract from the "protectiveness" of any passive films on the Fe - 12% Cr alloy.

Figure 62 presents log passivation current density vs. log chloride ion molarity diagrams constructed from potentiokinetic polarization data (Appendix 11) for the Fe - 12% Cr alloy in H_2 -saturated solutions of pH 5.4, 8.8 and 10.8. Passivation current densities appear to be relatively independent of chloride ion molarity for the solutions studied [55, 154].

Figure 63 is a log passivation current density vs. pH diagram constructed from potentiokinetic polarization data (Appendix 8) for the Fe - 12% Cr alloy in 0.1 M (Molar) Cl^- , H_2 -saturated solutions. A tendency is noted for increasing passivation current densities with decreasing pH's.

Figure 64 is a plot of the metal chloride solution ($[Fe]/[Cr] = 7.82$) scan data (Appendix 19) for the "Teflon Gasket" samples, superimposed on the log passivation current density line for the Fe - 12% Cr alloy in 0.1 M (molar) Cl^- , H_2 -saturated solutions (from Figure 63). There appears to be rough agreement down to pH's of about 3.7, again indicating the possibility that the predominant role of the metal chlorides in dilute solutions may be to control the solution pH.

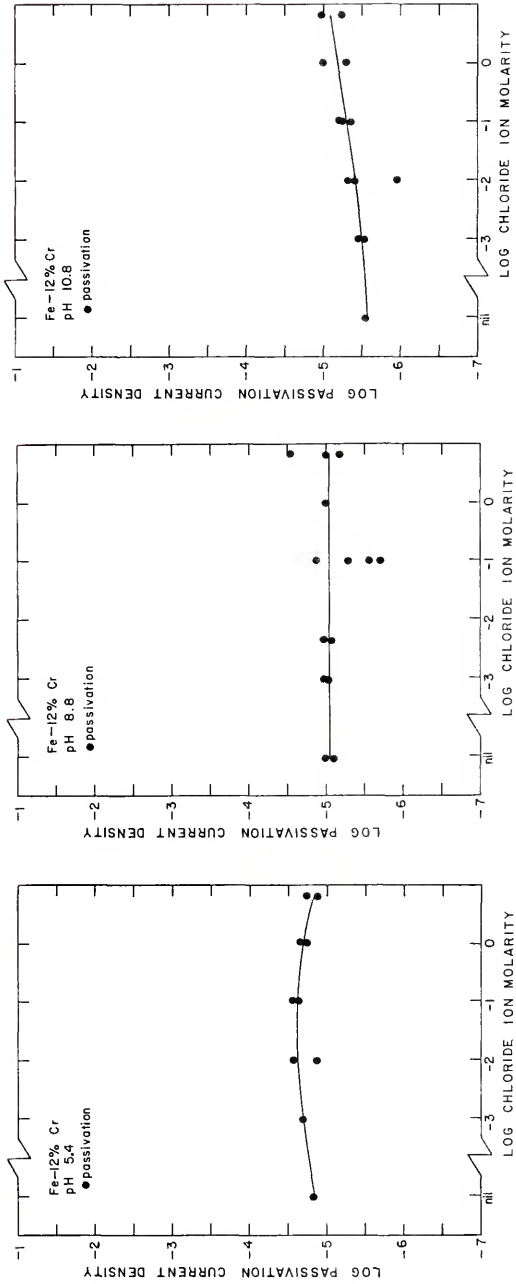


Figure 62. Log passivation current density (a/cm^2) vs. log chloride ion molarity diagrams constructed from potentiokinetic polarization data for the Fe - 12% Cr alloy in H_2O -saturated solutions of pH 5.4, 8.8 and 10.8.

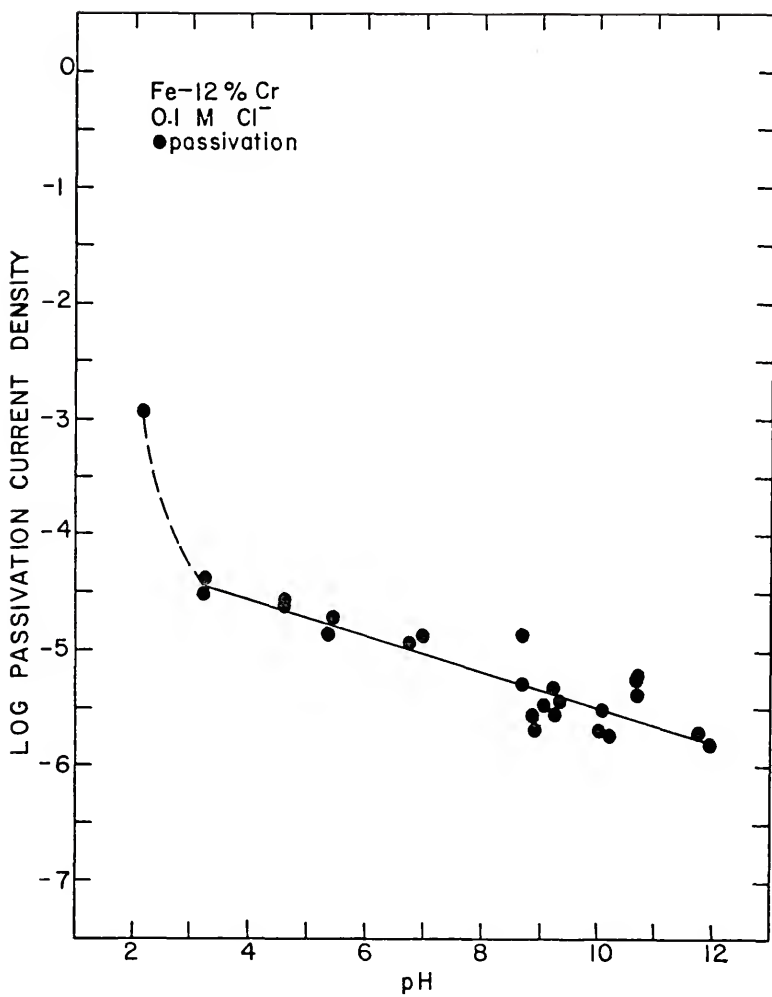


Figure 63. Log passivation current density (a/cm^2) vs. pH diagram constructed from potentiokinetic polarization data for the Fe - 12% Cr alloy in 0.1 M (molar) Cl⁻, H₂-saturated solutions.

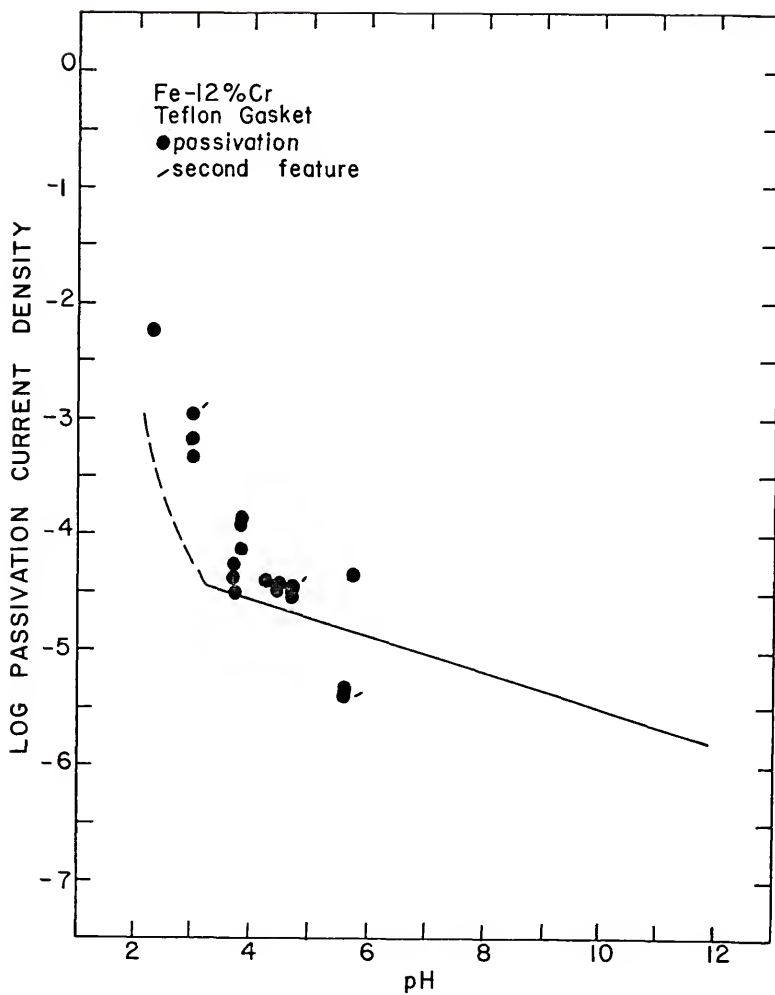


Figure 64. Metal chloride solution ($[\text{Fe}]/[\text{Cr}] = 7.82$) scan data superimposed on the log passivation current density (a/cm^2) line for the Fe - 12% Cr alloy in 0.1 M (molar) Cl^- , H_2 -saturated solutions (from Figure 63).

The apparent disagreement at lower pH's (more concentrated solutions of metal chlorides) may be a result of the increased chloride ion concentration. Chin and Nobe [183], investigating the dissolution kinetics of iron in acidic chloride media $\{0.1 \text{ N HClO}_4 + x\text{N NaCl} + y\text{N NaClO}_4 (x + y = 1.9)\}$ by potentiostatic polarization, observed that an increase in the chloride ion concentration, at a constant pH (~ 1), increased the dissolution rate of iron.

4.6 Potentiostatic Titration Results

The technique of titrating a particular solution into an electrochemical cell containing a solid metallic electrode, potentiostated at a given electrochemical potential while monitoring the applied current, hereafter referred to as "potentiostatic titration," was described for the case of chloride titrations in Section 2.4.1.6.

4.6.1 pH Titrations

Potentiostatic pH titrations for the Fe - 12% Cr alloy were conducted in the standard electrochemical polarization cell described in Appendix 12. As was mentioned at the beginning of Chapter 3, an additional hole was drilled in the Teflon lid to permit the insertion of a combination glass/Ag-AgCl pH electrode into the cell. A 250 ml burette was inserted in the thermometer hole.

The initial solutions were 0.1 M NaCl or 0.1 M NaCl + $\sim 0.001 \text{ M NaOH}$ ($\text{pH} \approx 10$). The solutions were either H_2 -saturated or O_2 -saturated. The titrant was 0.1 M HCl, H_2 -saturated for the H_2 -saturated solutions. The painted-off Fe - 12% Cr alloy samples were potentiostated at

either -0.250 or -0.300 v_{SCE} (0.000 or -0.050 v_{SHE}). The 0.1 M HCl was added in increments, while monitoring both pH and applied current.

After an increment had been added, pH and applied current readings were taken 3-5 min later. The critical pH necessary for the breakdown of passivity was considered to be that corresponding to an applied current density of just less than $+25$ $\mu\text{a}/\text{cm}^2$. The results, given in Table 8, were used to help establish the vertical lines separating the corrosion region from the passivation and pitting regions on the experimental potential vs. pH diagrams for the Fe - 12% Cr alloy in 0.1 M Cl^- solutions presented in Figures 20 and 21.

4.6.2 Metal Chloride Titrations

The metal chloride titrations for the Fe - 12% Cr alloy were conducted similarly to the pH titrations, except that the titrant was 0.1 M NaCl + 0.1 M $\text{CrCl}_3 \cdot 6\text{H}_2\text{O}$ + 0.782 M $\text{FeCl}_2 \cdot 4\text{H}_2\text{O}$ ([Fe]/[Cr] ratio of 7.82 for the Fe - 12% Cr alloy). The purpose was to determine the critical concentration of metal chlorides necessary for the breakdown of passivity. The initial solutions were 0.1 M NaCl, H_2 -saturated. The Fe - 12% alloy samples were potentiostated at -0.100 , -0.150 , -0.250 and -0.350 v_{SCE} ($+0.150$, $+0.100$, 0.000 and -0.100 v_{SHE}).

The procedure was to record the volume increments of metal chloride solution added and, after a waiting period of 3 min, the pH and applied current were recorded. The critical amount of metal chloride solution and pH necessary for the breakdown of passivity was considered to be that corresponding to an applied current density of just less than $+25$ $\mu\text{a}/\text{cm}^2$.

TABLE 8

pH TITRATION RESULTS: Fe-12% Cr ALLOY

Run No.	Purging Gas	Holding Potential (v _{SCE})	(pH) Initial	[Cl ⁻] (M)	(pH) Critical
KS-130	H ₂	-0.250	10.8	0.1	2.9
KS-131	H ₂	-0.250	10.8	0.1	3.0
KS-244	H ₂	-0.250	6.3	0.1	2.9
KS-239	H ₂	-0.300	7.1	0.1	2.7
KS-243	H ₂	-0.300	6.5	0.1	2.7
KS-241	O ₂	-0.250	5.6	0.1	2.3
KS-245	O ₂	-0.250	5.6	0.1	2.4
KS-242	O ₂	-0.300	5.7	0.1	2.3
KS-140	H ₂	-0.250	10.6	1.0	3.6

The final volume of solution in the standard electrochemical cell was measured immediately after each run. This volume, the volume of titrant added, and the concentration of the titrant were then used to calculate the critical concentration of metal chlorides.

The results are given in Table 9. The concentrations of metal chlorides necessary for the breakdown of passivity on the Fe - 12% Cr alloy are more dilute than those attained in the artificial occluded cells. This supports the idea that an active pit or crevice (for this alloy) may propagate to an extent precluding the possibility of a "repassivation" mechanism unless there is dilution of the contents of the pit or crevice.

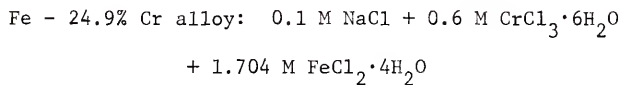
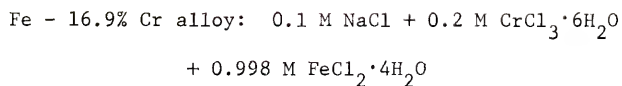
In addition, the critical pH observed for the Fe - 12% Cr metal chloride titrations at $-0.250 v_{SCE}$ ($0.000 v_{SHE}$) of 3.3 to 3.4 appears to be significantly higher than that observed for the pH titrations at the same potential (critical pH of 2.9 to 3.0). This may be due in part to a slightly higher final $[Cl^-]$ for the metal chloride titrations (0.17 M vs. 0.1 M) and in part to an increased tendency for crevice attack in metal chloride solutions.

Metal chloride titration experiments were conducted for the Fe - 5.0% Cr, Fe-16.9% Cr and Fe - 24.9% Cr alloys at $-0.250 v_{SCE}$ ($0.000 v_{SHE}$). The results (including the Fe - 12% Cr results) are given in Table 10. The Fe - 5.0% Cr alloy underwent a breakdown in passivity almost immediately, without the addition of any metal chloride solution (possibly due to the lack of any buffers in the initial solution). The compositions of the titrants used for the Fe - 16.9% Cr and Fe - 24.9% Cr alloys were as follows:

TABLE 9

METAL CHLORIDE TITRATION RESULTS: Fe-12% Cr ALLOY,
0.1M NaCl, H₂-SATURATED INITIAL SOLUTIONS

Run No.	Holding Potential (V _{SCE})	[Cr ⁺⁺⁺] (M) Critical	[Fe ⁺⁺] (M) Critical	[Cl ⁻] (M) Critical	(pH) Critical
KS-254	-0.100	0	0	0.10	6.9
KS-255	-0.100	3.78×10^{-3}	2.96×10^{-2}	0.17	3.8
KS-252	-0.150	5.24×10^{-3}	4.10×10^{-2}	0.20	3.2
KS-253	-0.150	5.34×10^{-3}	4.18×10^{-2}	0.20	3.1
KS-222	-0.250	4.12×10^{-3}	3.22×10^{-2}	0.18	3.3
KS-223	-0.250	4.03×10^{-3}	3.15×10^{-2}	0.18	3.4
KS-248	-0.350	$<1.88 \times 10^{-4}$	$<1.47 \times 10^{-3}$	0.10	>4.2
KS-249	-0.350	$<1.12 \times 10^{-4}$	$<8.76 \times 10^{-4}$	0.10	>4.3



A sample calculation of the $[\text{Fe}]/[\text{Cr}]$ ratio for an alloy (Fe - 12% Cr), taking into account the presence of carbides, is included in Appendix 16.

Table 10 shows that the critical concentrations of metal chlorides necessary for the breakdown of passivity at this potential ($-0.250 v_{\text{SCE}}$; $0.000 v_{\text{SHE}}$) increase with increasing Cr content in the alloy. The Fe - 5.0% Cr alloy (and, presumably, the Fe - 0.5% Cr and Fe - 2.0% Cr alloys) can tolerate little or no metal chlorides, the Fe - 12% Cr alloy can tolerate rather low concentrations of metal chlorides, and the Fe - 16.9% Cr and Fe - 24.9% Cr alloys can tolerate more concentrated metal chloride solutions.

The results given in Table 10 appear to support the earlier suggestion that the Fe - 0.5% Cr, Fe - 2.0% Cr and Fe - 5.0% Cr "protection potentials" (as determined by cyclic potentiokinetic polarization scans) were indicative of a predominately "deactivation" mechanism, that the Fe - 16.9% Cr and Fe - 24.9% Cr "protection potentials" were indicative of a predominately "repassivation" mechanism, and that the Fe - 12% Cr "protection potentials" were indicative of transitional behavior (either or both mechanisms being operative).

TABLE 10

METAL CHLORIDE TITRATION RESULTS: Fe - 5.0% Cr, Fe - 12% Cr, Fe - 16.9% Cr AND
 Fe - 24.9% Cr ALLOYS 0.1 M NaCl, H₂-SATURATED INITIAL SOLUTIONS,
 HOLDING POTENTIAL -0.250 v_{SCE} (0.000 v_{SHE})

Run No.	Alloy	[Cr ⁺⁺⁺] (M) Critical	[Fe ⁺⁺] (M) Critical	[Cl ⁻] (M) Critical	(pH) Critical
KS-278	Fe-5.0% Cr	0	0	0.1	5.6
KS-222	Fe-12% Cr	4.12×10^{-3}	3.22×10^{-2}	0.18	3.3
KS-223	Fe-12% Cr	4.03×10^{-3}	3.15×10^{-2}	0.18	3.4
KS-322	Fe-16.9% Cr	0.116	0.579	1.61	1.9
KS-323	Fe-16.9% Cr	0.103	0.514	1.44	2.0
KS-327	Fe-24.9% Cr	0.432	1.23	3.85	0.9
KS-328	Fe-24.9% Cr	0.445	1.26	3.96	0.9

CHAPTER 5

CONCLUSIONS

1. The "protection potential," as determined from cyclic potentiokinetic polarization curves, although influenced somewhat by both alloy composition and environment, is nonetheless of considerable engineering importance since it provides information with regard to the propagation stage of pitting or crevice (occluded cell) corrosion.

2. Both "repassivation" and "deactivation" mechanisms appear to be operative in determining the "protection potential" for the binary Fe-Cr alloys, depending upon the particular alloy/environment system.

3. The "protection potential," as determined from cyclic potentiokinetic polarization curves, appears to be useful in establishing the potential/pH/[Cl⁻] ranges for which a particular Fe-Cr alloy may be anodically or cathodically protected in a given environment.

4. Careful judgment must be exercised in applying "protection potential" results for one alloy/environment system to other alloy/environment systems.

5. When the "protection potential" approximately equals the corresponding zero current potential (out scan) this is taken as being indicative of a "deactivation" mechanism, reflecting an instantaneous mixed potential involving active metal dissolution and hydrogen evolution.

6. When the "protection potential" is determined to be above (more noble than) the equilibrium hydrogen electrode potential

(taking into account localized acidification by metal hydrolysis) this is believed indicative of a "repassivation" mechanism. For example, an assumed local pH of ~ 0 corresponds to an equilibrium hydrogen electrode potential of $0.000 \text{ v}_{\text{SHE}}$. Hence "protection potentials" appreciably above (more noble than) $0.000 \text{ v}_{\text{SHE}}$ at this pH may be indicative of a "repassivation" mechanism.

7. At any pH, "protection potentials" slightly more noble than the equilibrium hydrogen electrode potential may nonetheless be indicative of a "deactivation" mechanism since localized acidification would raise (make more noble) the equilibrium hydrogen electrode potential locally.

8. Concerning cyclic potentiokinetic polarization scans in H_2 -saturated solutions, a second out scan (noble direction) conducted immediately after recording the "protection potential" appears useful in discriminating between "deactivation" and "repassivation" mechanisms.

9. It may be possible for both "repassivation" and "deactivation" mechanisms to operate simultaneously, some pits (or crevices) deactivating and some repassivating.

10. "Protection potentials," for alkaline bulk solutions, which roughly parallel (but are more noble than) the equilibrium hydrogen electrode ("a") line nonetheless may be indicative of a "deactivation" mechanism. The potential/pH path resulting from localized acidification and drop in potential (occasioned or assisted by the presence of solid oxide or hydroxide corrosion products) is postulated to intersect the "a" line (equilibrium hydrogen electrode potential locus) at

different points, depending upon bulk solution pH. Under these circumstances the "deactivation" would occur within local occluded cells at potentials more active than the equilibrium hydrogen electrode potential.

Concerning "protection potential" (E_p) data obtained from cyclic potentiokinetic polarization scans in 0.1 M (molar) Cl^- , H_2 -saturated electrolytes:

11. The "protection potential" commonly tends to increase (become more noble) with increasing chromium content for binary Fe-Cr alloys.

12. The relatively low (active) "protection potential" data for the Fe - 0.5% Cr, Fe - 2.0% Cr and Fe - 5.0% Cr alloys suggest that a "deactivation" mechanism predominates for these alloys.

13. The relatively high (noble) "protection potential" data for the Fe - 16.9% Cr and Fe - 24.9% Cr alloys suggest that a "repassivation" mechanism predominates for these alloys.

14. The relatively high (noble) and relatively low (active) observed "protection potential" data for the Fe - 12% Cr alloy suggests that transitional or combined mechanisms are operative for this alloy.

15. The "protection potential" data for the Fe - 0.5% Cr, Fe - 2.0% Cr and Fe - 5.0% Cr alloys approach the zero current potential line of each alloy in acidic solutions, exhibit a break or discontinuity at about pH 8, and roughly parallel the equilibrium hydrogen electrode ("a") line for pH's above 8. According to

conclusions 5 and 10, this behavior may be rationalized in terms of a "deactivation" mechanism.

16. The "protection potential" data for the Fe - 12% Cr alloy increase (become more noble) with increasing pH in acidic solutions and roughly parallel the equilibrium hydrogen electrode ("a") line for pH's above 8. By using the technique of making a second out scan (immediately after recording the "protection potential"), a "deactivation" mechanism appeared to be operative for pH's below 3.2 - 4.4 and above 9.7 - 10.9, with a "repassivation" mechanism being operative for intermediate pH's.

17. Concerning "protection potential" (E_p) data obtained from cyclic potentiokinetic polarization scans in H_2 -saturated solutions of nominal pH 5.4, 8.8 and 10.8 for the Fe - 0.5% Cr, Fe - 2.0% Cr, Fe - 12% Cr and Fe - 16.9% Cr alloys, the "protection potential" commonly appears to decrease (become more active) with increasing bulk chloride ion concentration. This behavior is consistent with the assumption of a tendency for a change in mechanism (for some alloys) from "repassivation" to "deactivation."

18. Concerning "protection potential" (E_p) vs. extent of propagation data obtained from cyclic potentiokinetic polarization scans for the Fe - 12% Cr alloy in 0.1 M Cl^- , H_2 -saturated solutions of nominal pH 10.1, the "protection potential" tends to decrease (become more active) with increasing extent of propagation. A break or discontinuity in the data suggests a possible change in mechanism (from "repassivation" to "deactivation"). The single-pit data appear to be relatively independent of the extent of propagation, implying

that one result of continuing propagation of a multi-pit sample may be to increase the number of active pits and thereby increase the chances for one or more of these pits to remain in the active state.

The following conclusions concern artificial occluded cell experiments in solutions initially 0.1 M (molar) Cl^- for Armco Fe and the Fe - 12% Cr alloy:

19. The artificial occluded cells for the Fe - 12% Cr alloy attained lower (more acidic) pH's than did similar cells for Armco Fe and eventually attained potentials and pH's corresponding to a potential/pH region of active metal dissolution. It appears that an active pit (or crevice) of the Fe - 12% Cr alloy may propagate to an extent precluding the possibility of a "repassivation" mechanism unless there is dilution of the contents of the pit (or crevice).

20. Results for the Fe - 12% Cr alloy give no evidence of macroscopic dealloying, based on atomic absorption analyses. The total metal chlorides in solution correspond approximately to the relationship $[\text{Cl}] = (2)[\text{Fe}] + (3)[\text{Cr}]$, based on atomic absorption analyses and potentiometric AgNO_3 titrations.

21. Thermodynamic calculations, combined with artificial occluded cell results for the Fe - 12% Cr alloy, predict CrCl^{++} to be quantitatively predominant but suggest that CrOH^{++} may be one of the pH-limiting species in active pits and crevices of this alloy.

CHAPTER 6

RECOMMENDATIONS FOR FURTHER RESEARCH

The results of this investigation reveal several areas of research which should be fruitful, from both scientific and economic points of view:

1. The technique of making a second out scan (noble direction) immediately after recording the "protection potential" should be applied to other alloys and electrolytes. It may be useful to incorporate this procedure into routine determinations of the "protection potential" from cyclic potentiokinetic polarization curves.

2. A detailed study of the "protection potential" in actual sea water is needed, complete with corroborative, long-term, potentiostatic corrosion tests.

3. Metal chloride titrations should be carried out for alloys of higher chromium content to see if a critical chromium content exists, above which the alloy would be completely resistant to metal chloride solutions.

4. Additional work is needed to determine how the local chemistry of active occluded cells in NaCl solutions compares with that in sea water (for example, how the chemistry is influenced by the presence of microorganisms).

5. A detailed study of hydrolysis mechanisms, perhaps including more elaborate thermodynamic calculations and experimental techniques (including the use of ion-sensitive electrodes and colorimetry), is needed to better understand the chemistry inside active occluded cells.

APPENDICES

APPENDIX 1
ALLOY CHARACTERIZATION

The compositions of the iron-chromium alloys under investigation are given in Table 11. The microstructures of the alloys have been described elsewhere [55]. It was concluded that although the microstructures of the six iron-chromium alloys were seen to differ greatly, the electrochemical data were independent of the observed microstructures.

Figure 65 is a phase diagram for the Fe-Cr system, according to Hansen [184]. It should be noted that this diagram does not take into account the effects of C or other alloying elements. It can be seen the γ phase no longer forms above approximately 13 weight percent Cr.

Early work on the Fe - 12% Cr alloy was done in the as-forged condition. Later an annealing heat treatment [185] was performed in order to facilitate sample preparation. The details of the heat treatment, which was carried out under an argon atmosphere, were as follows:

1. Hold at 1585°F for 6-12 hours.
2. Furnace cool to 1350°F.
3. Hold at 1350°F for 6-12 hours.
4. Furnace cool.

The as-forged hardness and annealed hardness were approximately Rockwell C45 and Rockwell B75, respectively. The as-forged and annealed microstructures are given in Figures 66 and 67.

TABLE 11

COMPOSITIONS OF BINARY IRON-CHROMIUM ALLOYS UNDER INVESTIGATION

Alloy	Cr	C	Mn	P	S	Si	Cu	Ni	Source
1	0.5	0.15	1.3	0.011	0.037	0.22	0.09	0.12	USS
2	2.0	0.16	1.4	0.010	0.022	0.22	0.09	0.03	USS
3	5.0	0.16	1.4	0.010	0.022	0.19	0.09	0.05	USS
4	12.0	0.15	0.3*	NA	0.012*	NA	0.09*	0.08*	NRL
5	16.9	0.17	1.3	0.014	0.018	0.17	0.09	0.11	USS
6	24.9	0.09	0.82	0.020	0.015	0.22	0.08	0.29	USS

USS--United States Steel Corporation, Monroeville, Pennsylvania

NRL--Naval Research Laboratory, Washington, D. C.

*X-ray Fluorescence Analysis

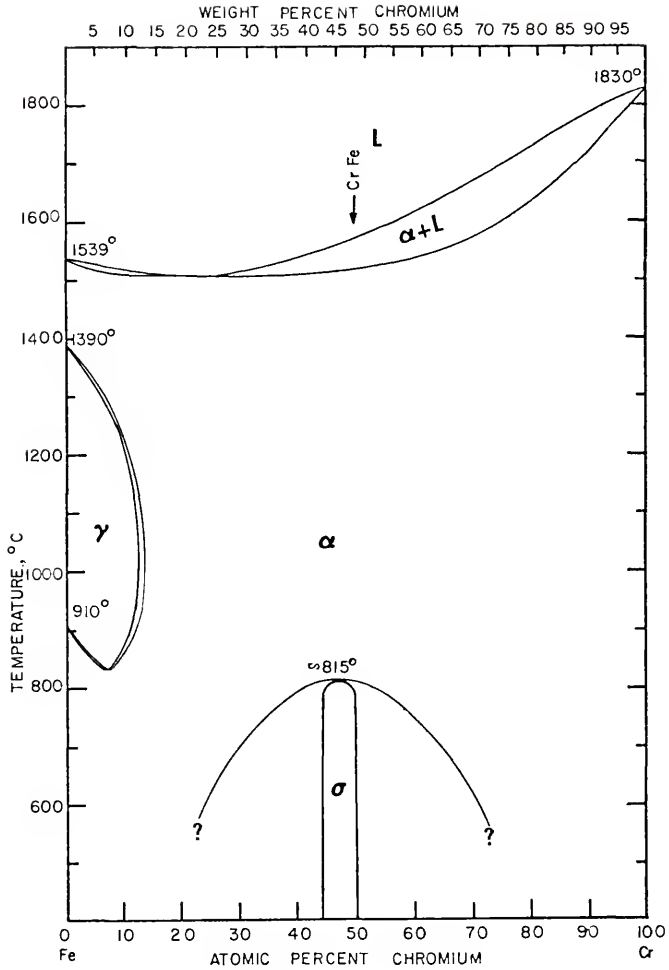


Figure 65. Phase diagram for the Fe-Cr system, according to Hansen [184, p. 527].

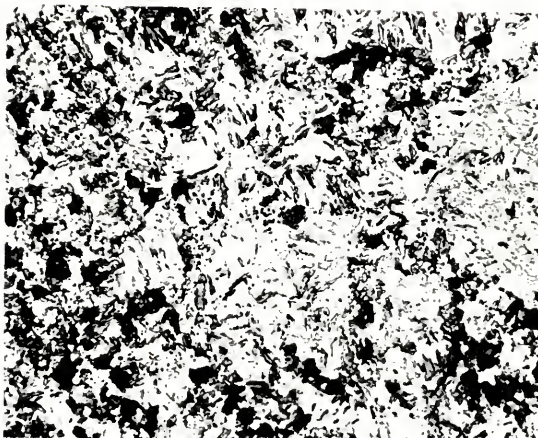


Figure 66. Photomicrograph of the as-forged Fe - 12% Cr alloy showing delta ferrite in a martensite matrix (magnification 500 X).



Figure 67. Photomicrograph of the annealed Fe - 12% Cr alloy showing a matrix of equiaxed ferrite grains, with randomly dispersed particles of chromium carbide (magnification 500 X).

The as-forged microstructure appears to consist of delta ferrite in a martensite matrix [186]. The annealed microstructure appears to consist of a matrix of equiaxed ferrite grains, with randomly dispersed particles of chromium carbide [186].

APPENDIX 2

STANDARD ELECTROCHEMICAL POLARIZATION CELL

The standard electrochemical polarization cell employed during this investigation has been discussed elsewhere [157, 54, 55, 154]. A schematic drawing of the standard cell appears in Figure 68. The cell is constructed of Pyrex^{*} glass with a Teflon⁺ lid bolted to a polycarbonate Van-Stone backing ring, resulting in a gastight system. A bright platinum screen serves as an auxiliary electrode. The Haber-Luggin probe electrically connects the cell via a glass bridge filled with electrolyte to a beaker containing a saturated calomel reference electrode.

The gas (hydrogen) diffuser provides for continuous purging of the electrolyte during the experiment [187]. Prior to transferring the electrolyte into the cell, air is displaced from the cell and the electrolyte is vacuum deaerated. Appendix 5 shows a calculation of the concentration of oxygen remaining in the electrolyte after deaeration. The solution in the cell is constantly stirred using either a water-powered or an electric magnetic stirrer.

* Trade name of Corning Glass Works.

+ Trade name of E. I. du Pont de Nemours and Co., Inc.

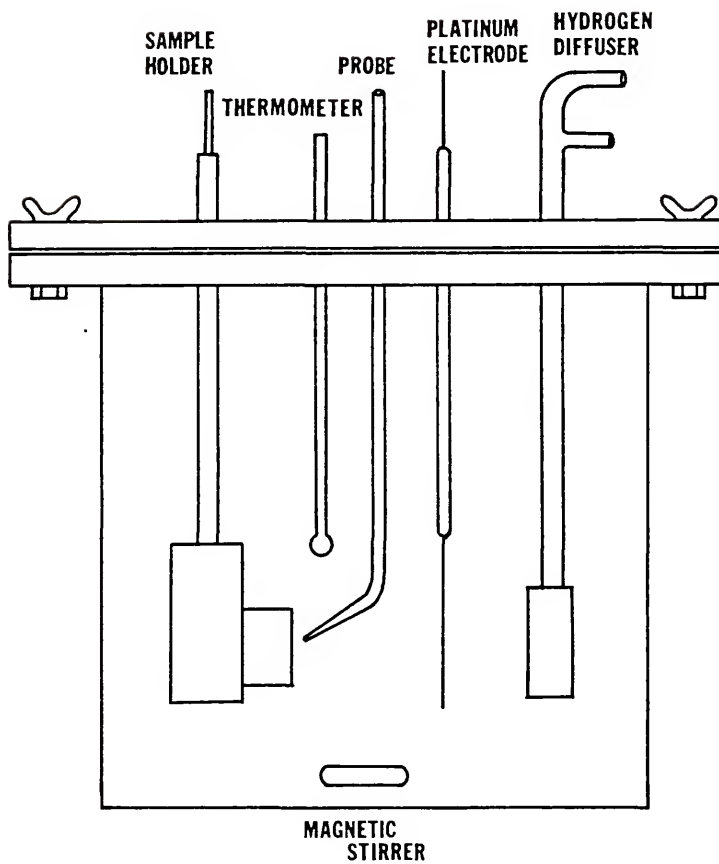
CORROSION CELL SCHEMATIC

Figure 68. Standard electrochemical polarization cell used during this investigation.

APPENDIX 3

SAMPLE PREPARATION AND MOUNTING

The effects of sample preparation variables were discussed elsewhere [55]. Early samples were hand-ground dry through 4/0 emery papers. Later samples were hand-ground wet through 600 grit silicon carbide papers. The two methods gave reproducible and similar results.

The hand-ground samples were hand-cleaned in a laboratory detergent, rinsed with distilled/deionized water and air dried. Samples were then stored in a desiccator, when necessary, or in open air.

Two sample mounting techniques were used: a Teflon^{*}/polycarbonate demountable sample holder [188, 189] and painting off with Microshield⁺ lacquer. The sample holder was used for most ordinary potentiokinetic scans, while painting off was used for most other experiments.

Figure 69 shows the sample holder, the main body of which is constructed of Teflon to prevent reaction with the electrolyte. Electrical contact with the sample is provided by copper parts encased in Teflon. A polycarbonate nut holds the sample in place and exposes one cm² of the sample to the electrolyte. The Teflon gasket minimizes crevice effects and avoids leakage.

The painted-off samples were prepared by attaching (either by soldering or by spot welding) an insulated copper wire to the sample and then painting off all but approximately one cm² of sample area. The lacquer was very effective in minimizing crevice effects.

* Trade name of E. I. du Pont de Nemours and Co., Inc.

+ Trade name of Michigan Chrome and Chemical Co.

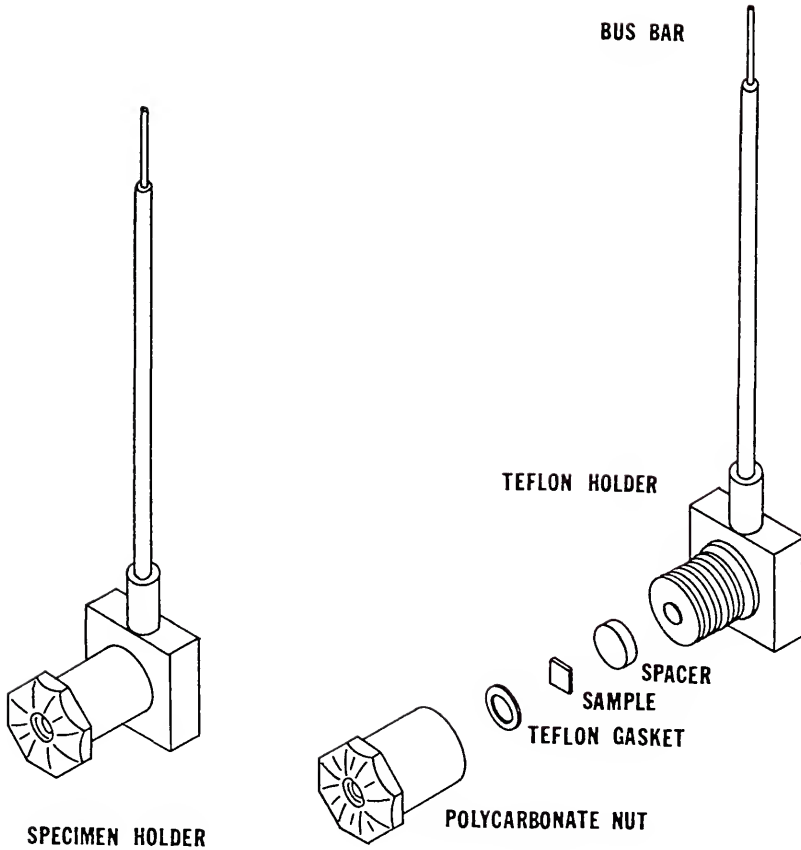


Figure 69. Assembled and exploded views of sample holder [188, 189].

APPENDIX 4
ELECTROLYTES

The electrolytes used in this investigation were aqueous solutions made up of combinations of NaCl, HCl, NaOH and the following buffers [93]:

potassium hydrogen phthalate-- $\text{KHC}_8\text{H}_4\text{O}_4$ (pH = 4.0)

sodium bicarbonate -- NaHCO_3 (pH = 8.6)

sodium borate -- $\text{Na}_2\text{B}_4\text{O}_7$ (pH = 9.2)

The compositions of the 0.1 M chloride solutions are given in Table 12. Other chloride concentrations (from nil to saturation) were obtained for the pH 5.4, 8.9, 10.8 and 11.0 solutions by varying (or eliminating) the concentration of NaCl. All electrolytes were made up with distilled/deionized water. All chemicals were analytical reagent grade.

TABLE 12
0.1 M Cl⁻ ELECTROLYTES

pH (\pm 0.2)	Composition
2.1	0.090 M NaCl 0.010 M HCl
3.2	0.098 M NaCl 0.002 M HCl 0.005 M KHC ₈ H ₄ O ₄
4.0	0.100 M NaCl 0.002 M NaOH 0.088 M KHC ₈ H ₄ O ₄
4.5	0.100 M NaCl 0.016 M NaOH 0.074 M KHC ₈ H ₄ O ₄
5.0	0.100 M NaCl 0.030 M NaOH 0.060 M KHC ₈ H ₄ O ₄
5.4	0.100 M NaCl 0.038 M NaOH 0.052 M KHC ₈ H ₄ O ₄
5.9	0.100 M NaCl 0.038 M NaOH 0.052 M KHC ₈ H ₄ O ₄
6.5-7.5	0.100 M NaCl
6.9	0.100 M NaCl 0.046 M NaOH 0.046 M KHC ₈ H ₄ O ₄
8.5	0.100 M NaCl 0.010 M NaHCO ₃
8.9	0.100 M NaCl 0.100 M NaHCO ₃
9.1	0.100 M NaCl 0.010 M NaOH 0.100 M NaHCO ₃

TABLE 12 (Continued)

pH (\pm 0.2)	Composition
9.3	0.100 M NaCl 0.002 M NaOH 0.022 M $\text{Na}_2\text{B}_4\text{O}_7 \cdot 10 \text{H}_2\text{O}$
10.0	0.100 M NaCl 0.0003 M NaOH
10.1	0.100 M NaCl 0.001 M NaOH 0.003 M NaHCO_3
10.8	0.100 M NaCl 0.022 M NaOH 0.010 M $\text{Na}_2\text{B}_4\text{O}_7 \cdot 10 \text{H}_2\text{O}$
11.0	0.100 M NaCl 0.001 M NaOH
11.9	0.100 M NaCl 0.010 M NaOH

APPENDIX 5

DEAERATION OF ELECTROLYTES

The Welch Duo-Seal Model 1405H vacuum pump, used in this investigation, has the following specifications:

- 1) Ultimate pressure $P_u = 5 \times 10^{-5}$ mm Hg.
- 2) Free air displacement = 33.4 liters/minute.
- 3) Pumping speed = 7.5 liters/minute.

The solubility of oxygen in sea water is related to the temperature and chloride content of the sea water [190] by:

$$S_{O_2} \text{ (STP)} = 10.291 - 0.2809t + 0.006009t^2 + 0.0000632t^2 \\ - \pi_{Cl} (0.1161 - 0.003922t + 0.0000631t^2)$$

where $t = 0$ to 28°C .

$\pi_{Cl} = 0$ to 20 parts per thousand chloride in sea water

For $t = 25^\circ\text{C}$, $\pi_{Cl} = 3.55$ (10^{-1} molar chloride)

$S_{O_2} \text{ (STP)} = 8.93 \text{ cm}^3 \text{ O}_2$ per liter of electrolyte

$$\frac{P_u}{P} = \frac{S_{O_2} \text{ (after pumping)}}{S_{O_2} \text{ (STP)}} : S_{O_2} \text{ (after pumping)} = \frac{P_u}{P} \times S_{O_2} \text{ (STP)}$$

$$S_{O_2} \text{ (after pumping)} = \frac{5 \times 10^{-5} \text{ mm Hg}}{760 \text{ mm Hg}} \times \frac{8.93 \text{ cm}^3 \text{ O}_2}{\text{liter electrolyte}}$$

$$S_{O_2} \text{ (after pumping)} = \frac{5.88 \times 10^{-7} \text{ cm}^3}{\text{liter electrolyte}} .$$

APPENDIX 6

LIST OF EQUIPMENT

1. Magna AnatroI Research Potentiostat
Model 4700M with attached Linear Scan Unit
Model 4510
2. TRW Research Potentiostat Model 200A with attached Linear Scan
Unit Model 202A
3. Hewlett-Packard Sanborn Differential Amplifier Model 8875A
4. Hewlett-Packard Logarithmic Converter Model 7561A
5. Varian X-Y Recorder Model F-100
6. Hewlett-Packard X-Y Recorder
Model 7005B
7. Honeywell X-Y Recorder Model 550
8. Hewlett-Packard Moseley X-Y Recorder Model 7000A
9. Berkleonics CEA shielded Line Isolator Model CEA 33
10. Welch Duo-Seal Vacuum Pump Model 1405H
11. Wenking Potentiostat Model 68TA1 with attached Motor Potentiometer
Model MP165
12. Keithley Electrometer Model 602
13. Keithley pH Electrode Adapter Model 6013
14. Keithley Isolating Amplifier Model 399
15. Hewlett-Packard Moseley Strip Chart Recorder Model 680
16. Beckman pH Meter Expandomatic Model SS-2
17. Hewlett-Packard Digital Voltmeter Model 3440A
18. Keithley Digital Multimeter Model 160
19. Hewlett-Packard D.C. Power Supply Model 6216A
20. Tektronix Storage Oscilloscope Type 564 with attached Time Base
Type 2B67 and Plug-In Type 2A63

21. Tektronix Oscilloscope Camera System Type C-27
22. Corning Calomel Reference Electrode Number 476001
23. Corning Semi-Micro Combination pH Electrode Number 476050
24. Corning Rugged Combination pH Electrode Number 476051
25. Heath Malmstadt-Enke Atomic Absorption Spectrophotometer Model EV-703-D with Techtron Slot-type Burner Type AB51
26. Barnstead Still Model A1013
27. Illinois Water Treatment Ion Exchange Column Model Research II
28. Englehard Deoxo Gas Purifier Model D-25-2300

APPENDIX 7

ZERO-IMPEDANCE AMMETER

An electrical schematic diagram of the zero-impedance ammeter used in this investigation is shown in Figure 70. The basic design and theory of operation of such a circuit was discussed by Lauer and Mansfield [191]. The device uses a Philbrick Model 1009 operational amplifier in conjunction with a negative-feedback circuit which effectively eliminates internal resistance errors during current measurements.

ZERO - RESISTANCE AMMETER

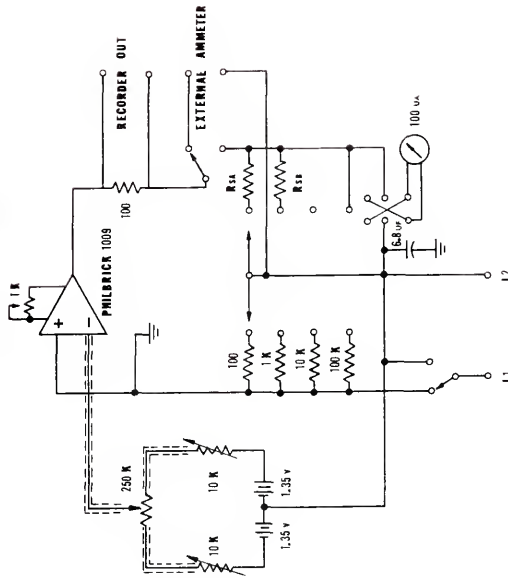


Figure 70. Electrical schematic diagram of zero-impedance ammeter used to eliminate internal resistance errors during current measurements. J1 and J2 represent the test leads, and RSA and RSB represent appropriate meter shunt resistors. The 15 v power supply is not shown.

APPENDIX 8

EXPERIMENTAL POTENTIAL VS. pH DIAGRAMS AND CHARACTERISTIC
VALUES FROM CYCLIC POTENTIOKINETIC POLARIZATION
CURVES FOR Fe-Cr ALLOYS IN 0.1 M Cl^- , H_2 -SATURATED
(OR O_2 -SATURATED) SOLUTIONS

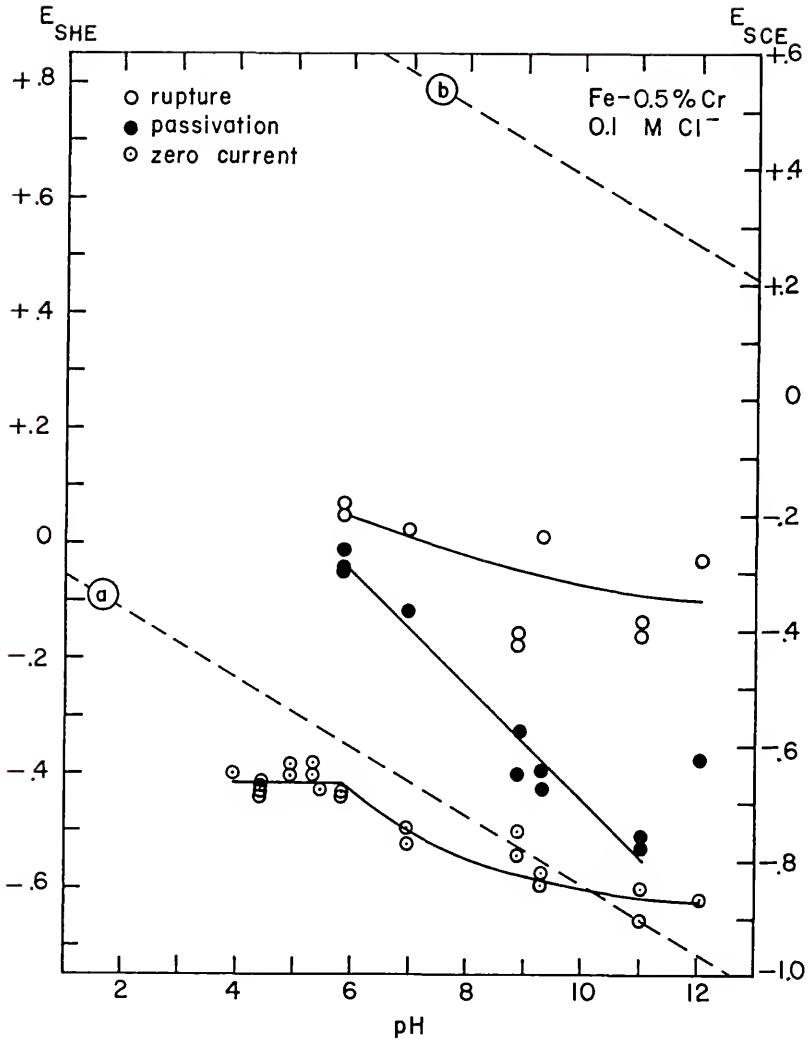


Figure 71. Experimental potential vs. pH diagram for the Fe - 0.5% Cr alloy in 0.1 M Cl⁻, H₂-saturated solutions.

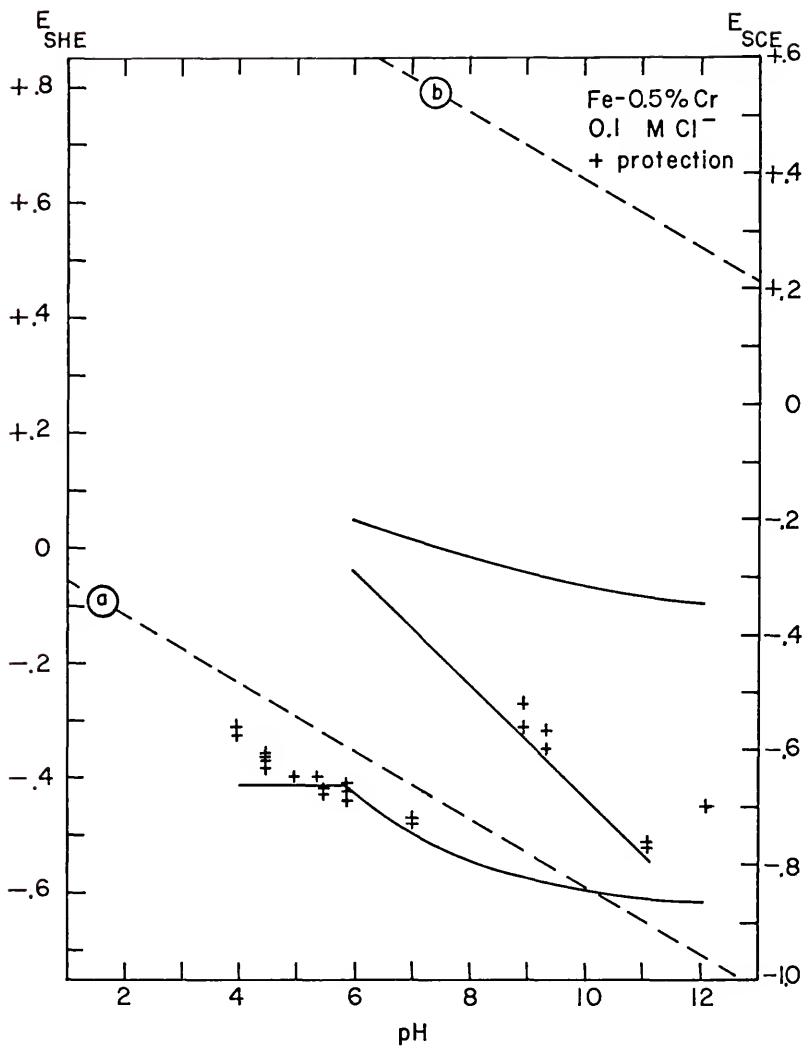


Figure 72. "Protection potential" (E_p) data for the Fe - 0.5% Cr alloy, superimposed on the zero current potential, primary passivation potential and rupture potential lines taken from Figure 71.

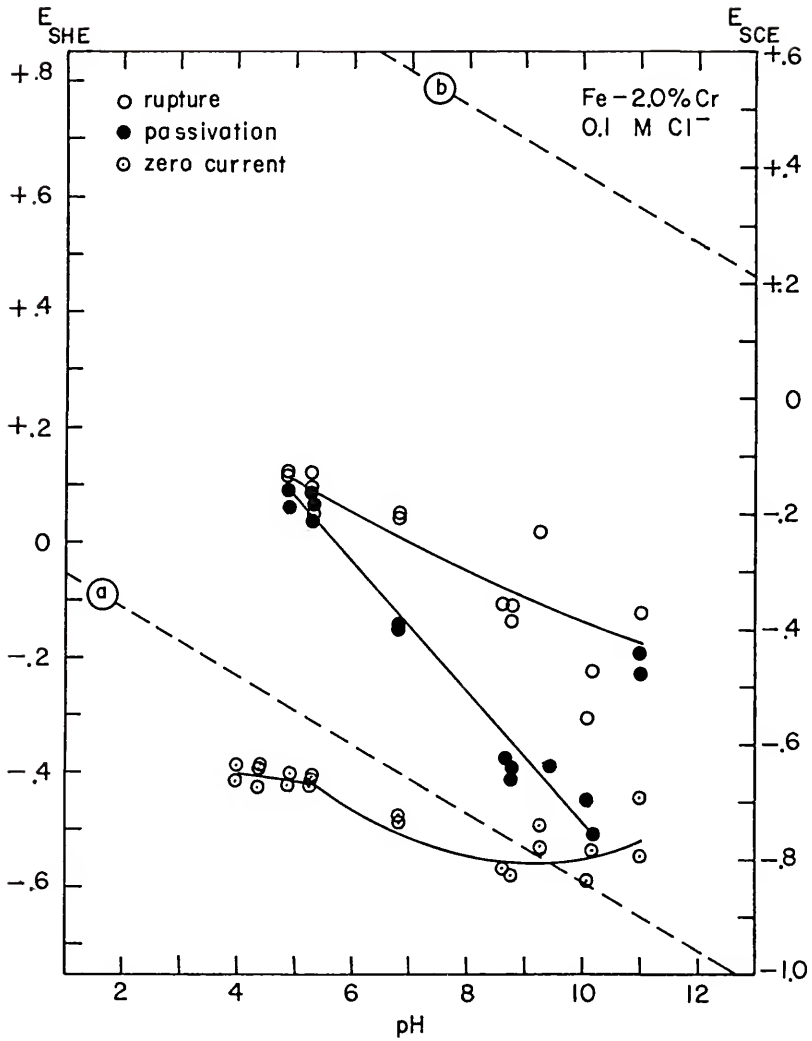


Figure 73. Experimental potential vs. pH diagram for the Fe - 2.0% Cr alloy in 0.1 M Cl⁻, H₂-saturated solutions.

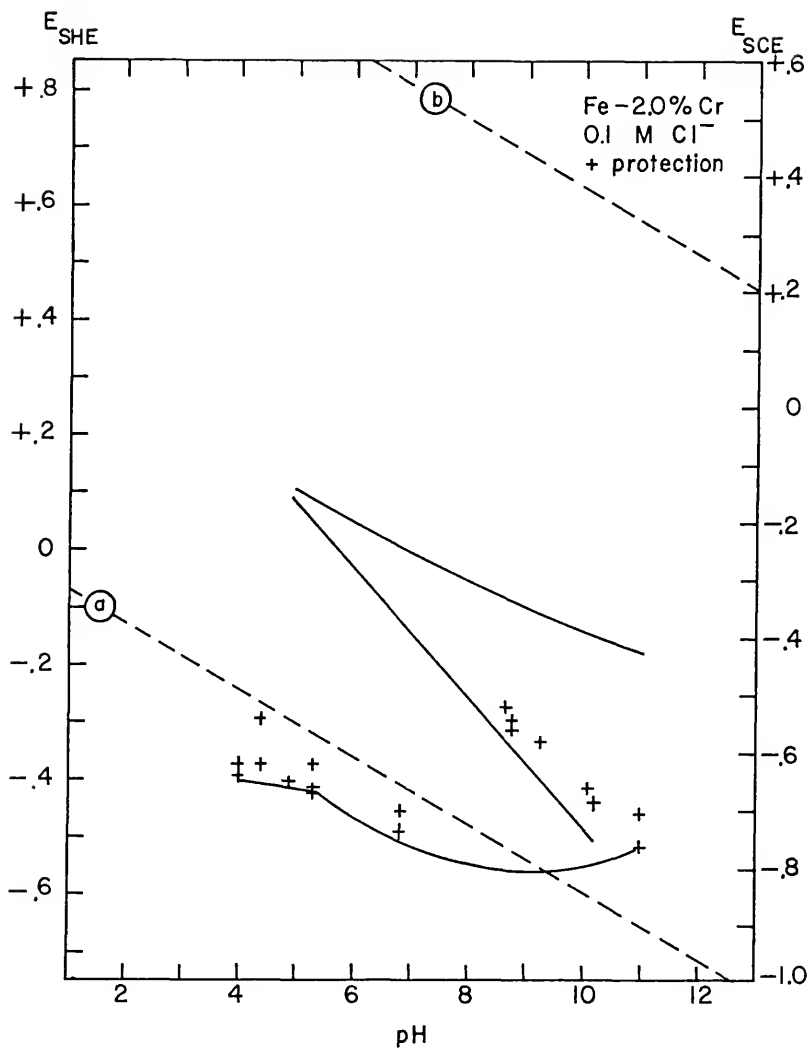


Figure 74. "Protection potential" (E_p) data for the Fe - 2.0% Cr alloy, superimposed on the zero current potential, primary passivation potential and rupture potential lines taken from Figure 73.

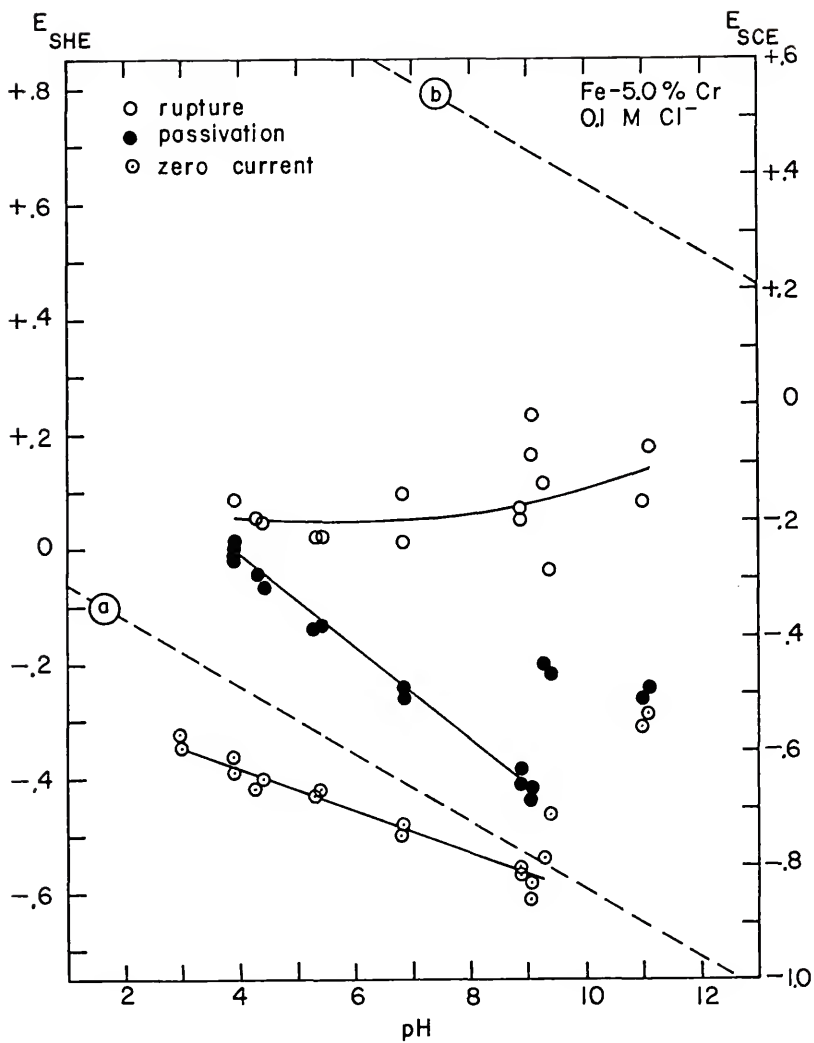


Figure 75. Experimental potential vs. pH diagram for the Fe - 5.0% Cr alloy in 0.1 M Cl⁻, H₂-saturated solutions.

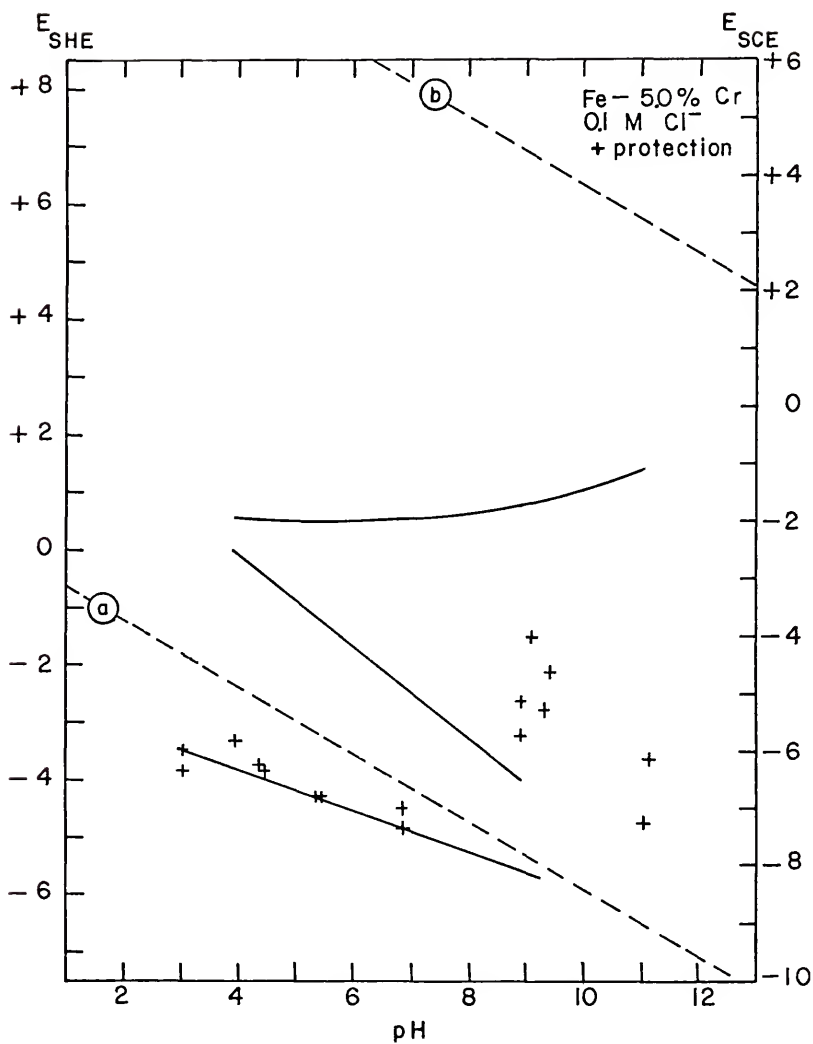


Figure 76. "Protection potential" (E_p) data for the Fe - 5.0% Cr alloy, superimposed on the zero current potential, primary passivation potential and rupture potential lines taken from Figure 75.

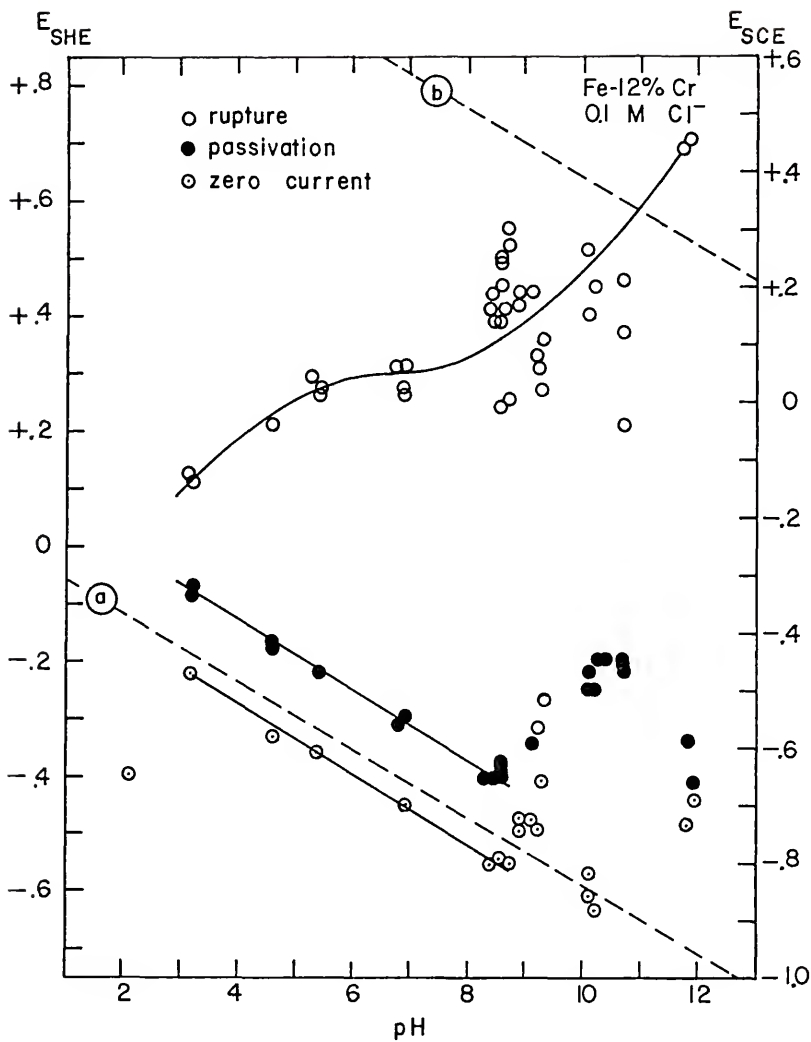


Figure 77. Experimental potential vs. pH diagram for the Fe - 12% Cr alloy in 0.1 M, H₂-saturated solutions.

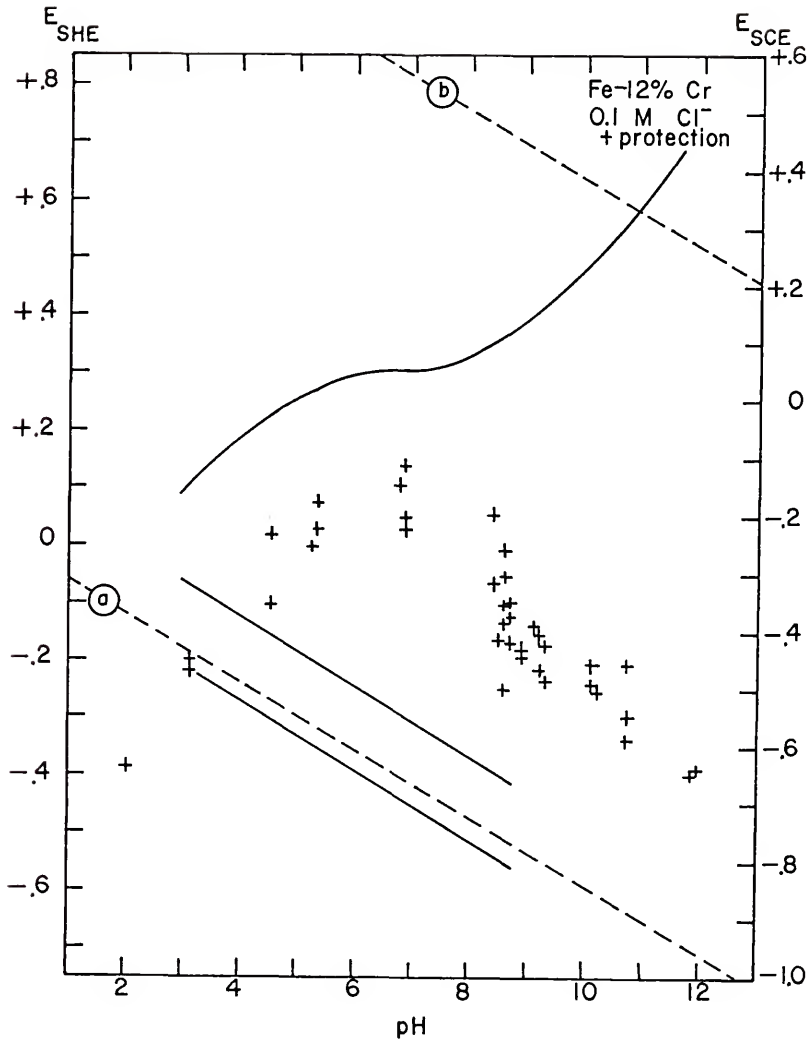


Figure 78. "Protection potential" (E_p) data for the Fe - 12% Cr alloy, superimposed on the zero current potential, primary passivation potential and rupture potential lines taken from Figure 77.

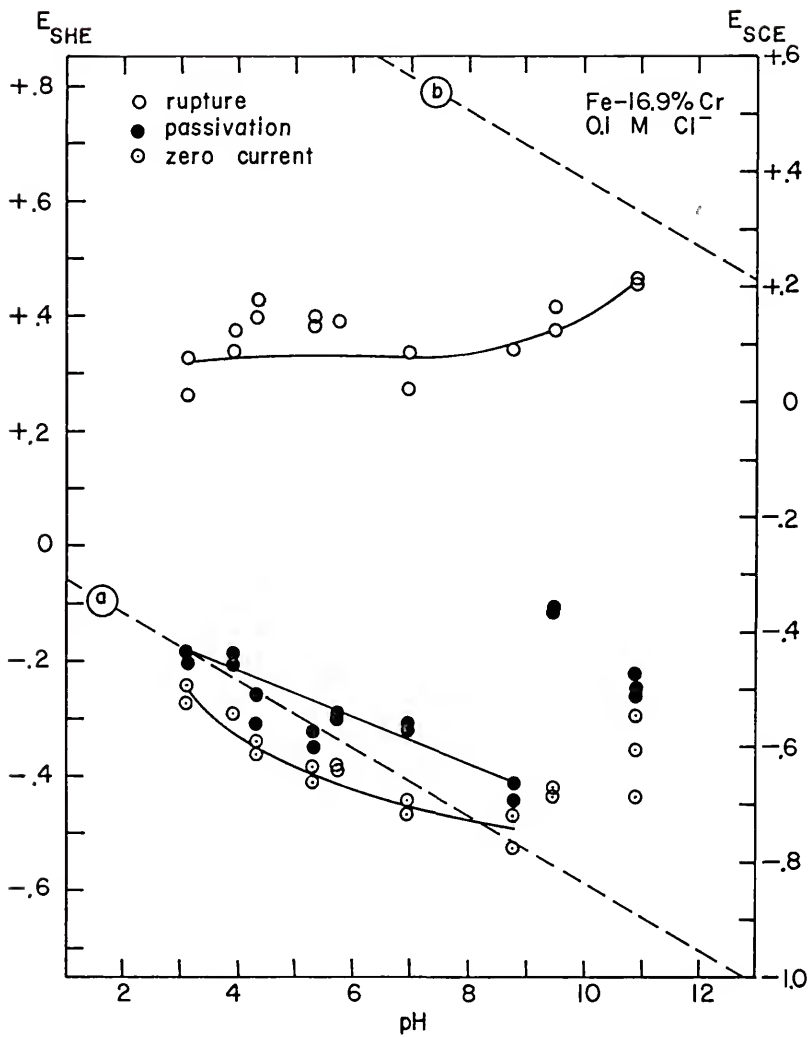


Figure 79. Experimental potential vs. pH diagram for the Fe - 16.9% Cr alloy in 0.1 M Cl⁻, H₂-saturated solutions.

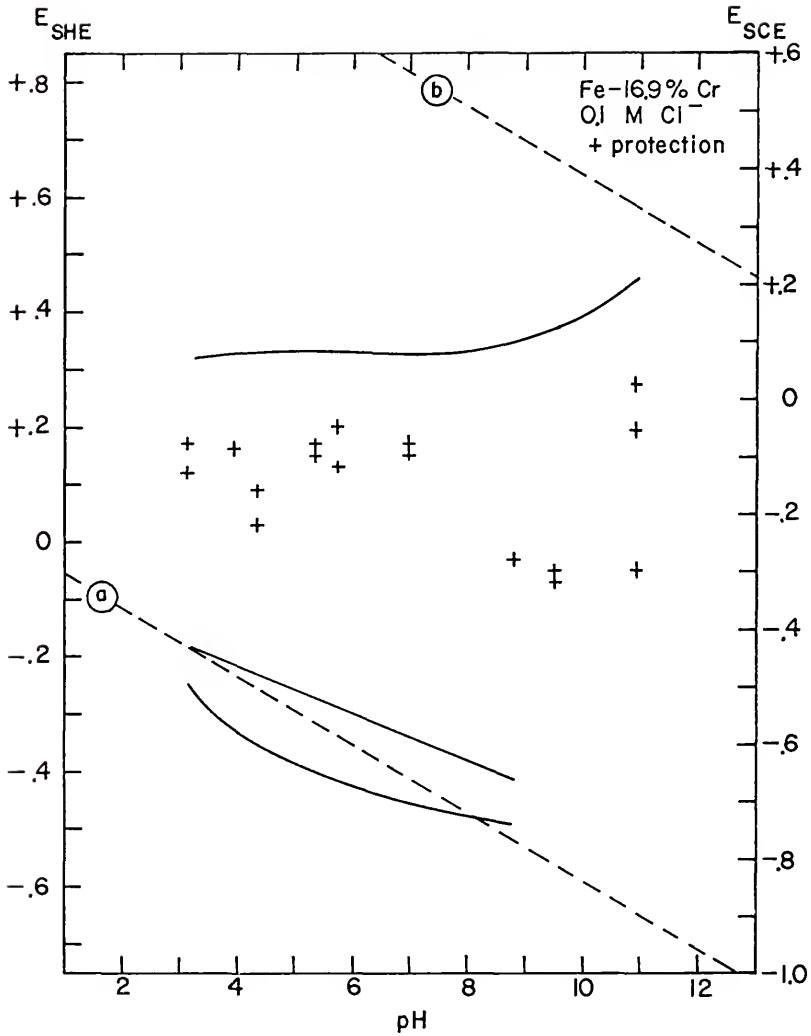


Figure 80. "Protection potential" (E_p) data for the Fe - 16.9% Cr alloy, superimposed on the zero current potential, primary passivation potential and rupture potential lines taken from Figure 79.

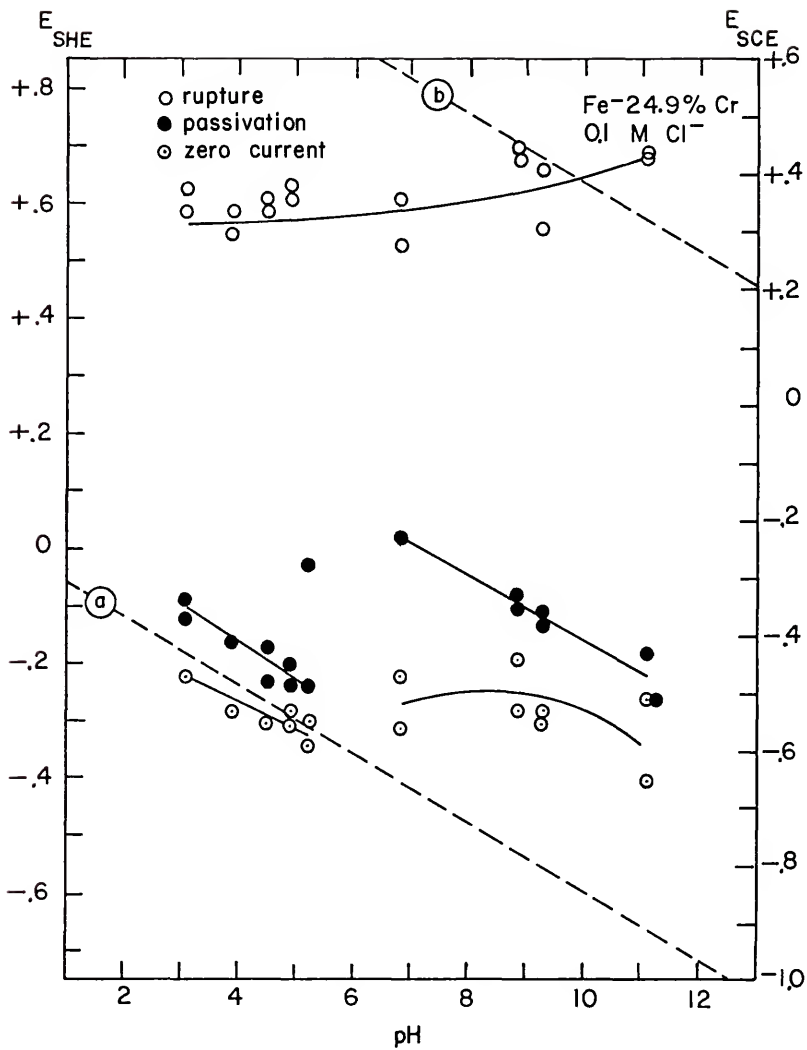


Figure 81. Experimental potential vs. pH diagram for the Fe - 24.9% Cr alloy in 0.1 M Cl⁻, H₂-saturated solutions.

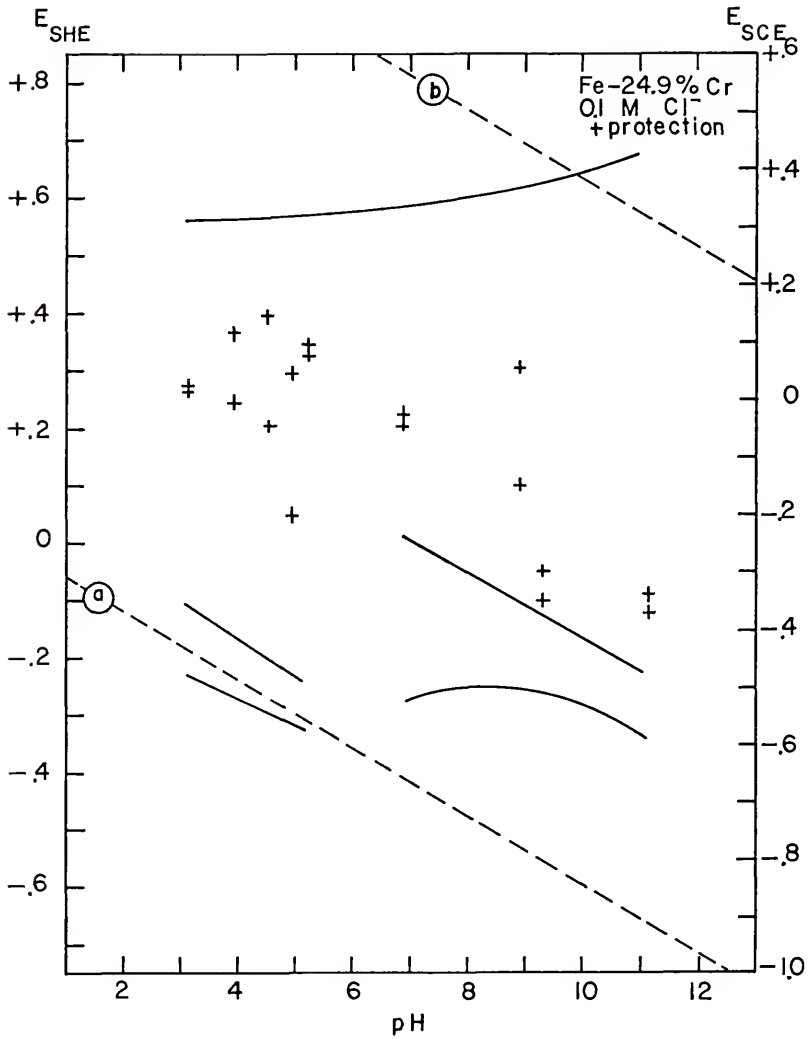


Figure 82. "Protection potential" (E_p) data for the Fe - 24.9% Cr alloy, superimposed on the zero current potential, primary passivation potential and rupture potential lines taken from Figure 81.

TABLE 13

CHARACTERISTIC VALUES FROM CYCLIC POTENTIOKINETIC POLARIZATION
CURVES FOR THE Fe-0.5% Cr ALLOY IN 0.1MCl₂, H₂-SATURATED SOLUTIONS⁺

Run No.	pH	Zero Current Potential (V SCE)	Passivation Potential (V SCE)	Log Passivation Current Density (a/cm ²)	Rupture Potential (V SCE)	"Protection Potential" (V SCE)
*RC-154	4.0	-0.650	-	-	-	-0.565
RC-132	4.0	-0.650	-	-	-	-0.580
RC-29	4.5	-0.675	-	-	-	-0.615
RC-30	4.5	-0.665	-	-	-	-0.620
RC-148	4.5	-0.690	-	-	-	-0.635
RC-149	4.5	-0.680	-	-	-	-0.610
RC-138	5.0	-0.650	-	-	-	-0.650
RC-139	5.0	-0.635	-	-	-	-
RC-133	5.4	-0.650	-	-	-	-
RC-151	5.4	-0.630	-	-	-	-0.650
RC-27	5.5	-0.670	-	-	-	-0.670
RC-28	5.5	-0.670	-	-	-	-0.680
RC-124	5.9	-0.690	-0.265	-2.41	-0.190	-0.690
RC-140	5.9	-0.680	-0.300	-2.26	-0.190	-0.660

TABLE 13 (Continued)

Run No.	pH	Zero Current Potential (V _{SCE})	Passivation Potential (V _{SCE})	Log Passivation Current Density (a/cm ²)	Rupture Potential (V _{SCE})	"Protection Potential" (V _{SCE})
RC-141	5.9	-0.680	-0.300	-2.26	-0.200	-0.675
RC-25	7.0	-0.745	-0.370	-2.85	-0.230	-0.720
RC-26	7.0	-0.770	-0.370	-2.85	-0.230	-0.730
RC-23	8.9	-0.750	-0.580	-3.83	-0.410	-0.565
RC-24	8.9	-0.790	-0.650	-4.35	-0.425	-0.525
RC-16	9.3	-0.820	-0.675	-5.00	-0.240	-0.600
RC-18	9.3	-0.840	-0.640	-5.02	-0.240	-0.570
RC-31	11.0	-0.845	-0.775	-5.48	-0.385	-0.760
RC-32	11.0	-0.900	-0.755	-5.15	-0.410	-0.770
RC-176	12.0	-0.865	-0.620	-5.22	-0.280	-0.700

*Run numbers prefixed "RC" performed by R. L. Cusumano [55].

+ [55]

TABLE 14

CHARACTERISTIC VALUES FROM CYCLIC POTENTIOKINETIC POLARIZATION CURVES FOR THE Fe-2.0% Cr ALLOY IN 0.1M CL₂, H₂-SATURATED SOLUTIONS⁺

Run No.	pH	Zero Current Potential (V _{SCE})	Passivation Potential (V _{SCE})	Log Passivation Current Density (a/cm ²)	Rupture Potential (V _{SCE})	"Protection Potential" (V _{SCE})
RC-147	4.1	-0.660	-	-	-	-0.640
RC-144	4.1	-0.630	-	-	-	-0.620
RC-37	4.5	-0.635	-	-	-	-0.620
RC-38	4.5	-0.635	-	-	-	-0.620
RC-152	4.5	-0.640	-	-	-	-0.545
RC-142	4.5	-0.670	-	-	-	-0.620
RC-145	5.0	-0.665	-0.185	-2.25	-0.135	-0.650
RC-146	5.0	-0.650	-0.155	-2.31	-0.130	-0.650
RC-35	5.4	-0.660	-0.180	-2.25	-0.130	-0.660
RC-36	5.4	-0.670	-0.160	-2.30	-0.155	-0.670
RC-143	5.4	-0.650	-0.205	-2.47	-0.195	-0.620
RC-33	6.9	-0.720	-0.390	-3.05	-0.195	-0.735
RC-34	6.9	-0.730	-0.400	-3.15	-0.200	-0.700

TABLE 14 (Continued)

Run No.	pH	Zero Current Potential (V _{SCE})	Passivation Potential (V _{SCE})	Log Passivation Current Density (a/cm ²)	Rupture Potential (V _{SCE})	"Protection Potential" (V _{SCE})
RC-150	8.7	-0.810	-0.620	-4.39	-0.355	-0.520
RC-39	8.8	-0.820	-0.635	-4.45	-0.355	-0.560
RC-40	8.8	-0.820	-0.650	-4.35	-0.385	-0.545
RC-41	9.3	-0.735	-0.620	-5.35	-0.230	-0.580
RC-42	9.3	-0.775	-0.620	-5.15	-0.230	-0.580
RC-166	10.1	-0.830	-0.690	-5.00	-0.550	-0.660
RC-160	10.2	-0.780	-0.750	-5.10	-0.470	-0.685
RC-47	11.0	-0.790	-0.475	-5.35	-0.370	-0.705
RC-48	11.0	-0.690	-0.440	-5.35	-0.370	-0.760

+ [55]

TABLE 15

CHARACTERISTIC VALUES FROM CYCLIC POTENTIOKINETIC POLARIZATION CURVES FOR THE Fe-5.0% Cr ALLOY IN 0.1M Cl⁻, H₂-SATURATED SOLUTIONS†

Run No.	pH	Zero Current Potential (VSCE)	Passivation Potential (VSCE)	Log Passivation Current Density (a/cm ²)	Rupture Potential (VSCE)	"Protection Potential" (VSCE)
RC-153	3.1	-0.570	-	-	-	-0.595
RC-175	3.1	-0.590	-	-	-	-0.630
RC-155	4.0	-0.635	-0.250	-2.85	-0.160	-0.580
RC-156	4.0	-0.635	-0.260	-2.89	-0.160	-0.580
RC-157	4.0	-0.610	-0.240	-2.85	-0.160	-0.580
RC-158	4.0	-0.610	-0.270	-2.94	-0.160	-0.580
* JS-9	4.4	-0.665	-0.295	-2.78	-0.195	-0.620
JS-8	4.5	-0.645	-0.310	-3.00	-0.205	-0.630
JS-11	5.4	-0.675	-0.385	-3.10	-0.230	-0.675
JS-10	5.5	-0.665	-0.380	-3.08	-0.230	-0.675
JS-12	6.9	-0.740	-0.500	-3.68	-0.155	-0.730
JS-13	6.9	-0.725	-0.490	-3.74	-0.235	-0.695
JS-14	8.9	-0.800	-0.650	-4.86	-0.180	-0.570

TABLE 15 (Continued)

Run No.	pH	Zero Current Potential (V SCE)	Passivation Potential (V SCE)	Log Passivation Current Density (a/cm ²)	Rupture Potential (V SCE)	"Protection Potential" (V SCE)
JS-15	8.9	-0.810	-0.630	-4.79	-0.200	-0.510
RC-163	9.1	-0.825	-0.680	-4.85	-0.020	-0.400
RC-164	9.1	-0.845	-0.665	-4.64	-0.909	-
JS-19	9.3	-0.785	-0.450	-5.47	-0.135	-0.525
JS-16	9.4	-0.710	-0.460	-5.42	-0.285	-0.460
RC-177	11.0	-0.550	-0.510	-5.52	-0.170	-0.720
JS-21	11.1	-0.535	-0.490	-5.22	-0.075	-0.610

*Run numbers prefixed "JS" performed by J. S. Snodgrass [55].

+ [55]

TABLE 16
 CHARACTERISTIC VALUES FROM CYCLIC POTENTIOKINETIC POLARIZATION
 CURVES FOR THE Fe-12% Cr ALLOY IN 0.1M Cl^- , H_2 -SATURATED SOLUTIONS

Run No.	pH	Zero Current Potential (V/SCE)	Passivation Potential (V/SCE)	Log Passivation Current Density (a/cm^2)	Rupture Potential (V/SCE)	"Protection Potential" (V/SCE)	Extent of Propagation, Q/A (coul/cm^2)
*KS-82	2.1	-0.595	-0.370	-2.89	-	-0.630	-
KS-83	2.1	-0.595	-0.370	-2.89	-	-0.630	-
RC-134	3.2	-0.475	-0.275	-4.49	-0.130	-0.465	1.10
RC-135	3.2	-0.470	-0.285	-4.40	-0.140	-0.445	0.778
KS-14	4.6	-0.580	-0.420	-4.62	-0.040	-0.350	0.168
KS-15	4.6	-0.580	-0.430	-4.65	-0.040	-0.230	0.219
KS-74	5.3	-0.620	-0.440	-4.92	+0.040	-0.250	0.0807
KS-12	5.4	-0.615	-0.470	-4.74	+0.010	-0.220	0.269
KS-13	5.4	-0.600	-0.470	-4.70	+0.020	-0.175	0.277
KS-11	6.8	-0.700	-0.560	-4.96	+0.060	-0.145	0.278
KS-8	6.9	-0.700	-0.550	-4.90	+0.010	-0.220	0.142
KS-9	6.9	-0.695	-0.550	-4.90	+0.060	-0.110	0.189
KS-10	6.9	-0.340	-	-	+0.020	-0.200	1.89
KS-76	8.4	-0.810	-0.650	-5.33	+0.190	-0.315	0.232

TABLE 16 (Continued)

Run No.	pH	Zero Current Potential (V SCE)	Passivation Potential (V SCE)	Log Passivation Current Density (a/cm ²)	Rupture Potential (V SCE)	"Protection Potential" (V SCE)	Extent of Propagation, Q/A (coul/cm ²)
KS-77	8.4	-0.795	-0.650	-5.29	+0.160	-0.195	0.228
KS-80	8.5	-0.810	-0.650	-5.26	+0.140	-0.410	0.420
KS-72	8.6	-0.780	-0.650	-5.54	+0.250	-0.350	0.650
KS-73	8.6	-0.795	-0.660	-5.58	+0.200	-0.255	0.343
KS-75	8.6	-0.820	-0.680	-5.18	+0.160	-0.300	0.389
KS-78	8.6	-0.790	-0.280	-4.89	-0.010	-0.380	0.227
KS-79	8.6	-0.790	-0.670	-5.39	+0.240	-0.300	1.03
KS-81	8.6	-0.800	-0.660	-5.12	+0.140	-0.495	0.861
KS-71	8.7	-0.400	-	-	0.000	-0.345	0.945
RC-169	8.7	-0.800	-0.675	-4.88	+0.270	-0.415	0.949
RC-170	8.7	-0.795	-0.745	-5.30	+0.300	-0.370	0.121
KS-18	8.9	-0.740	-0.600	-5.70	+0.170	-0.440	1.17
KS-19	8.9	-0.725	-0.620	-5.55	+0.190	-0.425	1.54
RC-136	9.1	-0.725	-0.595	-5.52	+0.190	-0.385	0.372

TABLE 16 (Continued)

Run No.	pH	Zero Current Potential (V/SCE)	Passivation Potential (V/SCE)	Log Passivation Current Density (a/cm ²)	Rupture Potential (V/SCE)	"Protection Potential" (V/SCE)	Extent of Propagation, Q/A (coul/cm ²)
KS-3	9.2	-0.570	-0.330	-5.55	+0.080	-0.460	0.904
KS-7	9.2	-0.740	-0.320	-5.36	+0.060	-0.400	0.332
KS-1	9.3	-0.660	-0.330	-5.46	+0.110	-0.420	1.54
KS-2	9.3	-0.520	-0.345	-5.46	+0.020	-0.480	0.790
KS-150	10.1	-0.820	-0.500	-5.72	+0.150	-0.485	-
KS-152	10.1	-0.860	-0.470	-5.52	+0.260	-0.450	0.860
KS-151	10.2	-0.885	-0.500	-5.54	+0.200	-0.500	-
KS-4	10.7	-0.800	-0.445	-5.27	+0.210	-0.450	0.898
KS-5	10.7	-0.720	-0.460	-5.24	-0.040	-0.540	0.232
KS-6	10.7	-0.850	-0.470	-5.37	+0.120	-0.580	2.09
KS-207	11.8	-0.730	-0.590	-5.74	+0.440	-0.640	4.31
KS-206	11.9	-0.690	-0.660	-5.74	+0.460	-0.630	5.91

*Run numbers prefixed "KS" performed by K. K. Starr.

TABLE 17

 CHARACTERISTIC VALUES FROM CYCLIC POTENTIOKINETIC POLARIZATION
 CURVES FOR THE Fe-12% Cr ALLOY IN 0.1M Cl⁻, O₂-SATURATED SOLUTIONS

Run No.	pH	Zero Current Potential (^v SCE)	Passivation Potential (^v SCE)	Log Passivation Current Density (a/cm ²)	Rupture Potential (^v SCE)	"Protection Potential" (^v SCE)
*JB-1	2.4	-0.490	-	-	-0.70	-0.505
JB-2	2.4	-0.480	-	-	-0.065	-0.505
JB-16	3.9	-0.415	-	-	+0.100	-0.265
JB-3	4.0	-0.485	-	-	+0.120	-0.240
JB-4	4.0	-0.450	-	-	+0.025	-0.225
JB-8	5.4	-0.330	-	-	+0.105	-0.110
JB-9	5.4	-0.330	-	-	+0.140	-0.105
JB-7	7.0	-0.135	-	-	+0.170	-0.175
JB-5	7.4	-0.160	-	-	+0.300	-0.095
JB-6	7.4	-0.200	-	-	+0.170	-0.150
JB-10	8.5	-0.265	-	-	+0.140	-0.220
JB-12	8.6	-0.245	-	-	+0.280	-0.200
JB-11	8.8	-0.275	-	-	+0.280	-0.225
JB-13	8.8	-0.270	-	-	+0.560	-0.295

TABLE 17 (Continued)

Run No.	pH	Zero Current Potential (VSCE)	Passivation Potential (VSCE)	Log Passivation Current Density (a/cm ²)	Rupture Potential (VSCE)	"Protection Potential" (VSCE)
JB-15	10.0	-0.280	-	-	+0.215	-0.200
JB-14	10.1	-0.285	-	-	+0.185	-0.240
JB-17	11.5	-0.415	-	-	+0.200	-0.380
JB-18	11.6	-0.390	-	-	+0.160	-0.415

*Run numbers prefixed "JB" were conducted by J. M. Bowers

TABLE 18

CHARACTERISTIC VALUES FROM CYCLIC POTENTIOKINETIC POLARIZATION CURVES FOR THE Fe-16.9% Cr ALLOY IN 0.1N Cl⁻, H₂-SATURATED SOLUTIONS[†]

Run No.	pH	Zero Current Potential (V _{SCE})	Passivation Potential (V _{SCE})	Log Passivation Current Density (a/cm ²)	Rupture Potential (V _{SCE})	"Protection Potential" (V _{SCE})
RC-171	3.2	-0.490	-0.435	-4.70	+0.070	-0.130
RC-172	3.2	-0.520	-0.450	-4.40	+0.010	-0.080
RC-127	4.0	-0.540	-0.440	-4.90	+0.120	-0.090
RC-128	4.0	-0.540	-0.455	-4.85	+0.080	-0.090
JS-26	4.4	-0.610	-0.560	-4.75	+0.140	-0.220
JS-27	4.4	-0.590	-0.510	-4.88	+0.170	-0.160
JS-28	5.4	-0.660	-0.600	-4.87	+0.140	-0.080
JS-29	5.4	-0.630	-0.570	-5.06	+0.130	-0.105
RC-121	5.8	-0.630	-0.550	-5.08	+0.135	-0.050
RC-122	5.8	-0.635	-0.545	-5.00	+0.135	-0.120
JS-30	7.0	-0.690	-0.560	-5.18	+0.080	-0.100
JS-31	7.0	-0.710	-0.570	-5.07	+0.020	-0.080
JS-32	8.8	-0.710	-0.690	-5.81	+0.090	-0.280

TABLE 18 (Continued)

Run No.	pH	Zero Current Potential (VSCE)	Passivation Potential (VSCE)	Lot Passivation Current Density (a/cm ²)	Rupture Potential (VSCE)	"Protection Potential" (VSCE)
JS-33	8.8	-0.770	-0.660	-5.31	+0.090	-0.280
JS-34	9.5	-0.670	-0.360	-5.38	+0.120	-0.320
JS-35	9.5	-0.680	-0.370	-5.39	+0.160	-0.300
JS-36	10.9	-0.540	-0.470	-5.30	+0.210	-0.060
JS-37	10.9	-0.680	-0.500	-5.26	+0.200	+0.020
RC-78	10.9	-0.600	-0.510	-5.52	+0.200	-0.300

+ [55]

TABLE 19
 CHARACTERISTIC VALUES FROM CYCLIC POTENTIOKINETIC POLARIZATION
 CURVES FOR THE Fe-24.9% Cr ALLOY IN 0.1 M Cl^- , H_2 -SATURATED SOLUTIONS⁺

Run No.	pH	Zero Current Potential (V _{SCE})	Passivation Potential (V _{SCE})	Log Passivation Current Density (a/cm ²)	Rupture Potential (V _{SCE})	"Protection Potential" (V _{SCE})
RC-129	3.2	-0.470	-0.340	-5.26	+0.330	+0.010
RC-131	3.2	-0.470	-0.370	-5.17	+0.370	+0.020
RC-125	4.0	-0.530	-0.410	-5.19	+0.290	-0.010
RC-126	4.0	-0.530	-0.410	-5.13	+0.330	+0.110
*KE-1	4.6	-0.550	-0.480	-5.34	+0.330	+0.140
KE-2	4.6	-0.550	-0.420	-5.42	+0.350	-0.050
RC-173	5.0	-0.555	-0.485	-5.10	+0.350	-0.205
RC-174	5.0	-0.530	-0.450	-5.00	+0.375	+0.040
KE-3	5.3	-0.590	-0.490	-5.42	+0.320	+0.070
KE-4	5.3	-0.550	-0.280	-5.41	+0.330	+0.090
KE-5	6.9	-0.470	-0.230	-5.62	+0.350	-0.050
KE-6	6.9	-0.560	-0.230	-5.55	+0.270	-0.030
KE-7	8.9	-0.440	-0.330	-5.85	+0.420	+0.050

TABLE 19 (Continued)

Run No.	pH	Zero Current Potential (V SCE)	Passivation Potential (V SCE)	Log Passivation Current Density (a/cm ²)	Rupture Potential (V SCE)	"Protection Potential" (V SCE)
KE-8	8.9	-0.530	-0.350	-5.57	+0.440	-0.150
KE-9	9.3	-0.550	-0.380	-5.70	+0.300	-0.300
KE-10	9.3	-0.530	-0.360	-5.77	+0.400	-0.350
KE-11	11.1	-0.650	-0.510	-5.85	+0.430	-0.370
KE-12	11.1	-0.510	-0.430	-5.89	+0.420	-0.340

*Run numbers prefixed "KE" were performed by K. D. Efird [55].

+ [55]

APPENDIX 9

SPECIAL CYCLIC POTENTIOKINETIC POLARIZATION SCANS
FOR THE Fe - 12% Cr ALLOY IN 0.1 M Cl^- ,
 H_2 -SATURATED SOLUTIONS

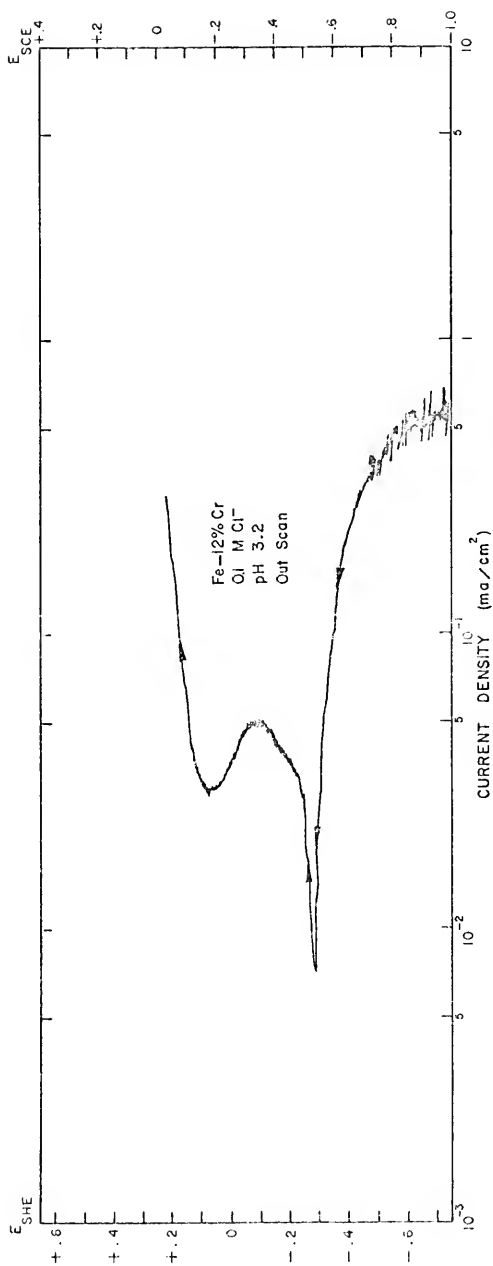


Figure 83. Out-scan portion of special cyclic potentiokinetic polarization scan for the Fe - 12% Cr alloy in 0.1 M Cl⁻, H₂-saturated solution of pH 3.2.

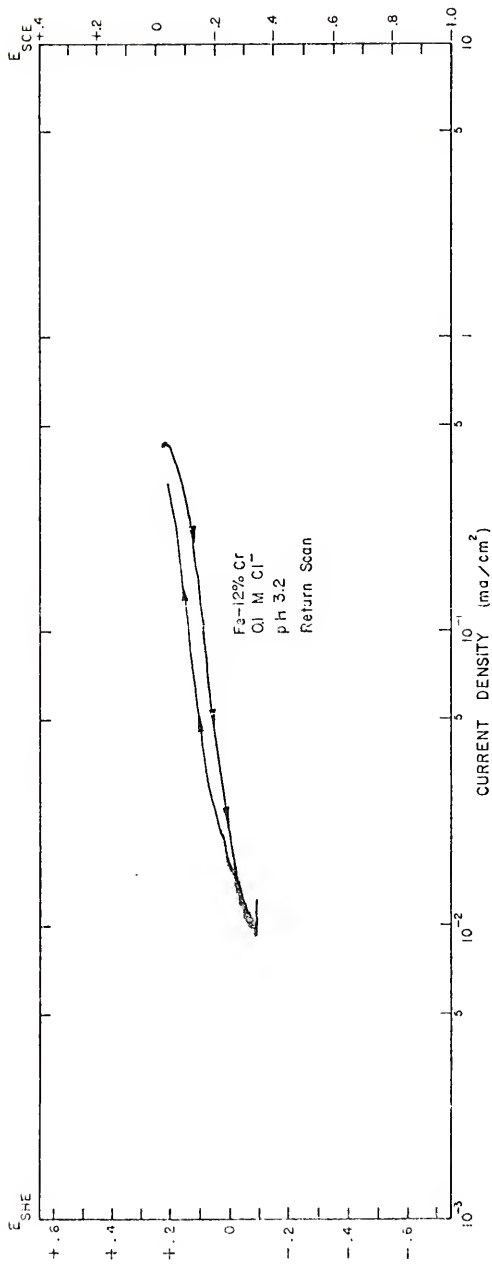


Figure 84. Return-scan portion of special cyclic potentiokinetic polarization scan for the Fe - 12% Cr alloy in 0.1 M Cl^- , H_2O -saturated solution of pH 3.2.

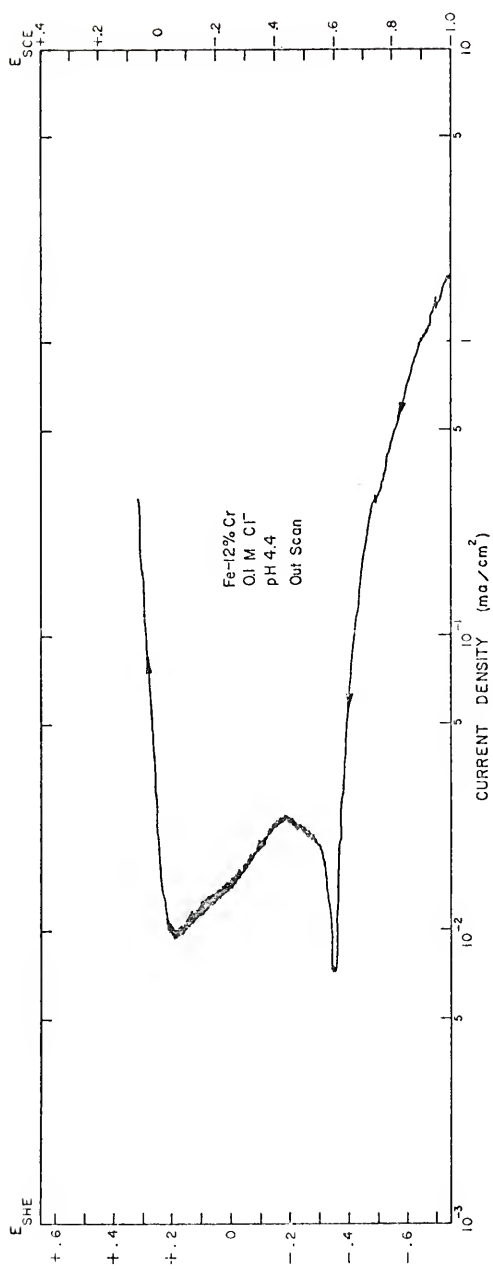


Figure 85. Out-scan portion of special cyclic potentiokinetic polarization scan for the Fe - 12% Cr alloy in 0.1 M Cl⁻, H₂-saturated solution of pH 4.4.

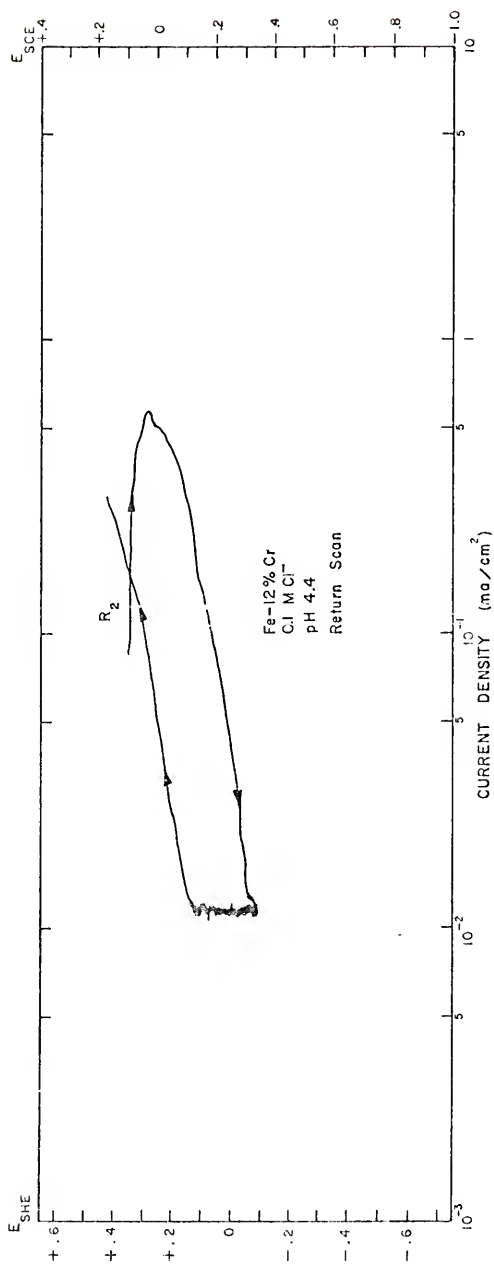


Figure 86. Return-scan portion of special cyclic potentiokinetic polarization scan for the Fe - 12% Cr alloy in 0.1 M Cl⁻, H₂-saturated solution of pH 4.4.

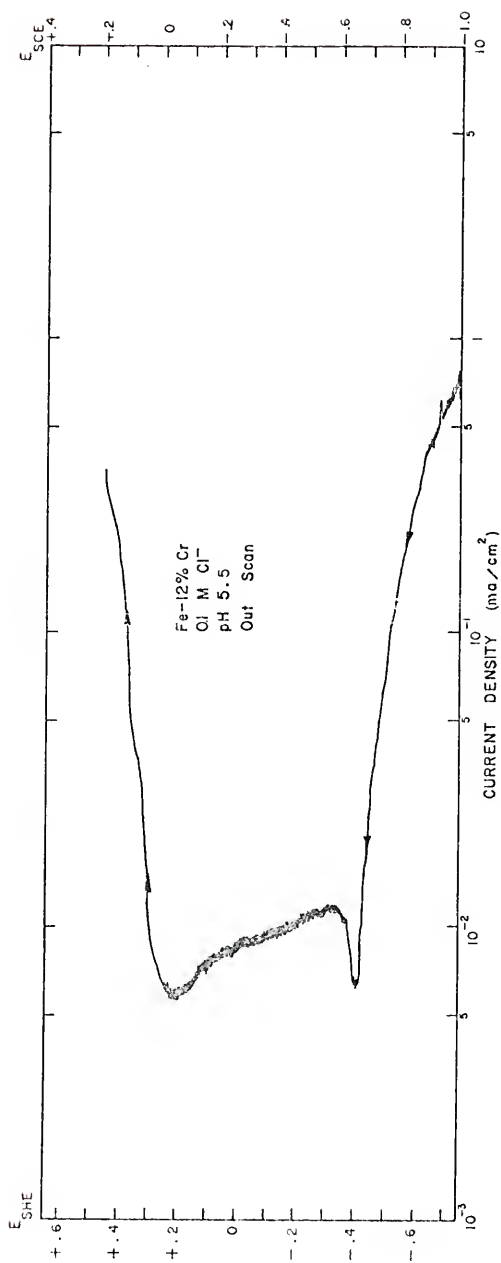


Figure 87. Out-scan portion of special cyclic potentiokinetic polarization scan for the Fe - 12% Cr alloy in 0.1 M Cl^- , H_2 -saturated solution of pH 5.5.

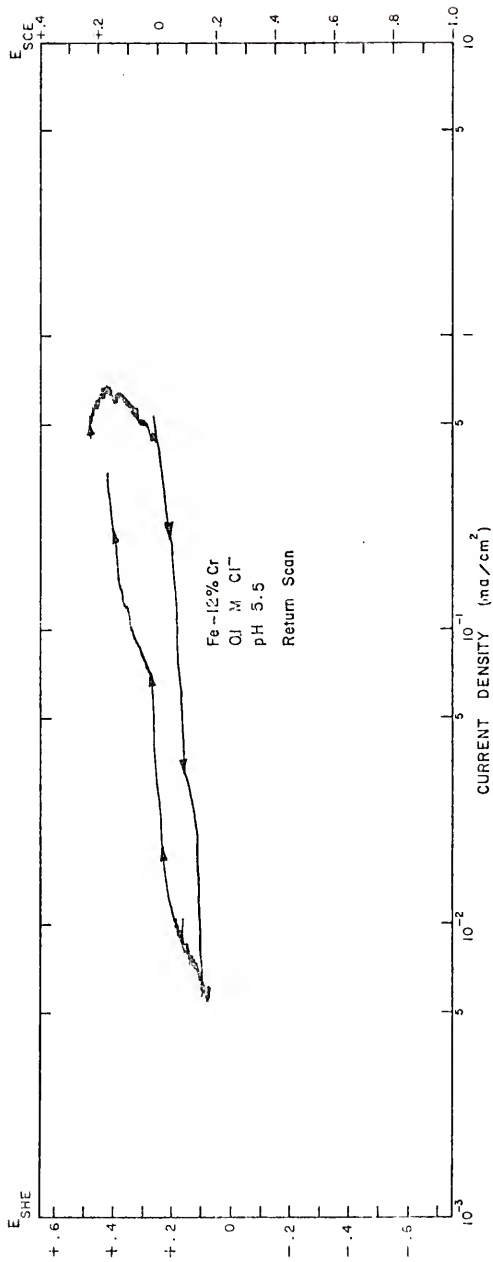


Figure 88. Return-scan portion of special cyclic potentiokinetic polarization scan for the Fe - 12% Cr alloy in 0.1 M Cl^- , H_2 -saturated solution of pH 5.5.

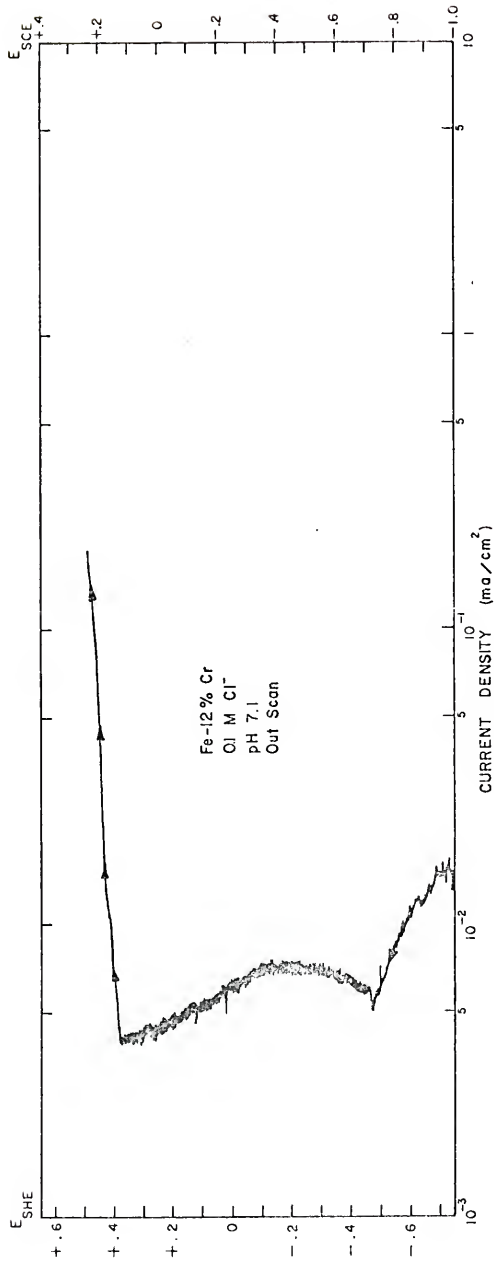


Figure 89. Out-scan portion of special cyclic potentiokinetic polarization scan for the Fe - 12% Cr alloy in 0.1 M Cl⁻, H₂-saturated solution of pH 7.1.

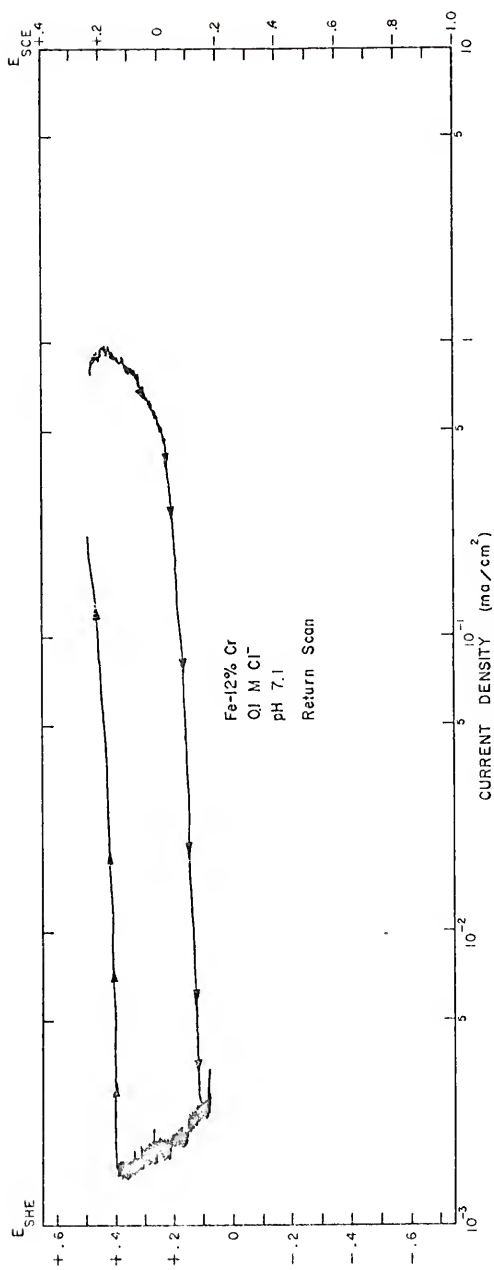


Figure 90. Return-scan portion of special cyclic potentiokinetic polarization scan for the Fe - 12% Cr alloy in 0.1 M Cl⁻, H₂-saturated solution of pH 7.1.

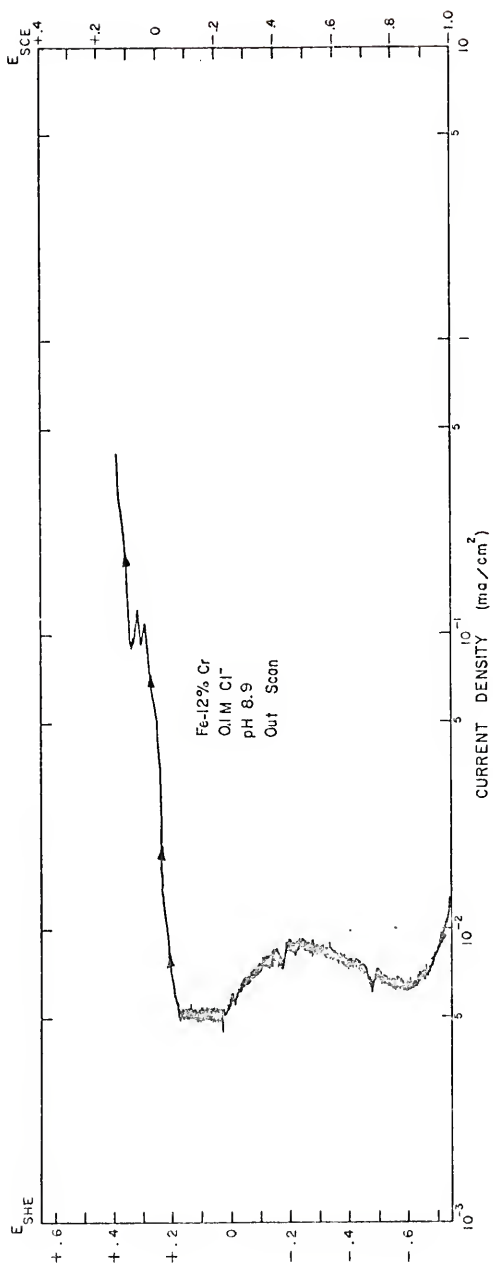


Figure 91. Out-scan portion of special cyclic potentiokinetic polarization scan for the Fe - 12% Cr alloy in 0.1 M Cl^- , H_2 -saturated solution of pH 8.9.

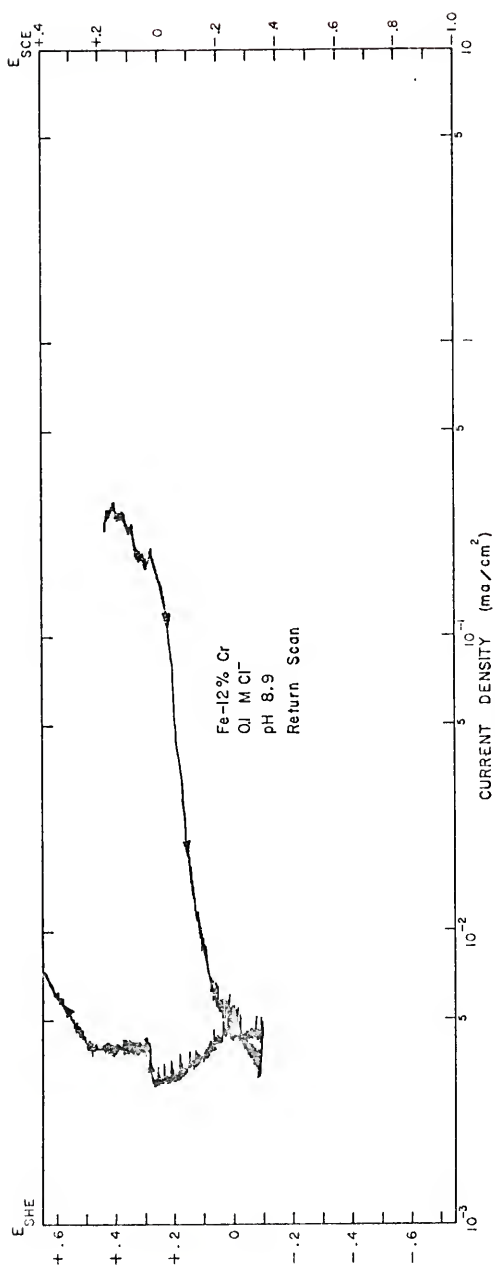


Figure 92. Return-scan portion of special cyclic potentiokinetic polarization scan for the Fe - 12% Cr alloy in 0.1 M Cl⁻, H₂-saturated solution of pH 8.9.

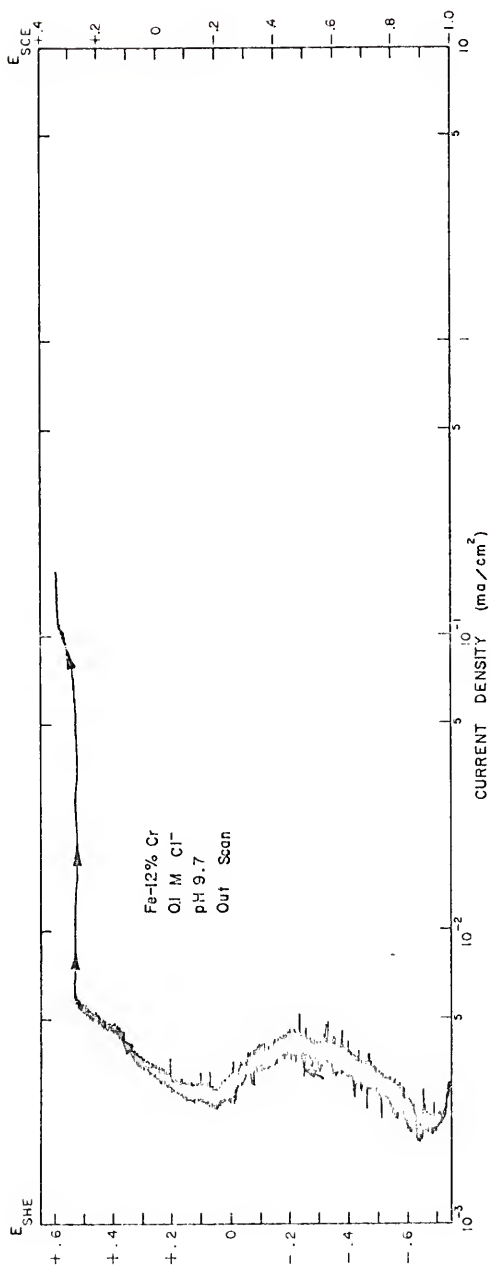


Figure 93. Out-scan portion of special cyclic potentiokinetic polarization scan for the Fe - 12% Cr alloy in 0.1 M Cl⁻, H₂-saturated solution of pH 9.7.

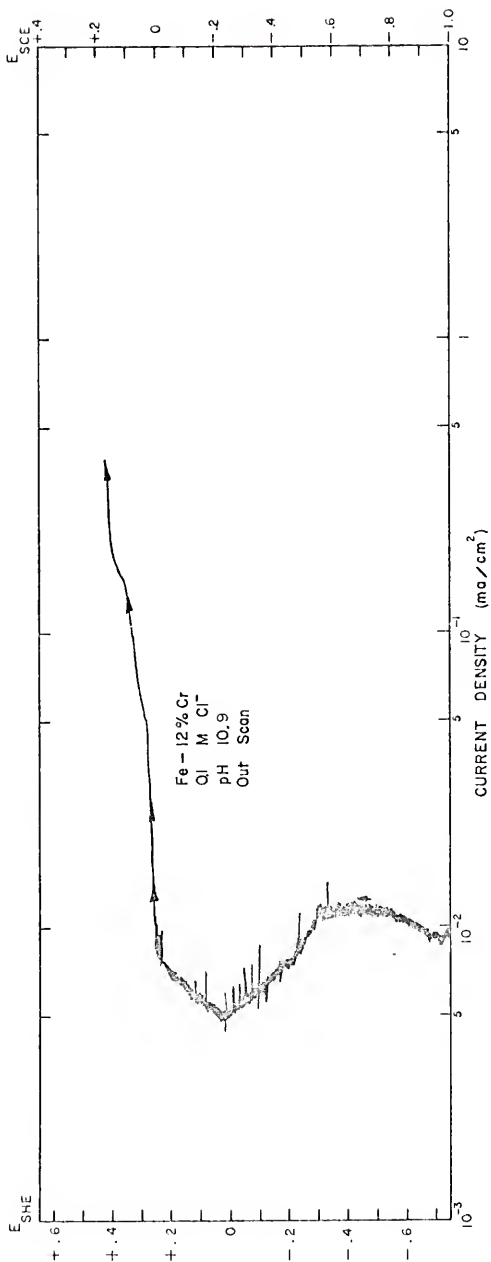


Figure 95. Out-scan portion of special cyclic potentiokinetic polarization scan for the Fe - 12% Cr alloy in 0.1 M Cl⁻; H₂-saturated solution of pH 10.9.

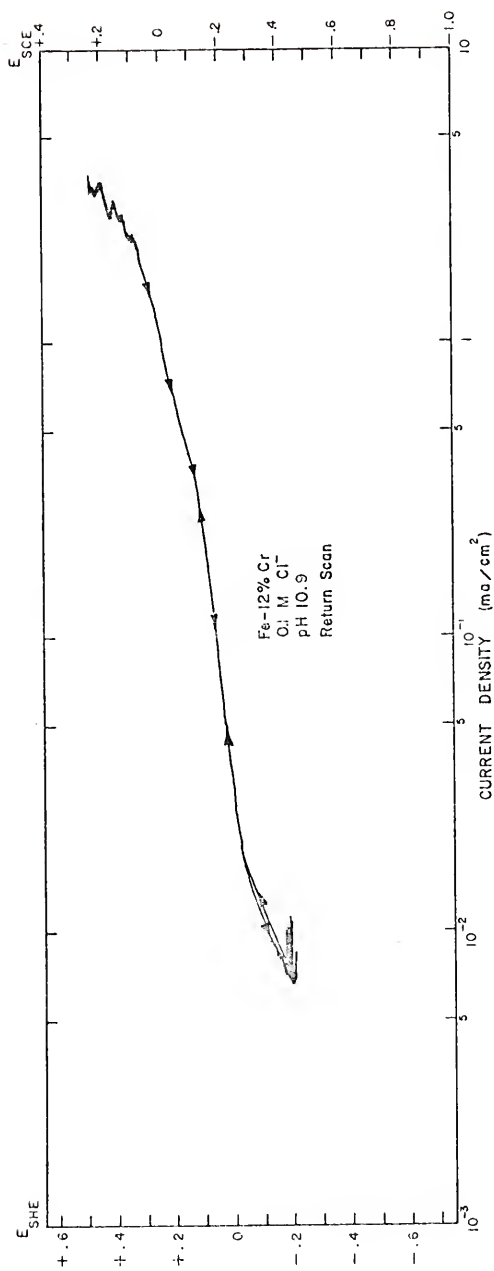


Figure 96. Return-scan portion of special cyclic potentiokinetic polarization scan for the Fe - 12% Cr alloy in 0.1 M Cl^- , H_2 -saturated solution of pH 10.9.

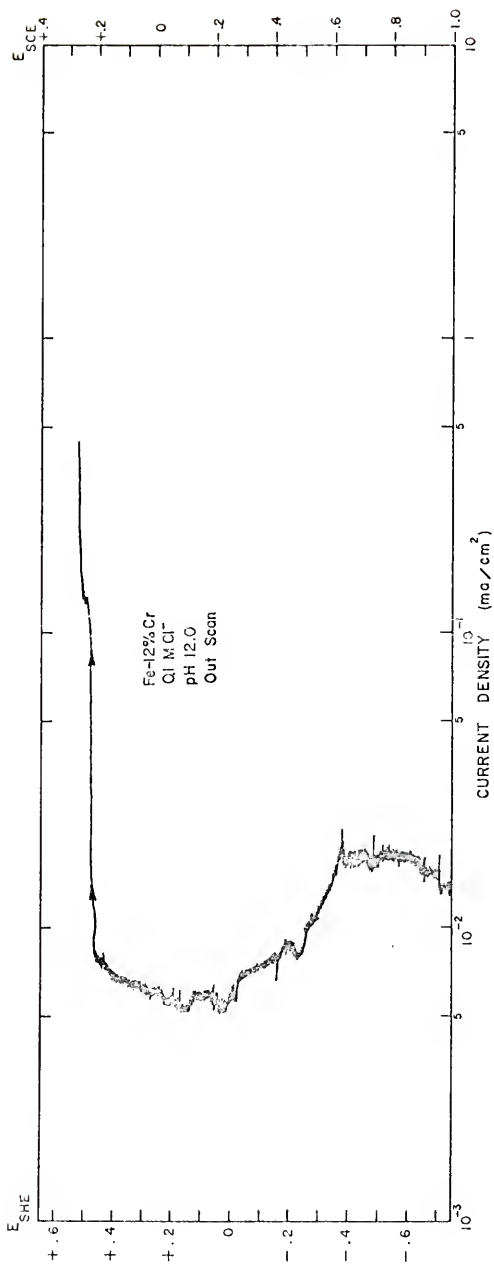


Figure 97. Out-scan portion of special cyclic potentiokinetic polarization scan for the Fe - 12% Cr alloy in 0.1 M Cl^- , H_2 -saturated solution of pH 12.0.

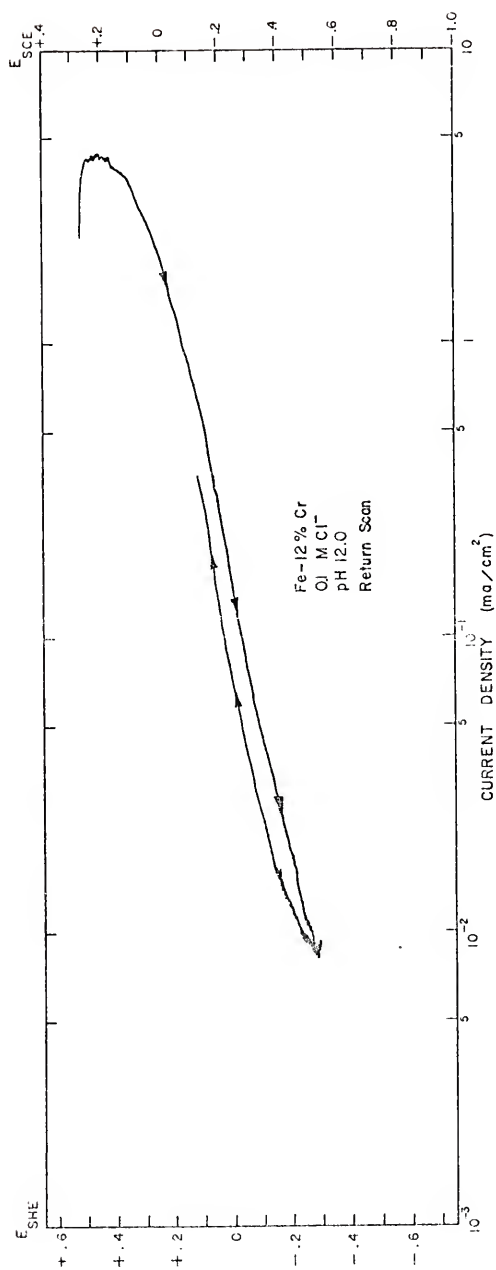


Figure 98. Return-scan portion of special cyclic potentiokinetic polarization scan for the Fe - 12% Cr alloy in 0.1 M Cl⁻, H₂-saturated solution of pH 12.0.

APPENDIX 10

SPECIAL CYCLIC POTENTIOKINETIC POLARIZATION SCANS FOR THE
Fe - 12% Cr ALLOY IN 0.1 M Cl^- , H_2 -SATURATED SOLUTIONS,
USING PAINTED-OFF SAMPLES APPROXIMATELY 1 cm^2 IN AREA

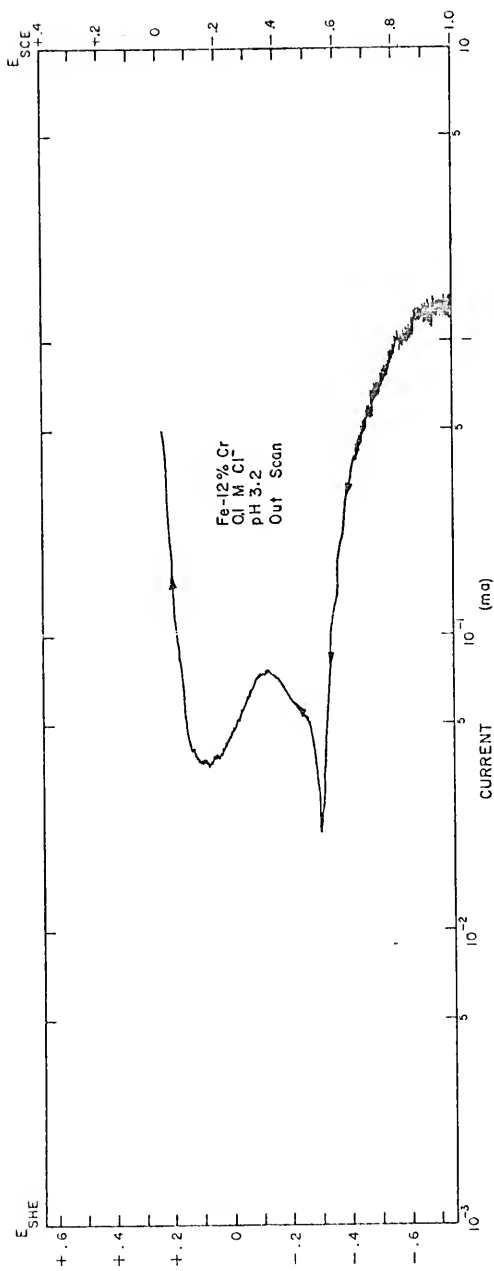


Figure 99. Out-scan portion of special cyclic potentiokinetic polarization scan for the Fe - 12% Cr alloy in 0.1 M Cl⁻, H₂-saturated solution of pH 3.2, using painted-off sample approximately 1 cm² in area.

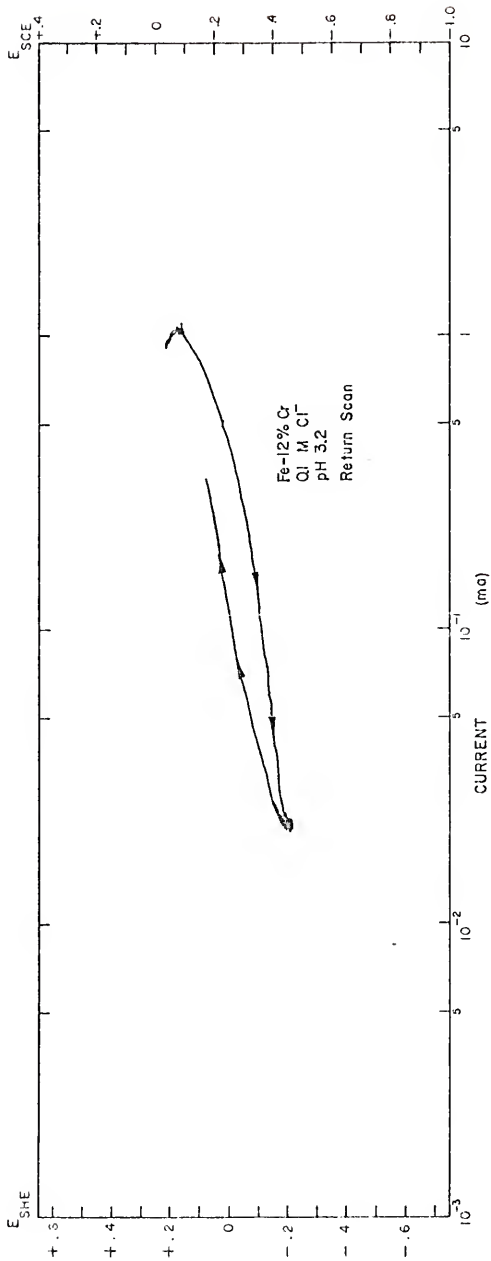


Figure 100. Return-scan portion of special potentiokinetic polarization scan for the Fe - 12% Cr alloy in 0.1 M Cl⁻, H₂-saturated solution of pH 3.2, using painted-off sample approximately 1cm² in area.

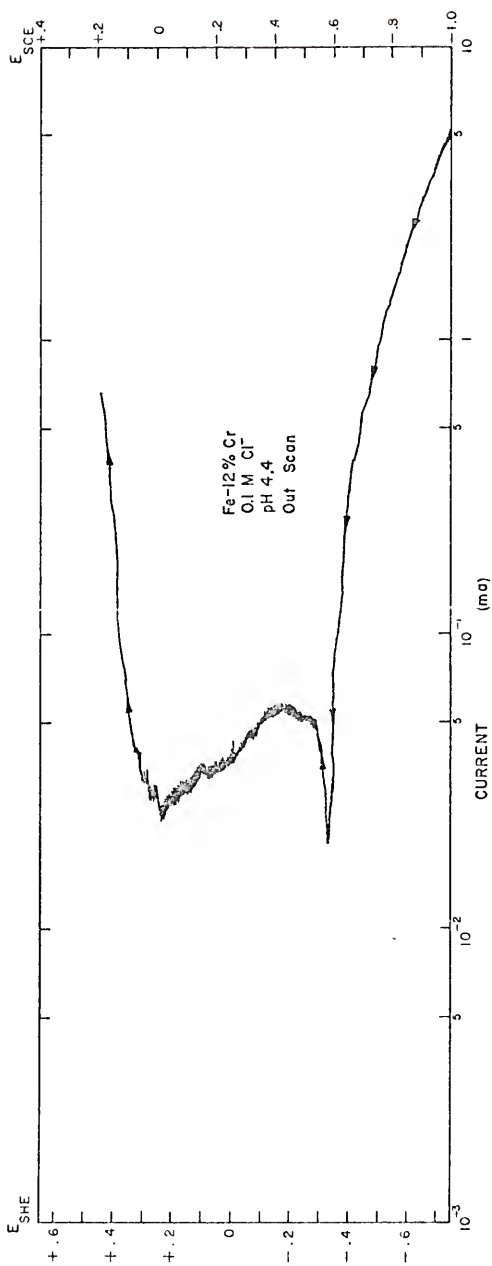


Figure 101. Out-scan portion of special cyclic potentiokinetic polarization scan for the Fe - 12% Cr alloy in 0.1 M Cl⁻, H₂-saturated solution of pH 4.4, using painted-off sample approximately 1 cm² in area.

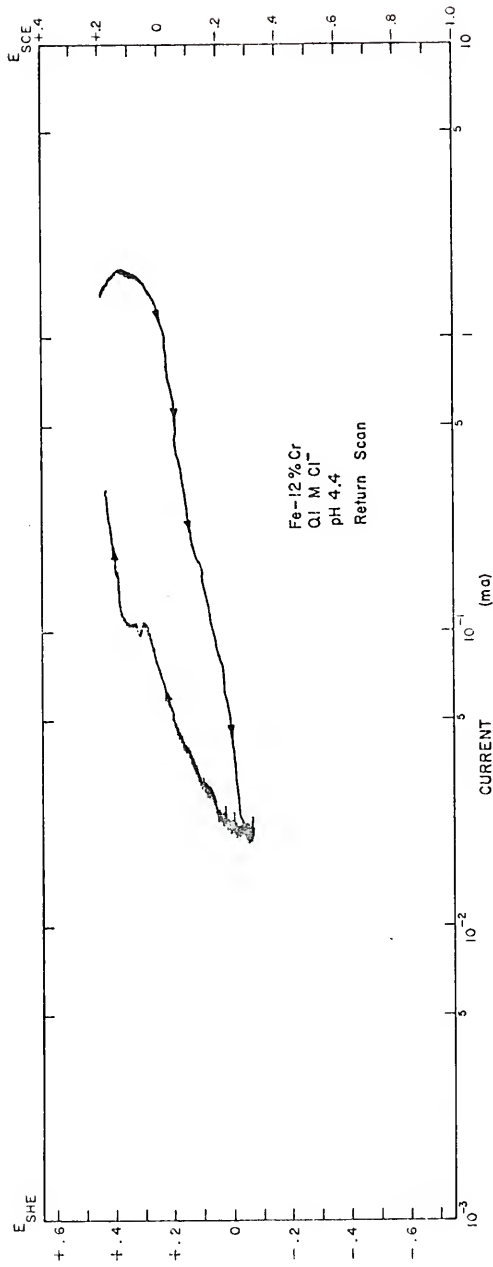


Figure 102. Return-scan portion of special cyclic potentiokinetic polarization scan for the Fe - 12% Cr alloy in 0.1 M Cl⁻, H₂-saturated solution of pH 4.4, using painted-off sample approximately 1 cm² in area.

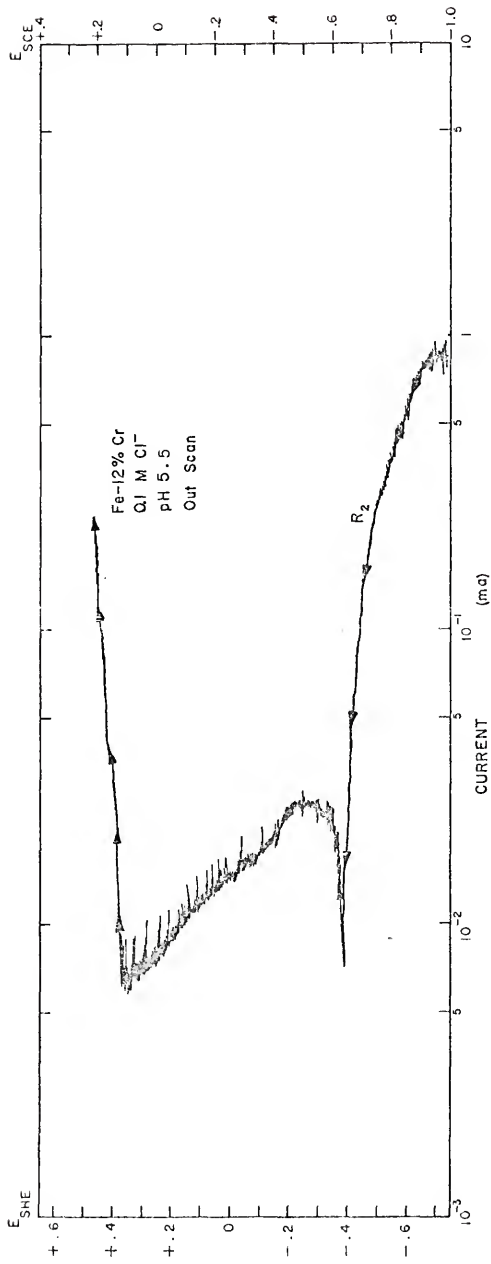


Figure 103. Out-scan portion of special cyclic potentiokinetic polarization scan for the Fe - 12% Cr alloy in 0.1 M Cl^- , H_2 -saturated solution of pH 5.5, using painted-off sample approximately 1 cm^2 in area.

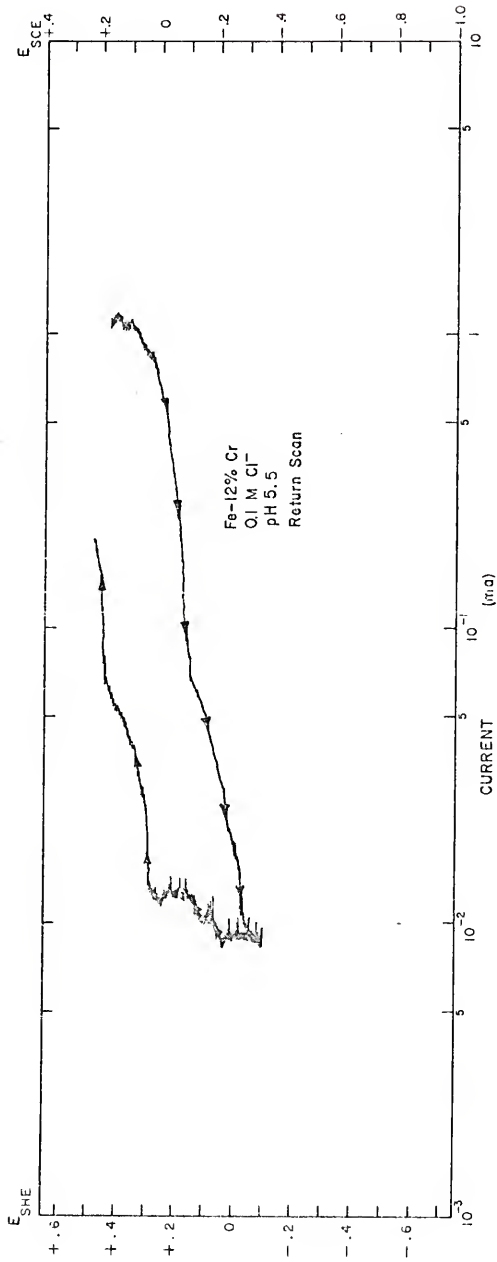


Figure 104. Return-scan portion of special cyclic potentiokinetic polarization scan for the Fe - 12% Cr alloy in 0.1 M Cl⁻, H₂O-saturated solution of pH 5.5, using painted-off sample approximately 1 cm² in area.

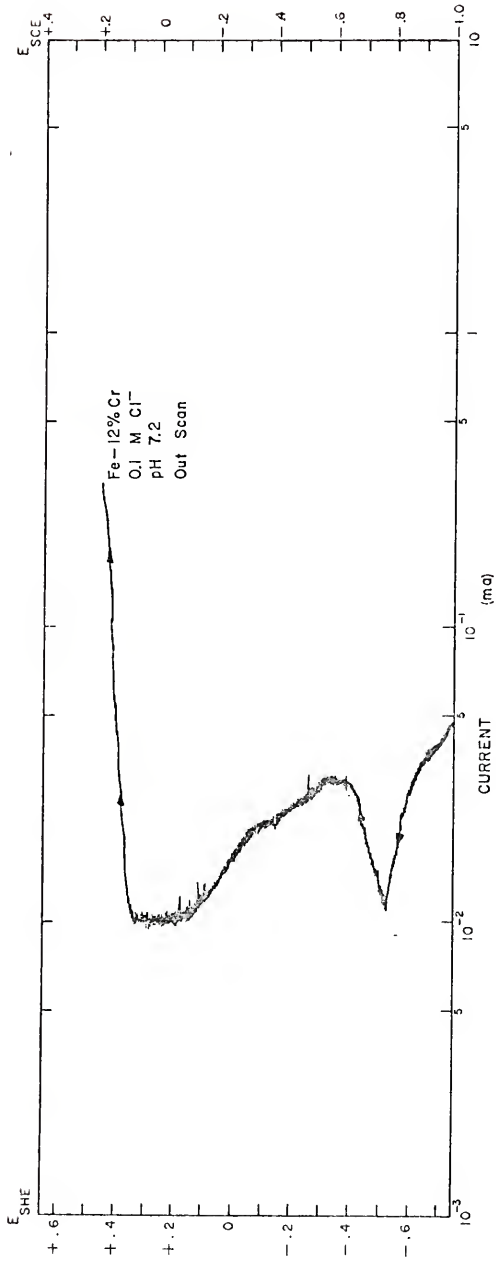


Figure 105. Out-scan portion of special cyclic potentiokinetic polarization scan for the Fe - 12% Cr alloy in 0.1 M Cl⁻, H₂-saturated solution of pH 7.2, using painted-off sample approximately 1 cm² in area.

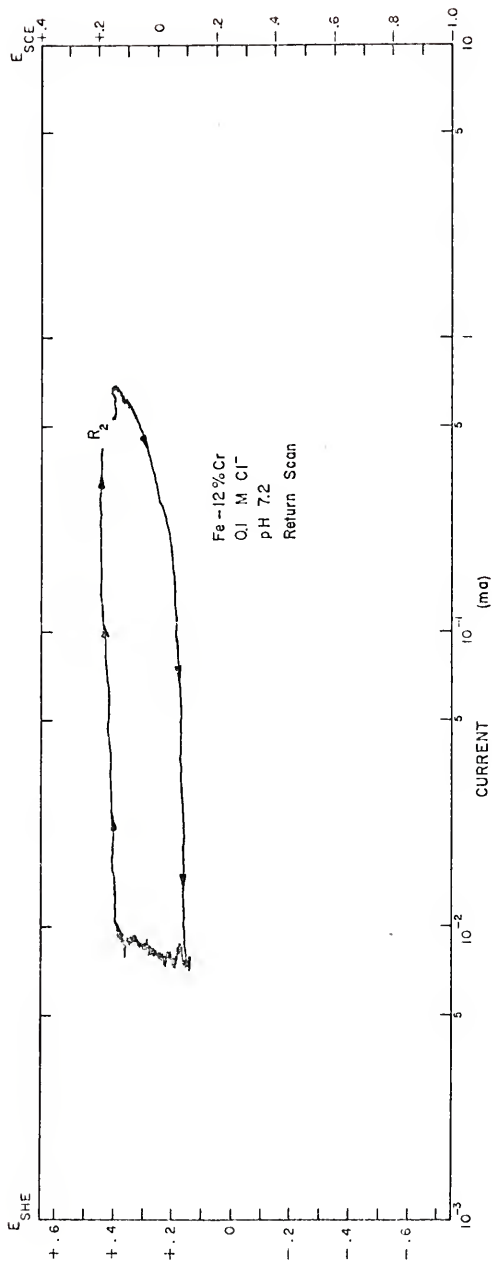


Figure 106. Return-scan portion of special potentiokinetic polarization scan for the Fe - 12% Cr alloy in 0.1 M Cl⁻, H₂-saturated solution of pH 7.2, using painted-off sample approximately 1 cm² in area.

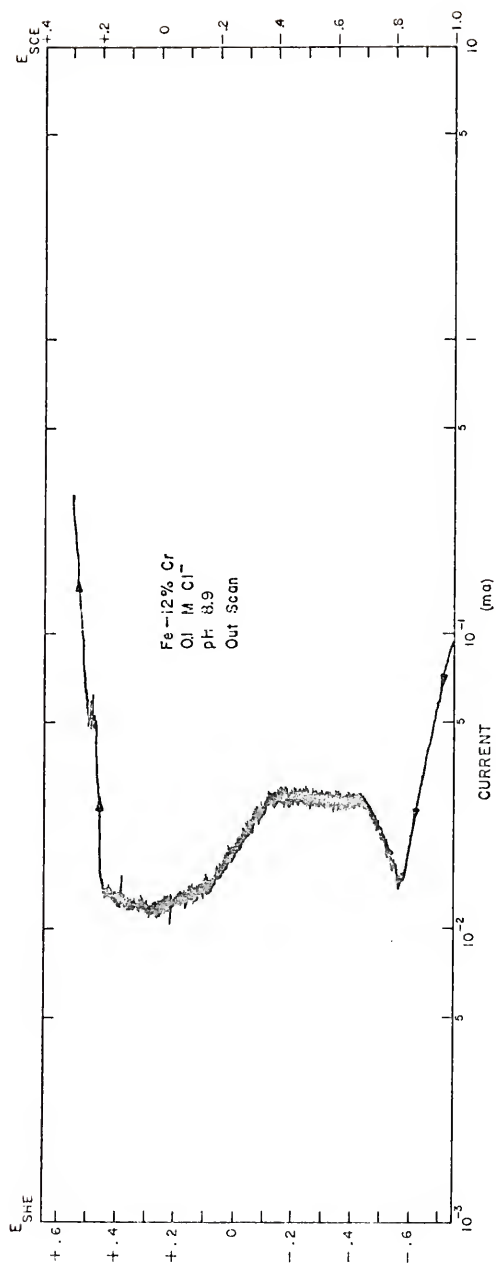


Figure 107. Out-scan portion of special cyclic potentiokinetic polarization scan for the Fe - 12% Cr alloy in 0.1 M Cl⁻, H₂-saturated solution of pH 8.9, using painted-off sample approximately 1 cm² in area.

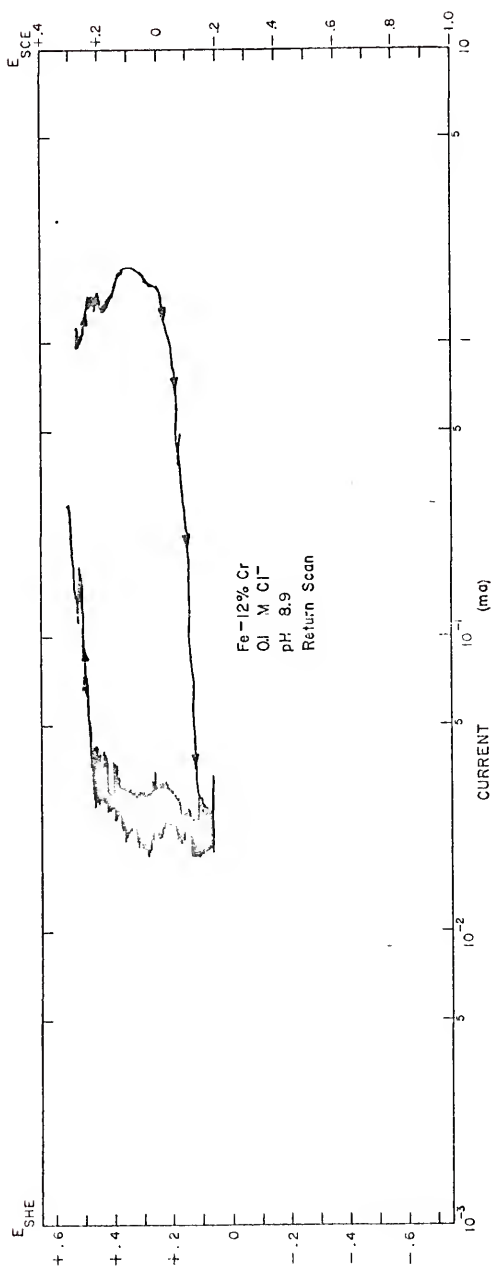


Figure 108. Return-scan portion of special cyclic potentiokinetic polarization scan for the Fe - 12% Cr alloy in 0.1 M Cl⁻, H₂-saturated solution of pH 8.9, using painted-off sample approximately 1 cm² in area.

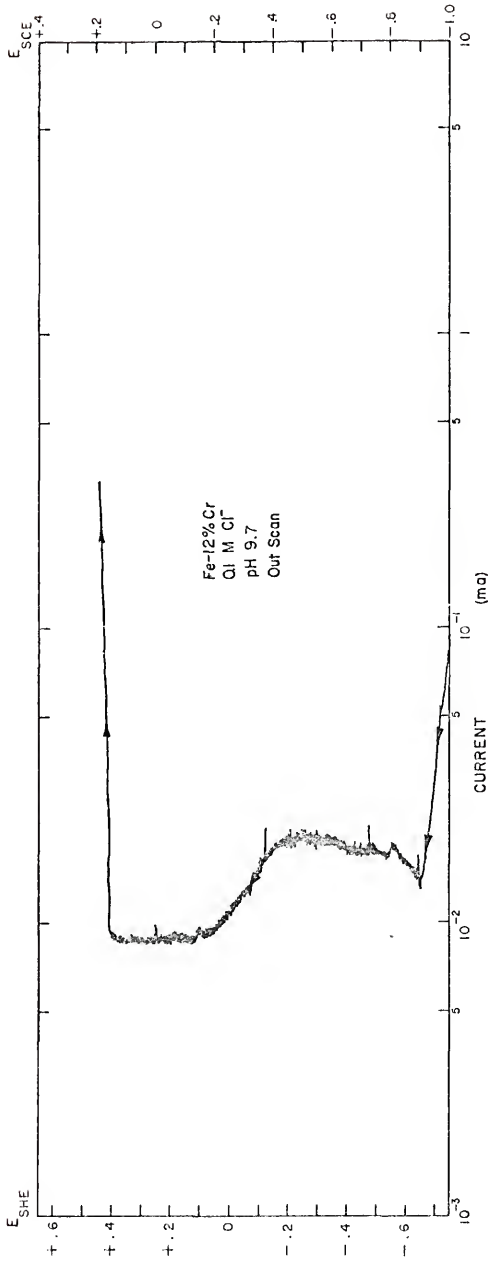


Figure 109. Out-scan portion of special cyclic potentiokinetic polarization scan for the Fe - 12% Cr alloy in 0.1 M Cl⁻, H₂-saturated solution of pH 9.7, using painted-off sample approximately 1 cm² in area.

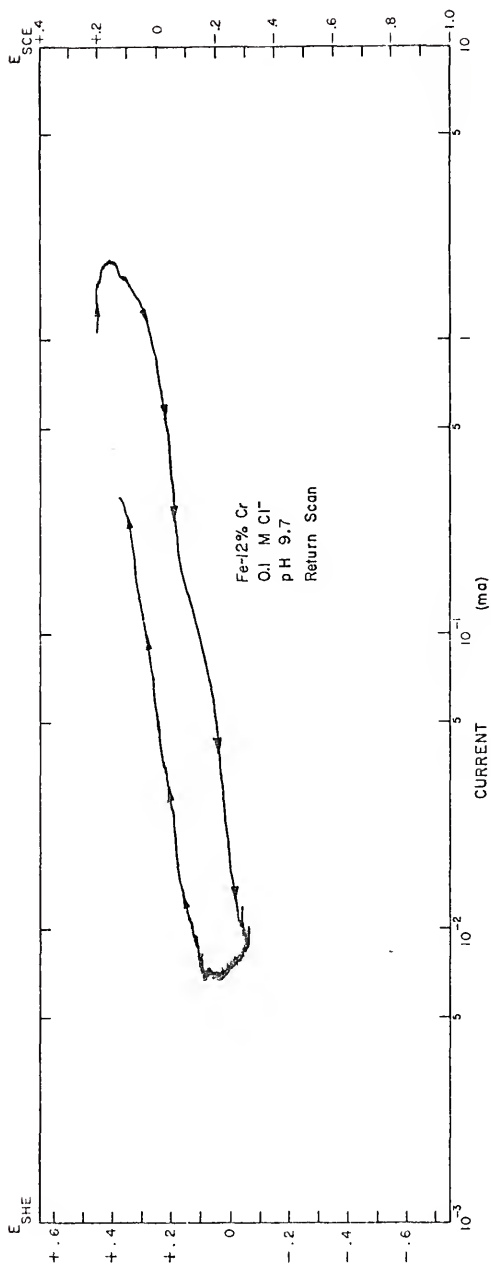


Figure 110. Return-scan portion of special cyclic potentiokinetic polarization scan for the Fe - 12% Cr alloy in 0.1 M Cl⁻, H₂O-saturated solution of pH 9.7, using painted-off sample approximately 1 cm² in area.

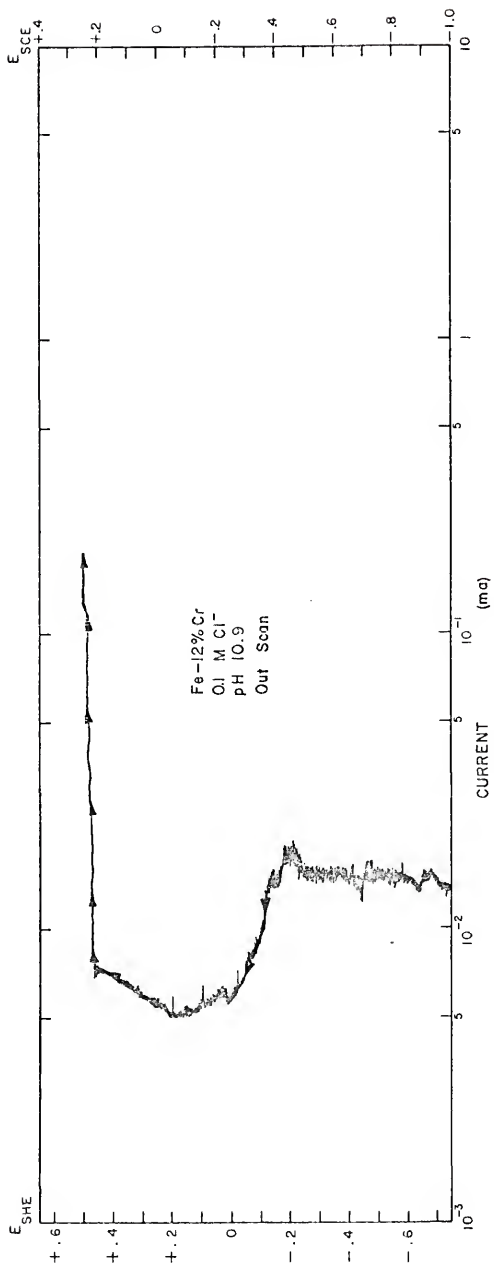


Figure 111. Out-scan portion of special cyclic potentiokinetic polarization scan for the Fe - 12% Cr alloy in 0.1 M Cl^- , H_2 -saturated solution of pH 10.9, using painted-off sample approximately 1 cm^2 in area.

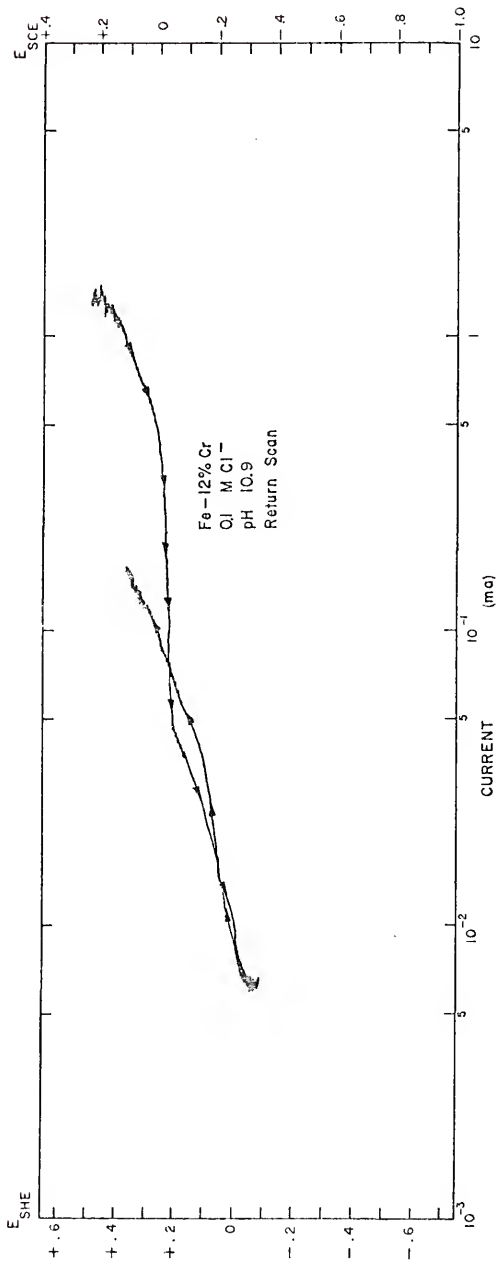


Figure 112. Return-scan portion of special cyclic potentiokinetic polarization scan for the Fe - 12% Cr alloy in 0.1 M Cl⁻, H₂-saturated solution of pH 10.9, using painted-off sample approximately 1 cm² in area.

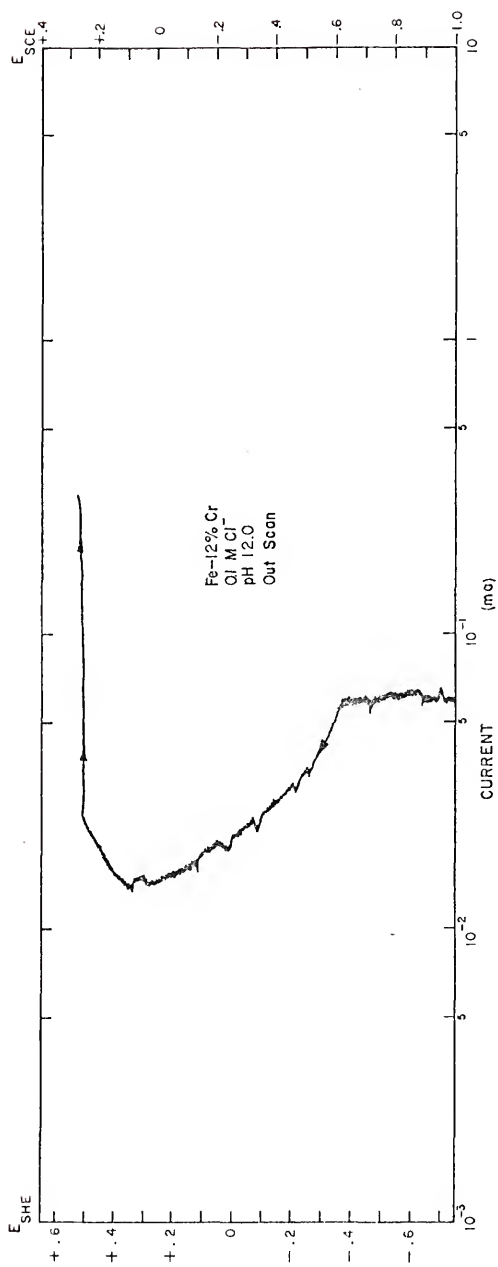


Figure 113. Out-scan portion of special cyclic potentiokinetic polarization scan for the Fe - 12% Cr alloy in 0.1 M Cl⁻, H₂-saturated solution of pH 12.0, using painted-off sample approximately 1 cm² in area.

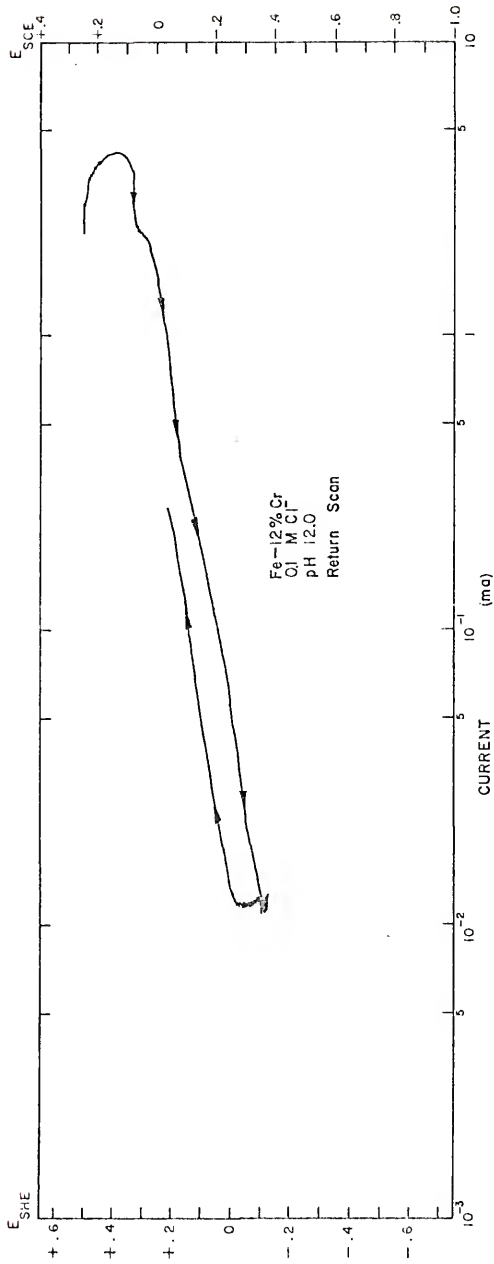


Figure 114. Return-scan portion of special cyclic potentiokinetic polarization scan for the Fe - 12% Cr alloy in 0.1 M Cl⁻, H₂O-saturated solution of pH 12.0, using painted-off sample approximately 1 cm² in area.

APPENDIX 11

EXPERIMENTAL POTENTIAL VS. LOG CHLORIDE ION MOLARITY DIAGRAMS AND
CHARACTERISTIC VALUES FROM CYCLIC POTENTIOKINETIC POLARIZATION
CURVES FOR Fe-Cr ALLOYS IN H₂-SATURATED SOLUTIONS
OF NOMINAL pH 5.4, 8.8 AND 10.8

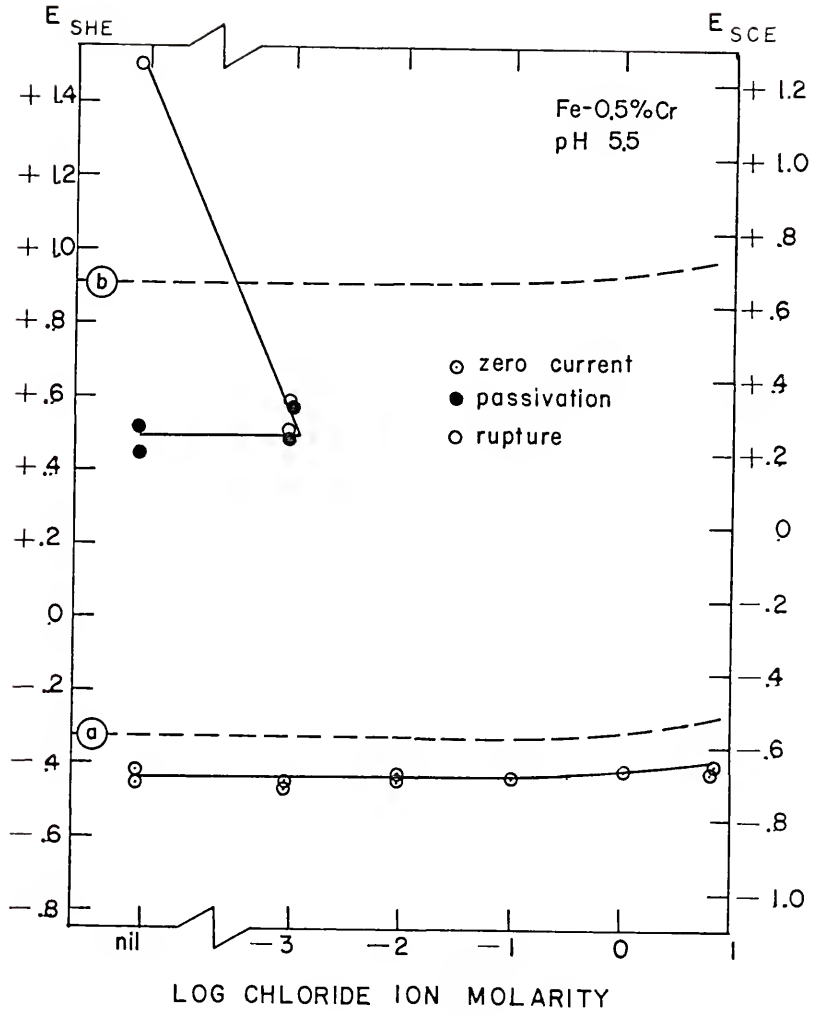


Figure 115. Potential vs. log chloride ion molarity diagram for the Fe - 0.5% Cr alloy in H_2 -saturated solutions of pH 5.5.

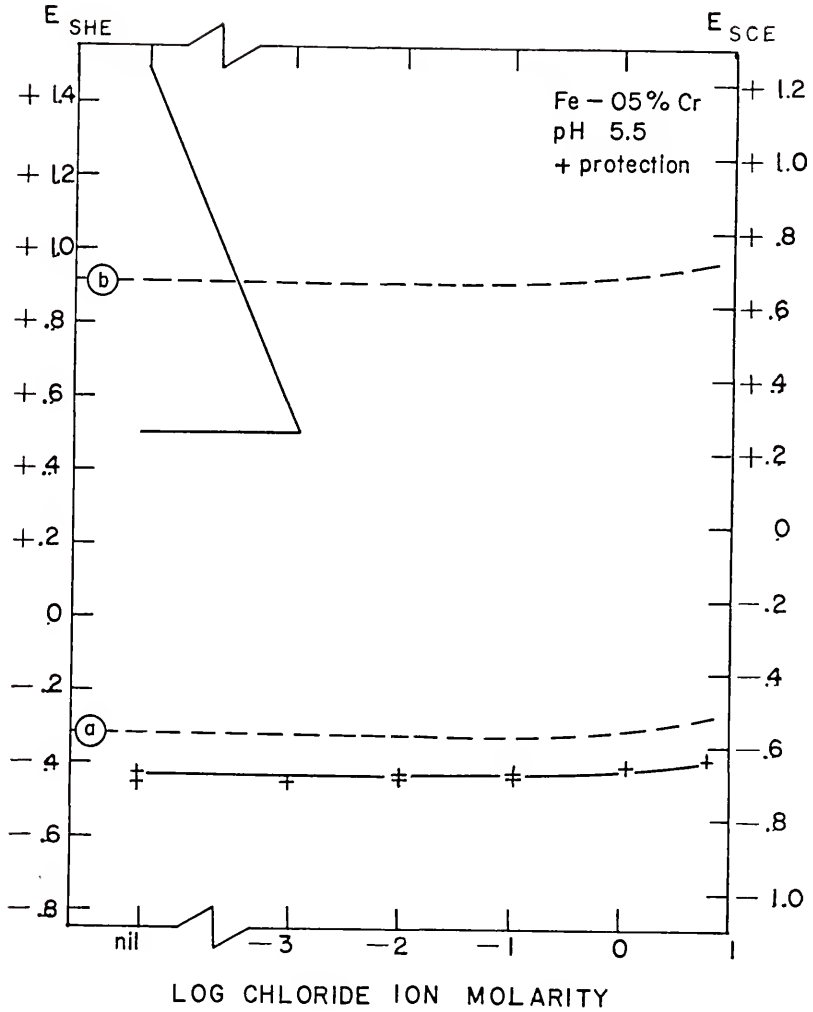


Figure 116. "Protection potential" (E_p) data, superimposed on the zero current potential, primary passivation potential and rupture potential lines taken from Figure 115.

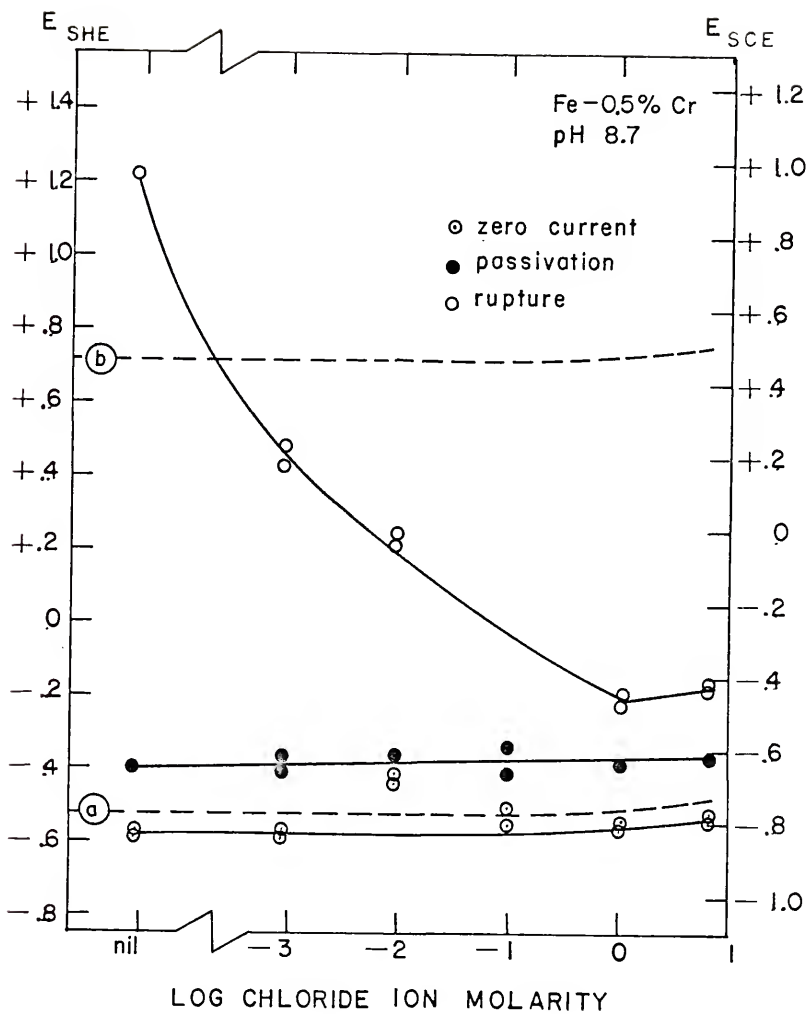


Figure 117. Potential vs. log chloride ion molarity diagram for the Fe - 0.5% Cr alloy in H₂-saturated solutions of pH 8.7.

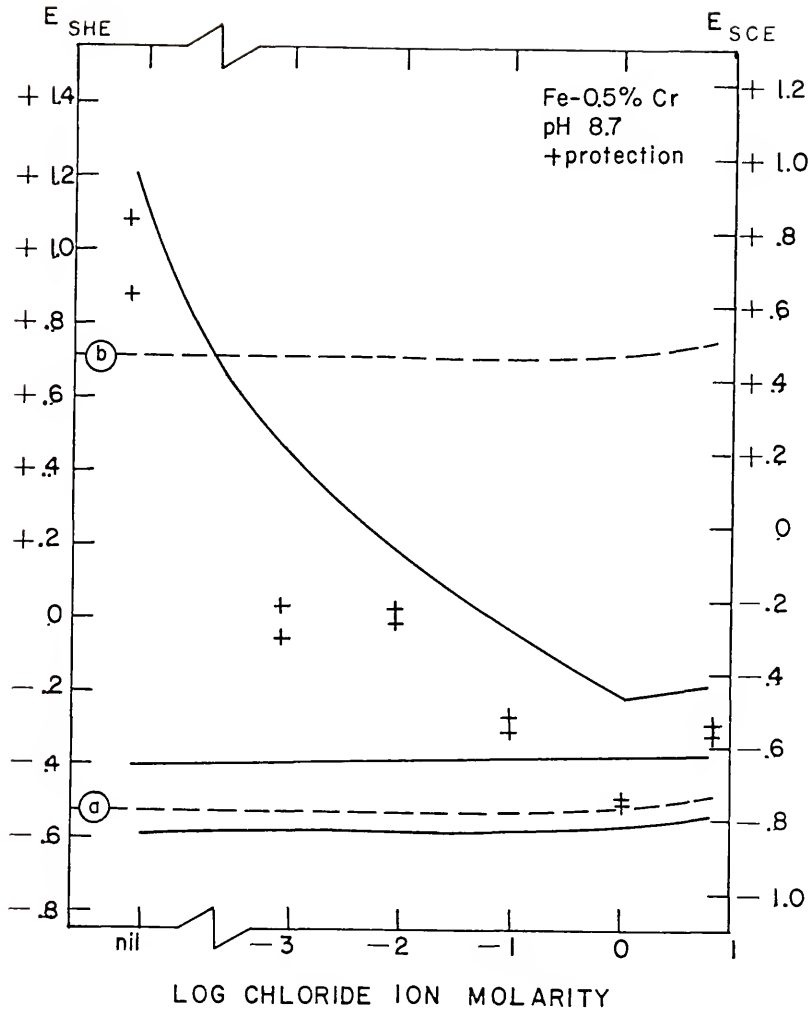


Figure 118. "Protection potential" (E_p) data, superimposed on the zero current potential, primary passivation potential and rupture potential lines taken from Figure 117.

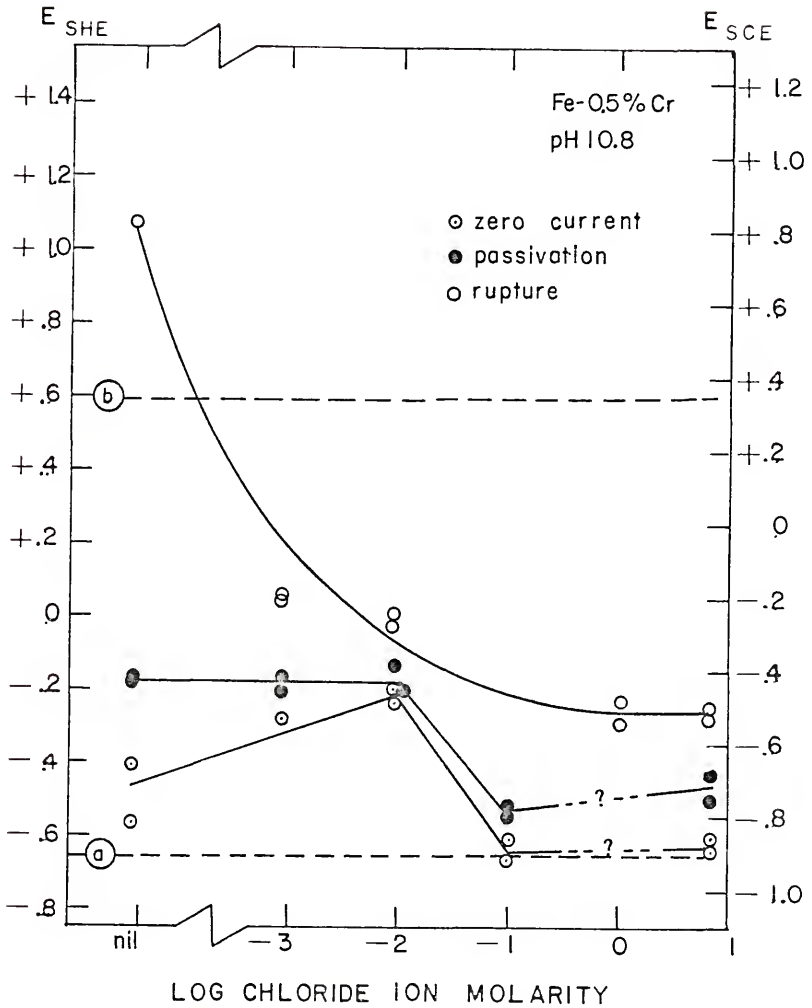


Figure 119. Potential vs. log chloride ion molarity diagram for the Fe - 0.5% Cr alloy in H_2 -saturated solutions of pH 10.8.

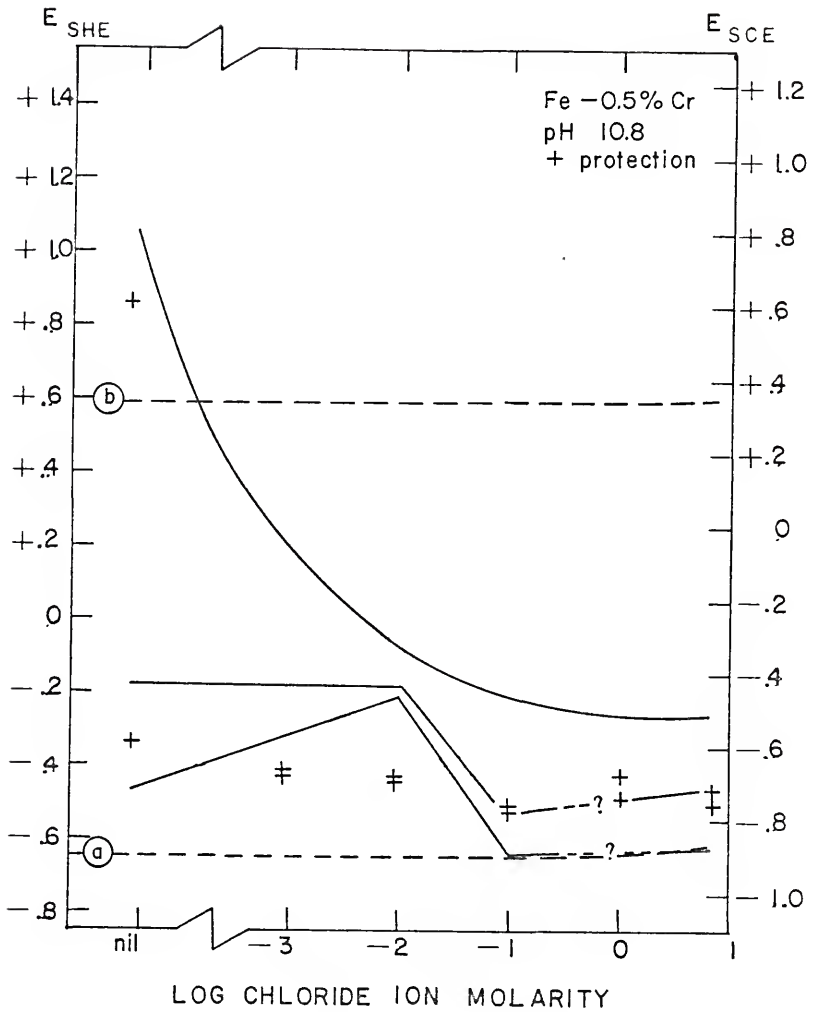


Figure 120. "Protection potential" (E_p) data, superimposed on the zero current potential, primary passivation potential and rupture potential lines taken from Figure 119.

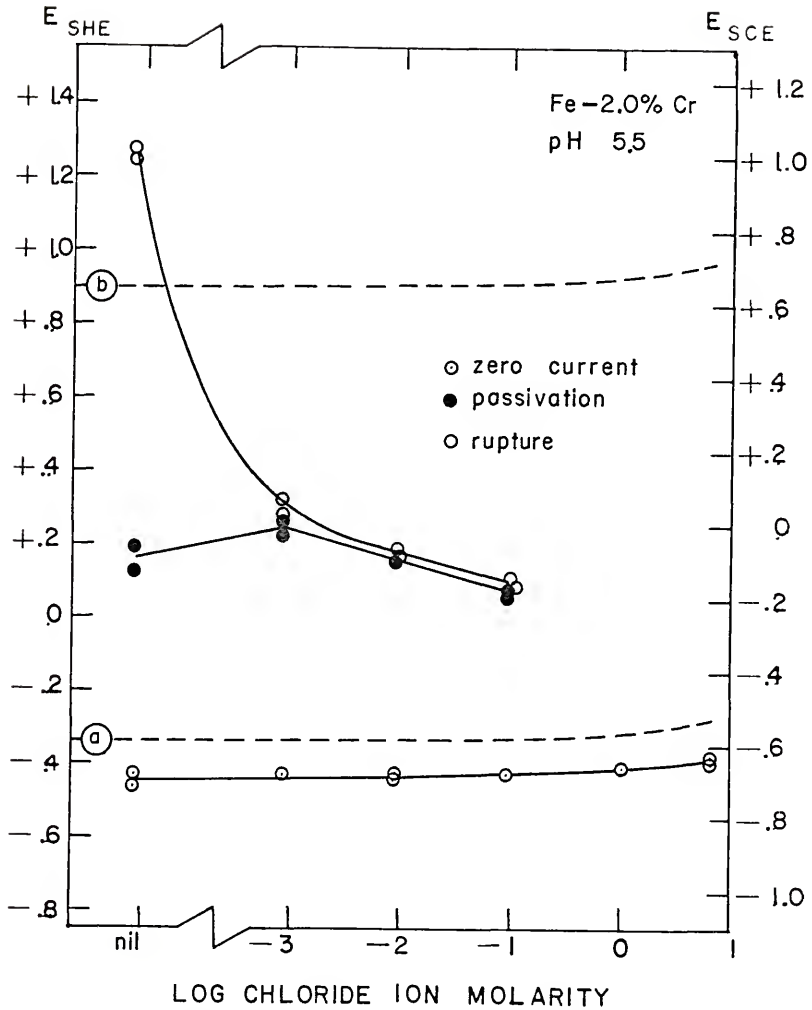


Figure 121. Potential vs. log chloride ion molarity diagram for the Fe - 2.0% Cr alloy in H_2 -saturated solutions of pH 5.5.

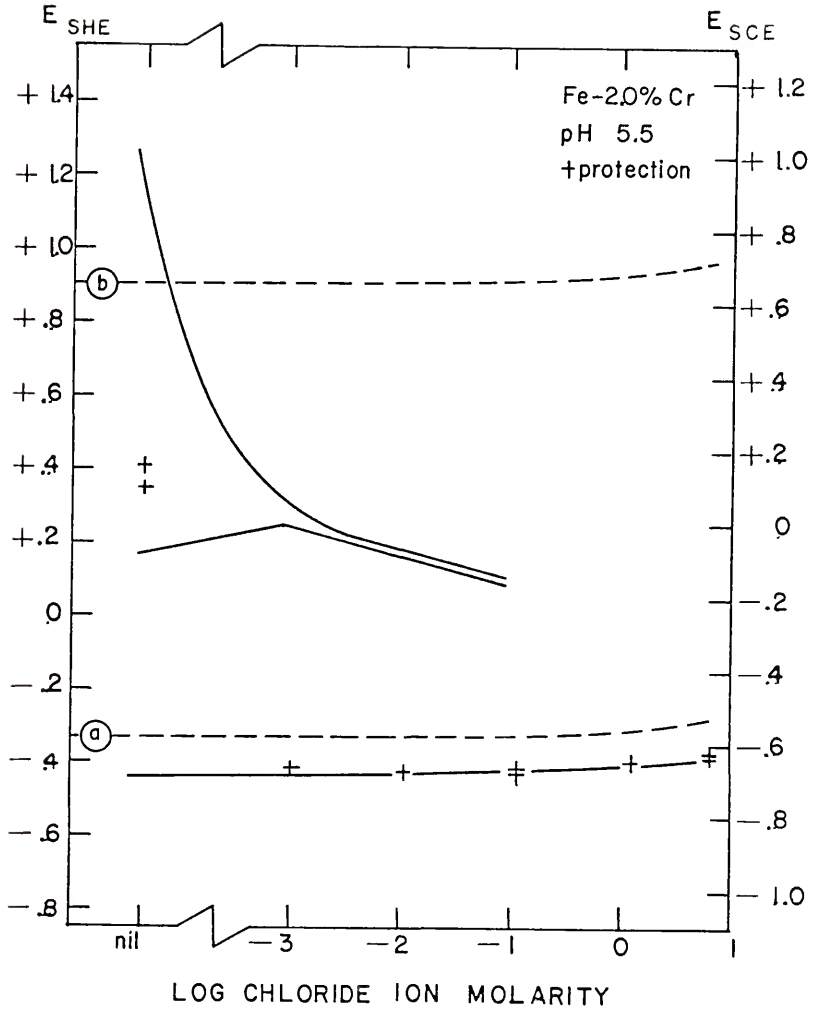


Figure 122. "Protection potential" (E_p) data, superimposed on the zero current potential, primary passivation potential and rupture potential lines taken from Figure 121.

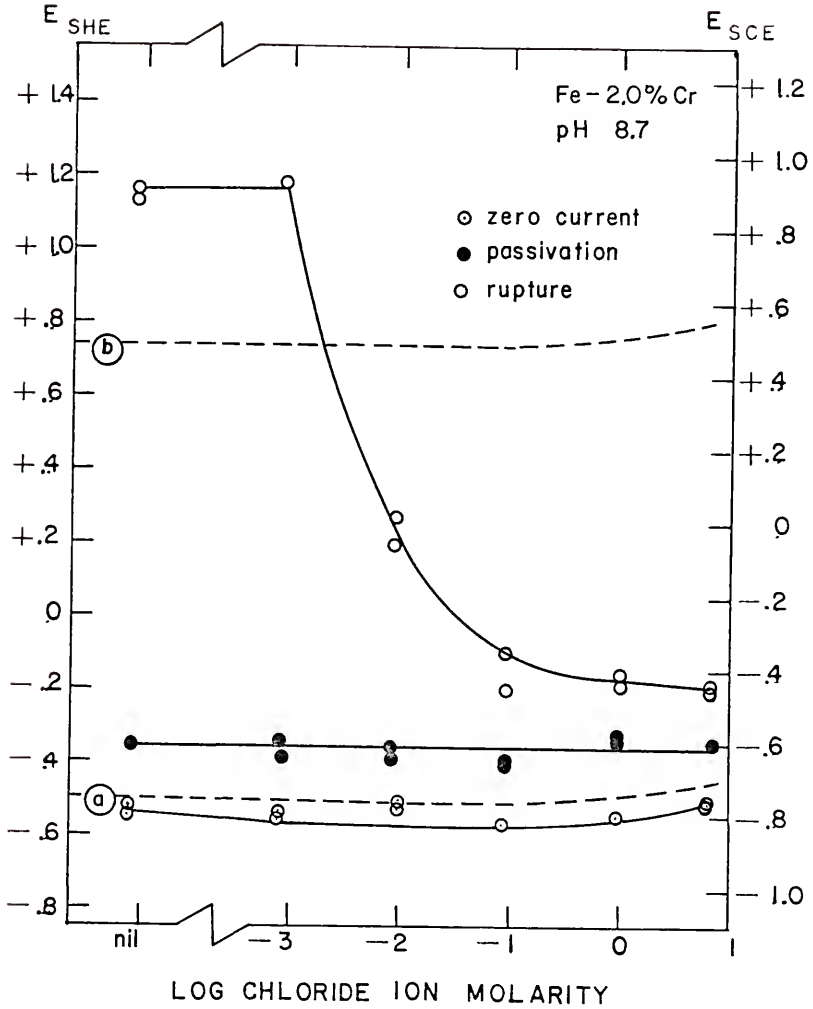


Figure 123. Potential vs. log chloride ion molarity diagram for the Fe - 2.0% Cr alloy in H₂-saturated solutions of pH 8.7.

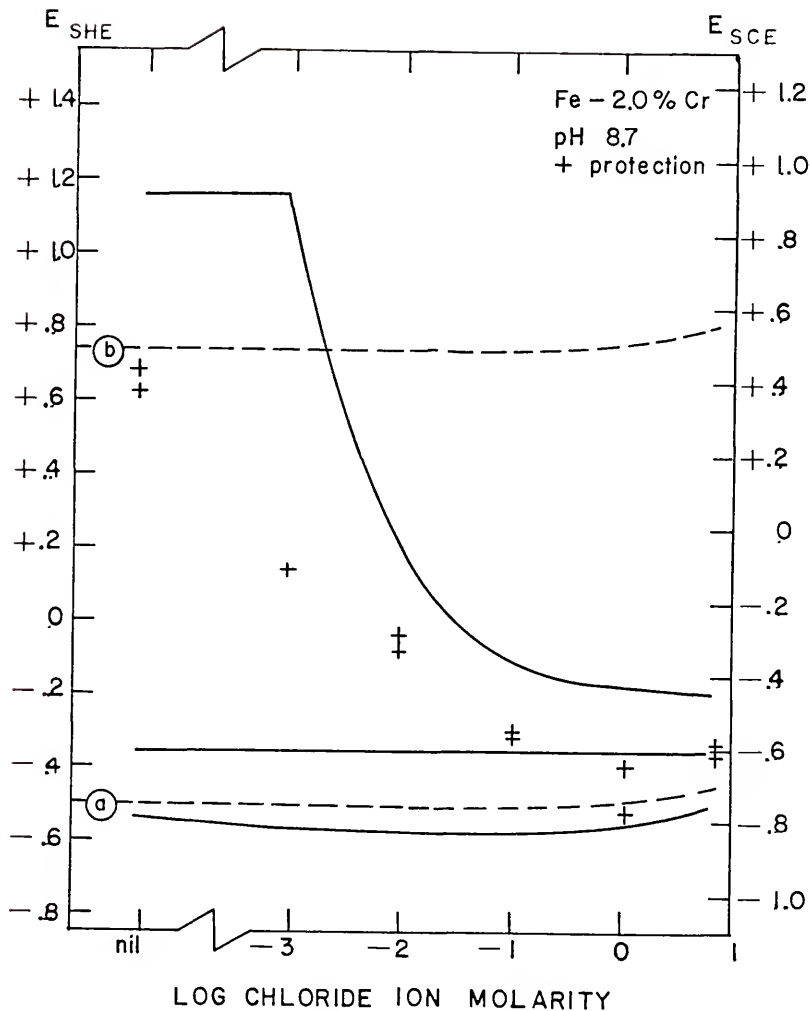


Figure 124. "Protection potential" (E_p) data, superimposed on the zero current potential, primary passivation potential and rupture potential lines taken from Figure 123.

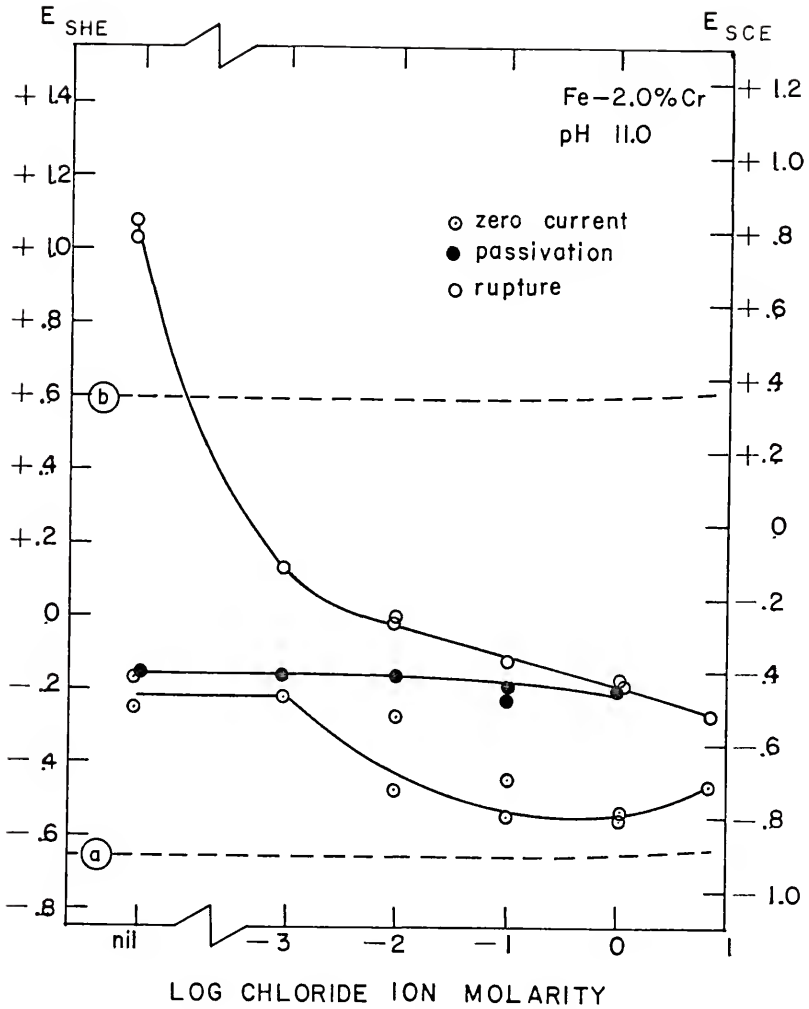


Figure 125. Potential vs. log chloride ion molarity diagram for the Fe - 2.0% Cr alloy in H₂-saturated solutions of pH 11.0.

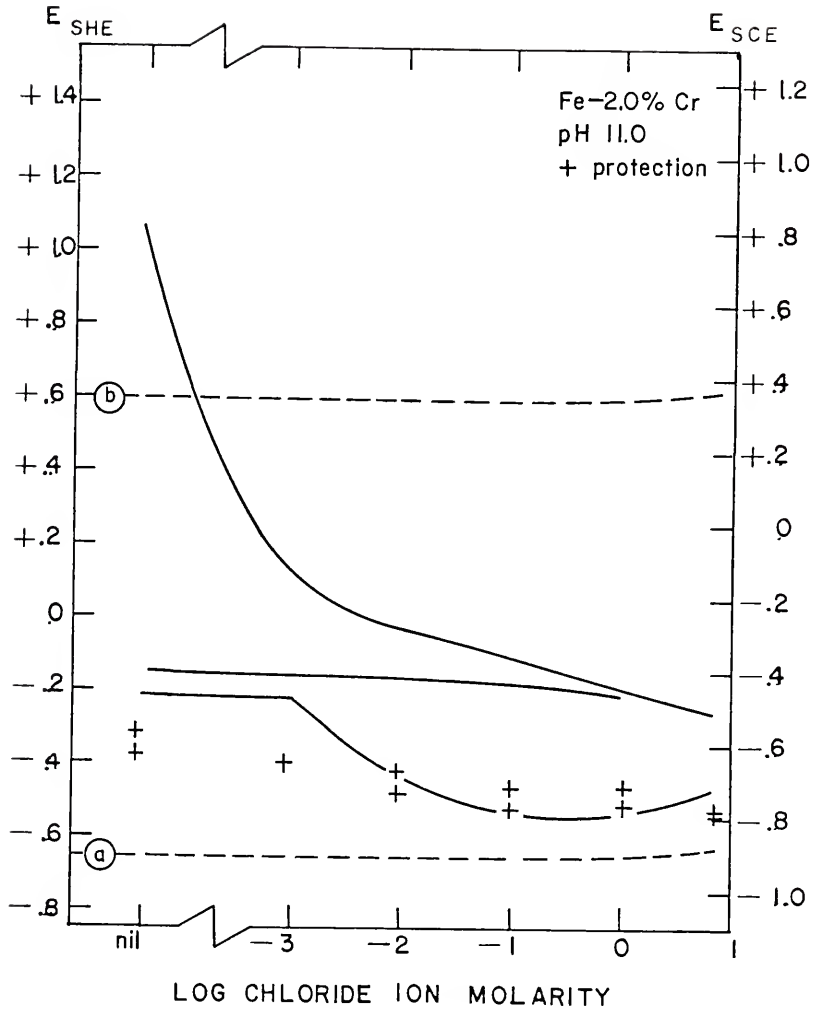


Figure 126. "Protection potential" (E_p) data, superimposed on the zero current potential, primary passivation potential and rupture potential lines taken from Figure 125.

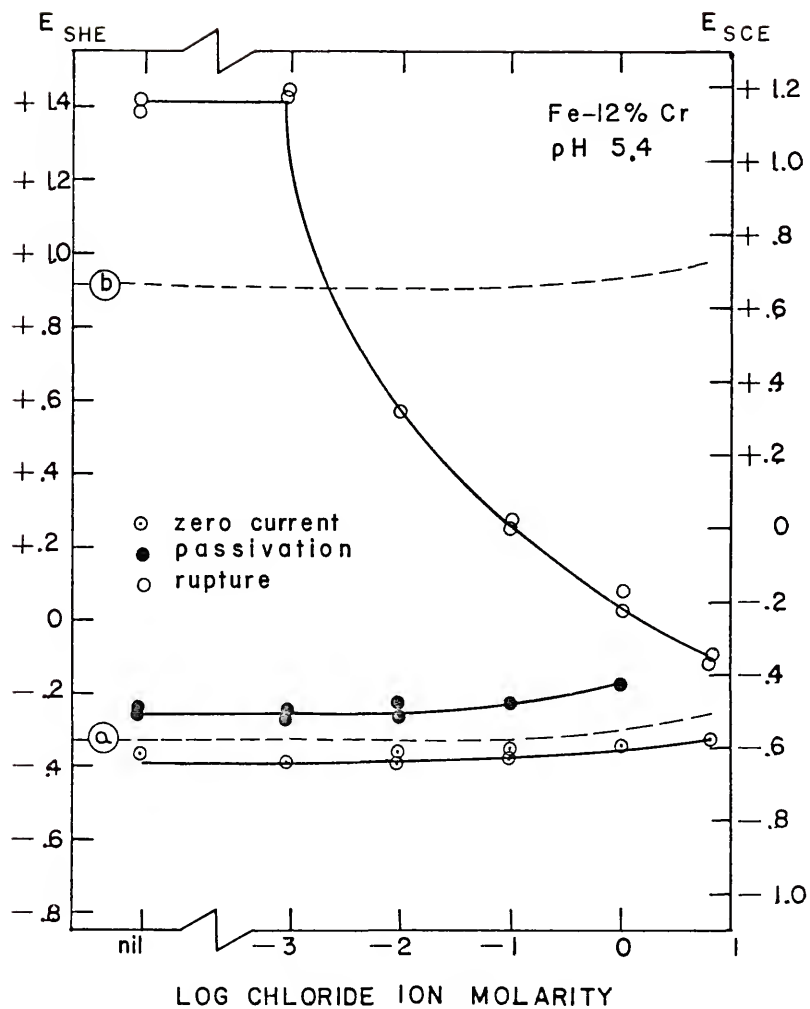


Figure 127. Potential vs. log chloride ion molarity diagram for the Fe - 12% Cr alloy in H_2 -saturated solutions of pH 5.4.

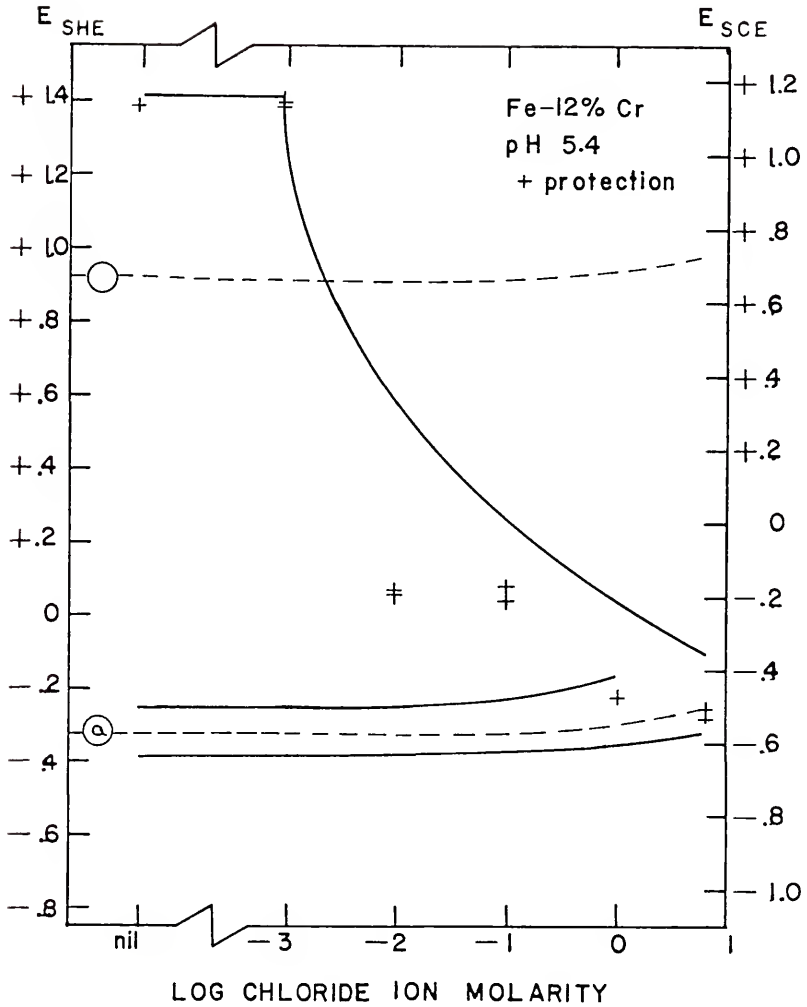


Figure 128. "Protection potential" (E_p) data, superimposed on the zero current potential, primary passivation potential and rupture potential lines taken from Figure 127.

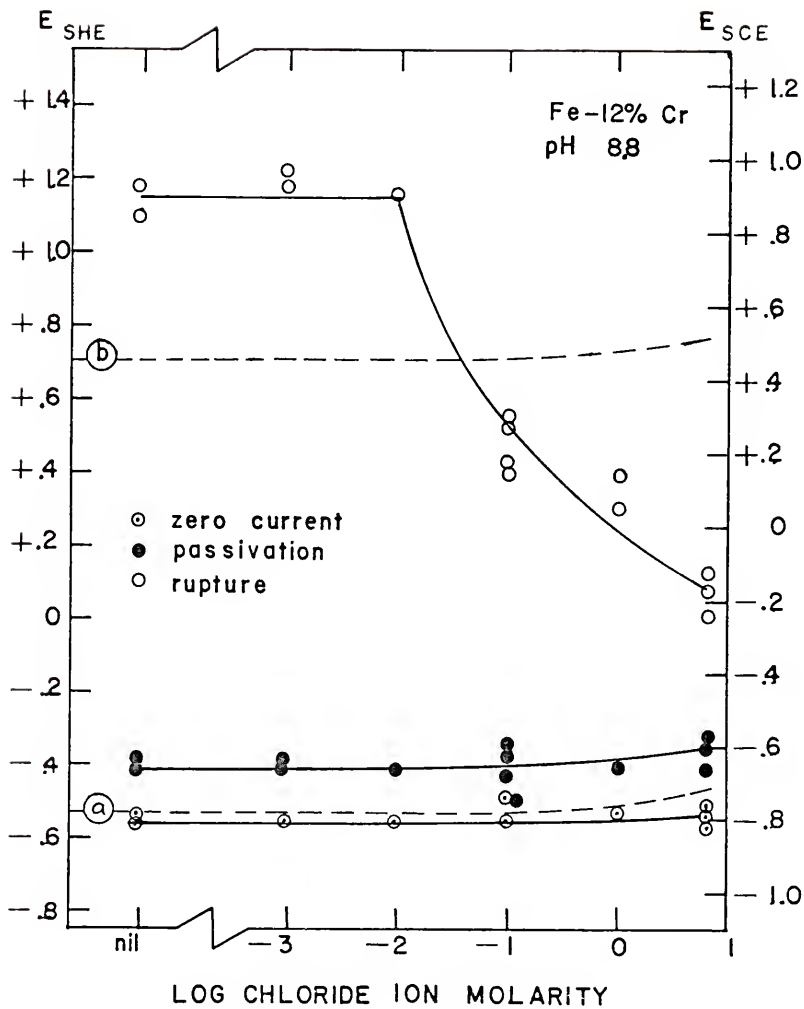


Figure 129. Potential vs. log chloride ion molarity diagram for the Fe - 12% Cr alloy in H_2 -saturated solutions of pH 8.8.

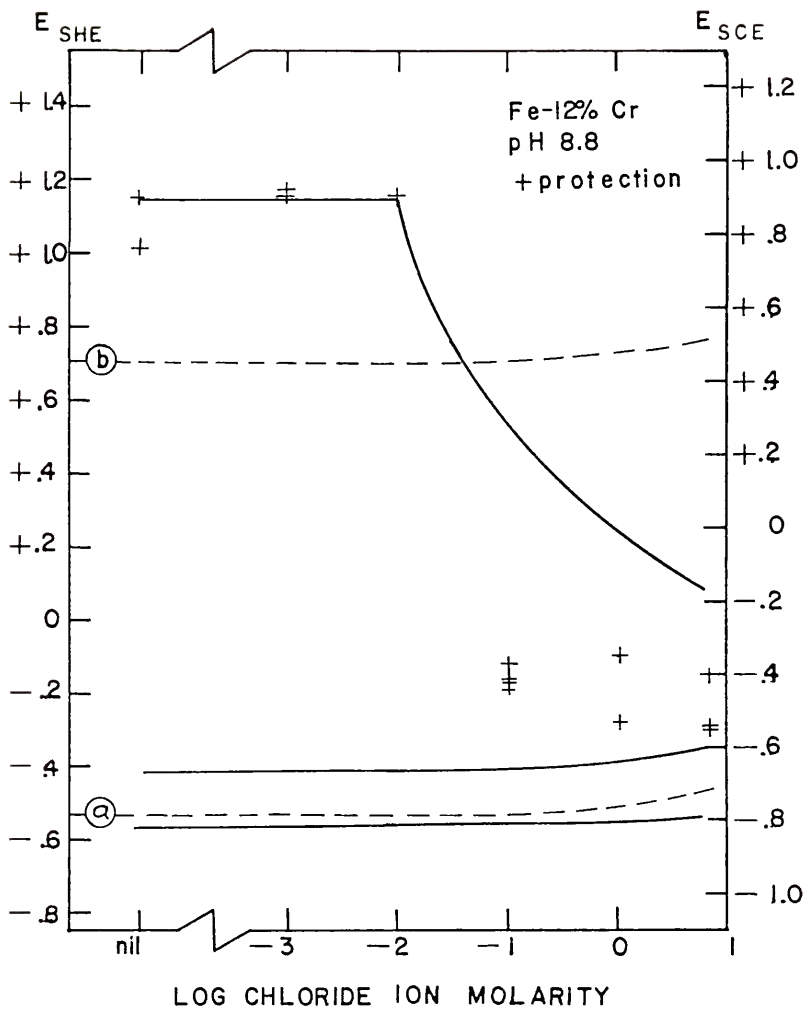


Figure 130. "Protection potential" (E_p) data, superimposed on the zero current potential, primary passivation potential and rupture potential lines taken from Figure 129.

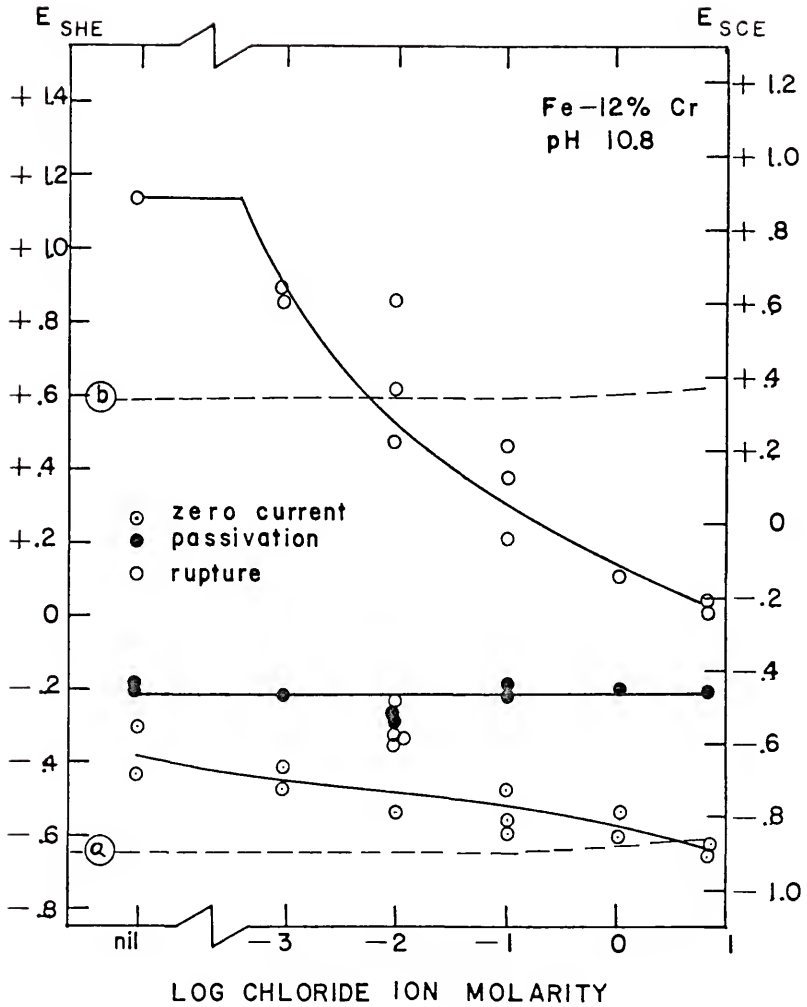


Figure 131. Potential vs. log chloride ion molarity diagram for the Fe - 12% Cr alloy in H_2 -saturated solutions of pH 10.8.

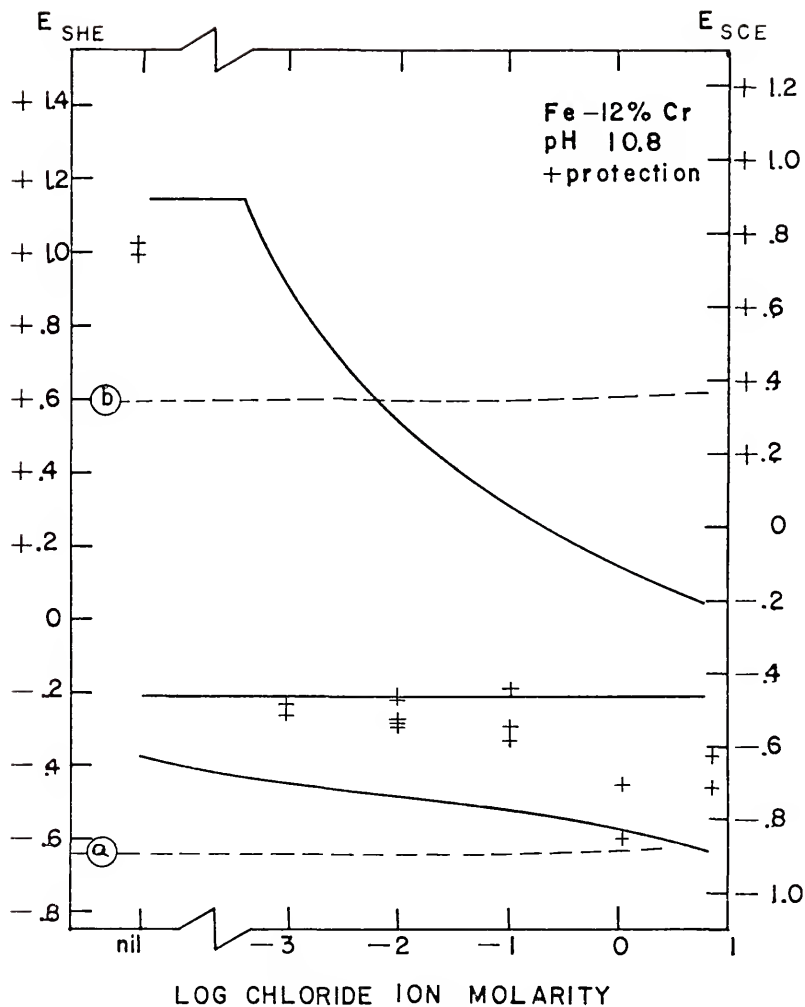


Figure 132. "Protection potential" (E_p) data, superimposed on the zero current potential, primary passivation potential and rupture potential lines taken from Figure 131.

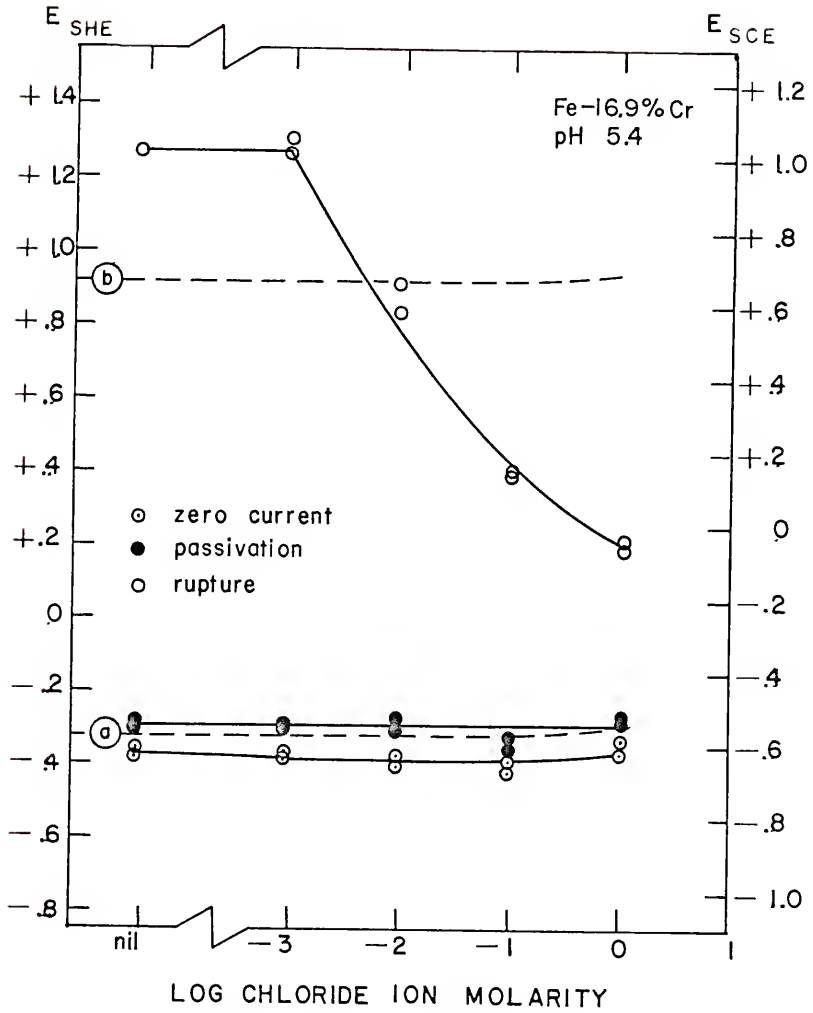


Figure 133. Potential vs. log chloride ion molarity diagram for the Fe - 16.9% Cr alloy in H_2 -saturated solutions of pH 5.4.

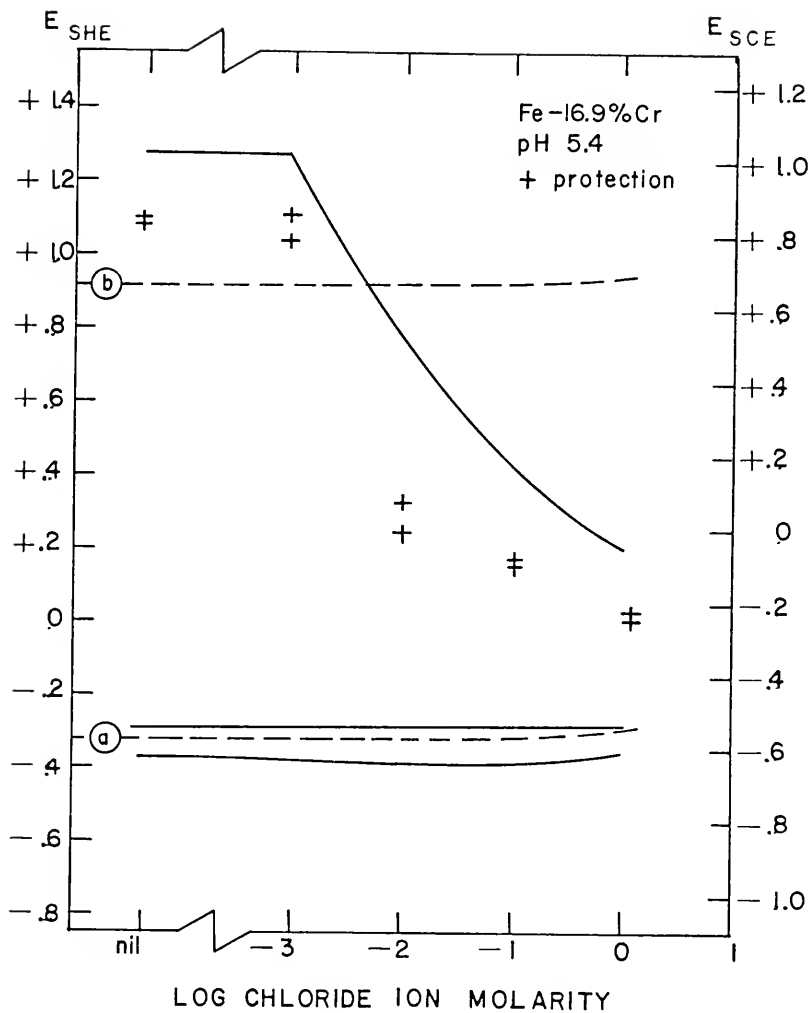


Figure 134. "Protection potential" (E_p) data, superimposed on the zero current potential, primary passivation potential and rupture potential lines taken from Figure 133.

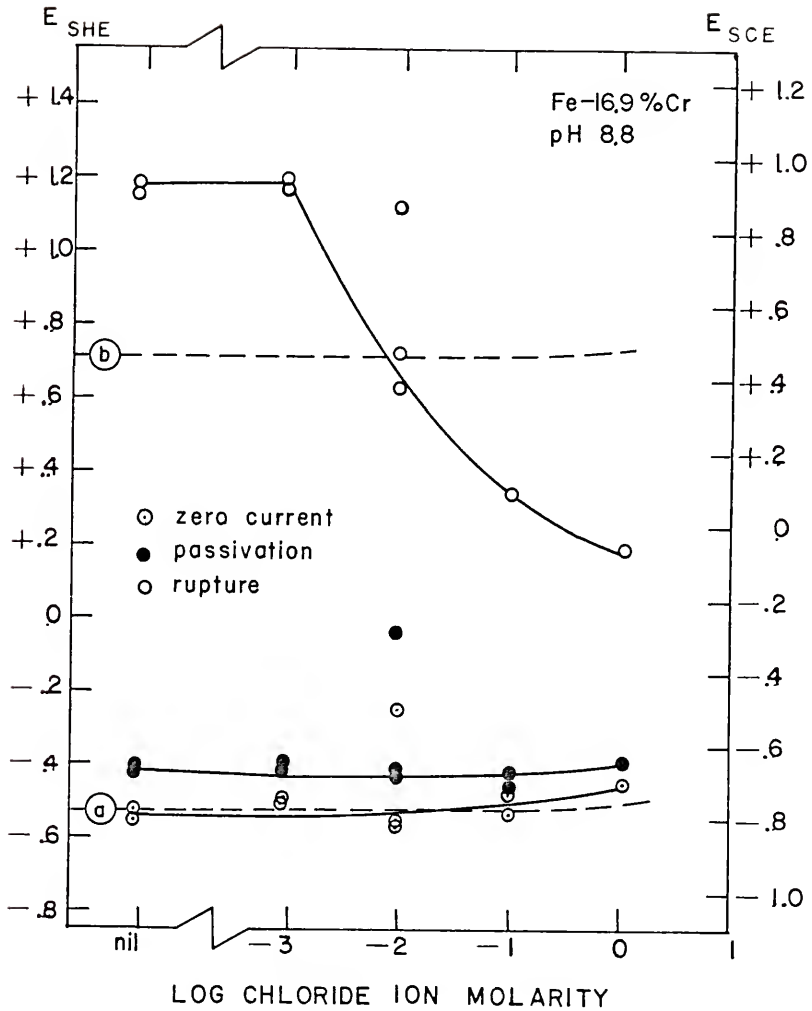


Figure 135. Potential vs. log chloride ion molarity diagram for the Fe - 16.9% Cr alloy in H_2 -saturated solutions of pH 8.8.

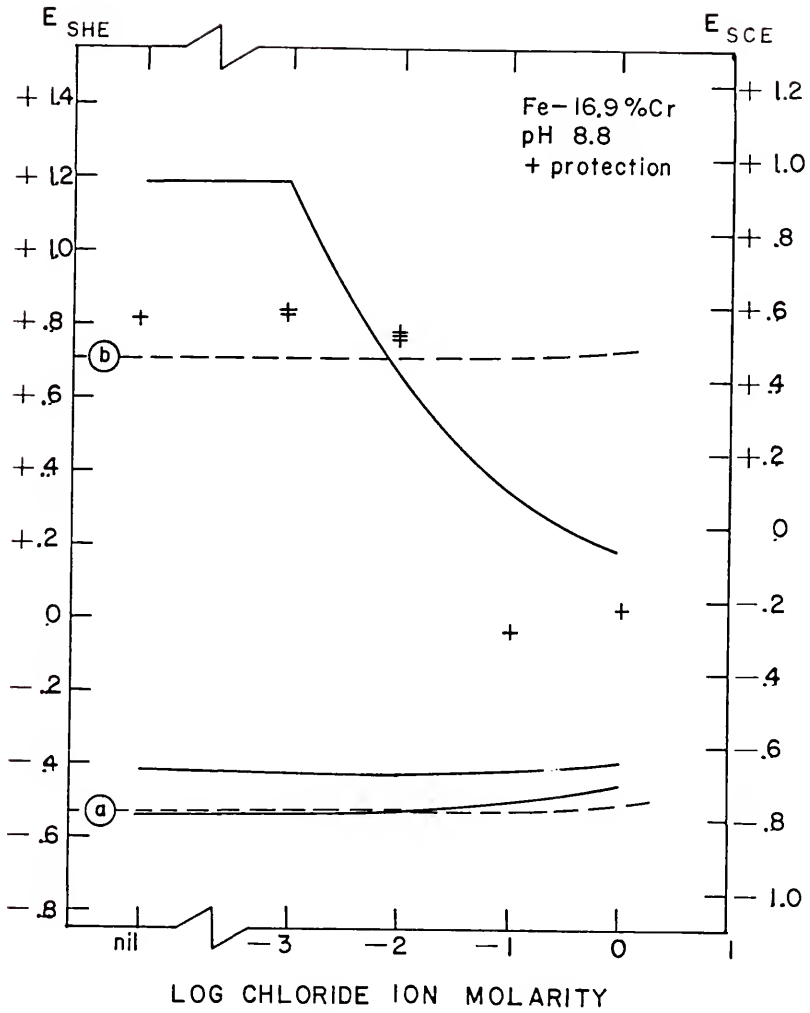


Figure 136. "Protection potential" (E_p) data, superimposed on the zero current potential, primary passivation potential and rupture potential lines taken from Figure 135.

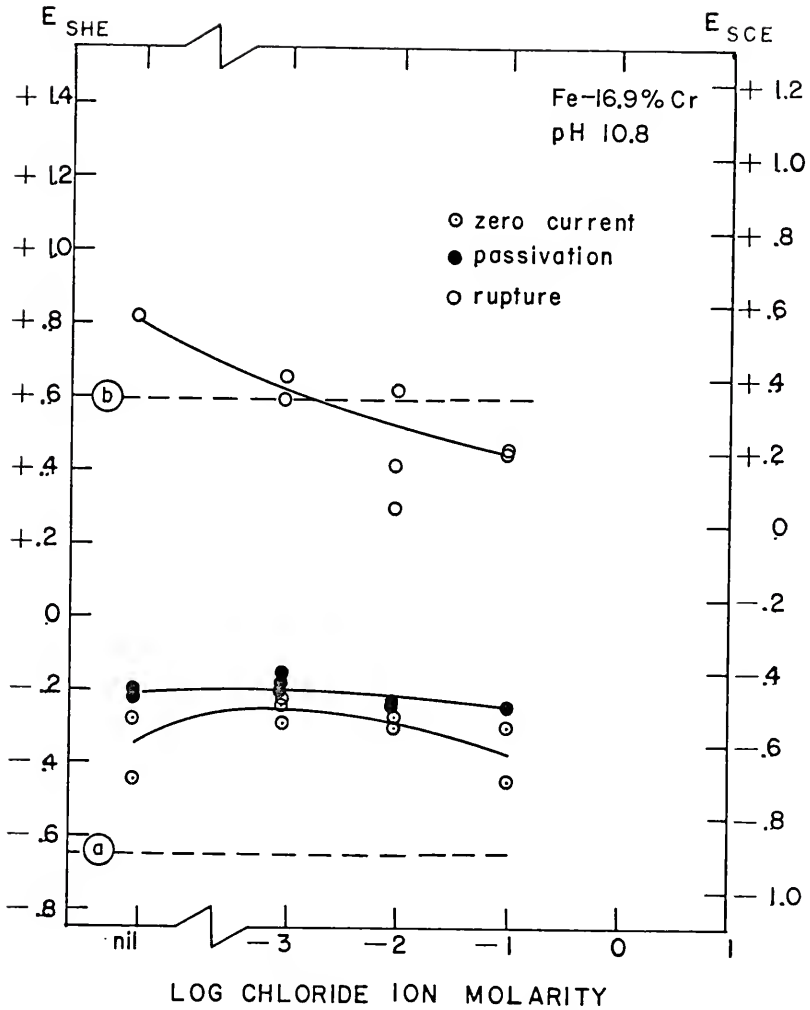


Figure 137. Potential vs. log chloride ion molarity diagram for the Fe - 16.9% Cr alloy in H_2 -saturated solutions of pH 10.8.

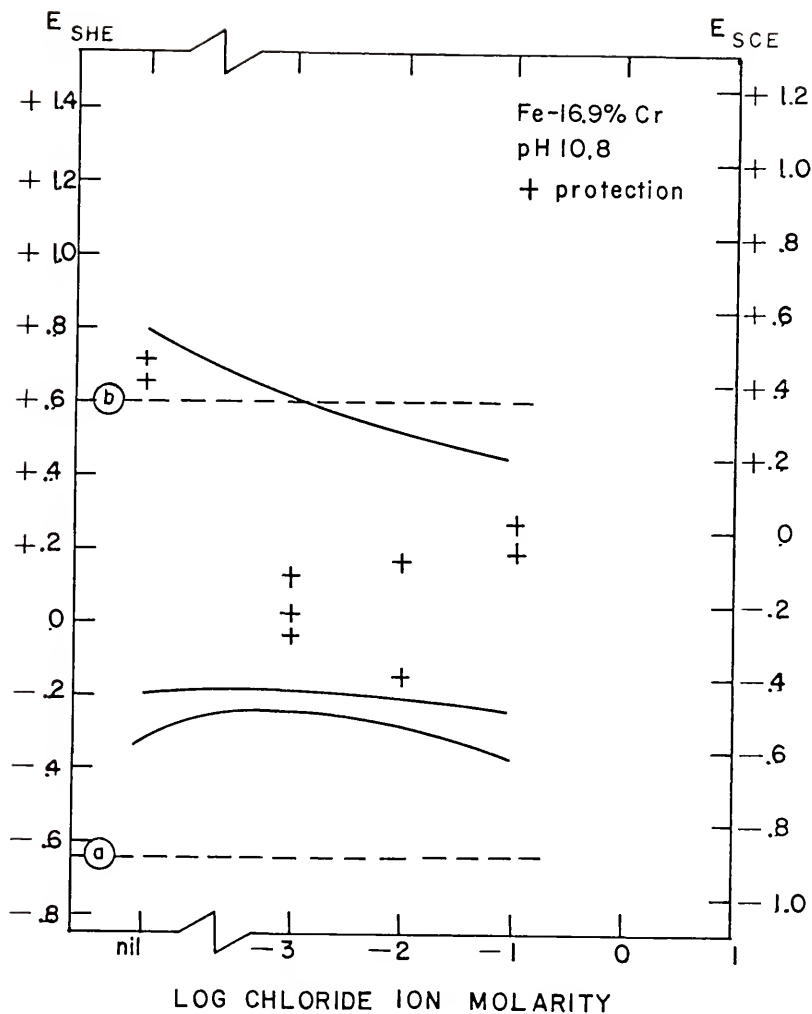


Figure 138. "Protection potential" (E_p) data, superimposed on the zero current potential, primary passivation potential and rupture potential lines taken from Figure 137.

TABLE 20
 CHARACTERISTIC VALUES FROM CYCLIC POTENTIOKINETIC
 POLARIZATION CURVES FOR THE Fe-0.5% Cr ALLOY
 IN H₂-SATURATED SOLUTIONS[†]

Run No.	Log Chloride ion Molarity (M)	pH	Zero Current Potential (VSCE)	Passivation Potential (VSCE)	Log Passivation Current Density (a/cm ²)	Rupture Potential (VSCE)	"Protection Potential" (VSCE)
*RC-68	-6.0	5.5	-0.660	-0.200	-2.13	+1.240	-0.660
RC-79	-6.0	5.5	-0.690	-0.260	-2.10	+1.240	-0.690
RC-66	-6.0	8.7	-0.815	-0.640	-4.10	+0.960	+0.620
RC-67	-6.0	8.7	-0.820	-0.640	-4.10	+0.960	+0.820
RC-75	-6.0	10.8	-0.650	-0.420	-5.57	+0.820	-0.580
RC-76	-6.0	10.8	-0.800	-0.410	-5.41	+0.820	+0.600
RC-92	-3.0	5.5	-0.685	+0.320	-2.17	+0.330	-0.690
RC-93	-3.0	5.5	-0.690	+0.230	-2.21	+0.250	-0.690
RC-87	-3.0	8.7	-0.830	-0.640	-4.12	+0.180	-0.310
RC-88	-3.0	8.7	-0.810	-0.610	-4.00	+0.230	-0.220
RC-84	-3.0	10.7	-0.520	-0.410	-5.41	-0.190	-0.660
RC-85	-3.0	10.7	-0.520	-0.440	-5.60	-0.200	-0.670
RC-57	-2.0	5.5	-0.665	-	-	-	-0.670

TABLE 20 (Continued)

 CHARACTERISTIC VALUES FROM CYCLIC POTENTIOKINETIC
 POLARIZATION CURVES FOR THE Fe-0.5% Cr ALLOY
 IN H₂-SATURATED SOLUTIONS[†]

Run No.	Log Chloride ion Molarity (M)	pH	Zero Current Potential (VSCE)	Passivation Potential (VSCE)	Log Passivation Current Density (a/cm ²)	Rupture Potential (VSCE)	"Protection Potential" (VSCE)
RC-58	-2.0	5.5	-0.685	-	-	-	-0.680
RC-59	-2.0	8.7	-0.650	-0.610	-4.00	-0.005	-0.270
RC-60	-2.0	8.7	-0.675	-0.620	-4.17	-0.035	-0.230
RC-61	-2.0	11.0	-0.440	-0.380	-6.08	-0.240	-0.690
RC-63	-2.0	11.0	-0.480	-0.440	-5.52	-0.270	-0.680
RC-27	-1.0	5.5	-0.670	-	-	-	-0.670
RC-28	-1.0	5.5	-0.670	-	-	-	-0.680
RC-23	-1.0	8.9	-0.750	-0.580	-3.83	-0.410	-0.565
RC-24	-1.0	8.9	-0.790	-0.650	-4.35	-0.425	-0.525
RC-31	-1.0	11.0	-0.845	-0.775	-5.48	-0.385	-0.760
RC-32	-1.0	11.0	-0.900	-0.755	-5.15	-0.410	-0.770
RC-100	-0.0	4.9	-0.650	-	-	-	-0.650
RC-101	-0.0	4.9	-0.650	-	-	-	-0.650

TABLE 20 (Continued)

 CHARACTERISTIC VALUES FROM CYCLIC POTENTIOKINETIC
 POLARIZATION CURVES FOR THE Fe-0.5% Cr ALLOY
 IN H₂-SATURATED SOLUTIONS

Run No.	Log Chloride Ion Molarity (M)	pH	Zero Current Potential (VSCE)	Passivation Potential (VSCE)	Log Passivation Current Density (a/cm ²)	Rupture Potential (VSCE)	"Protection Potential" (VSCE)
RC-96	0.0	8.3	-0.800	-0.610	-3.75	-0.440	-0.745
RC-97	0.0	8.3	-0.790	-0.610	-4.10	-0.460	-0.760
RC-102	0.0	10.6	-0.470	-	-	-	-0.745
RC-104	0.0	10.6	-0.525	-	-	-	-0.680
RC-119	0.8	4.6	-0.645	-	-	-	-0.630
RC-120	0.8	4.6	-0.640	-	-	-	-0.630
RC-110	0.8	7.6	-0.760	-0.595	-4.05	-0.410	-0.580
RC-111	0.8	7.6	-0.775	-0.605	-4.15	-0.425	-0.550
RC-117	0.8	10.6	-0.875	-0.735	-5.69	-0.495	-0.765
RC-118	0.8	10.6	-0.840	-0.670	-5.69	-0.510	-0.720

*Run numbers prefixed "RC" performed by R. L. Cusumano [54].

+ [54]

TABLE 21

CHARACTERISTIC VALUES FROM CYCLIC POTENTIOKINETIC
POLARIZATION CURVES FOR THE Fe-2.0% Cr ALLOY
IN H₂-SATURATED SOLUTIONS†

Run No.	Log Chloride Ion Molarity (M)	pH	Zero Current Potential (VSCE)	Passivation Potential (VSCE)	Log Passivation Current Density (a/cm ²)	Rupture Potential (VSCE)	"Protection" Potential" (VSCE)
RC-70	-6.0	5.5	-0.690	-0.050	-3.58	+1.020	+0.150
RC-72	-6.0	5.5	-0.660	-0.110	-3.54	+0.990	+0.090
RC-64	-6.0	8.7	-0.780	-0.610	-5.67	+0.880	+0.370
RC-65	-6.0	8.7	-0.800	-0.610	-5.72	+0.850	+0.430
RC-55	-6.0	11.0	-0.420	-0.410	-7.81	+0.810	-0.560
RC-56	-6.0	11.0	-0.500	-0.410	-6.48	+0.770	-0.620
RC-89	-3.0	5.5	-0.660	-0.020	-3.57	+0.040	-0.660
RC-90	-3.0	5.5	-0.660	-0.010	-3.56	+0.080	-0.660
RC-78	-3.0	8.8	-0.800	-0.610	-5.61	+0.900	-0.110
RC-79	-3.0	8.8	-0.810	-0.640	-5.68	+0.900	-
RC-82	-3.0	10.8	-0.470	-0.410	-6.36	-0.120	-0.640
RC-86	-3.0	10.8	-0.470	-0.410	-6.36	-0.120	-0.640
RC-49	-2.0	5.5	-0.660	-0.080	-3.60	-0.060	-0.670

TABLE 21 (Continued)

 CHARACTERISTIC VALUES FROM CYCLIC POTENTIOKINETIC
 POLARIZATION CURVES FOR THE Fe-2.0% Cr ALLOY
 IN H₂-SATURATED SOLUTIONS⁺

Run No.	Log Chloride ion Molarity (M)	pH	Zero Current Potential (VSCE)	Passivation Potential (VSCE)	Log Passivation Current Density (a/cm ²)	Rupture Potential (VSCE)	"Protection" Potential" (VSCE)
RC-50	-2.0	5.5	-0.670	-0.090	-3.59	-0.075	-0.670
RC-52	-2.0	8.7	-0.780	-0.640	-5.61	-0.070	-0.285
RC-53	-2.0	8.7	-0.760	-0.610	-5.71	-0.005	-0.330
RC-80	-2.0	10.8	-0.720	-0.410	-6.70	-0.250	-0.720
RC-81	-2.0	10.8	-0.520	-0.410	-6.74	-0.270	-0.660
RC-35	-1.0	5.4	-0.663	-0.180	-2.25	-0.130	-0.660
RC-36	-1.0	5.4	-0.670	-0.160	-2.30	-0.155	-0.670
RC-39	-1.0	8.8	-0.820	-0.635	-4.45	-0.355	-0.560
RC-40	-1.0	8.8	-0.820	-0.650	-4.35	-0.385	-0.545
RC-47	-1.0	11.0	-0.790	-0.475	-5.35	-0.370	-0.705
RC-48	-1.0	11.0	-0.690	-0.440	-5.35	-0.370	-0.760
RC-98	0.0	4.9	-0640	-	-	-	-0.640
RC-99	0.0	4.9	-0.640	-	-	-	-0.640

TABLE 21 (Continued)

CHARACTERISTIC VALUES FROM CYCLIC POTENTIOKINETIC
POLARIZATION CURVES FOR THE Fe-2.0% Cr ALLOY
IN H₂-SATURATED SOLUTIONS⁺

Run No.	Log Chloride ion Molarity (M)	pH	Zero Current Potential (VSCE)	Passivation Potential (VSCE)	Log Passivation Current Density (a/cm ²)	Rupture Potential (VSCE)	"Protection Potential" (VSCE)
RC-94	0.0	8.2	-0.800	-0.585	-4.04	-0.425	-0.640
RC-95	0.0	8.2	-0.800	-0.595	-4.00	-0.440	-0.765
RC-106	0.0	10.6	-0.775	-0.450	-5.25	-0.440	-0.700
RC-107	0.0	10.6	-0.800	-0.455	-6.95	-0.425	-0.750
RC-112	0.8	4.5	-0.620	-	-	-	-0.620
RC-113	0.8	4.5	-0.635	-	-	-	-0.635
RC-108	0.8	7.6	-0.755	-0.610	-5.60	-0.435	-0.580
RC-109	0.8	7.6	-0.760	-0.610	-5.51	-0.455	-0.610
RC-115	0.8	10.6	-0.710	-	-	-0.495	-0.765
RC-116	0.8	10.6	-0.710	-	-	-0.525	-0.760

+ [54]

TABLE 22

CHARACTERISTIC VALUES FROM CYCLIC POTENTIOKINETIC
POLARIZATION CURVES FOR THE Fe-1.2% Cr ALLOY
IN H₂-SATURATED SOLUTIONS⁺

Run No.	Log Chloride Ion Molarity (M)	pH	Zero Current Potential (VSCE)	Passivation Potential (VSCE)	Log Passivation Current Density (a/cm ²)	Rupture Potential (VSCE)	"Protection" Potential" (VSCE)
*KS-36	-6.0	5.4	-0.610	-0.500	-4.84	+1.140	+1.120
KS-37	-6.0	5.4	-0.610	-0.490	-4.84	+1.160	+1.120
KS-34	-6.0	8.6	-0.800	-0.660	-5.00	+0.920	+0.900
KS-35	-6.0	8.7	-0.790	-0.640	-5.07	+0.840	+0.760
KS-38	-6.0	10.8	-0.680	-0.450	-5.57	+0.780	+0.770
KS-39	-6.0	10.8	-0.550	-0.440	-5.55	+0.780	+0.740
KS-44	-3.0	5.4	-0.630	-0.510	-4.72	+1.170	+1.130
KS-45	-3.0	5.4	-0.630	-0.500	-4.72	+1.180	+1.120
KS-42	-3.0	8.7	-0.800	-0.660	-5.03	+0.920	+0.900
KS-43	-3.0	8.7	-0.800	-0.640	-5.00	+0.960	+0.920
KS-40	-3.0	10.7	-0.660	-0.460	-5.48	+0.640	-0.510
KS-41	-3.0	10.7	-0.720	-0.460	-5.52	+0.600	-0.480
KS-28	-2.0	5.5	-0.610	-0.470	-4.88	+0.310	-0.200

TABLE 22 (Continued)

 CHARACTERISTIC VALUES FROM CYCLIC POTENTIOKINETIC
 POLARIZATION CURVES FOR THE Fe-12% Cr ALLOY
 IN H₂-SATURATED SOLUTIONS

Run No.	Log Chloride ion Molarity (M)	pH	Zero Current Potential (VSCE)	Passivation Potential (VSCE)	Log Passivation Current Density (a/cm ²)	Rupture Potential (VSCE)	"Protection" Potential" (VSCE)
KS-29	-2.0	5.5	-0.630	-0.510	-4.59	+0.315	-0.190
KS-32	-2.0	8.7	-0.800	-0.660	-5.07	+0.900	+0.900
KS-33	-2.0	8.7	-0.800	-0.660	-5.01	+0.900	+0.900
KS-30	-2.0	10.6	-0.580	-0.450	-5.33	+0.220	-0.530
KS-31	-2.0	10.7	-0.560	-0.460	-5.40	+0.360	-0.540
KS-20	-2.0	10.9	-0.780	-0.480	-5.42	+0.600	-0.470
KS-21	-2.0	10.9	-0.480	-0.450	-5.96	+0.600	-0.520
KS-12	-1.0	5.4	-0.610	-0.470	-4.74	+0.010	-0.220
KS-13	-1.0	5.4	-0.600	-0.470	-4.87	+0.020	-0.180
KS-18	-1.0	8.9	-0.740	-0.600	-5.70	+0.175	-0.440
KS-19	-1.0	8.9	-0.725	-0.620	-5.55	+0.145	-0.425
KS-4	-1.0	10.7	-0.800	-0.445	-5.27	+0.210	-0.450

TABLE 22 (Continued)

 CHARACTERISTIC VALUES FROM CYCLIC POTENTIOKINETIC
 POLARIZATION CURVES FOR THE Fe-12% Cr ALLOY
 IN H₂-SATURATED SOLUTIONS

Run No.	Log Chloride ion Molarity (M)	pH	Zero Current Potential (VSCE)	Passivation Potential (VSCE)	Log Passivation Current Density (a/cm ²)	Rupture Potential (VSCE)	"Protection Potential" (VSCE)
KS-5	-1.0	10.7	-0.720	-0.460	-5.24	-0.040	-0.540
KS-6	-1.0	10.7	-0.830	-0.470	-5.37	+0.120	-0.580
KS-48	0.0	4.9	-0.590	-0.420	-4.72	-0.210	-0.480
KS-49	0.0	4.9	-0.590	-0.420	-4.68	-0.170	-0.480
KS-47	0.0	8.2	-0.775	-0.650	-5.00	+0.050	-0.530
KS-46	0.0	8.3	-0.785	-0.650	-4.99	+0.140	-0.350
KS-50	0.0	10.3	-0.840	-0.450	-5.00	-0.120	-0.845
KS-51	0.0	10.4	-0.780	-0.450	-5.30	-0.140	-0.700
KS-55	0.78	4.3	-0.565	-	-	-0.345	-0.510
KS-56	0.78	4.3	-0.575	-	-	-0.365	-0.535
KS-52	0.78	7.7	-0.810	-0.660	-4.53	-0.240	-0.550
KS-53	0.78	7.7	-0.780	-0.600	-5.00	-0.175	-0.405
KS-54	0.78	7.7	-0.760	-0.570	-5.16	-0.130	-0.540

TABLE 22 (Continued)

CHARACTERISTIC VALUES FROM CYCLIC POTENTIOKINETIC
POLARIZATION CURVES FOR THE Fe-12% Cr ALLOY
IN H₂-SATURATED SOLUTIONS

Run No.	Log Chloride ion Molarity (M)	pH	Zero Current Potential (VSCE)	Passivation Potential (VSCE)	Log Passivation Current Density (a/cm ²)	Rupture Potential (VSCE)	"Protection Potential" (VSCE)
KS-57	0.78	10.4	-0.900	-0.450	-4.98	-0.215	-0.620
KS-58	0.78	10.4	-0.870	-0.450	-5.25	-0.230	-0.705

*Run numbers prefixed "KS" performed by K. K. Starr [54]

+ [54]

TABLE 23
 CHARACTERISTIC VALUES FROM CYCLIC POTENTIOKINETIC
 POLARIZATION CURVES FOR THE Fe-16.9% Cr ALLOY
 IN H₂-SATURATED SOLUTIONS[†]

Run No.	Log Chloride ion Molarity (M)	pH	Zero Current Potential (VSCE)	Passivation Potential (VSCE)	Log Passivation Current Density (a/cm ²)	Rupture Potential (VSCE)	"Protection Potential" (VSCE)
*JS-50	-6.0	5.4	-0.600	-0.530	-5.03	+1.000	+0.830
JS-51	-6.0	5.4	-0.620	-0.540	-5.04	+1.000	+0.810
JS-48	-6.0	8.7	-0.760	-0.640	-5.32	+0.900	+0.560
JS-49	-6.0	8.7	-0.780	-0.660	-5.24	+0.920	+0.560
JS-46	-6.0	10.8	-0.680	-0.460	-5.48	+0.560	+0.400
JS-47	-6.0	10.8	-0.520	-0.440	-5.50	+0.560	+0.460
JS-52	-3.0	5.4	-0.610	-0.540	-5.03	+1.03	+0.840
JS-53	-3.0	5.4	-0.630	-0.550	-5.00	+0.990	+0.770
JS-54	-3.0	8.8	-0.730	-0.630	-5.60	+0.930	+0.570
JS-55	-3.0	8.8	-0.740	-0.650	-5.50	+0.940	+0.580
JS-56	-3.0	10.8	-0.530	-0.450	-5.57	+0.400	-0.280
JS-57	-3.0	10.7	-0.480	-0.430	-5.62	+0.340	-0.220
JS-58	-3.0	10.8	-0.470	-0.410	-5.58	+0.400	-0.120

TABLE 23 (Continued)

CHARACTERISTIC VALUES FROM CYCLIC POTENTIOKINETIC
POLARIZATION CURVES FOR THE Fe-16.9% Cr ALLOY
IN H₂-SATURATED SOLUTIONS[†]

Run No.	Log Chloride Ion Molarity (M)	pH	Zero Current Potential (VSCE)	Passivation Potential (VSCE)	Log Passivation Current Density (a/cm ²)	Rupture Potential (VSCE)	"Protection" Potential" (VSCE)
JS-38	-2.0	5.4	-0.640	-0.550	-5.14	+0.570	+0.070
JS-39	-2.0	5.4	-0.620	-0.520	-5.08	+0.650	-0.010
JS-40	-2.0	8.8	-0.490	-0.280	-5.33	+0.470	+0.510
JS-41	-2.0	8.9	-0.800	-0.650	-5.25	+0.380	+0.520
JS-42	-2.0	8.9	-0.790	-0.680	-5.30	+0.860	+0.500
JS-43	-2.0	10.7	-0.520	-0.460	-5.33	+0.160	-0.080
JS-44	-2.0	10.7	-0.540	-0.480	-5.40	+0.050	-0.390
JS-45	-2.0	10.8	-0.530	-0.470	-5.45	+0.360	-0.080
JS-28	-1.0	5.4	-0.660	-0.600	-4.87	+0.140	-0.080
JS-29	-1.0	5.4	-0.630	-0.570	-5.06	+0.130	-0.105
JS-32	-1.0	8.8	-0.710	-0.690	-5.81	+0.090	-0.280
JS-33	-1.0	8.8	-0.770	-0.660	-5.31	+0.090	-0.280
JS-36	-1.0	10.9	-0.540	-0.480	-5.30	+0.210	-0.060

TABLE 23 (Continued)

CHARACTERISTIC VALUES FROM CYCLIC POTENTIOKINETIC
POLARIZATION CURVES FOR THE Fe-16.9% Cr ALLOY
IN H₂-SATURATED SOLUTIONS*

Run No.	Log Chloride ion Molarity (M)	pH	Zero Current Potential (VSCE)	Passivation Potential (VSCE)	Log Passivation Current Density (a/cm ²)	Rupture Potential (VSCE)	"Protection" Potential" (VSCE)
JS-37	-1.0	10.9	-0.680	-0.500	-5.26	+0.200	+0.020
JS-59	0.0	4.9	-0.610	-0.530	-5.00	-0.040	-0.250
JS-60	0.0	4.9	-0.580	-0.520	-5.30	-0.060	-0.220
JS-61	0.0	8.2	-0.690	-0.630	-5.87	-0.060	-0.220

*Run numbers prefixed "JS" performed by J. S. Snodgrass [54].

+ [54]

APPENDIX 12

GALVANOSTATIC POLARIZATION EXPERIMENT DATA FOR THE Fe -
12% IN A 0.1 M Cl⁻, H₂-SATURATED SOLUTIONS
OF NOMINAL pH 10.1

TABLE 24

GALVANOSTATIC POLARIZATION EXPERIMENT DATA FOR THE Fe-12% Cr ALLOY IN A
0.1 M Cl^- , H_2 -SATURATED SOLUTION OF pH 10.1: RUN NO. KS-145
(SAMPLE AREA \approx 0.95 cm^2)

Q (coul)	E_{mix} at 0 min (V SCE)	E_{mix} at 1 min (V SCE)	E_{mix} at 10 min (V SCE)	E_{mix} at 20 min (V SCE)	E_{mix} at 30 min (V SCE)
10^{-2}	-0.316	-0.464	-0.465	-0.465	-0.465
10^{-1}	-0.338	-0.518	-0.524	-0.520	-0.512
10^0	-0.304	-0.554	-0.602	-0.610	-0.610
10^1	-0.380	-0.560	-0.617	-0.637	-0.646

TABLE 25

GALVANOSTATIC POLARIZATION EXPERIMENT DATA FOR THE Fe-12% Cr ALLOY IN A
0.1 M Cl^- , H_2 -SATURATED SOLUTION OF pH 10.0: RUN NO. KS-146
(SAMPLE AREA \approx 1.13 cm^2)

Q (coul)	E_{mix} at 0 min (V SCE)	E_{mix} at 1 min (V SCE)	E_{mix} at 10 min (V SCE)	E_{mix} at 20 min (V SCE)	E_{mix} at 30 min (V SCE)
10^{-2}	-0.260	-0.477	-0.472	-0.464	-0.458
10^{-1}	-0.278	-0.497	-0.520	-0.513	-0.502
10^0	-0.304	-0.563	-0.610	-0.617	-0.618
10^1	-0.360	-0.563	-0.622	-0.641	-0.652

TABLE 26

GALVANOSTATIC POLARIZATION EXPERIMENT DATA FOR THE Fe-12% Cr ALLOY IN A
 0.1 M Cl^- , H_2 -SATURATED SOLUTION OF pH 10.1: RUN NO. KS-148
 (SAMPLE AREA = 1.33 cm^2)

Q (coul)	E_{mix} at 0 min (v _{SCE})	E_{mix} at 15 sec (v _{SCE})	E_{mix} at 30 sec (v _{SCE})	E_{mix} at 45 sec (v _{SCE})	E_{mix} at 1 min (v _{SCE})
10^{-2}	-0.116	-0.440	-0.450	-0.456	-0.460
10^{-1}	-0.220	-0.496	-0.512	-0.524	-0.528
10^0	-0.280	-0.508	-0.536	-0.545	-0.550
10^1	-0.0300	-0.516	-0.543	-0.556	-0.562

TABLE 27

GALVANOSTATIC POLARIZATION EXPERIMENT DATA FOR THE Fe-12% Cr ALLOY IN A
 0.1 M Cl^- , H_2 -SATURATED SOLUTION OF pH 10.1: RUN NO. KS-149
 (SAMPLE AREA = 1.33 cm^2)

Q (coul)	E_{mix} at 0 min (v _{SCE})	E_{mix} at 15 sec (v _{SCE})	E_{mix} at 30 sec (v _{SCE})	E_{mix} at 45 sec (v _{SCE})	E_{mix} at 1 min (v _{SCE})
10^{-2}	-0.114	-0.442	-0.444	-0.444	-0.444
10^{-1}	-0.200	-0.468	-0.476	-0.478	-0.480
10^0	-0.220	-0.457	-0.516	-0.533	-0.542
10^1	-0.280	-0.500	-0.525	-0.536	-0.540

APPENDIX 13

GALVANOSTATIC SINGLE-PIT POLARIZATION EXPERIMENT DATA
FOR THE Fe - 12% Cr ALLOY IN 0.1 M Cl^- , H_2 -SATURATED
SOLUTIONS OF NOMINAL pH 10.2

TABLE 28

SINGLE-PIT GALVANOSTATIC POLARIZATION EXPERIMENT DATA FOR THE Fe-12% Cr ALLOY IN A
 0.1 M Cl^- , H_2 -SATURATED SOLUTION OF pH 10.2: RUN NO. KS-185 (SAMPLE AREA = 0.000883 cm^2)

Q/A (coul/cm^2)	E_{mix} at 0 min (VSCE)	E_{mix} at 30 sec (VSCE)	E_{mix} at 1 min (VSCE)	E_{mix} at 10 min (VSCE)	E_{mix} at 20 min (VSCE)	E_{mix} at 30 min (VSCE)
10^0	-0.378	-0.438	-0.418	-0.290	-0.250	-0.232
10^1	-0.470	-0.593	-0.602	-0.602	-0.603	-0.597
10^2	-0.450	-0.552	-0.747	-0.646	-0.658	-0.650
10^3	-0.520	-0.598	-0.596	-0.608	-0.653	-0.693

TABLE 29

SINGLE-PIT GALVANOSTATIC POLARIZATION EXPERIMENT DATA FOR THE Fe-12% Cr ALLOY IN A
 0.1 MCl⁻, H₂-SATURATED SOLUTION OF pH 10.1; RUN NO. KS-186 (SAMPLE AREA = 0.000883 cm²)

Q/A (coul/cm ²)	Emix at 0 min (VSCE)	Emix at 30 sec (VSCE)	Emix at 1 min (VSCE)	Emix at 10 min (VSCE)	Emix at 20 min (VSCE)	Emix at 30 min (VSCE)
10 ⁰	-0.320	-0.790	-0.806	-0.792	-0.774	-0.760
10 ¹	-0.450	-0.676	-0.812	-0.848	-0.827	-0.808
10 ²	-0.510	-0.602	-0.617	-0.878	-0.860	-0.840
10 ³	-0.550	-0.607	-0.592	-0.752	-0.710	-0.748

TABLE 30

SINGLE-PIT GALVANOSTATIC POLARIZATION EXPERIMENT DATA FOR THE Fe-12% Cr ALLOY IN A
 0.1MCl⁻, H₂-SATURATED SOLUTION OF pH 10.2: RUN NO. KS-187 (SAMPLE AREA = 0.000883 cm²)

Q/A (coul/cm ²)	E _{mix} at 0 min (VSCE)	E _{mix} at 30 sec (VSCE)	E _{mix} at 1 min (VSCE)	E _{mix} at 10 min (VSCE)	E _{mix} at 20 min (VSCE)	E _{mix} at 30 min (VSCE)
10 ⁰	-0.330	-0.778	-0.776	-0.698	-0.654	-0.615
10 ¹	-0.384	-0.740	-0.848	-0.778	-0.730	-0.697
10 ²	-0.460	-0.606	-0.626	-0.852	-0.812	-0.798
10 ³	-0.540	-0.580	-0.580	-0.636	-0.693	-0.748

APPENDIX 14

ARTIFICIAL OCCLUDED CELL DATA FOR THE Fe - 12% Cr ALLOY
AND ARMCO Fe IN SOLUTIONS INITIALLY 0.1 M Cl^-

TABLE 31

ARTIFICIAL OCCLUDED CELL DATA FOR THE Fe-12% Cr ALLOY AND ARMCO Fe IN SOLUTIONS INITIALLY 0.1 MCl⁻

Run No.	Alloy	pH of Initial Solution	Purging Gas (Bulk Solution)	Applied Potential (VSCE)	Elapsed Time (hr)	Occluded Cell Potential (v SCE)	Occluded Cell pH	Occluded Cell Current Density (ma/cm ²)
KS-102	Fe-12% Cr	8.4	H ₂	Free Corr. +0.150	0	-0.336	8.38	~0
					1.33	-0.178	7.28	+0.50
					4.50	-0.266	6.00	+0.67
KS-103	Fe-12% Cr	8.6	H ₂	Free Corr. +0.150	25.50	-0.502	2.75	+0.67
					0	-0.364	8.58	~0
					1.17	-0.089	7.60	+0.33
					2.17	-0.103	7.20	+0.42
					7.17	-0.207	6.22	+0.58
KS-104	Fe-12% Cr	8.5	O ₂	Free Corr. 0.000	23.17	-0.455	2.90	+1.33
					28.25	-0.473	2.77	+1.33
					42.75	-0.492	2.75	+1.25
					0	-0.369	8.50	~0
					2.67	-0.186	6.75	+0.29
KS-105	Fe-12% Cr	8.5	O ₂	Free Corr. 0.000	23.67	-0.460	3.18	+0.96
					27.00	-0.471	2.87	+1.03
					44.50	-0.482	2.65	+1.26
					0	-0.148	8.49	~0
					5.50	-0.001	8.49	+0.023
					19.00	-0.021	6.35	+0.078
					43.67	-0.019	5.98	+0.066
					71.83	-0.022	5.15	+0.061
					101.67	-0.144	4.67	+0.46
					118.83	-0.363	3.24	+0.91
					137.67	-0.451	2.77	+1.66

TABLE 31 (Continued)
 ARTIFICIAL OCCLUDED CELL DATA FOR THE Fe-12% Cr ALLOY AND ARMCO Fe IN SOLUTIONS INITIALLY 0.1M CL⁻

Run No.	Alloy	pH of Initial Solution	Purging Gas (Bulk Solution)	Applied Potential (VSCE)	Elapsed Time (hr)	Occluded Cell Potential (VSCE)	Occluded Cell pH	Occluded Cell Current Density (ma/cm ²)
KS-108	Fe-12% Cr	10.3	O ₂	Free Corr. 0.000	148.50	-0.440	2.68	+2.39
					165.17	-0.464	2.45	+2.68
					236.50	-	2.87	0
					0	-0.170	10.26	~0
					5.92	-0.195	3.72	+0.68
					22.00	-0.365	3.22	+0.60
KS-113	Fe-12% Cr	10.0	O ₂	Free Corr. 0.000	32.00	-0.465	3.00	+0.94
					43.33	-0.468	2.87	+1.02
					55.00	-0.465	2.70	+1.38
					68.25	-0.467	2.60	+1.64
					78.42	-0.470	2.60	+3.76
					164.33	-	3.29	0
KS-123	Fe-12% Cr	9.6	O ₂	Free Corr. 0.000	0	-0.208	10.02	~0
					7.00	-0.160	3.97	+0.97
					22.50	-0.447	3.33	+0.40
					295.17	-	3.98	0
					0	-0.201	4.72	~0
					4.50	-0.220	3.87	+0.73
KS-123	Fe-12% Cr	9.6	O ₂	Free Corr. 0.000	20.25	-0.390	2.98	+1.60
					27.42	-0.426	2.81	+1.83
					44.50	-0.458	2.65	+2.10
					68.83	-	2.83	0

TABLE 31 (Continued)

ARTIFICIAL OCCLUDED CELL DATA FOR THE Fe-12% Cr ALLOY AND ARMCO Fe IN SOLUTIONS INITIALLY 0.1M Cl⁻

Run No.	Alloy	pH of Initial Solution	Purging Gas (Bulk Solution)	Applied Potential (VSCE)	Elapsed Time (hr)	Occluded Cell Potential (VSCE)	Occluded Cell pH	Occluded Cell Current Density (ma/cm ²)
KS-125	Armco Fe	5.1	O ₂	Free Corr. 0.000	0	-0.342	5.08	~0
					2.33	-0.384	5.00	+1.52
					17.67	-0.493	4.27	+2.32
					24.17	-0.512	4.18	+2.36
					43.50	-0.528	4.12	+2.40
KS-126	Armco Fe	9.9	O ₂	Free Corr. 0.000	0	-0.372	9.90	~0
					0.33	-0.242	9.85	+1.31
					4.83	-0.396	4.60	+2.14
					18.83	-0.469	4.03	+2.93
					29.00	-0.471	3.96	+3.04
					-	3.86	-	
KS-120	Fe-12% Cr	10.0	O ₂	Free Corr. 0.000	0	-0.382	4.36	~0
					0.83	-0.305	4.15	+0.50
					14.25	-0.334	3.18	+0.44
					25.25	-0.404	3.13	+0.47
					40.00	-0.442	2.81	+0.59
					-0.444	2.77	+0.44	
					-0.446	2.75	+0.37	
				-0.570	185.00	-	3.31	0

APPENDIX 15

ANALYSES OF FINAL ARTIFICIAL OCCLUDED CELL SOLUTIONS
FOR THE Fe - 12% Cr ALLOY AND ARMCO Fe
IN SOLUTIONS INITIALLY 0.1 M Cl^-

TABLE 32

ANALYSES OF FINAL ARTIFICIAL OCCLUDED CELL SOLUTIONS FOR THE Fe-12% Cr ALLOY AND ARMCO Fe IN SOLUTIONS INITIALLY 0.1 MCl⁻

Run No.	[Fe] (M)	[Cr] (M)	Log [Cr] (M)	[Cl] (M)
KS-102	0.115	0.0129	-1.89	0.341
KS-103	0.222	0.0273	-1.56	0.553
KS-104	0.210	0.0273	-1.56	0.247
KS-105	0.406	0.0538	-1.27	0.664
KS-108	0.240	0.0281	-1.55	0.559
KS-113	0.145	0.0144	-1.84	0.327
KS-120	0.158	0.0192	-1.72	0.393
KS-123	0.150	0.0166	-1.78	0.377
KS-125	0.204	Armco Fe	-	0.499
KS-126	0.401	Armco Fe	-	0.834

APPENDIX 16

CARBIDE CALCULATIONS

The chemical analysis given by the Naval Research Laboratories for the Fe - 12% Cr alloy was nominally 12.0% Cr, 0.15% C. Minor alloying elements will be neglected for the calculations made herein and for simplicity the balance of the alloy will be assumed to be Fe (87.85%). The solid line in Figure 48 was calculated, ignoring the presence of carbides, as follows:

assuming 100 gm of alloy,

$$12.0 \text{ gm Cr} \div (12/51.996)(6.023 \times 10^{23}) \text{ Cr atoms} \\ = 1.390 \times 10^{23} \text{ Cr atoms}$$

$$0.15 \text{ gm C} \div (0.15/12.011)(6.023 \times 10^{23}) \text{ C atoms} \\ = 1.390 \times 10^{23} \text{ C atoms}$$

$$87.85 \text{ gm Fe} \div (87.85/55.847)(6.023 \times 10^{23}) \text{ Fe atoms} \\ = 9.474 \times 10^{23} \text{ Fe atoms}$$

$$[\text{Fe}]/[\text{Cr}] = (9.474 \times 10^{23}) / (1.390 \times 10^{23}) \\ = 6.82$$

$$\therefore [\text{Fe}] = (6.82)[\text{Cr}]$$

The dashed line in Figure 48 was calculated, taking into account the presence of carbides, making the following assumptions:

1. All C above about 0.02% will be present in the form of carbides [1, p. 59].
2. The predominate carbide for the Fe - 12% Cr alloy (and for the Fe - 16.9% Cr and Fe - 24.9% Cr alloys) will be $(\text{Cr}, \text{Fe})_{23}\text{C}_6$, containing about 25% Fe [192, pp. 65 and 75].
3. The $(\text{Cr}, \text{Fe})_{23}\text{C}_6$ will not undergo dissolution [1, pp. 59-60].

An experiment was performed which suggests that the above assumptions may be reasonable. An Fe - 12% Cr sample was potentiostated at $-0.365 v_{SCE}$ ($-0.115 v_{SHE}$) for approximately 45 hr in a $0.25 M FeCl_2 \cdot 4H_2O + 0.034 M CrCl_3 \cdot 6H_2O$ solution (of the order of the concentrations of the artificial occluded cell solutions). The initial and final applied current densities were $+1.4$ and $+2.4$ ma/cm^2 , respectively. After the run, the corroded sample was placed immediately in an X-ray diffractometer. The resulting peaks were identified as being due to Fe-Cr and $Cr_{23}C_6$.

Assuming 100 gm of alloy,

$$\begin{aligned} 12.0 \text{ gm Cr} &\Rightarrow (12/51.996)(6.023 \times 10^{23}) \text{ Cr atoms} \\ &= 1.390 \times 10^{23} \text{ Cr atoms} \end{aligned}$$

$$\begin{aligned} 0.13 \text{ gm C net } (0.15 - 0.02) &\Rightarrow (0.13/12.011)(6.023 \times 10^{23}) \text{ C atoms} \\ &= 0.065 \times 10^{23} \text{ C atoms} \end{aligned}$$

$$\begin{aligned} 87.85 \text{ gm Fe} &\Rightarrow (87.85/55.847)(6.023 \times 10^{23}) \text{ Fe atoms} \\ &= 9.474 \times 10^{23} \text{ Fe atoms} \end{aligned}$$

$$\begin{aligned} (Cr, Fe)_{23}C_6 &\Rightarrow (\text{no. metal atoms})/(\text{no. C atoms}) = \frac{23}{6} \\ &= 3.833 \end{aligned}$$

$$\text{no. Cr atoms tied up} = (0.065 \times 10^{23})(3.833)(0.75) = 0.187 \times 10^{23}$$

$$\text{leaving } (1.390 - 0.187) \times 10^{23} = 1.203 \times 10^{23} \text{ Cr atoms}$$

$$\text{no. Fe atoms tied up} = (0.065 \times 10^{23})(3.833)(0.25) = 0.062 \times 10^{23}$$

$$\text{leaving } (9.474 - 0.062) \times 10^{23} = 9.412 \times 10^{23} \text{ Fe atoms}$$

$$\begin{aligned} [Fe]/[Cr] &= (9.412 \times 10^{23})/(1.203 \times 10^{23}) \\ &= 7.82 \end{aligned}$$

$$\therefore [Fe] = 7.82 [Cr]$$

Similar calculations were carried out for the Fe - 16.9% Cr and Fe - 24.9% Cr alloys (making the same assumptions, but taking into account minor alloying elements). The results are

$$\text{Fe} - 16.9\% \text{ Cr} \quad [\text{Fe}]/[\text{Cr}] = 4.99$$

$$\text{Fe} - 24.9\% \text{ Cr} \quad [\text{Fe}]/[\text{Cr}] = 2.84.$$

APPENDIX 17

CALCULATED EQUILIBRIUM POTENTIAL VS. pH (POURBAIX) DIAGRAMS,
THERMODYNAMIC DATA AND PERTINENT EQUATIONS

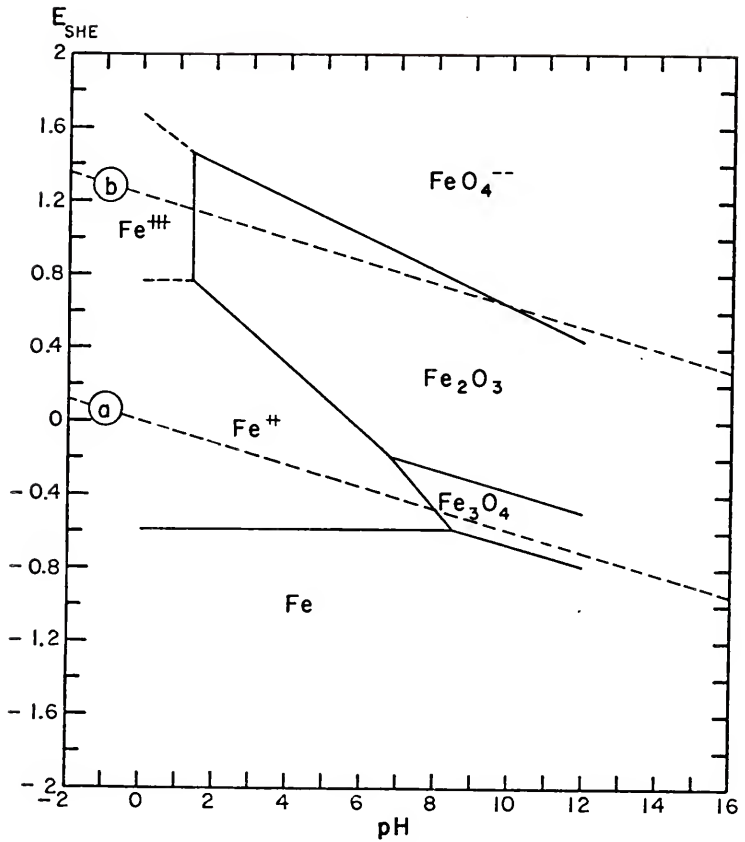


Figure 139. Calculated equilibrium potential vs. pH (Pourbaix) diagram for the Fe-H₂O system. The activities of all dissolved species were taken to be 10^{-6} .

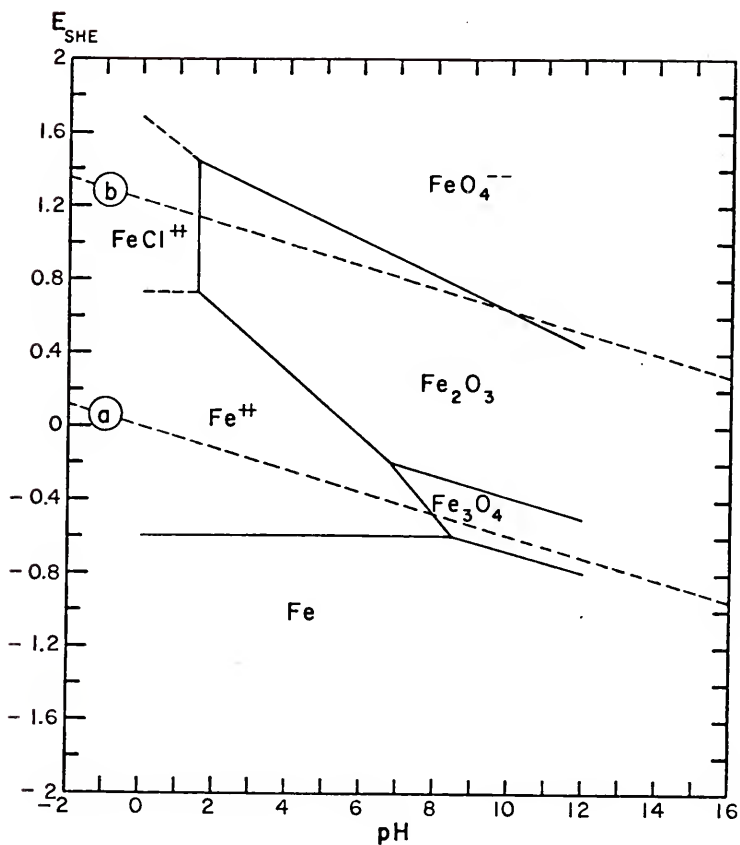


Figure 140. Calculated equilibrium potential vs. pH (Pourbaix) diagram for the Fe-Cl⁻-H₂O system. The activity of Cl⁻ was taken to be 0.1 and the activities of all other dissolved species were taken to be 10⁻⁶.

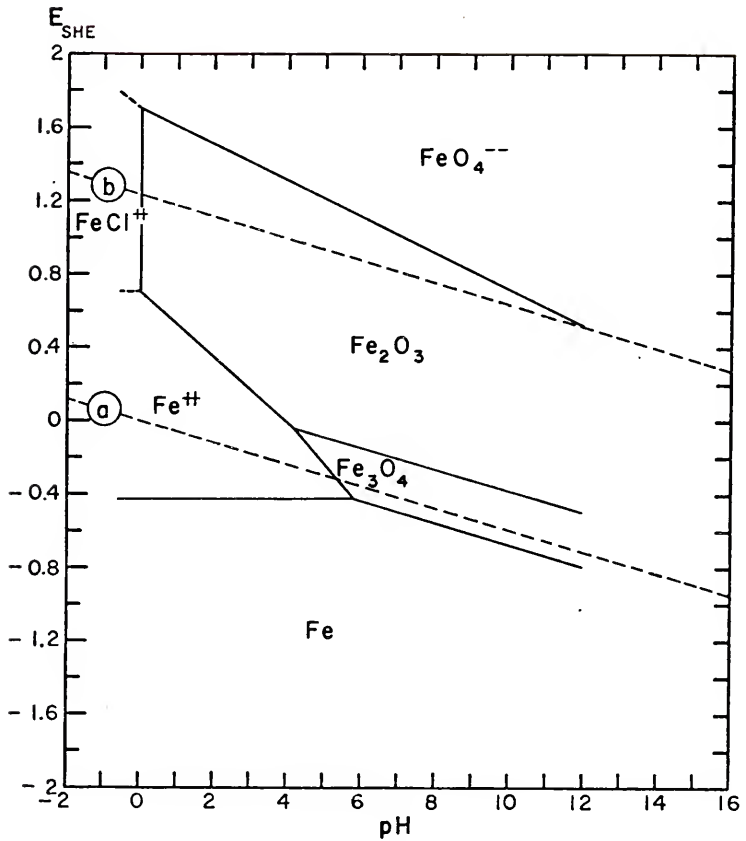


Figure 141. Specially calculated equilibrium potential vs. pH (Pourbaix) diagram for the Fe-Cl⁻-H₂O system. The activity of Cl⁻ was taken to be 0.373 and the activities of all other dissolved species were taken to be 0.156.

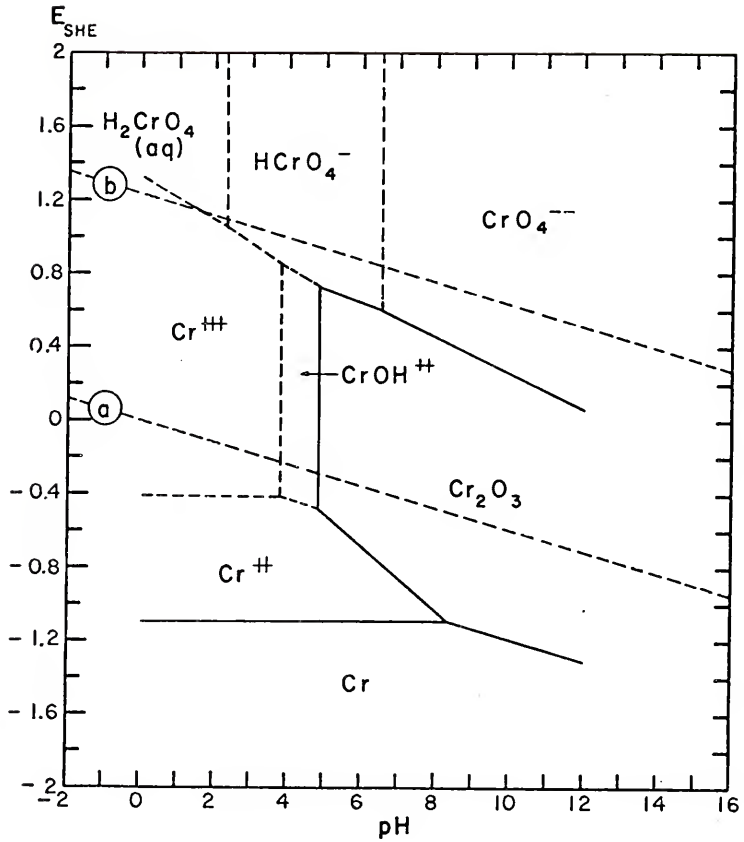


Figure 142. Calculated equilibrium potential vs. pH (Pourbaix) diagram for the Cr-H₂O system. The activities of all dissolved species were taken to be 10^{-6} .

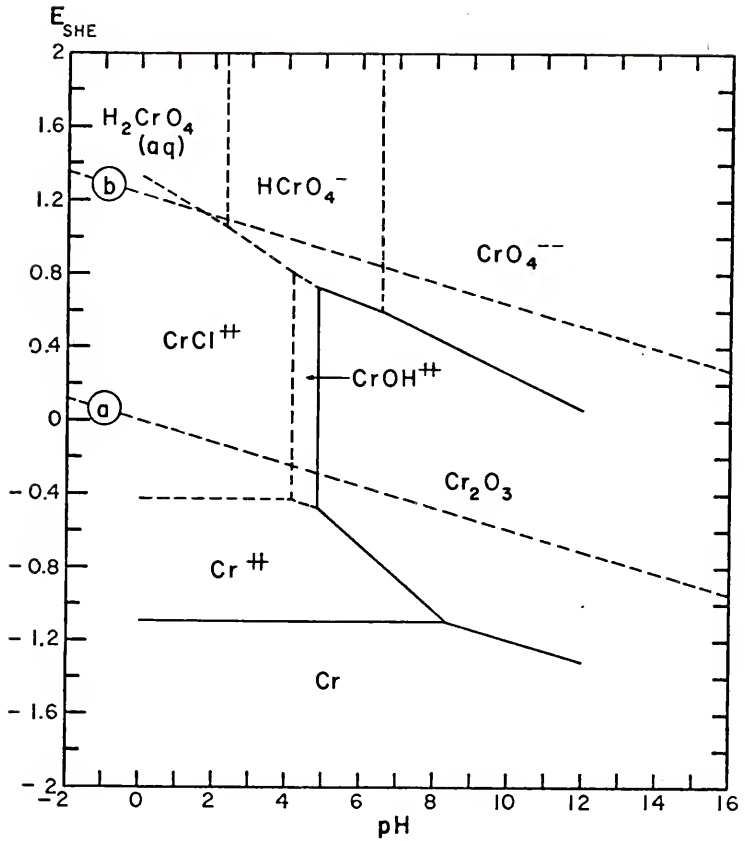


Figure 143. Calculated equilibrium potential vs. pH (Pourbaix) diagram for the Cr-Cl⁻-H₂O system. The activity of Cl⁻ was taken to be 0.1 and the activities of all other dissolved species were taken to be 10⁻⁶.

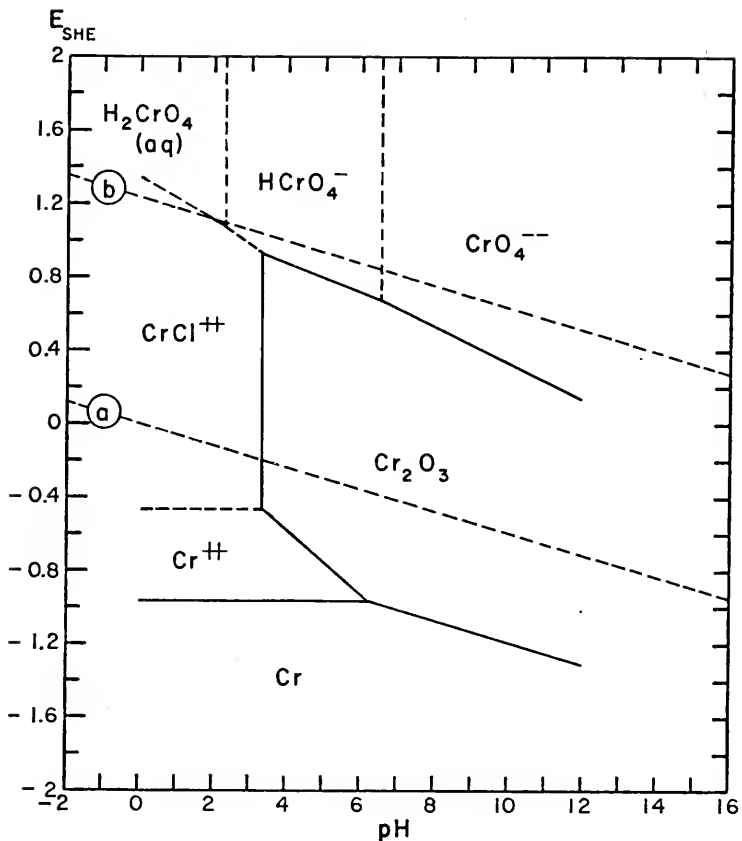


Figure 144. Specially calculated equilibrium potential vs. pH (Pourbaix) diagram for the Cr-Cl⁻-H₂O system.

The activity of Cl⁻ was taken to be 0.373 and the activities of all other dissolved species were taken to be 0.02.

TABLE 33

FREE ENERGY OF FORMATION DATA FOR
Fe-CONTAINING SPECIES CONSIDERED

<u>Species</u>	<u>Free Energy of Formation (Cal/mole)</u>	<u>Source</u>
Fe	0	[193]
Fe(OH) ₂	-116,300	[193]
Fe ₃ O ₄	-242,700	[193]
Fe ₂ O ₃	-177,400	[193]
Fe ⁺⁺	- 18,850	[193]
Fe ⁺⁺⁺	- 1,100	[193]
FeOH ⁺	- 62,470	[179]*
FeOH ⁺⁺	- 54,830	[193]
Fe(OH) ₂ ⁺	-106,470	[176]*
HFeO ₂ ⁻	- 90,300	[193]
FeO ₄ ⁻⁻	-111,685	[171]
Fe ₂ (OH) ₂ ⁺⁺⁺⁺	-11,670	[176]*
Fe ₄ (OH) ₃ ⁹⁺	-166,450	[176]*
FeCl ⁺	- 50,220	est. from FeCl ₂
FeCl ₂ (aq)	- 81,590	[193]
FeCl ₂	- 72,260	[193]
FeCl ⁺⁺	- 34,490	[176]*
FeCl ₂ ⁺	- 66,700	[193]
FeCl ₃ (aq)	- 95,200	[193]
FeCl ₃	- 79,840	[193]

* Calculated from reference data

TABLE 34

FREE ENERGY OF FORMATION DATA FOR
Cr-CONTAINING SPECIES CONSIDERED

<u>Species</u>	<u>Free Energy of Formation (Cal/mole)</u>	<u>Source</u>
Cr	0	-
Cr(OH) ₂	-140,500	[171]
Cr ₂ O ₃	-252,900	[193]
Cr(OH) ₄	-242,380	[171]
CrO ₃	-120,000	[171]
Cr ⁺⁺	- 42,100	[171]
Cr ⁺⁺⁺	- 51,500	[171]
CrOH ⁺⁺	-103,090	[176]*
Cr(OH) ₂ ⁺	-151,200	[171]
CrO ₂ ⁻	-128,090	[171]
CrO ₃ ⁻⁻⁻	-144,220	[171]
H ₂ CrO ₄ (aq)	-185,920	[171]
HCrO ₄ ⁻	-182,800	[193]
CrO ₄ ⁻⁻	-173,960	[193]
Cr ₂ O ₇ ⁻⁻	-311,000	[193]
CrCl ₂	- 85,100	[193]
CrCl ⁺⁺	- 84,770	[176]*
CrCl ₂ ⁺	-116,240	[176]*
CrCl ₃	-116,200	[193]
CrO ₂ Cl(aq)	-122,100	[193]

* Calculated from reference data

TABLE 35

PERTINENT NERNST EQUATIONS FOR THE Fe-H₂O SYSTEM POTENTIAL VS. pH
(POURBAIX) DIAGRAM (ACTIVITIES OF ALL DISSOLVED SPECIES TAKEN TO BE 10⁻⁶)

Species	Nernst Equation
Fe/Fe ₃ O ₄	E = -0.086 - 0.0591 pH
Fe/Fe ⁺⁺	E = -0.586
Fe ₃ O ₄ /Fe ₂ O ₃	E = 0.214 - 0.0591 pH
Fe ₃ O ₄ /Fe ⁺⁺	E = 1.412 - 0.2364 pH
Fe ₂ O ₃ /Fe ⁺⁺	E = 1.013 - 0.1773 pH
Fe ₂ O ₃ /Fe ⁺⁺⁺	pH = 1.37
Fe ₂ O ₃ /FeO ₄ ⁻⁻	E = 1.598 - 0.0985 pH
Fe ⁺⁺ /Fe ⁺⁺⁺	E = 0.770
Fe ⁺⁺⁺ /FeO ₄ ⁻⁻	E = 1.679 - 0.1576 pH

TABLE 36

PERTINENT NERNST EQUATIONS FOR THE $\text{Fe}-\text{Cl}^- - \text{H}_2\text{O}$ SYSTEM POTENTIAL
 VS. pH (POURBAIX) DIAGRAM (ACTIVITY OF Cl^- TAKEN TO BE 0.1
 AND ACTIVITIES OF ALL OTHER DISSOLVED SPECIES TAKEN TO BE 10^{-6})

Species	Nernst Equation
$\text{Fe}/\text{Fe}_3\text{O}_4$	$E = -0.086 - 0.0591 \text{ pH}$
Fe/Fe^{++}	$E = -0.586$
$\text{Fe}_3\text{O}_4/\text{Fe}_2\text{O}_3$	$E = 0.214 - 0.0591 \text{ pH}$
$\text{Fe}_3\text{O}_4/\text{Fe}^{++}$	$E = 1.412 - 0.2364 \text{ pH}$
$\text{Fe}_2\text{O}_3/\text{Fe}^{++}$	$E = 1.013 - 0.1773 \text{ pH}$
$\text{Fe}_2\text{O}_3/\text{FeCl}^{++}$	$\text{pH} = 1.53$
$\text{Fe}_2\text{O}_3/\text{FeO}_4^{--}$	$E = 1.598 - 0.0985$
$\text{Fe}^{++}/\text{FeCl}^{++}$	$E = 0.741$
$\text{FeO}_4^{--}/\text{FeCl}^{++}$	$E = 1.689 - 0.1576 \text{ pH}$

TABLE 37

PERTINENT NERNST EQUATIONS FOR THE SPECIAL $\text{Fe}-\text{Cl}^- - \text{H}_2\text{O}$ SYSTEM POTENTIAL VS. pH (POURBAIX) DIAGRAM (ACTIVITY OF Cl^- TAKEN TO BE 0.373 AND ACTIVITIES OF ALL OTHER DISSOLVED SPECIES TAKEN TO BE 0.156)

Species	Nernst Equation
$\text{Fe}/\text{Fe}_3\text{O}_4$	$E = -0.086 - 0.0591 \text{ pH}$
Fe/Fe^{++}	$E = -0.432$
$\text{Fe}_3\text{O}_4/\text{Fe}_2\text{O}_3$	$E = 0.214 - 0.0591 \text{ pH}$
$\text{Fe}_3\text{O}_4/\text{Fe}^{++}$	$E = 0.952 - 0.2364 \text{ pH}$
$\text{Fe}_2\text{O}_3/\text{Fe}^{++}$	$E = 0.706 - 0.1773 \text{ pH}$
$\text{Fe}_2\text{O}_3/\text{FeCl}^{++}$	$\text{pH} = -0.01$
$\text{Fe}_2\text{O}_3/\text{FeO}_4^{--}$	$E = 1.700 - 0.0985 \text{ pH}$
$\text{Fe}^{++}/\text{FeCl}^{++}$	$E = 0.708$
$\text{FeO}_4^{--}/\text{FeCl}^{++}$	$E = 1.700 - 0.1576 \text{ pH}$

TABLE 38

PERTINENT NERNST EQUATIONS FOR THE Fe-H₂O SYSTEM POTENTIAL VS. pH
(POURBAIX) DIAGRAM (ACTIVITIES OF ALL DISSOLVED SPECIES TAKEN TO BE 10⁻⁶)

Species	Nernst Equation
Cr/Cr ₂ O ₃	E = -0.599 - 0.0591 pH
Cr/Cr ⁺⁺	E = -1.090
Cr ₂ O ₃ /Cr ⁺⁺	E = 0.384 - 0.1773 pH
Cr ₂ O ₃ /CrOH ⁺⁺	pH = 4.83
Cr ₂ O ₃ /HCrO ₄ ⁻	E = 1.116 - 0.0788 pH
Cr ₂ O ₃ /CrO ₄ ⁻⁻	E = 1.244 - 0.0985 pH
Cr ⁺⁺ /Cr ⁺⁺⁺	E = -0.407
Cr ⁺⁺ /CrOH ⁺⁺	E = -0.186 - 0.0591 pH
Cr ⁺⁺⁺ /CrOH ⁺⁺	pH = 3.74
Cr ⁺⁺⁺ /H ₂ CrO ₄ (aq)	E = 1.335 - 0.1182 pH
Cr ⁺⁺⁺ /HCrO ₄ ⁻	E = 1.380 - 0.1379 pH
CrOH ⁺⁺ /HCrO ₄ ⁻	E = 1.306 - 0.1182 pH
H ₂ CrO ₄ (aq)/HCrO ₄ ⁻	pH = 2.29
HCrO ₄ ⁻ /CrO ₄ ⁻⁻	pH = 6.48

TABLE 39

PERTINENT NERNST EQUATIONS FOR THE Fe-Cl⁻-H₂O SYSTEM POTENTIAL VS. pH (POURBAIX) DIAGRAM (ACTIVITY OF Cl⁻ TAKEN TO BE 0.1 AND ACTIVITIES OF ALL OTHER DISSOLVED SPECIES TAKEN TO BE 10⁻⁶)

Species	Nernst Equation
Cr/Cr ₂ O ₃	E = -0.599 -0.0591 pH
Cr/Cr ⁺⁺	E = -1.090
Cr ₂ O ₃ /Cr ⁺⁺	E = 0.384 -0.1773 pH
Cr ₂ O ₃ /CrOH ⁺⁺	pH = 4.83
Cr ₂ O ₃ /HCrO ₄ ⁻	E = 1.116 -0.0788 pH
Cr ₂ O ₃ /CrO ₄ ⁻⁻	E = 1.244 -0.0985 pH
Cr ⁺⁺ /CrCl ⁺⁺	E = -0.431
Cr ⁺⁺ /CrOH ⁺⁺	E = -0.186 -0.0591 pH
CrOH ⁺⁺ /CrCl ⁺⁺	pH = 4.13
H ₂ CrO ₄ (aq)/CrCl ⁺⁺	E = 1.342 -0.1182 pH
HCrO ₄ ⁻ /CrCl ⁺⁺	E = 1.388 -0.1379 pH
CrOH ⁺⁺ /HCrO ₄ ⁻	E = 1.306 -0.1182 pH
H ₂ CrO ₄ (aq)/HCrO ₄ ⁻	pH = 2.29
HCrO ₄ ⁻ /CrO ₄ ⁻⁻	pH = 6.48

TABLE 40
 PERTINENT NERNST EQUATIONS FOR THE SPECIAL Cr-Cl⁻-H₂O SYSTEM POTENTIAL
 VS. pH (POURBAIX) DIAGRAM (ACTIVITY OF Cl⁻ TAKEN TO BE 0.373 AND ACTIVITIES
 OF ALL OTHER DISSOLVED SPECIES TAKEN TO BE 0.02)

Species	Nernst Equation
Cr/Cr ₂ O ₃	E = -0.599-0.0591 pH
Cr/Cr ⁺⁺	E = -0.963
Cr ₂ O ₃ /Cr ⁺⁺	E = 0.130 -0.1773 pH
Cr ₂ O ₃ /HCrO ₄ ⁻	E = 1.200 -0.0788 pH
Cr ₂ O ₃ /CrO ₄ ⁻⁻	E = 1.328 -0.0985
Cr ₂ O ₃ /CrCl ⁺⁺	pH = 3.35
Cr ⁺⁺ /CrCl ⁺⁺	E = -0.465
H ₂ CrO ₄ (aq)/HCrO ₄ ⁻	pH = 2.29
H ₂ CrO ₄ (aq)/CrCl ⁺⁺	E = 1.354 -0.1182 pH
HCrO ₄ ⁻ /CrO ₄ ⁻⁻	pH = 6.48
HCrO ₄ ⁻ /CrCl ⁺⁺	E = 1.399 -0.1379 pH

APPENDIX 18

HYDROLYSIS CALCULATIONS AND RESULTS

FORTRAN IV COMPUTER PROGRAMS

HYD1E

```

C1=1.1175E-14
1  READ, FMAX,C2,C3,C4,N
2  PHMIN=-(1.0/2.0)*ALOG10(C1+C2*FMAX)
3  EMAX=C3+C4*ALOG10(FMAX)
4  PRINT, FMAX,PHMIN,EMAX,C2,C3,C4,N
5  DO 9I=1,16
6  PH=-(1.0/2.0)*ALOG10(C1+C2*10.0**(I-1))
7  IF(PH-6.97587)8,8,1
8  E=C3+C4*(1-I)
9  PRINT, 1-I,PH,E,C2,C3,C4,N
10 GO TO 1

```

HYD2A

```

C1=1.1175E-14
1  READ, FMAX,C2,C3,C4,N
2  PHMIN=-(1.0/3.0)*(ALOG10(C2)+2.0*ALOG10(FMAX))-0.10
3  EMAX=C3+C4*ALOG10(FMAX)
4  PRINT, FMAX,PHMIN,EMAX,C2,C3,C4,N
5  DO 9I=1,16
6  PH=-(1.0/3.0)*(ALOG10(C2)+2.0*ALOG10(10.0**(I-1)))-0.10
7  IF(PH-6.97588)8,8,1
8  E=C3+C4*(1-I)
9  PRINT, 1-I,PH,E,C2,C3,C4,N
10 GO TO 1

```

HYD3A

```

C1=1.1175E-14
1  READ, FMAX,C2,C3,C4,N
2  PHMIN=-(1.0/3.0)*(ALOG10(C2)+1.0*ALOG10(FMAX))-0.10
3  EMAX=C3+C4*ALOG10(FMAX)
4  PRINT, FMAX,PHMIN,EMAX,C2,C3,C4,N
5  DO 9I=1,16
6  PH=-(1.0/3.0)*(ALOG10(C2)+1.0*ALOG10(10.0**(I-1)))-0.10
7  IF(PH-6.97588)8,8,1
8  E=C3+C4*(1-I)
9  PRINT, 1-I,PH,E,C2,C3,C4,N
10 GO TO 1

```

HYD4A

```
C1=1.1175E-14
1  READ, FMAX,C2,C3,C4,N
2  PHMIN=- (1.0/4.0)*(ALOG10(C2)+4.0*ALOG10(FMAX))-0.12
3  EMAX=C3+C4*ALOG10(FMAX)
4  PRINT, FMAX,PHMIN,EMAX,C2,C3,C4,N
5  DO 9I=1,16
6  PH=- (1.0/4.0)*(ALOG10(C2)+4.0*ALOG10(10.0**(1-I)))-0.12
7  IF (PH-6.97588)8,8,1
8  E=C3+C4*(1-I)
9  PRINT, 1-I,PH,E,C2,C3,C4,N
10 GO TO 1
```

TABLE 41

DATA USED FOR HYD1E, HYD2E, HYD3A AND HYD4A COMPUTER PROGRAMS

FMAX = saturated solution
 C2 = hydrolysis equilibrium constant
 C3 = intercept of Nernst equation
 C4 = slope of Nernst equation

<u>Hydrolysis Product</u>	<u>FMAX (M)</u>	<u>C2</u>	<u>C3 (v SHE)</u>	<u>C4 (v)</u>	<u>Program Type</u>
FeOH^+	4.463	2.630 E-10	-0.440	+0.0295	HYD1E
FeOH^{++}	5.497	6.761 E-3	-0.037	+0.0197	HYD1E
$\text{Fe}(\text{OH})_2^+$	5.497	1.349 E-6	-0.037	+0.0197	HYD3A
$\{\text{Fe}_2(\text{OH})_2\}^{4+}$	5.497	1.380 E-3	-0.037	+0.0197	HYD2A
$\{\text{Fe}_4(\text{OH})_3\}^{9+}$	5.497	1.349 E-6	-0.037	+0.0197	HYD4A
CrOH^{++}	9.050	1.820 E-4	-0.744	+0.0197	HYD1E
$\text{Cr}(\text{OH})_2^+$	9.050	1.092 E-10	-0.744	+0.0197	HYD3A
NiOH^+	4.409	1.778 E-10	-0.250	+0.0295	HYD1E
CrOH^{++} (Fe - 12% Cr alloy)	0.570	1.820 E-4	-0.414	+0.0295	HYD1E

TABLE 42
HYDROLYSIS CALCULATION RESULTS

Log Metal Ion Concentration (M)	pH	Potential (v SHE)	Log Metal Ion Concentration (M)	pH	Potential (v SHE)
FeOH ⁺ : PHMIN = 4.46, EMAX = -0.421					
0	4.79	-0.440	0	1.86	-0.037
- 1	5.29	-0.470	- 1	2.20	-0.057
- 2	5.79	-0.500	- 2	2.52	-0.076
- 3	6.29	-0.528	- 3	2.86	-0.096
- 4	6.71	-0.558	- 4	3.19	-0.116
- 5	6.93	-0.587	- 5	3.52	-0.136
- 6	6.97	-0.617	- 6	3.86	-0.155
FeOH ⁺⁺ : PHMIN = 0.71, EMAX = -0.022					
0	1.08	-0.037	- 9	4.86	-0.215
- 1	1.58	-0.056	-10	5.19	-0.234
- 2	2.08	-0.076	-11	5.52	-0.254
- 3	2.58	-0.096	-12	5.86	-0.273
- 4	3.08	-0.116	-13	6.19	-0.293
- 5	3.58	-0.136	-14	6.52	-0.313
- 6	4.08	-0.155	-15	6.86	-0.332
- 7	4.58	-0.174			
- 8	5.08	-0.194			
- 9	5.58	-0.214			
-10	6.08	-0.234			
-11	6.55	-0.254			
-12	6.87	-0.274			
-13	6.96	-0.294			

TABLE 42 (Continued)

Log Metal Ion Concentration (M)	pH	Potential (v SHE)	Log Metal Ion Concentration (M)	pH	Potential (v SHE)
$\{\text{Fe}_2(\text{OH})_2\}^{4+}$	PHMIN = 0.36, EMAX = -0.022		CrOH^{++}	PHMIN = 1.39, EMAX = -0.725	
0	0.85	-0.037	0	1.87	-0.744
- 1	1.52	-0.057	- 1	2.37	-0.764
- 2	2.19	-0.076	- 2	2.87	-0.783
- 3	2.85	-0.096	- 3	3.37	-0.803
- 4	3.52	-0.116	- 4	3.87	-0.823
- 5	4.19	-0.136	- 5	4.37	-0.842
- 6	4.85	-0.155	- 6	4.87	-0.862
- 7	5.52	-0.175	- 7	5.37	-0.882
- 8	6.19	-0.195	- 8	5.87	-0.902
- 9	6.85	-0.214	- 9	6.36	-0.921
			-10	6.77	-0.941
			-11	6.94	-0.961
			-12	6.97	-0.980
$\{\text{Fe}_4(\text{OH})_3\}^{9+}$	PHMIN = 0.61, EMAX = -0.022				
0	1.35	-0.037			
- 1	2.35	-0.057			
- 2	3.35	-0.076			
- 3	4.35	-0.096			
- 4	5.35	-0.116			
- 5	6.35	-0.136			

TABLE 42 (Continued)

Log Metal Ion Concentration (M)	pH	Potential (v SHE)	Log Metal Ion Concentration (M)	pH	Potential (v SHE)
Cr(OH)_2^+ : PHMIN = 2.90, EMAX = -0.725					
0	3.22	-0.744	0	1.87	-0.414
-1	3.55	-0.764	-1	2.37	-0.444
-2	3.89	-0.783	-2	2.87	-0.473
-3	4.22	-0.803	-3	3.37	-0.502
-4	4.55	-0.823	-4	3.87	-0.532
-5	4.89	-0.842	-5	4.37	-0.561
-6	5.22	-0.862	-6	4.87	-0.591
-7	5.55	-0.882	-7	5.37	-0.620
-8	5.89	-0.902	-8	5.87	-0.650
-9	6.22	-0.921	-9	6.36	-0.680
-10	6.55	-0.941	-10	6.77	-0.709
NiOH^+ : PHMIN = 4.55, EMAX = -0.231					
0	4.88	-0.250	-11	6.94	-0.738
-1	5.37	-0.280	-12	6.97	-0.768
-2	5.87	-0.309			
-3	6.36	-0.338			
-4	6.77	-0.368			
-5	6.94	-0.398			
-6	6.97	-0.427			

CrOH^{++} : PHMIN = 1.99, EMAX = -0.421
(Fe - 12% Cr Alloy)

APPENDIX 19

CYCLIC POTENTIOKINETIC POLARIZATION SCAN DATA FOR THE
Fe - 12% Cr ALLOY IN H₂-SATURATED METAL CHLORIDE SOLUTIONS

TABLE 43

CYCLIC POTENTIOKINETIC POLARIZATION SCAN DATA FOR THE
Fe - 12% Cr ALLOY IN H₂O-SATURATED METAL CHLORIDE SOLUTIONS
("TEFLON GASKET" SAMPLES)

Run No.	(M) [Cl ⁻]	pH	Log		Zero Current Potential (v SCE)	Passiva- tion Potential (v SCE)	Passiva- tion Current Density (a/cm ²)	Second Passiva- tion Potential (v SCE)	Log Second Passiva- tion Current Density (a/cm ²)	Chromic Ion Molarity	Return Peak Potential (v SCE)	Rupture Potential (v SCE)	"Protection Potential" (v SCE)
			Passiva- tion Current Density (a/cm ²)	Second Passiva- tion Potential (v SCE)									
KS-194	0.10	5.60	-	-	-0.590	-	-	-	nil	-	+0.080	-0.052	
KS-195	0.10	5.60	-0.390	-5.37	-0.580	-0.135	-5.40	-	nil	-	+0.070	-0.164	
KS-196	0.10	5.60	-	-	-0.525	-	-	-	nil	-	+0.100	-0.064	
KS-193	0.10	5.70	-0.120	-4.35	-0.450	-	-	-	nil	-	+0.080	-0.044	
KS-191	0.10	5.76	-	-	-0.382	-	-	-	nil	-	+0.108	-0.556	
KS-192	0.10	5.76	-	-	-0.690	-	-	-	nil	-	+0.060	-0.458	
KS-197	0.10	4.58	-0.380	-4.49	-0.660	-	-	-	5 x 10 ⁻⁵	-	-0.010	-0.560	
KS-198	0.10	4.63	-0.460	-4.51	-0.638	-0.350	-4.46	-	5 x 10 ⁻⁵	-	-0.040	-0.560	
KS-214	0.10	4.33	-0.390	-4.43	-0.560	-	-	-	10 ⁻⁴	-	-0.085	-0.250	
KS-213	0.10	4.35	-0.395	-4.44	-0.580	-	-	-	10 ⁻⁴	-	-0.095	-0.263	
KS-215	0.10	4.37	-0.400	-4.47	-0.566	-	-	-	10 ⁻⁴	-	-0.060	-0.508	
KS-210	0.12	3.82	-0.360	-3.96	-0.570	-	-	-	5 x 10 ⁻⁴	-	-0.178	-0.536	
KS-211	0.12	3.84	-0.355	-4.14	-0.560	-	-	-	5 x 10 ⁻⁴	-	-0.205	-0.538	
KS-212	0.12	3.84	-0.355	-3.92	-0.568	-	-	-	5 x 10 ⁻⁴	-	-0.120	-0.520	

TABLE 43 (Continued)

Run No.	[Cl ⁻] (M)	pH	Zero Current Potential (v _{SCE})	Passiva- tion Potential (v _{SCE})	Log Passiva- tion Current Density (a/cm ²)	Second Passiva- tion Potential (v _{SCE})	Log Second Passiva- tion Current Density (a/cm ²)	Chromic Ion Molarity	Return Peak Potential (v _{SCE})	Rupture Potential (v _{SCE})	"Protection Potential" (v _{SCE})
KS-217	0.14	3.68	-0.542	-0.340	-4.28	-	-	10 ⁻³	-0.340	-0.100	-0.275
KS-218	0.14	3.68	-0.530	-0.335	-4.49	-	-	10 ⁻³	-0.375	-0.040	-0.518
KS-216	0.14	3.70	-0.540	-0.340	-4.37	-	-	10 ⁻³	-0.375	-0.030	-0.275
KS-219	0.47	3.05	-0.600	-0.440	-3.21	-0.260	-2.89	10 ⁻²	-0.295	-0.170	-0.647
KS-220	0.47	3.05	-0.600	-0.450	-3.31	-0.265	-2.89	10 ⁻²	-0.295	-0.180	-0.650
KS-221	3.83	2.25	-0.580	-0.390	-2.26	-	-	10 ⁻¹	-0.430	-0.340	-0.600

BIBLIOGRAPHY

1. M. G. Fontana and N. D. Greene, Corrosion Engineering, McGraw-Hill Book Co., 1967.
2. B. F. Brown, "Technical Note: The Concept of the Occluded Corrosion Cell," Corrosion, 26, 249-250 (Aug. 1970).
3. M. Pourbaix, L. Klimzack-Mathieu, C. Mertens, J. Meunier, C. Vanleugenhaghe, L. de Munck, J. Laureys, L. Neelemans and M. Warzee, "Potentiokinetic and Corrosimetric Investigations of the Corrosion Behavior of Alloy Steels," Corrosion Science, 3, 239-259 (1963).
4. "NACE Glossary of Corrosion Terms," Corrosion, 20, 267t-268t (Aug. 1964).
5. N. D. Greene and M. G. Fontana, "A Critical Analysis of Pitting Corrosion," Corrosion, 15, 25t-31t (Jan. 1959).
6. C. Wagner and W. Traud, "Über die Deutung von Korrosionsvorgängen durch Überlagerung von elektrochemischen Teilvorgängen und über die Potentialbildung an Mischelektroden," Zeitschrift für Elektrochemie, 44, 391-402 (1938).
7. K. J. Vetter, Electrochemical Kinetics. Theoretical and Experimental Aspects, Translated by Scripta Technica, Inc., Academic Press, 1967.
8. "Standard Method of Total Immersion Corrosion Test of Stainless Steels," A.S.T.M. Designation: A 279-63, A.S.T.M. Standards, Part 3, Steel Sheet, Strip, Bar, Rod, Wire; Metallic Coated Products, Am. Soc. for Testing and Materials, Philadelphia, 268-276, 1968.
9. "Recommended Practice for Conventions Applicable to Electrochemical Measurements in Corrosion Testing," A.S.T.M. Designation: G 3-68, Annual A.S.T.M. Standards, Part 31, Metals-Physical, Mechanical, Nondestructive, Corrosion Tests, Metallography, Am. Soc. for Testing and Materials, Philadelphia, 940-950, 1970.
10. S. Brenner, "Method for Testing the Resistance of Stainless Steels to Local Corrosive Attack," Journal of the Iron and Steel Institute, 135, 101P-111P (1937).
11. N. D. Greene, "The Classical Potentiostat: Its Application to the Study of Passivity," Corrosion, 15, 369t-372t (July 1959).
12. J. E. Reinhoehl, F. H. Beck, and M. G. Fontana, "Effect of Polarization Rate in Potentiokinetic Anodic Polarization of Iron in 1 N H₂SO₄," Corrosion, 26, 141-150 (April 1970).

13. H. P. Leckie, "A Contribution to the Applicability of Critical Pitting Potentials," J. Electrochem. Soc., 117, 1152-1153 (Sept. 1970).
14. "Recommended Practice for Standard Reference Method for Making Potentiostatic and Potentiodynamic Anodic Polarization Measurements," A.S.T.M. Designation: G 6-69, Annual A.S.T.M. Standards, Part 31, Metals-Physical, Mechanical, Nondestructive, Corrosion Tests, Metallography, Am. Soc. for Testing and Materials, Philadelphia, 964-975, 1970.
15. N. D. Greene, Experimental Electrode Kinetics, Rensselaer Polytechnic Institute, Troy, New York, 1965.
16. Ja. M. Kolotyrkin, "Effects of Anions on the Dissolution Kinetics of Metals," J. Electrochem. Soc., 108, 209-216 (1961).
17. Ja. M. Kolotyrkin, "Pitting Corrosion of Metals," Corrosion, 19, 261t-268t (Aug. 1963).
18. T. P. Hoar, "On Corrosion-Resistant Materials," J. Electrochem. Soc., 117, 17C-22C (Jan. 1970).
19. E. H. Wyche, L. R. Voigt, and F. L. LaQue, "Corrosion in Crevices," J. Electrochem. Soc., 89, 149-166 (1946).
20. H. H. Uhlig, Corrosion and Corrosion Control, John Wiley and Sons, Inc., 1964.
21. V. M. Novakovsky, "Thermodynamic and Kinetic Causes of Passivity," Electrochimica Acta, 10, 353-365 (1965).
22. N. Tomashov and G. P. Chernova, Passivity and Protection of Metals Against Corrosion, Plenum Press, 1967.
23. J. O'M. Bockris and A. K. N. Reddy, Modern Electrochemistry, Volume 2, Plenum Press, New York, 1970.
24. G. Okamoto, "Passive Film of 18-8 Stainless Steel--Structure and Its Function," paper presented at the International Congress on Metallic Corrosion, Tokyo, Japan, May 21-27, 1972.
25. H. H. Uhlig and J. Wulff, "The Nature of Passivity in Stainless Steels and Other Alloys, I and II," Trans. Am. Inst. Min. & Met. Engrs., 135, 494-534 (1939).
26. H. H. Uhlig, "Adsorbed and Reaction-Product Films on Metals," J. Electrochem. Soc., 97, 215C-220C (Nov. 1950).
27. Marcel Pourbaix, "Significance of Protection Potential in Pitting and Intergranular Corrosion," Corrosion, 26, 431-438 (Oct. 1970).

28. C. W. Borgmann, "Initial Corrosion Rate of Mild Steel, Influence of the Cation," Ind. and Eng. Chem., 29, 814-821 (1937).
29. R. T. Foley, "Role of the Chloride Ion in Iron Corrosion," Corrosion, 26, 58-70 (Feb. 1970).
30. D. M. Brasher, "Role of the Anion in Relation to Metallic Corrosion and Inhibition," Nature, 193, 868-869 (1962).
31. H. P. Leckie and H. H. Uhlig, "Environmental Factors Affecting the Critical Potential for Pitting in 18-8 Stainless Steel," J. Electrochem. Soc., 113, 1262-1267 (1966).
32. Z. Szklarska-Smialowska, "Review of Literature on Pitting Corrosion Published Since 1960," Corrosion, 27, 223-233 (June 1971).
33. P. M. Aziz and H. P. Godard, "Pitting Corrosion Characteristics of Aluminum," Ind. and Eng. Chem., 44, 1791-1795 (1952).
34. M. A. Streicher, "Pitting Corrosion of 18 Cr-8 Ni Stainless Steel," J. Electrochem. Soc., 103, 375-389 (1956).
35. B. Kabanov, R. Burstein, and A. Frumkin, "Kinetics of Electrode Processes on the Iron Electrode," Discuss. Far. Soc., No. 1, 259-269 (1947).
36. I. L. Rosenfeld and I. S. Danilov, "Electrochemical Aspects of Pitting Corrosion," Corrosion Science, 7, 129-142 (1967).
37. U. R. Evans, "The Passivity of Metals, Part 1 - The Isolation of the Protective Film," J. Chem. Soc. (London), 1020-1040 (1927).
38. T. P. Hoar, "General Discussion," Discussion of the Faraday Soc. on Electrode Processes, No. 1, Gurney and Jackson, London, 299-300 (1947).
39. T. P. Hoar, "The Breakdown and Repair of Oxide Films on Iron," Trans. Far. Soc., 45, 683-693 (1949).
40. H.-J. Engell and N. D. Stolica, "Untersuchungen über Lochfrass an passiven Elektroden aus unlegierten Stahl in chlorionenhaltiger Schwefelsäure," Archiv für das Eisenhüttenwesen, 30, 239-248 (1959).
41. H. Kaesche, "Kurze Mitteilung, Anodischer Grenzstrom und Lochfrass von Aluminium in Alkalischen Neutralsalzlösungen," Zeitschrift für Physikalische Chemie, Neue Folge, 26, 138-142 (1960).
42. K. J. Vetter, "Eine thermodynamische Theorie zur Lochfrasskorrosion," Berichte der Bunsengesellschaft, 69, 683-688 (1965).

43. T. P. Hoar and W. R. Jacob, "Breakdown of Passivity of Stainless Steel by Halide Ions," Nature, 216, 1299-1301 (1967).
44. J. E. Reinehl and F. H. Beck, "Passivity and Anodic Protection," Corrosion, 25, 233-242 (June 1969).
45. F. Fenwick, "Protective Films on Ferrous Alloys," Ind. and Eng. Chem., 27, 1095-1099 (1935).
46. H. H. Uhlig, "Pitting of Stainless Steels," Trans. Am. Inst. Min. & Met. Eng., 140, 411-432 (1940).
47. H. A. Liebhafsky and A. E. Newkirk, "Corrosion of Stainless Steel in Ferric Chloride Solution," Corrosion, 12, 92t-98t (Feb. 1956).
48. C. M. Mahla and N. A. Nielsen, "Passivation of Stainless Steel," Trans. Electrochem. Soc., 89, 167-194 (1946).
49. L. Klimzack-Mathieu, C. Mertens, J. Meunier, M. Pourbaix, and C. Vanlengenhaghe, "Sur le Comportement d'Aciers Allies en Solution Chloruree. Influence de la Temperature sur les Tension de 'Rupture,' et de 'Protection,' d'Aciers, et sur les Concentrations de 'Rupture,' et de 'Protection' en chlorure (Solutions Bicarboniques)," Report No. 105, CEBELCOR, Brussels, Belgium (1962).
50. Z. Szklarska-Smialowska and M. Janik-Czachor, "The Analysis of Electrochemical Methods for the Determination of Characteristic Potentials of Pitting Corrosion," Corrosion Science, 11, 901-914 (1971).
51. A. P. Bond, "Pitting Corrosion - A Review of Recent Advances in Testing Methods and Interpretation," Localized Corrosion - Cause of Metal Failure, ASTM STP 516, Am. Soc. for Testing and Materials, 250-261, 1972.
52. L. Klimzack-Mathieu, J. Meunier, M. Pourbaix, and C. Vanleughenaghe, "Sur le Comportement d'Aciers Allies en Solution Bicarbonique. Influence de Chlorure et d'Oxydants," Report No. 103, CEBELCOR, Brussels, Belgium (1962).
53. K. Nobe and R. F. Tobias, "Anodic Potentiostatic Polarization of Iron in Sulfuric Acid: Effect of Chloride Ions," Corrosion, 20, 263t-266t (Aug. 1964).
54. E. D. Verink, Jr., "Construction of Pourbaix Diagrams for Alloy Systems with Special Application to the Binary Fe-Cr System," A Report to the Advanced Research Project Agency, Eng. and Ind. Exp. Sta., College of Eng., U. of Fla., Gainesville, June 10, 1970.

55. R. L. Cusumano, "The Establishment of a Three-Dimensional (Potential-pH-Composition) Diagram for Binary Fe-Cr Alloys in 0.1 Molar Chloride Solutions," Master's Thesis, University of Florida, 1971.
56. R. F. Steigerwald, "Effect of Cr Content on Pitting Behavior of Fe-Cr Alloys," Corrosion, 22, 107-112 (April 1966).
57. K. G. Weil and D. Menzel, "Die Einwirkung von Halogenionen auf passives Eisen," Zeitschrift für Elektrochemie, 63, 669-673 (1959).
58. W. Schwenk, "Theory of Stainless Steel Pitting," Corrosion, 20, 129t-137t (April 1964).
59. W. Schwenk, "Diskussion der Eigenschaften des Lochfrasspotentials Nichtrostender Stähle in Zusammenhang mit seinen Bestimmungsmethoden," Corrosion Science, 5, 245-254 (1965).
60. N. Stolica, "Pitting Corrosion on Fe-Cr Alloys," Corrosion Science, 9, 205-216 (1969).
61. F. A. Champion, "New Methods for the Examination of Corroded Metal," J. Inst. Metals (London), 69, 47-67 (1943).
62. H. W. Pickering and R. P. Frankenthal, "A Transmission Electron Microscope Study of the Breakdown of Passivity on Fe - 24% Cr," J. Electrochem. Soc., 112, 761-767 (Aug. 1965).
63. J. A. Richardson and G. C. Wood, "A Study of the Pitting Corrosion of Al by Scanning Electron Microscopy," Corrosion Science, 10, 313-323 (1970).
64. R. P. Frankenthal and H. W. Pickering, "On the Mechanism of Localized Corrosion of Iron and Stainless Steel. II. Morphological Studies," J. Electrochem. Soc., 119, 1304-1310 (1972).
65. T. P. Hoar, "The Production and Breakdown of the Passivity of Metals," Corrosion Science, 7, 341-355 (1967).
66. J. N. Agar and T. P. Hoar, "The Influence of Change of Size in Electrochemical Systems," Discuss. Far. Soc., No. 1, 158-162 (1947).
67. J. T. Waber, "Study of a Size Effect in Galvanic Corrosion," Corrosion, 13, 95t-102t (Feb. 1957).
68. R. H. Brown and R. B. Mears, "The Electrochemistry of Corrosion," Trans. Electrochem. Soc., 74, 495-517 (1938).
69. R. H. Brown and R. B. Mears, "Application of Electrochemical Measurements to Studies of the Corrosion of 18-8 Stainless Steel," Trans. Far. Soc., 35, 467-474 (1939).

70. L. J. Benson, R. H. Brown, and R. B. Mears, "Electrochemical Studies of the Corrosion of Steel and Magnesium in Partly Inhibited Solutions," Trans. Electrochem. Soc., 76, 259-269 (1939).
71. N. D. Greene and M. G. Fontana, "An Electrochemical Study of Pitting Corrosion in Stainless Steels, Part 1 - Pit Growth," Corrosion, 15, 32t-38t (Jan. 1959).
72. N. D. Greene and M. G. Fontana, "An Electrochemical Study of Pitting Corrosion in Stainless Steels, Part 2 - Polarization Measurements," Corrosion, 15, 39t-44t (Jan. 1959).
73. G. A. W. Murray, "Artificial Pits for Quantitative Studies of Corrosion of Aluminum Alloys in Natural Waters," Corrosion, 20, 329t-334t (Oct. 1964).
74. G. Herbsleb and H.-J. Engell, "Untersuchungen über das Verhalten von aktivem und passivem Eisen in Schwefelsäure und über die Zerstörung der Passivschicht auf Eisen durch Chlorionen," für Elektrochemie, 65, 881-887 (1961).
75. H. W. Pickering and R. P. Frankenthal, "On the Mechanism of Localized Corrosion of Iron and Stainless Steel. I. Electrochemical Studies," J. Electrochem. Soc., 119, 1297-1304 (1972).
76. G. W. Akimov, "Electrode Potentials, Part 2 of 2 Parts," Corrosion, 11, 515t-534t (Dec. 1955).
77. R. Piontelli, "Electrochemical Behavior of Metals as a Basis for the Study of Corrosion," Corrosion, 9, 115-122 (April 1953).
78. M. J. Pryor, "Corrosion of Steel in Dilute Solutions of Sodium Salts of Weak Acids," Corrosion, 9, 467-477 (Dec. 1953).
79. E. Heyn and O. Bauer, "Influence of the Treatment on the Solubility of Steel in Sulphuric Acid, and Deductions Therefrom as to the Nature of the Treatment to Which the Material has Been Previously Subjected," J. Iron and Steel Inst., 79, 109-117 (1909).
80. Z. A. Foroulis and H. H. Uhlig, "Effect of Velocity and Oxygen on Corrosion of Iron in Sulfuric Acid," J. Electrochem. Soc., 111, 13-17 (Jan. 1964).
81. G. Herbsleb and H.-J. Engell, "Untersuchungen über die Lochfrasskorrosion des passiven Eisens in chlorionenhaltiger Schwefelsäure," Werkstoffe und Korrosion, 17, 365-376 (1966).
82. C. J. Cron, J. H. Payer, and R. W. Staehle, "Dissolution Behavior of Fe-Fe₃C Structures as a Function of pH, Potential, and Anion - An Electron Microscopic Study," Corrosion, 27, 1-25 (Jan. 1971).

83. H. H. Strehblow and K. J. Vetter, "Ermittlung der Zusammensetzung der Oberfläche von Korrosionslöchern auf Eisen während des Lochfrasses mittels der Elektronenmikrosonde," Berichte der Bunsen - Gesellschaft für Physikalische Chemie, 75, 822-829 (1971).
84. J. R. Baylis, "Factors Other Than Dissolved Oxygen Influencing the Corrosion of Iron Pipes," Ind. and Eng. Chem., 18, 370-380 (1926).
85. U. R. Evans, "The Electrochemical Character of Corrosion," J. Inst. Metals, 30, 239-297 (1923).
86. J. Aston, "The Effect of Rust Upon the Corrosion of Iron and Steel," Trans. Am. Electrochem. Soc., 29, 449-468 (1916).
87. E. D. Parsons, H. H. Cudd, and H. L. Lochte, "Synthetic Corrosion Pits and the Analysis of Their Contents," J. Phys. Chem., 45, 1339-1345 (1941).
88. B. E. Wilde and E. Williams, "The Use of Current/Voltage Curves for the Study of Localized Corrosion and Passivity Breakdown on Stainless Steels in Chloride Media," Electrochimica Acta, 16, 1971-1985 (1971).
89. M. J. Sienko and R. A. Plane, Chemistry, Second Edition, McGraw-Hill Book Co., Inc., New York, 1961.
90. G. W. Whitman, R. P. Russell, and V. J. Altieri, "Effect of Hydrogen-Ion Concentration on the Submerged Corrosion of Steel," Ind. and Eng. Chem., 16, 665-670 (1924).
91. A. Seidell, Solubilities of Inorganic and Metal Organic Compounds, Vol. 1, 3rd Edition, D. Van Nostrand Company, Inc., New York, 1940.
92. W. F. Linke, Solubilities of Inorganic and Metal Organic Compounds, Vol. 1, 4th Edition, D. Van Nostrand Company, Inc., New York, 1958.
93. Handbook of Chemistry and Physics, R. C. Weast, Editor, The Chemical Rubber Co., Cleveland, Ohio, 51st Edition, 1970-71.
94. Barrow, Physical Chemistry, McGraw-Hill Book Co., Inc., New York, 1961.
95. W. D. France, Jr. and N. D. Greene, "Comparison of Chemically and Electrolytically Induced Pitting Corrosion," Corrosion, 26, 1-4 (Jan. 1970).
96. U. R. Evans, "The Distribution and Velocity of the Corrosion of Metals," J. Franklin Institute, 208, 45-58 (July 1929).
97. G. T. Colegate, "The Corrosion of the Austenitic Stainless Steels, Part II - Pitting and Intergranular Corrosion," Metallurgia, 41, 259-262 (1950).

98. R. May, "Some Observations on the Mechanism of Pitting Corrosion," J. Inst. Metals (London), 82, 65-74 (1953).
99. U. F. Franck, "Über die Stabilität von heterogenen Oberflächenstrukturen bei der Korrosion passivierbarer Metalle," Werkstoffe und Korrosion, 11, 401-410 (1960).
100. E. Brauns und W. Schwenk, "Untersuchung der Lochfrasskorrosion an chemisch Beständigen austenitischen Stählen," Archiv für das Eisenhüttenwesen, 32, 387-396 (June 1961).
101. W. Schwenk, "Diskussion über die Ursache und Stabilität der Lochfrasskorrosion in Zusammenhang mit dem 'Alles-odor-Nichts' - Gesetz der Passivität und Einem kinetischen Modell," Corrosion Science, 3, 107-121 (1963).
102. T. P. Hoar, D. C. Mears, and G. P. Rothwell, "The Relationships Between Anodic Passivity, Brightening and Pitting," Corrosion Science, 5, 279-289 (1965).
103. G. J. Schafer, J. R. Gabriel, and P. K. Foster, "On the Role of the Oxygen Concentration Cell in Crevice Corrosion and Pitting," J. Electrochem. Soc., 107, 1002-1004 (1960).
104. G. Bombara, "Stress-Corrosion Cracking and Crevice Corrosion in Passivable Alloys," Corrosion Science, 9, 519-533 (1969).
105. H. H. Uhlig, Ed., The Corrosion Handbook, John Wiley & Sons, Inc., New York, 172, 1948.
106. W. D. France, Jr., "Crevice Corrosion of Metals," Localized Corrosion - Cause of Metal Failure, ASTM STP 516, Am. Soc. for Testing and Materials, 164-200, 1972.
107. B. E. Wilde and E. Williams, "The Relevance of Accelerated Electrochemical Pitting Tests to the Long-Term Pitting and Crevice Corrosion Behavior of Stainless Steels in Marine Environments," J. Electrochem. Soc., 118, 1057-1062 (1971).
108. I. L. Rosenfeld and I. K. Marshakov, "Mechanism of Crevice Corrosion," Corrosion, 20, 115t-125t (April 1964).
109. R. J. McKay, "Corrosion by Electrolyte Concentration Cells," Trans. Am. Electrochem. Soc., 41, 201-215 (1922).
110. R. J. McKay, "The Common Occurrence of Corrosion by Electrolyte Concentration Cells," Ind. and Eng. Chem., 17, 23-24 (1925).
111. G. J. Scahfer and P. K. Foster, "The Role of the Metal-Ion Concentration Cell in Crevice Corrosion," J. Electrochem. Soc., 106, 468 (1959).

112. U. R. Evans, "Corrosion of Metals at Joints and Crevices," Engineering, 123, 362-363 (1927).
113. R. B. Mears and U. R. Evans, "Corrosion at Contact with Glass," Trans. Far. Soc., 30, 417-423 (1934).
114. Y. M. Korovin and I. B. Ulanovskii, "Effect of Oxygen Concentration and pH on Electrode Potential of Stainless Steels and Operation of Microcouples," Corrosion, 22, 16-20 (Jan. 1966).
115. B. E. Wilde and E. Williams, "On the Breakdown of Passivity on Stainless Steels in Halide Media," J. Electrochem. Soc., 116, 1539-1540 (1969).
116. G. Karlberg and G. Wranglén, "On the Mechanism of Crevice Corrosion of Stainless Cr Steels," Corrosion Science, 11, 499-510 (1971).
117. B. E. Wilde, "A Critical Appraisal of Some Popular Laboratory Electrochemical Tests for Prediction of the Localized Corrosion Resistance of Stainless Steels in Sea Water," Corrosion, 28, 283-291 (Aug. 1972).
118. I. L. Rosenfeld, "Review: Crevice Corrosion," The U. R. Evans International Conference on Localized Corrosion, Williamsburg, Virginia, Dec. 6-10, 1971.
119. N. D. Greene, W. D. France, Jr., and B. E. Wilde, "Technical Note: Electrode Mounting for Potentiostatic Anodic Polarization Studies," Corrosion, 21, 275-276 (Sept. 1965).
120. E. A. Lizlovs and A. P. Bond, "Anodic Polarization of Some Ferritic Stainless Steels in Chloride Media," J. Electrochem. Soc., 116, 574-579 (May 1969).
121. F. L. Rosenfeld and I. K. Marshakov, "Mechanism of Selective Linear Corrosion," Russian J. of Phys. Chem., English Trans., 35, 620-622 (1961).
122. O. B. Ellis and F. L. LaQue, "Area Effects in Crevice Corrosion," Corrosion, 7, 362-364 (Nov. 1951).
123. G. Bombara, D. Sinigaglia, and G. Taccani, "Geometrical Factors in Crevice Corrosion of Stainless Steels," Electrochim. Metal., 3, 81-94 (1968).
124. D. A. Vermilyea and C. S. Tedmon, Jr., "A Simple Crevice Corrosion Theory," J. Electrochem. Soc., 117, 437-440 (1970).
125. E. A. Lizlovs, "Technical Note, Polarization Cell for Potentiostatic Crevice Corrosion Testing," J. Electrochem. Soc., 117, 1335-1337 (Oct. 1970).

126. D. Sinigaglia, G. Taccani, and G. Bombara, "Crevice Corrosion of Austenitic Stainless Steels in Acid Solutions," Electrochim. Metal., 3, 297-312 (1968).
127. L. A. Larin and Z. A. Iofa, "A Study of the Mechanism of the Enhanced Corrosion of Iron at Three-Phase Boundaries," Russian J. of Phys. Chem., English Trans., 34, 703-706 (1960).
128. W. D. France, Jr. and N. D. Greene, Jr., "Passivation of Crevices During Anodic Protection," Corrosion, 24, 247-251 (Aug. 1968).
129. M. Pourbaix, "Bases Fondamentales de la Protection Cathodique, et Applications," Report No. 166 CEBELCOR, Brussels, Belgium, 1969.
130. K. D. Efird, "Crevice Corrosion of a Copper-Nickel Alloy and Its Relationship to the Experimental Pourbaix Diagram," Master's Thesis, University of Florida, 1970.
131. A. Pourbaix, "Etude de la Corrosion Localisee de l'Acier en Solutions Chlorurees," Report No. 198, CEBELCOR, Brussels, Belgium (Aug. 1971).
132. A. Pourbaix, "Characteristics of Localized Corrosion of Steel in Chloride Solutions," Corrosion, 27, 449-454 (Nov. 1971).
133. P. R. Rhodes, "Mechanism of Chloride Stress Corrosion Cracking of Austenitic Stainless Steels," Corrosion, 25, 462-472 (Nov. 1969).
134. G. Sandoz, C. T. Fujii and B. F. Brown, "Solution Chemistry Within Stress-Corrosion Cracks in Alloy Steels," Corrosion Science, 10, 839-845 (1970).
135. J. A. Smith, M. H. Peterson and B. F. Brown, "Electrochemical Conditions at the Tip of an Advancing Stress Corrosion Crack in AISI 4340 Steel," Corrosion, 26, 539-542 (Dec. 1970).
136. I. B. Ulanovskii and Iu. M. Korovin, "Corrosion of Stainless Steels at Points of Contact with Nonmetallic Materials," J. Appl. Chem. of the U.S.S.R. (Eng. Trans.), 31, 1352-1355 (1958).
137. M. H. Peterson, T. J. Lennox, Jr., and R. E. Groover, "A Study of Crevice Corrosion in Type 304 Stainless Steel," Materials Protection, 9, 23-26 (Jan. 1970).
138. B. F. Brown, C. T. Fujii and E. P. Dahlberg, "Methods for Studying the Solution Chemistry Within Stress Corrosion Cracks," J. Electrochem. Soc., 116, 218-219 (1969).
139. C. G. MacArthur, "Solubility of Oxygen in Salt Solutions and the Hydrates of these Salts," J. Phys. Chem., 20, 495-502 (1916).

140. "Solubilities of Gases in Liquids," International Critical Tables, 3, McGraw-Hill, New York, 1928.
141. M. A. Streicher, "The Time-Factor in Potentiostatic Studies of Intergranular Corrosion of Austenitic Stainless Steels," Corrosion Science, 9, 53-56 (1969).
142. R. J. Brigham, "Discussion: Chemically and Electrolytically Induced Pitting," Corrosion, 26, 200 (May 1970).
143. B. E. Wilde and E. Williams, "On the Correspondence Between Electrochemical and Chemical Accelerated Pitting Corrosion Tests," J. Electrochem. Soc., 117, 775-779 (June 1970).
144. F. L. LaQue, "Theoretical Studies and Laboratory Techniques in Sea Water Corrosion Testing Evaluation," Corrosion, 13, 303t-314t (May 1957).
145. K. G. Compton, "The Unique Environment of Sea Water and Its Effect on Corrosion of Metals," Corrosion, 26, 448-449 (Oct. 1970).
146. L. Klimzack-Mathieu, J. Meunier, M. Pourbaix, and C. Vanleughenaghe, "Sur le Comportement d'Aciers Allies en Solution Chloruree. Influence de Bicarbonate et de sulfate a 20°C," Report No. 104, CEBELCOR, Brussels, Belgium (1962).
147. M. Pourbaix, L. Klimzack-Mathieu, C. Mertens, J. Meunier, and C. Vanleughenaghe, "Etudes Potentiocinetiques et Corrosimetriques sur le Comportement d'Aciers Allies," Report No. 120, CEBELCOR, Brussels, Belgium (1962).
148. M. Pourbaix, J. Van Muylder, and P. Van Laer, "Sur la Tension d'Electrode du Cuivre en Presence d'Eau de Bruxelles. Influence de la Lumiere et des Conditions de Circulation de l'Eau," Report No. 125, CEBELCOR, Brussels, Belgium (1965).
149. J. Van Muylder, M. Pourbaix, and P. Van Laer, "Electrochemical Nature of the Pitting of Copper in Water and in Aqueous Chloride Solutions," Report E 61, CEBELCOR, Brussels, Belgium (1967).
150. M. Pourbaix, "Recent Applications of Electrode Potential Measurements in the Thermodynamics and Kinetics of Corrosion of Metals," Corrosion, 25, 267-281 (June 1969).
151. M. Pourbaix, "A Comparative Review of Electrochemical Methods of Assessing Corrosion and the Behavior in Practice of Corrodible Metals," Report E 50, CEBELCOR, Brussels, Belgium (1964).
152. E. D. Verink, Jr., J. S. Lee, III, and R. L. Cusumano, "Technical Note: Influence of Prior Electrochemical History on the Propagation of Localized Corrosion," Corrosion, 28, 348-349 (Sept. 1972).

153. E. D. Verink, Jr. and M. Pourbaix, "Use of Potentiokinetic Methods at Successively Increasing and Decreasing Electrode-Potentials in Developing Alloys for Saline Exposures," Report No. 191, CEBELCOR, Brussels, Belgium (1971).
154. E. D. Verink, Jr., and M. Pourbaix, "Use of Electrochemical Hysteresis Techniques in Developing Alloys for Saline Exposures," Corrosion, 27, 495-505 (Dec. 1971).
155. T. Suzuki and Y. Kitamura, "Critical Potential for Growth of Localized Corrosion of Stainless Steel in Chloride Media," Corrosion, 28, 1-6 (Jan. 1972).
156. T. S. Lee, III, "The Use of Experimentally Determined Potential vs. pH Diagrams to Elucidate the Influence of Solute Additions on the Passive Behavior of Binary Copper-Nickel Alloys in Solutions With and Without Chloride," Master's Thesis, University of Florida, 1972.
157. P. A. Parrish, "Use of Experimentally Determined Pourbaix Diagrams to Elucidate the Role of Iron in the Passive Behavior of Copper-Rich Alloys Containing Nickel," Master's Thesis, University of Florida, 1970.
158. R. H. Heidersbach, Jr., "The Dezincification of Alpha and Beta Brasses," Ph.D. Dissertation, University of Florida, December, 1971.
159. R. H. Heidersbach, Jr., and E. D. Verink, Jr., "The Dezincification of Alpha and Beta Brasses," Corrosion, 28, 397-418 (Nov. 1972).
160. E. D. Verink, Jr., and R. H. Heidersbach, Jr., "Evaluation of the Tendency for Dealloying in Metal Systems," Localized Corrosion - Cause of Metal Failure, ASTM STP 516, Am. Soc. for Testing and Materials, 303-322, 1972.
161. J. Van Muylder, N. de Zoubov, and M. Pourbaix, "Diagrammes d'Équilibres Tension - pH des Systèmes Cu-H₂O et Cu-Cl -H₂O à 25°C," Report No. 101, CEBELCOR, Brussels, Belgium (July 1962).
162. H. W. Pickering, Private Communication, University of Florida, Gainesville, Florida, June, 1972.
163. N. Pessall and C. Liu, "Determination of Critical Pitting Potentials of Stainless Steels in Aqueous Chloride Environments," Electrochimica Acta, 16, 1987-2003 (1971).
164. E. A. Lizlovs, "Crevice Corrosion of Some High-Purity Ferritic Stainless Steels," Localized Corrosion - Cause of Metal Failure, ASTM STP 516, Am. Soc. for Testing and Materials, 201-209, 1972.

165. W. D. France, Jr., and R. W. Lietz, "Improved Data Recording for Automatic Potentiodynamic Polarization Measurements," Corrosion, 24, 298-300 (Sept. 1968).
166. D. J. G. Ives and G. J. Janz, Reference Electrodes, Theory and Practice, Academic Press, New York and London, 1961.
167. American Public Health Association, Standard Methods for the Examination of Water and Wastewater, Twelfth Edition, Boyd Printing Co., Inc., 1966.
168. M. Pourbaix, Private Communication, University of Florida, Gainesville, Florida, Oct., 1972.
169. "Conductivity of Neutral Halides, Nitrates and Sulfates," International Critical Tables, 6, McGraw-Hill, New York, 230-240, 1928.
170. L. G. Sillen, "Graphic Presentation of Equilibrium Data," Chapter 8, Treatise on Analytical Chemistry, Part V, Theory and Practice, Volume V, Edited by I. M. Kolthoff and P. J. Elving, The Interscience Encyclopedia, Inc., New York, 277-317, 1959.
171. M. Pourbaix, Atlas of Electrochemical Equilibria in Aqueous Solutions, Translated from the French by James A. Franklin, Pergamon Press, 1966.
172. M. Pourbaix, "Les Facteurs Electrochimiques de la Corrosion Sous Tension," Report No. 199, CEBELCOR, Brussels, Belgium (Aug. 1971).
173. M. Pourbaix, "Electrochemical Aspects of Stress Corrosion Cracking," The Theory of Stress Corrosion Cracking in Alloys, Edited by J. C. Scully, N.A.T.O. Scientific Affairs Div., Brussels, Belgium, 17-63, 1971.
174. J. M. Bowers, T. S. Lee, III, and S. Maitra, Private Communication, University of Florida, Gainesville, Florida, Jan., 1973.
175. E. D. Verink, Jr., "A Technical Note: Simplified Procedure for Constructing Pourbaix Diagrams," Corrosion, 23, 371-372 (Dec. 1967).
176. S. F. Ashcroft and C. T. Mortimer, Thermochemistry of Transition Metal Complexes, Academic Press, London and New York, 1970.
177. C. L. Wilson and D. W. Wilson (Editors), Comprehensive Analytical Chemistry, Classical Analysis, Volume IB, Elsevier Publishing Co., 1960.

178. "Density (Specific Gravity) and Thermal Expansion (Under Atmospheric Pressure) of Aqueous Solutions of Inorganic Substances and of Strong Electrolytes," International Critical Tables, 3, McGraw-Hill, New York, 51-107, 1928.
179. F. H. Sweeton and C. F. Baes, Jr., "The Solubility of Magnetite and Hydrolysis of Ferrous Ion in Aqueous Solutions at Elevated Temperatures," J. Chem. Thermodynamics, 2, 479-500 (1970).
180. E. Deltombe, N. de Zoubov, and M. Pourbaix, "Comportement Electrochimique du Chrome, Diagramme d'Équilibre Tension-pH du Systeme Cr-H₂O, á 25°C," Report No. 41, CEBELCOR, Brussels, Belgium (Oct. 1956).
181. F. Feigl, Spot Tests in Inorganic Analysis, Translated by R. E. Desper, Elsevier Publishing Co., 1958.
182. T. Suzuki, M. Yamabe and Y. Kitamura, "Composition of Anolyte Within Pit Anode of Austenitic Stainless Steels in Chloride Solution," Corrosion, 29, 18-22 (Jan. 1973).
183. R. J. Chin and K. Nobe, "Electrodissolution Kinetics of Iron in Chloride Solutions IV. Acidic Solutions," J. Electrochem. Soc., 119, 1457-1461 (1972).
184. M. Hansen, Constitution of Binary Alloys, McGraw-Hill, 1958.
185. Metals Handbook, 8th Edition, "Heat Treating, Cleaning and Finishing," 2, American Society for Metals, Metals Park, Ohio, 1964.
186. Metals Handbook, 8th Edition, "Atlas of Microstructures of Industrial Alloys," 7, American Society for Metals, Metals Park, Ohio, 1972.
187. "Recommended Practice for a Standard Method for Making Potentiostatic and Potentiodynamic Anodic Polarization Measurements," A.S.T.M. Committee G-1, Subcommittee XI, April 10, 1968.
188. W. D. France, Jr., "A Specimen Holder for Precise Electrochemical Polarization Measurements on Metal Sheets and Foils," J. Electrochem. Soc., 114, 818-819 (1967).
189. J. R. Myers, E. G. Gruenler and L. A. Smulczenski, "Technical Note: Improved Working - Electrode Assembly for Electrochemical Measurements," Corrosion, 24, 352-353 (Oct. 1968).
190. International Critical Tables of Numerical Data, National Academy of Sciences, 3, Maple Press, York, Pa., 1929.

191. G. Lauer and F. Mansfeld, "Technical Note: Measurement of Galvanic Corrosion Current at Zero External Impedance," Corrosion, 504-506 (Nov. 1970).
192. A. B. Kinzel and W. Crafts, The Alloys of Iron and Chromium, I, Low-Chromium Alloys, McGraw-Hill Book Co., 1937.
193. "Selected Values of Chemical Thermodynamic Properties," NBS Technical Note 270-4, Institute for Materials Research, National Bureau of Standards, U. S. Government Printing Office, Washington, D.C. (May 1969).

BIOGRAPHICAL SKETCH

Kenneth Kirch Starr was born August 7, 1944, at Keokuk, Iowa. He attended public schools in several states and graduated from Edmunds High School, Sumter, South Carolina, in 1962. He received a Bachelor of Science degree in Metallurgical Engineering from Clemson University in May, 1966.

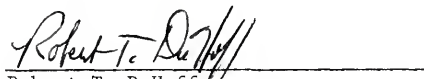
In September, 1966, he enrolled in the Graduate School of the University of Florida, receiving a Master of Engineering degree in Metallurgical Engineering in 1967. He has pursued the degree of Doctor of Philosophy in the Department of Materials Science and Engineering since that date.

Kenneth Kirch Starr is married to the former Barbara Jo Cantner. He is a member of Phi Kappa Phi, Tau Beta Pi, Alpha Sigma Mu, the American Society for Metals, the American Institute of Mining, Metallurgical and Petroleum Engineers, and the National Association of Corrosion Engineers.

I certify that I have read this study and that in my opinion it conforms to acceptable standards of scholarly presentation and is fully adequate, in scope and quality, as a dissertation for the degree of Doctor of Philosophy.


Ellis D. Verink, Jr., Chairman
Professor and Assistant Chairman
of Materials Science and
Engineering

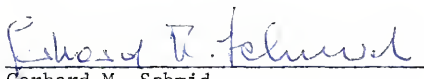
I certify that I have read this study and that in my opinion it conforms to acceptable standards of scholarly presentation and is fully adequate, in scope and quality, as a dissertation for the degree of Doctor of Philosophy.


Robert T. DeHoff
Professor of Materials Science
and Engineering

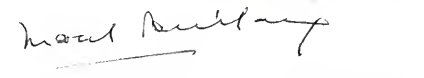
I certify that I have read this study and that in my opinion it conforms to acceptable standards of scholarly presentation and is fully adequate, in scope and quality, as a dissertation for the degree of Doctor of Philosophy.


John J. Hren
Professor of Materials Science
and Engineering

I certify that I have read this study and that in my opinion it conforms to acceptable standards of scholarly presentation and is fully adequate, in scope and quality, as a dissertation for the degree of Doctor of Philosophy.

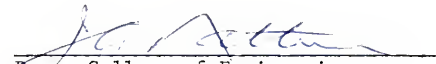

Gerhard M. Schmid
Associate Professor of Chemistry

I certify that I have read this study and that in my opinion it conforms to acceptable standards of scholarly presentation and is fully adequate, in scope and quality, as a dissertation for the degree of Doctor of Philosophy.


Marcel Pourbaix
Visiting Professor of Materials
Science and Engineering

This dissertation was submitted to the Dean of the College of Engineering and to the Graduate Council, and was accepted as partial fulfillment of the requirements for the degree of Doctor of Philosophy.

March, 1973



Dean, College of Engineering



Dean, Graduate School



UNIVERSITY OF FLORIDA



3 1262 08666 447 0